PHD

Mechanical factors influencing impaction bone grafting

Mak, Siu Yan

Award date:
2007

Awarding institution:
University of Bath

Link to publication

$\LaTeX\ 2_{\varepsilon}$

Mechanical factors influencing impaction bone grafting

Siu Yan Mak

for the degree of
Doctor of Philosophy

University of Bath
Department of Mechanical Engineering

October 2007

麦兆恩

‘This thesis is the result of three years of hard work and
collaboration of many minds and thoughts, and
I do believe strong commitment is the key to success.’

麥兆恩

Abstract

Impaction grafting for bone stock loss in revision total hip arthroplasty has been used for over a decade. This technique typically involves the insertion of a cemented highly polished stem into impacted morsellised allograft bone. The aim is to compensate for the bone stock loss after failed primary hip arthroplasty and to provide a mechanical and biological scaffold for mechanical support and bone remodelling. The primary objective of this study is to quantify and optimise the graft properties so as to provide maximum supportive forces to the stem, and, at the same time, to minimise the amount of per-operative and post-operative femoral fractures.

More than 60 parameters that could affect the mechanical properties of graft have been identified. Porcine bone from femoral heads was used in the study which was primarily divided into two parts: fundamental studies of the graft material, and *in-vitro* mechanical testing to replicate the clinical application of impaction bone grafting.

Various techniques of graft preparation including defatting of the graft were investigated. A die-plunger was employed to perform uni-axial compressive testing on the graft at varying strain rates. It was found that defatted graft demonstrated higher stiffness. Higher rates of loading resulted in increases in stiffness, hoop strain, axial force and Poisson's ratio. Pre-loading of the graft provided more predictable mechanical characteristics. Cyclic compressive testing showed that individual graft particles fractured during compression. In addition, it was found that the graft demonstrated increased viscoelastic properties at higher strain rates.

In-vitro mechanical testing was also performed to compare the level of mechanical stability of a cemented polished stem with a larger uncemented polished stem. Composite femora were used for this comparison. It was found that the cemented stem showed higher mechanical stability in terms of the level of micromotion and migration, and uncemented stem failed in a catastrophic manner.

The study provided information on how various factors contributed to the mechanical behaviour of bone graft and identified parameters that should be used when *in-vitro* testing of bone graft materials for use in impaction grafting.

Acknowledgements

This PhD thesis is the result of three years of hard work and has involved the kind contribution of many people's thoughts and ideas. I would like to thank my parents for support of my studies abroad. I would also like to express my thankfulness to Prof. Anthony Miles and Dr. James Cunningham for providing expert guidance, supervision and support.

I am very grateful to Dr. Ide Heyligers and Dr. Bernd Grimm for providing me with clinical experience in Netherlands at Atrium MC Heerlen Hospital. They gave me generous support during the time I was in Holland including allowing me to observe interesting operations and attend patient clinics. Mr. John Timperley gave me a valuable opportunity to observe an impaction grafting operation at the Princess Elizabeth Orthopaedic Centre in Exeter. I deeply appreciate all the explanations and guidance he provided during the operation.

I would like to thank Mr. Michael Katsimihas, Mr. Tim Holsgrove and Mr. Steven Smith for collaborating with me. I would also like to thank Mr. Richard Weston for his support with all aspects of the technical issue, Mr. Stephen Coombes for his support for the electronics of the testing apparatus, Mr. Colin Brain for his expertise in developing the high performance data acquisition software, all my colleagues for providing helpful distraction in the office.

Special thanks to Dr. Andrew Rees working as my LaTeX consultant for typesetting this tidy, organised and highly formatted thesis in LaTeX 2_ε format. I would also like to thank the Institution of Mechanical Engineers for sponsoring my conference visit in the United States. Last but not least, I would also like to thank the University of Bath, for providing a scholarship, without which my PhD would not have been possible.

Contents

List of Figures

List of Tables

Abbreviations

AMD	Apparent mass density
BMD	Bone mineral density
BMP	Bone morphogenic proteins
CCME	Consolidated constrained modulus of elasticity
CCPR	Consolidated constrained apparent Poisson's ratio
DNA	Deoxyribonucleic acid
DoE	Design of experiment
DOFs	Degree of freedoms
FEA	Finite element analysis
HA	Hydroxyapatite
HPVEE	Hewlett-Packard VEE
ICME	Impact constrained modulus of elasticity
ICPR	Impact constrained apparent Poisson's ratio
LaTeX	Text document (based on TeX)
LVDT	Linear variable displacement transducer
MCB	Morsellised cancellous bone
PIC	Proximal impaction cap
PID	Proportional-Integral-Derivative
PMMA	Polymethyl-methacrylate
PRV	Peak resistance value
QoL	Quality of life
RIG	Radial impaction grafting
RSA	Radiostereometric analysis
R-Sq	R-Square
SG	Strain gauge
TCP	Tricalcium-phosphate
THA	Total hip arthroplasty
THR	Total hip replacement
TCME	Total constrained modulus of elasticity
TCPR	Total constrained apparent Poisson's ratio

1. Introduction

1.1. Background

Currently, around 8 million people in the UK suffer from a wide range of hip disorders, though osteoarthritis is the most common. Total Hip Arthroplasty (THA) is a common treatment for osteoarthritis and is one of the most effective major surgical procedures performed in the National Health Service (NHS) [1]. Total hip replacement surgery helps to relieve pain, restores function and improves quality of life for patients with severe hip arthritis [2].

It has been estimated that more than 200,000 THA's are performed annually in the United States [3]. The UK National Joint Registry [4] reports that there were approximately 49,000 THA operations (primary 90.4%, revision 9.2%, others 0.4%) carried out in England and Wales in 2004. The majority of patients who require primary THA are in age range of $60 - 79$, and about $5 - 10\%$ of these patients experience complications of varying degrees of severity, including infection and joint loosening. For such cases, revision surgery may be required to replace the original prosthesis with a new one [1].

1.2. Total hip replacement

1.2.1. Primary hip replacement

Primary hip replacement involves replacing the femoral head and the acetabulum with artificial prostheses. The average cost of a primary hip replacement is £3,755 at 1998-99 prices [1]. The cost of the femoral component varies from £300 to around £2,000 depending on the component type [1]. Table 1.1 summarises all the patient characteristics for primary hip replacement procedures in 2004 across Wales and England [4]. As can be seen, approximately 94% of operations were performed for osteoarthritis.

	Primary THR			
	Cemented		Uncemented	
	Number	(%)	Number	(%)
Osteoarthritis	22,548	(94.0)	8,381	(93.6)
Avascular necrosis	774	(3.2)	341	(3.8)
Congenital dislocation/ dysplasia of hip	181	(0.8)	189	(2.1)
Fractured neck of femur	344	(1.4)	108	(1.2)
Seropositive rheumatoid arthritis	243	(1.0)	67	(0.8)
Failed international fixation	190	(0.8)	82	(0.9)
Other hip trauma	48	(0.2)	20	(0.2)
Previous arthrodesis	6	(0.03)	6	(0.1)
Other	559	(2.3)	255	(2.9)

Table 1.1.: Indications for primary hip replacement in Wales and England, 2004 (adapted from [4]).

1.2.2. Revision hip replacement

Revision hip replacement involves exchange or extraction of one or both of the implant components [5]. Murray *et al.* [6] reported that the revision rate is about 10% at ten years after initial THA, in which the major cause of revision hip replacement is aseptic loosening. However, the quality of life (QoL) for primary and revision hip operations both give a significant improvement in the QoL but function after revision may be less durable than after a primary arthroplasty [7]. Bozic *et al.* [8] compared the difference between primary and revision hip replacement, viz.:

- The mean total hospital cost was 30% higher for revision than for primary cases ($31,341 versus $24,170, $p < 0.0001$).
- The mean operative time was 41% longer for the revisions than for the primary procedures (4.5 hrs versus 3.2 hrs).
- The mean estimated blood loss was 160% higher (1348 ml versus 518 ml, $p < 0.0001$).
- The mean complication rate was 32% higher (29% versus 22%, $p = 0.072$).
- The mean length of the hospital stay was 16% longer (6.5 days versus 5.6 days, $p = 0.0005$).

1.2.3. Prosethetic components

The acetabular cup and femoral stem are the main components in total hip arthroplasty (Figure 1.1). The acetabular component replaces the acetabulum and typically consists of a ultra high molecular weight polyethylene liner with or without a metal backing shell. This provides a low friction bearing surface between the cup and the head of the femoral component. The femoral component typically consists of a stem and head component, the head component is fixed to the stem on a tapered spigot (Figure 1.2). However, in some early femoral stems versions (e.g. Charnley hip stem [9]), the head and the stem used to be a single component (monoblock design).

(a) (b)

Figure 1.1.: a) Acetabular component b) Femoral component (adapted from [10]).

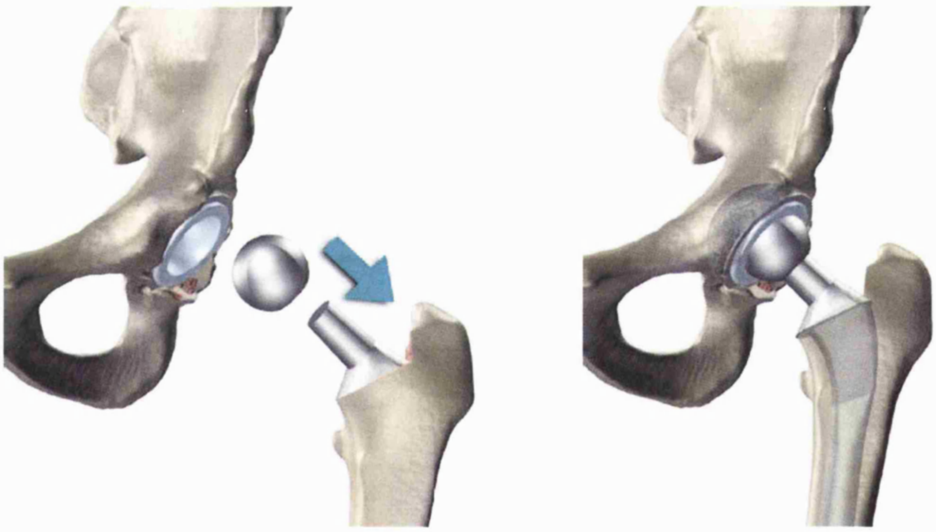

(a) (b)

Figure 1.2.: a) Insertion of the head. b) Fully installed hip implant (adapted from [10]).

Table 1.2 summarises some common methods for hip replacement. Various combination of materials for articulation included metal to polyethylene, ceramic to ceramic, metal to metal are available. A wide range of implant materials are also available for selection.

	Femoral stem
Method	press-fit (uncemented stem) [11], cementation (PMMA) [12]
	calcar support [13]
Material	cobalt-chrome [14], stainless steel [12, 15], titanium (Ti) alloys [16]
Geometry	collar [17], collarless [18], short [18], long [13], tapered [18], custom-made
Other	polished [12], matt surface [15], porous [11, 19], trabecular metal
	HA-TCP coating [20], titanium coating [21]
	Femoral head
Method	tapered locking with the stem, press-fit (resurfacing) [22]
Material	ceramic [23], metal [24]
Geometry	different offsets/diameters [24]
Other	modular design [25]
	Acetabular cup
Method	press-fit (uncemented cup), cementation [18]
Material	UHMWPE [26], ceramic [27], metal [28]
Geometry	threaded [16], different internal diameters [26]
Other	modular design, screw fixation [29], porous [30]
	trabecular metal, HA-TCP coating [30]

Table 1.2.: Common methods used for primary and revision hip replacement (not all combinations are available). Abbreviation: (PMMA) polymethylmethylacrylate, (HA-TCP) hydroxyapatite/tricalcium phosphate, (HDPE) higher density polyethylene, (UHMWPE), ultra high molecular weight polyethylene.

1.2.4. Complications in primary THA

According to the National Joint Registry 2004 [4], aseptic stem loosing (87.9%), osteolysis (31.8%) and pain are the major reasons for revision as shown in Table 1.3. The Swedish Arthroplasty Register 2005 [5] also reported also reported aseptic loosening is the main cause of failure in primary hip replacement which leads to revision hip replacement.

	Hip revision*			
	Single stage		Stage 1 of 2 stage	
	Number	(%)	Number	(%)
Aseptic loosening	2,343	(87.9)	127	(69.4)
Lysis	849	(31.8)	55	(30.1)
Pain	459	(17.2)	59	(15.8)
Dislocation/subluxation	363	(13.6)	8	(4.4)
Periprosthetic fracture	201	(7.5)	12	(6.6)
Infection	37	(1.4)	117	(63.9)
Malalignment	216	(8.1)	11	(6.0)
Fractured acetabulum	72	(2.7)	1	(0.5)
Fractured stem	59	(2.2)	2	(1.1)
Fractured femoral head	12	(0.4)	0	(0)
Incorrect sizing/head socket mismatch	9	(0.3)	2	(1.1)
Other	566	(21.2)	9	(4.9)

Table 1.3.: Indications for revision hip replacement in Wales and England, 2004 (adapted from [4]). *More than one indication may be selected for a single procedure so these numbers add up to more than the total number of procedures.

1.3. Fixation methods

Cemented and uncemented fixation techniques are widely used in hip replacement. The Swedish hip arthroplasty register 2005 [5] reported that there was a total of 13,848 THRs, of which approximately 12,700 (91.7%) were cemented and approximately 1,140 (8.3%) (Table 1.4 and Figure 1.3) were uncemented. Cemented fixation, as shown in Figure 1.4(a), uses the bone cement polymethyl-methacrylate (PMMA) as a grout to fix the femoral and acetabular components into the bone. Uncemented stems generally employ a press-fit stem which requires a tight fit between the femoral stem and the femoral canal.

Number of hips operated in Sweden, 2005			
13840 (Number of THR)*			
12700 (Cemented)**		1140 (Uncemented)**	
11600 (Primary)**	1100 (Revision)**	1020 (Primary)**	120 (Revision)**

Table 1.4.: Total number of total hip replacements in Swedish 2005 [5]. *The actual number of THRs is 13,848. **The values were estimated from Figure 1.3.

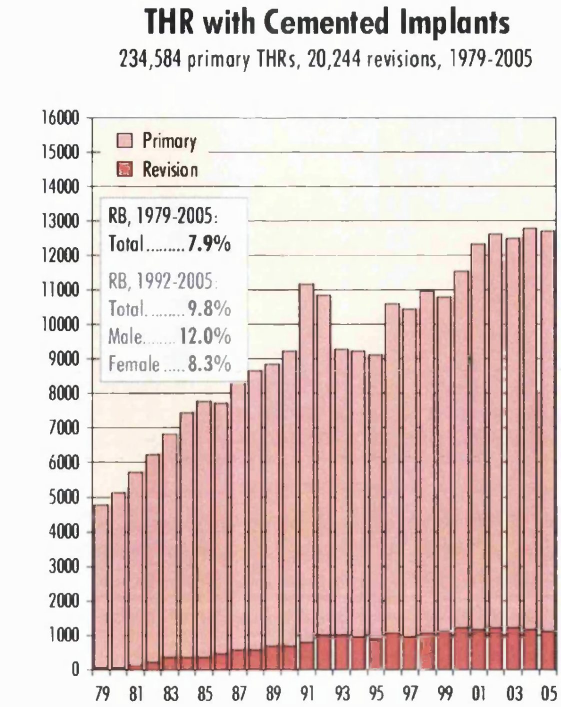

(a) Number of cemented THR

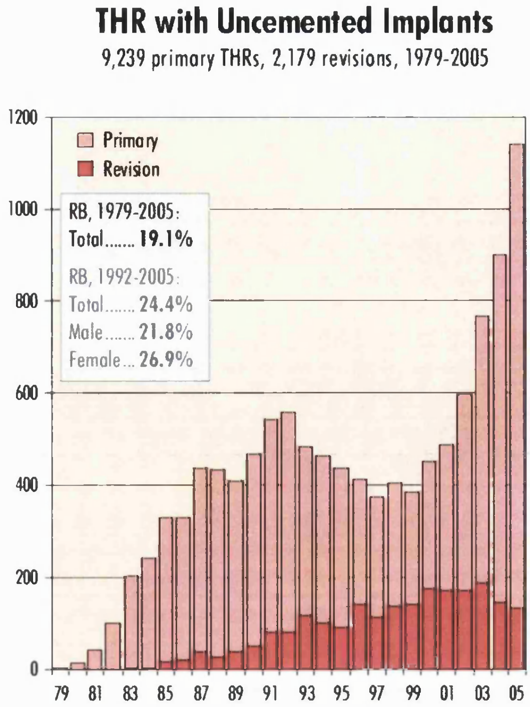

(b) Number of uncemented THR

Figure 1.3.: a) Total number of cemented implants (primary and revision) in total hip replacement. b) Total number of uncemented implants (primary and revision) in total hip replacement in Sweden 2005 (adapted from [5]).

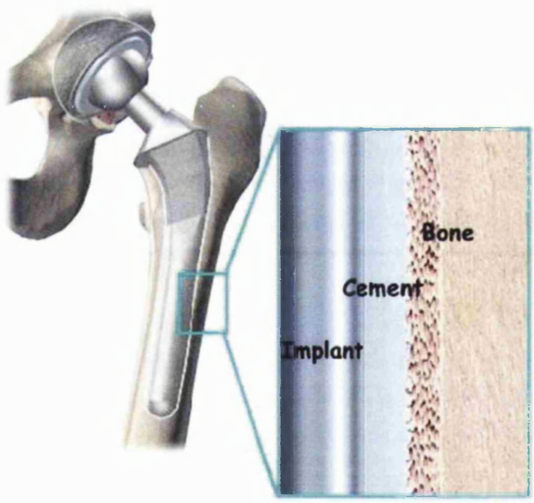

(a) Cemented prosthesis

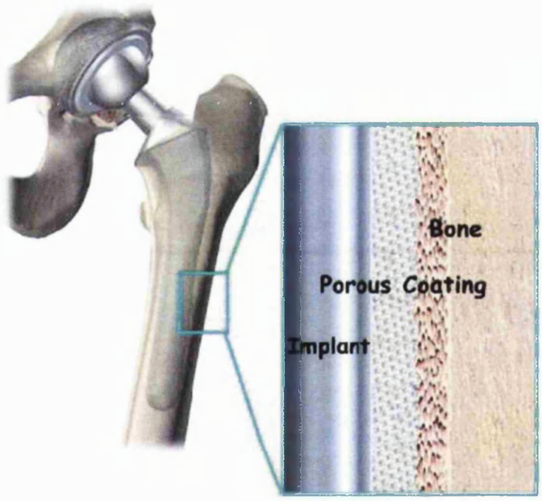

(b) Uncemented prosthesis

Figure 1.4.: a) Cemented technique with the use of bone cement to fix the prosthesis in position. b) Uncemented technique with the use of bone enhancement coating (adapted from [10]).

1.3.1. Primary hip replacement

In the Swedish hip arthroplasty register for 2005 [5] (see Table 1.4 on Page 5), there was a total of 11,600 (83.8%) primary cemented THRs, and there was a total of 1,020 (7.4%) primary uncemented THRs. The ratio between cemented to uncemented stem is therefore 11.4 : 1. Hence, the numbers of cemented stems in primary hip replacement were about ten times more than uncemented stem. In Wales and England 2004 [4], 44,262 primary hip replacements were performed. It is noted that the National Joint Registry, United Kingdom [4] classified the procedures into cemented, uncemented, hybrid and resurfacing hip arthroplasties. With this classification, a total of 23,992 (49.0%) cases were primary cemented THRs.

1.3.2. Revision hip replacement

In the Swedish hip arthroplasty register 2005 [5], there was a total of 1,100 (7.9%) revision cemented THRs, and there was a total of 120 (0.9%) revision uncemented THRs. The ratio between cemented to uncemented stems is 9.1 : 1, this ratio being similar to primary THRs. In Wales and England 2004 [4], there was a total of 4,516 (9.2%) revision THRs. However, the report did not specify the percentage of cemented and uncemented revisions.

1.4. Introduction to revision hip surgery

1.4.1. Approaches to revision surgery

Primary total hip arthroplasty has been shown to give great improvement in the quality of life [8]. Although the survival of THR is about 90% after 10 years [6, 31], a considerable number of patients require revision for aseptic loosening. There are two types of aseptic loosening: acetabular cup loosening and femoral stem loosening. Ornstein *et al.* [32] summarised the number of revision hip replacements, and there were 75% hip stem revisions (108 of 144) and 90% of acetabular cup revisions (130 of 144).

Revision surgery involves removal of the implants and insertion of new components. One of the major challenges in revision surgery for a failed femoral stem is the extensive loss of proximal bone stock in the femur, this mainly results from wear particulate induced osteolysis. The femoral cavity becomes enlarged and a primary hip stem is not suitable for revision hip replacement. Revision hip stems should therefore be used and there are various surgical methods and stem designs available for revision cases.

There are two main approaches to revision hip arthroplasty; insertion of a larger and longer cemented revision stem (Figure 1.5(a)), or an uncemented revision stem (Figure 1.5(b)). A major disadvantage with both of these approaches is that no attempt has been made to replace the bone lost and in the case of a further revision hip replacement, there is very poor bone stock and the revision surgery will be difficult.

Revision hip replacement can also be performed using the impaction of morsellised bone graft into femoral cavity so that a standard size stem can be used. A detailed discussion of impaction bone grafting will be given in the next section (see §1.4.2 on Page 8).

(a) Cemented revision stem (b) Uncemented revision stem

Figure 1.5.: a) Zimmer VerSys cemented revision hip prosthesis combined with long-stem cemented revision implant with those of a modular cemented calcar implant. b) Stryker Restoration modular uncemented revision implant (adapted from [13, 25]).

1.4.2. Introduction of impaction grafting

Impaction bone grafting (IBG) is a technique whereby morsellised bone graft is impacted into a cavity in order to compensate for bone loss and reconstruct the original shape of bone (e.g. femur, acetabulum). Impaction bone grafting with cement was first used for restoration of bone stock loss in revision total hip arthroplasty (THA), for reconstruction of acetabular protrusion in 1984 [33]. Gie *et al.* [12, 34] subsequently modified this technique and applied it to femoral reconstruction by impacting morsellised cancellous bone graft (MCB) into the medullary canal. This allows the insertion of a standard size of implant and permits the biological replacement of bone stock with the graft. The principal objective of impaction grafting is to secure the implant during revision THA and to provide a mechanical and biological scaffold for bone regeneration. Thus, the ultimate goal is to provide a favourable biological environment for bone remodelling. There has been scientific evidence of osteointegration showing that allograft chips have been replaced by viable cancellous bone after impaction grafting [35–38]. Collarless, polished and tapered stems have been extensively used in revision IBG [12, 39–41]. This particular type of implant design permits the implant to subside within the cement mantle, which generates radial compressive loading [12], and allows for self-tightening of the prosthesis as it subsides [42, 43]. It has also been suggested that these types of stems reduce wear particle induced osteolysis of the bone-cement interface [44] by sealing the bone-cement interface against ingress of wear debris.

In the past decade, a number of studies have recorded promising results [12, 35, 37, 39, 40, 43, 45–47], whereas numerous problems such as early subsidence and femoral fractures have also been reported [32, 41, 48, 49]. The nature of impaction grafting is a highly complex surgical process and its success depends on both biological and mechanical issues.

Table 1.5 provides a summary on the advantages and disadvantages on impaction grafting.

Method	Impaction grafting
Procedures	Impaction grafting with highly polished surface, bone cement PMMA is inserted
Advantages (+)	Allows use of standard stem size Bone stock compensation Integration between graft and host bone Standard stems size can be used Similar technique used in primary hip operation To date, high survivorship recorded in some studies [5]
Disadvantages (−)	Insufficient donor bone stock Toxicity of cement [50] Variability of bone quality Variable impaction techniques

Table 1.5.: Summary on the advantages and disadvantages on impaction grafting.

1.5. Bone classifications

Before performing impaction bone grafting, a radiograph is usually taken to assess the quality of the bone stock. This clinical assessment allows pre-operative planning on the size of the stem, the amount of graft required, and the need for other accessories such as mesh and cerclage wires. The quality of the bone stock loss is usually classified.

Two main classification methods have been used extensively to determine the amount of bone stock loss. The Endo-Klinik [51] and Gustilo and Pasternak [52] classifications as shown in Figure 1.6 and Figure 1.7 respectively and are both commonly used. These two classifications are similar for Type I and II deficiencies. The Gustilo and Pasternak scale provides a more accurate description of the thickness of the cortical bone, whilst for Type IV deficiency; the Endo-Klinik classification provides a more precise description of the damage to the femur. These classifications are described in detail below. It was found that the amount of subsidence of the Exeter stem was correlated with deficiency of bone stock graded on the Gustilo and Pasternak classification [40] (see §1.8.1 on Page 25).

1.5.1. Endo-Klinik

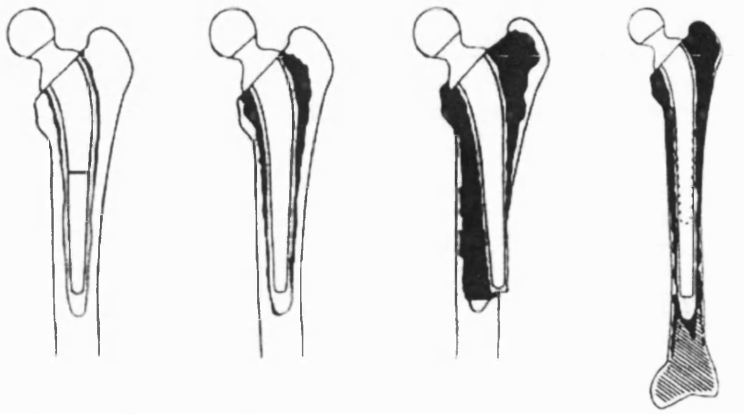

Figure 1.6.: Endo-Klinik classification (adapted from [51]).

- Type I – Radiolucent zone confined to the upper half of the cement mantle with clinical signs of loosening.
- Type II – Radiolucent zone around the cement mantle and endosteal erosion of the upper femur leading to widening of the medullary cavity.
- Type III – Widening of the medullary cavity by expansion of the upper femur with proximal bone loss and perforation.
- Type IV – Gross destruction of the upper and middle thirds of the femur with damage to the distal third and loss of support.

1.5.2. Gustilo and Pasternak

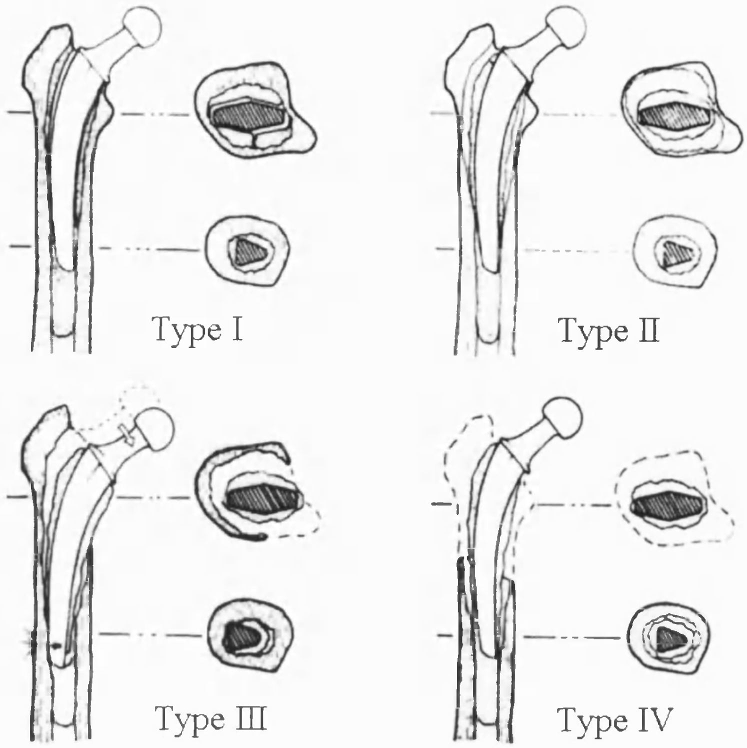

Figure 1.7.: Gustilo and Pasternak classification (adapted from [52]).

- Type I – Bone loss with minimal endosteal or inner cortical bone loss, i.e. loosening at the cement-metal-bone interface with < 50% thinning or a broken stem.
- Type II – Proximal femoral canal enlargement with cortical thinning of > 50% (almost all of the trabecular bone), and sometimes there is a lateral wall defect with an intact circumferential wall.
- Type III – Posterior-medial wall defect involving the lesser trochanter indicating instability.
- Type IV – Total circumferential loss of bone at varying distances below the lesser trochanter.

1.6. Impaction bone grafting techniques

1.6.1. Exeter impaction technique

The femoral impaction grafting technique was initially proposed for use in revision hip surgery by Gie *et al.* [12, 34] from the Princess Elizabeth Orthopaedic Hospital in Exeter, England. The technique described by the Exeter group is as follows: First, it is necessary to remove the loose prosthesis and all cement debris, any granulomata and fibrous membranes. In the case of any femoral cortical defects posing a subsequent fractures risk, it is recommended that prophylactic reconstruction by applying fine wire mesh with cerclage to reinforce the femoral shaft is carried out. An acrylic plug is then placed 2 cm distal to the most distal area of bone lysis for supporting the bone graft (Figure 1.8(a)). If there is a suitable cement plug drilled which is to be left *in-situ*, the largest impactor that will fit is placed down to the level of the plug, to act as a drill centralizer. A drill is passed through the impactor and the cement plug drilled and a guide wire is inserted [18]. If the required position lies beyond the isthmus, the cement plug is skewered with a percutaneous wire or seated on an earlier placed cement plug [53]. The canal is then filled distally with unwashed pure cancellous allograft bone chips. The allograft is prepared from fresh frozen femoral heads. Currently, two sizes of bone chips are prepared; those of 2 – 4 mm are used for distal canal and those of 5 – 10 mm for the proximal femur [53] (Savory *et al.* [54] recommends 3 – 4 mm and 8 – 10 mm for distal and proximal femur respectively). The graft may then inserted by a 10 cm^3 syringe [54].

The required distal impactors are sized depending on the size and the depth of the femoral canal as shown in Figure 1.8(b). The graft is then inserted and impacted using the sliding hammer (Figure 1.9). When the amount of graft reaches 8 – 10 cm below the level of the greater trochanter, a proximal phantom impactor which is two sizes larger than the template is used to vigorously impact the bone graft [12, 34] (Figure 1.10). The phantom is then removed carefully without distributing the graft and more chips are impacted. At the same time, the distal impactor is used alternatively until the mid-stem region is adequately packed [18]. The proximal impactor is used until the canal is fully filled with graft. This process is repeated until the canal has been filled up to the proximal end. For the most proximal area, a 'half-moon' impactor is used to impact the area around the trochanter.

After impaction, it is essential to ensure absolute axial and torsional stability of the proximal impactor as shown in Figure 1.11. The proximal impactor should be impossible to withdraw without using the sliding hammer [18]. Trial reduction *in-vivo* is then performed and the phantom is removed (Figure 1.12(a)). The canal is sucked dry and antibiotic-loaded cement is introduced in retrograde manner with a cement gun (Figure 1.12(b)). The proximal end is sealed and pressurised so that the cement can penetrate via the graft and create an interface between the graft and stem. A wingless Exeter stem centraliser is fitted to the end of the collarless, polished and tapered stem of pre-defined offset length and size before insertion with a leg-length gauge [53] (Figure 1.13(a)). The further pressurisation is achieved by applying a 'horse-collar' sponge so as to ensure the proximal cement is also pressured [54] (Figure 1.13(b)).

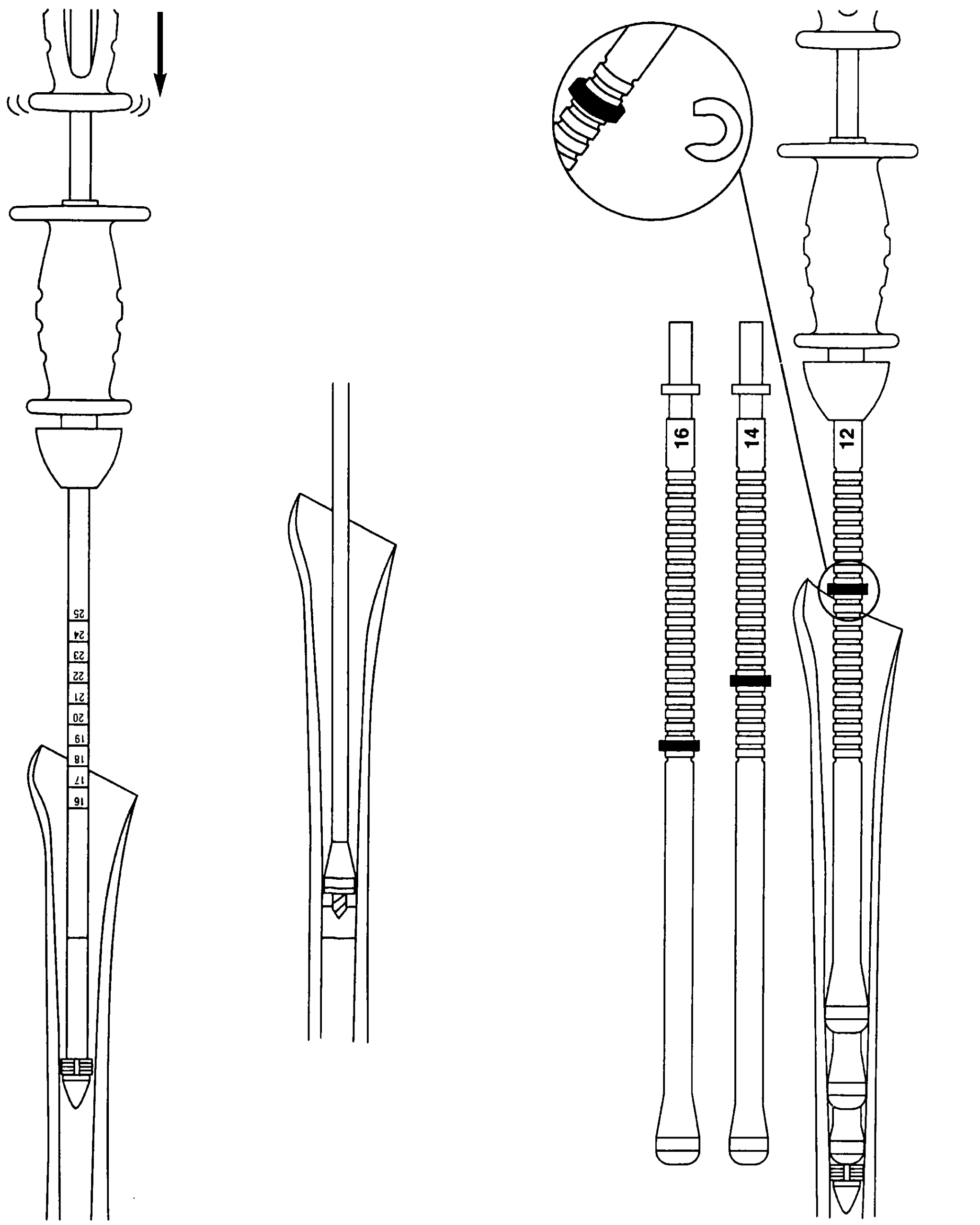

(a) Insertion of intramedullary plug (b) Sizing the proximal impactors

Figure 1.8.: Insertion of an intramedullary plug in the most distal area (also see Figure 1.14(g) on Page 18). Then the distal impactors were sized with a marker (adapted from [18]).

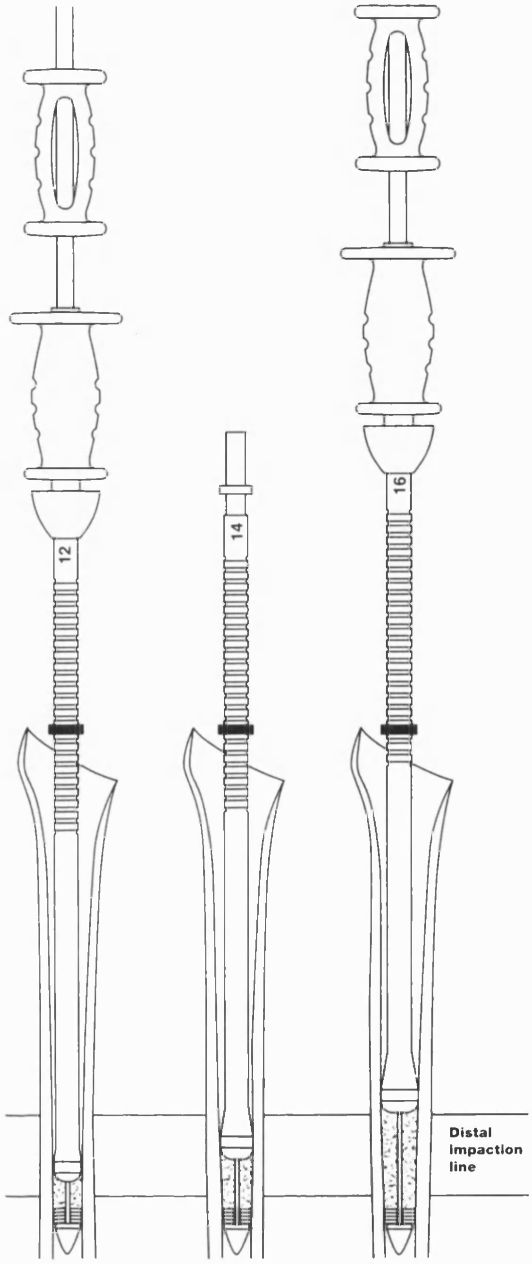

Figure 1.9.: The size of the distal impactors increase progressively (also see Figure 1.14(j) on Page 18) (adapted from [18]).

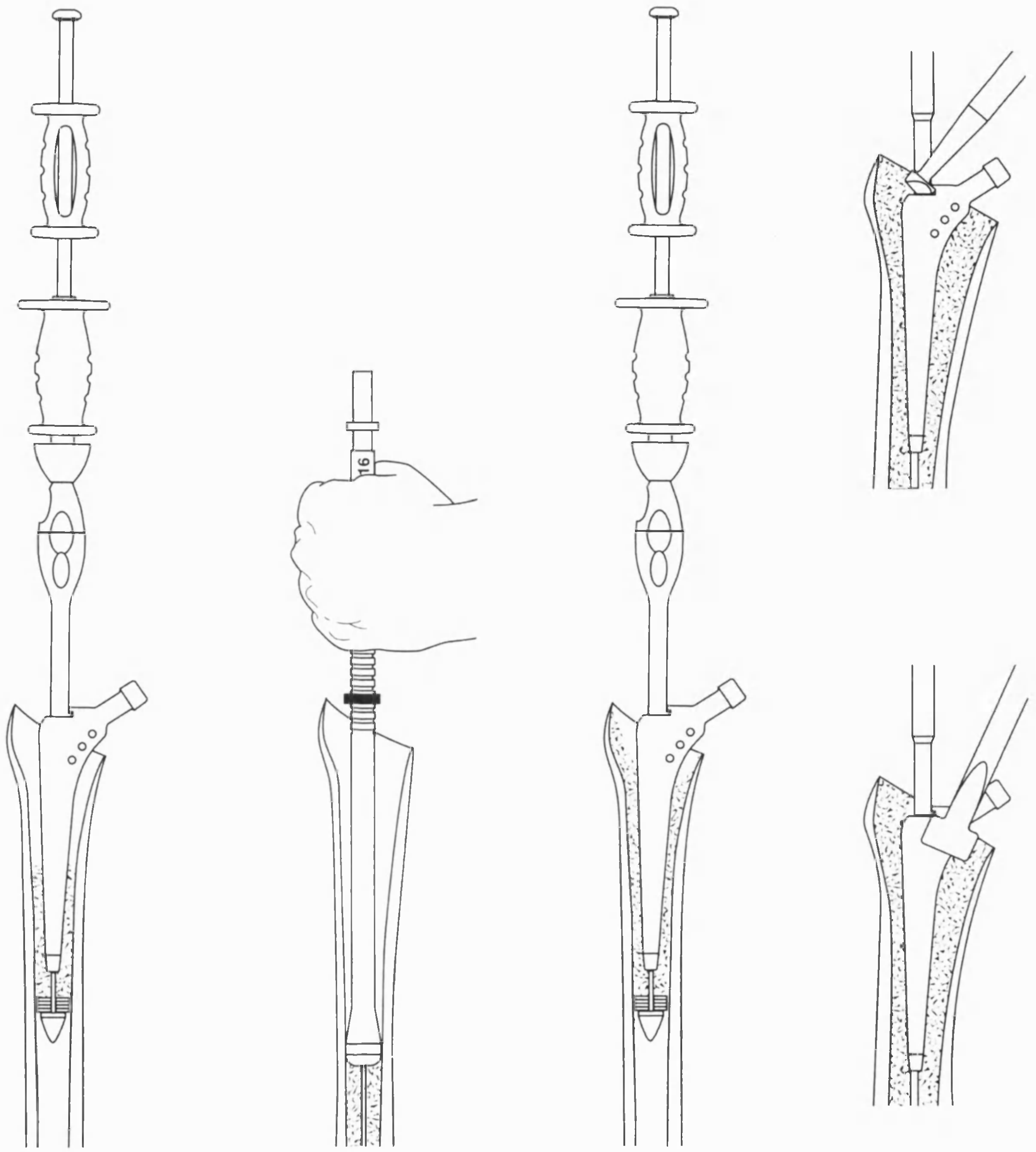

Figure 1.10.: After distal impaction, the proximal impactor should be driven vigorously into the chips (also see Figure 1.14(l) on Page 18). At the same time, the distal impactor is used alternatively until the mid-stem region is adequately packed. The proximal impactor is used until the canal is fully filled with graft. Using a 'half moon' impactor to impact the proximal areas (adapted from [18]).

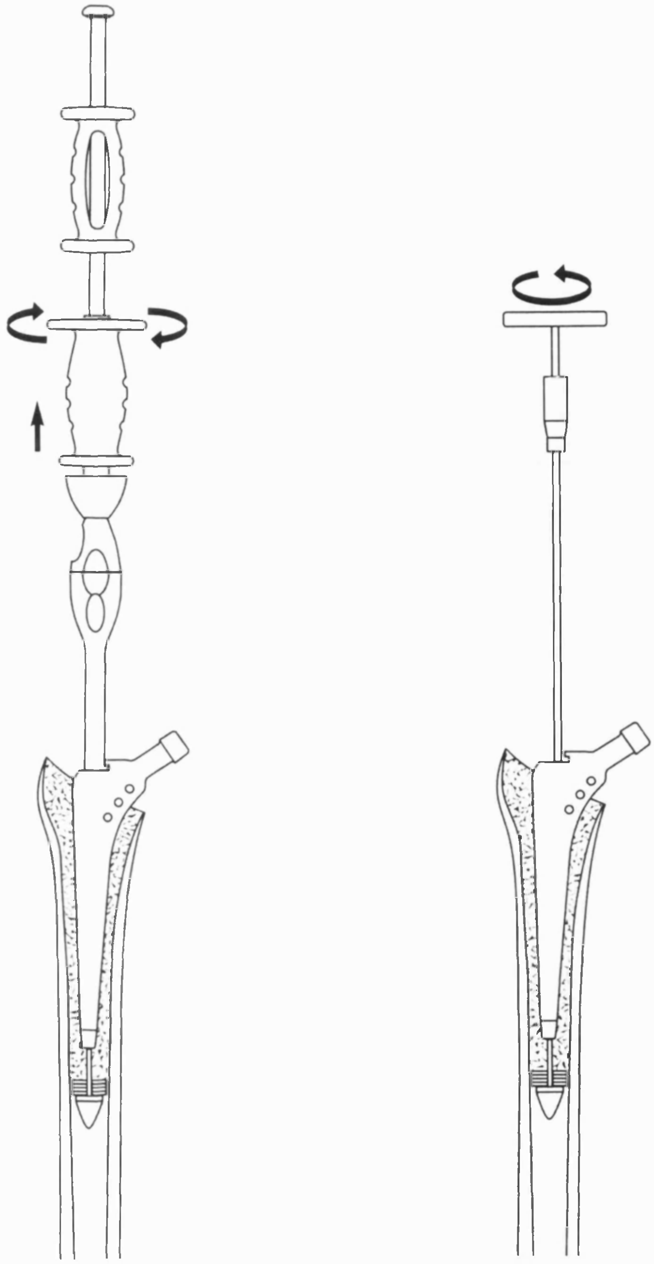

Figure 1.11.: The surgeon must then ensure absolute axial and torsional stability of the proximal impactor at the conclusion of packing (adapted from [18]).

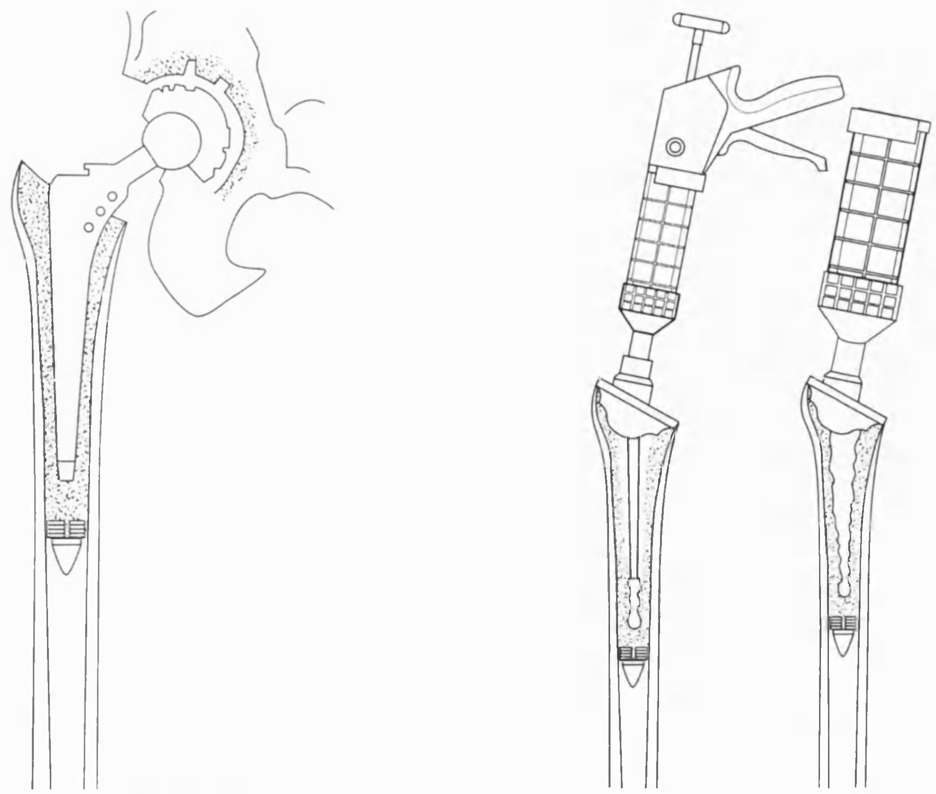

(a) Trial reduction

(b) Cement insertion

Figure 1.12.: A trial reduction is preformed to allow assessment of stability and leg length, and acts as a further guide for the depth of stem insertion (also see Figure 1.15(b) on Page 19). Then, cement was inserted in retrograde manner from the cement gun (also see Figure 1.15(e) on Page 19), using the tapered gun spout (adapted from [18]).

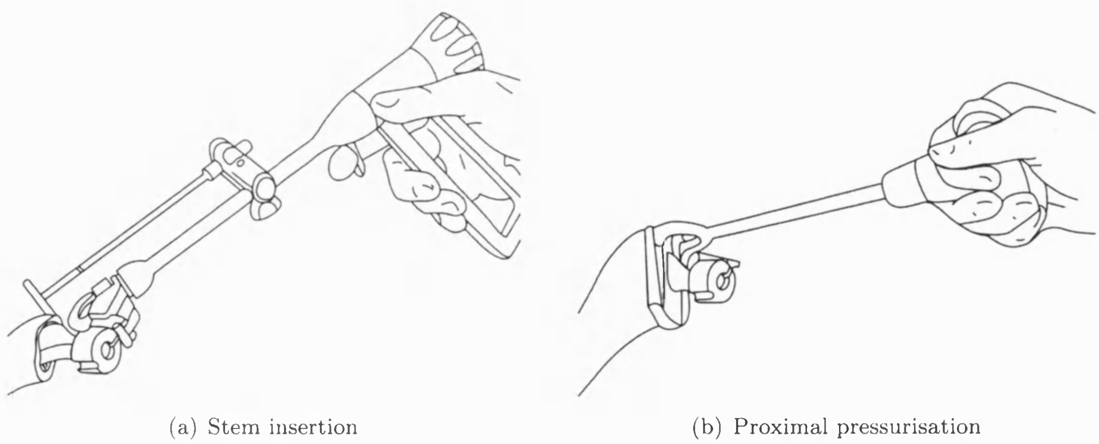

(a) Stem insertion

(b) Proximal pressurisation

Figure 1.13.: Insert the stem to its predetermined position by using the leg-length gauge (also see Figure 1.15(f) on Page 19). The introductor is removed when the insertion depth is achieved. A proximal seal is applied to pressure until the cement has polymerised (adapted from [18]).

Figure 1.14 and Figure 1.15 show a sequence of steps of the Exeter technique during the operation (as described in §1.6.1 on Page 12).


(a) Removal the old implant


(b) Removal of bone cement

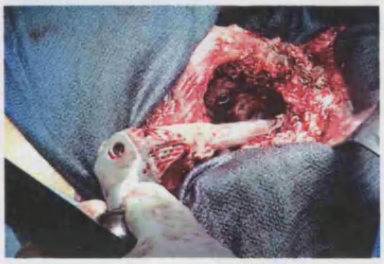
(c) Removal of implant

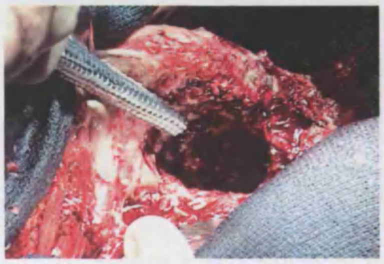
(d) Reaming the canal


(e) Determining the phantom size

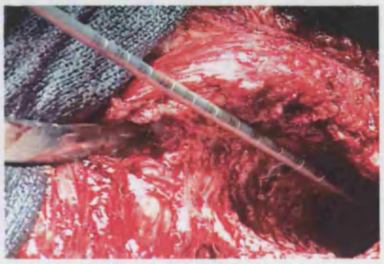
(f) Calibriation of guide wire


(g) Installation of distal plug


(h) Preparation of femoral heads


(i) Preparation of bone graft


(j) Distal impaction


(k) Reconstruction of femur

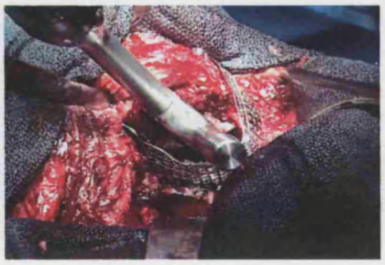
(l) Proximal impaction

Figure 1.14.: Surgical procedures of the Exeter technique (cont.) (adapted from [54]).

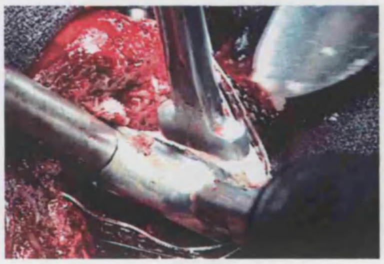

(a) Impaction by half-moon impactor

(b) Performing trial reduction

(c) Canal being sucked dry

(d) Cement insertion in retrograde manner

(e) Pressuration of canal

(f) Final insertion of stem

Figure 1.15.: Surgical procedures of the Exeter technique (adapted from [54]).

1.6.2. Implant design

Exeter stems are widely used for impaction grafting. A collarless design is employed to allow stem subsidence within the cement mantle; the surface is also highly polished so as to allow a low friction contact between the metal stem and the bone cement; the double-tapered shape also provides extra stability during subsidence due to wedge effect. Figure 1.16 shows the standard Exeter stem and the post-operative radiographs. Various standard sizes are also available depending on the size of the femoral canal of the patient. Different head/stem offset lengths are also available to accommodate the different anatomical requirements of the individual patients.

(a) Photograph of the Exeter stem

(b) Radiograph of the Exeter Stem

Figure 1.16.: a) Exeter collarless polished double-tapered stem, acetabular socket and distal centraliser. b) Post-operative radiography of Exeter cemented stem (adapted from [32]).

1.7. Alternative techniques used in impaction grafting

1.7.1. Radial impaction technique

Stulberg [42, 43] believed that complications from distal impaction might be related to the design of the Exeter stem rather than the impaction technique itself. The primary Exeter femoral stem with a limited number of neck lengths and offsets increased the likelihood of complications because the distal tip area of femoral shaft was often associated with a thin cortex either from loosening or extraction of the primary THR. Stulberg subsequently proposed a surgical technique called the radial impaction grafting (RIG) technique based on the procedures described by Gie *et al.* [12, 34]. The aims of RIG are to maximise the impaction of cancellous bone, minimise the potential for per- or post-operative fractures, and to allow the use of a variety of implants including different stem lengths, neck lengths and neck offsets. The recommended allograft is 80% cancellous bone and 20% cortical bone (instead of 100% cancellous). Tapered, polished impactors (instead of flat-end distal impactors) are introduced to impact the graft radially as shown in Figure 1.17. A polished, profile impactor is then used to create a neo-medullary canal and the stability of the final profile impactor is tested with a torque wrench (which does not exist in the Exeter technique). A trial reduction with the correct head-neck combination can then be performed, and cement is then introduced.

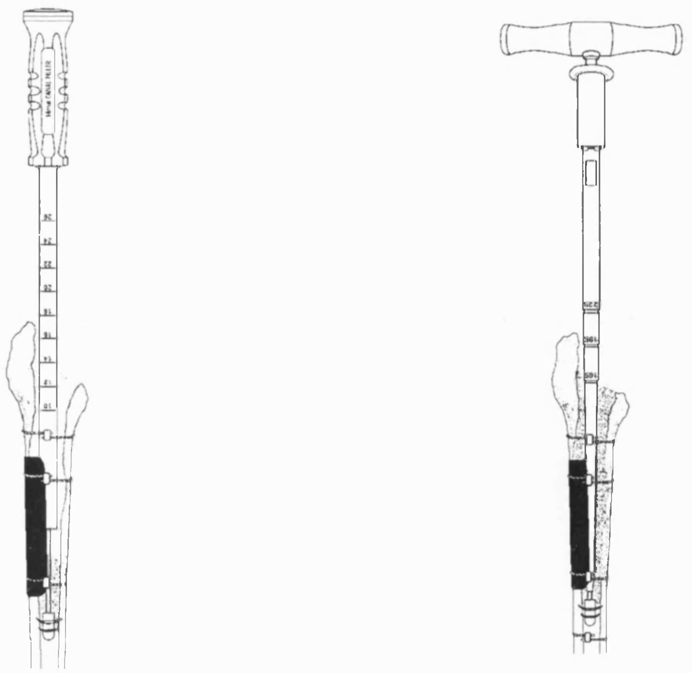

(a) Impacted with canal fillers (b) Impacted with tapered polished reamers

Figure 1.17.: Radial impaction technique (RIG) – a) The bone graft is impacted with canal fillers over guide wire. b) The bone graft is radially impacted with tapered polished reamers (adapted from [43]).

Regarding the choice of allograft, adding a small proportion of cortical bone into the cancellous bone can provide a good supportive structure and hence can increase the initial stability. However, not much research has been done on the effect on the short and long-term mechanical stability of mixing in cortical bone. Using a tapered polished impactor instead of flat-end distal impactor can minimise the risk of femoral fracture, as the bone graft is gradually impacted radially. In addition, the stress around the diaphyseal area would also be smaller because the bone graft is partially pre-impacted radially in advance, rather than being heavily driven outward by the proximal impactor as in the Exeter technique. Nevertheless, the Exeter technique compresses the bone graft more and it might provide better distal stability, but with a slightly high risk of fracture. Finally, a torque wrench is used to test the graft stability before introducing bone cement. The initial seven year results associated with this technique are encouraging; however, more research should be done on finding a compromise between the stem stability and the risk of fractures.

1.7.2. Modified Exeter technique

A modified technique has also been proposed by Thomasson *et al.* [55]. The goal of the modified Exeter technique is to achieve initial stability to prevent migration of the stem, despite the use of smaller bone chips, which can lead to subsidence and further revision if secondary stability is not obtained [55]. Fresh-frozen femoral allograft harvested at primary total hip arthroplasties is recommended. The canal is reamed to allow insertion of a hollow cylinder of graft as shown in Figure 1.18(a) and a distal plug is placed before introducing the 'graft gun'. The graft is morsellised with a 'cheese grater' acetabular reamer without particular attention to the size of the resultant chips. A Mersilene mesh (Ethicon, Neuilly-sur-Seine, France), as shown in Figure 1.18(b), is used to retain allograft at the desired locations and prevents the dispersion or extrusion of the graft through possible cortical defects the during impaction grafting. More allograft may be added if necessary before impacting with a tamp (proximal impactor). The size of the tamp is progressively increased as shown in Figure 1.19(a). The implant size is determined by the stable fit of a tamp of a particular size. This allows a 2 mm thick cement mantle around the stem. The definitive implant is inserted after cementation as shown in Figure 1.19(b) and Figure 1.20. Cement is placed in retrograde manner which is similar to the Exeter technique [12, 34]. Cementation is performed with Palacos (Biomet, Warsaw, Ind), which contains the antibiotic gentamicin.

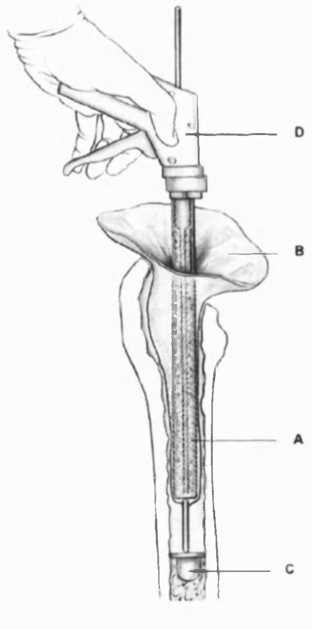

(a) Placement of the 'Graft gun'

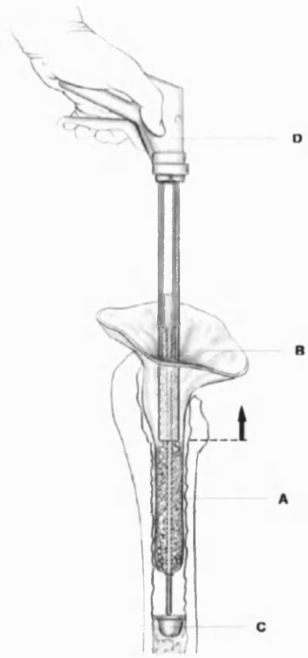

(b) Gradual retropulsion of the 'Graft gun'

Figure 1.18.: a) Placement of the 'Graft gun' (D) surrounded by its Mersilene mesh sheet (B), within the femoral canal. The medullary canal has been previously occluded distally with a polyethylene plug (C). b) Gradual retropulsion of the 'Graft gun' barrel, leaving in place the allograft around the gun shaft (adapted from [55]).

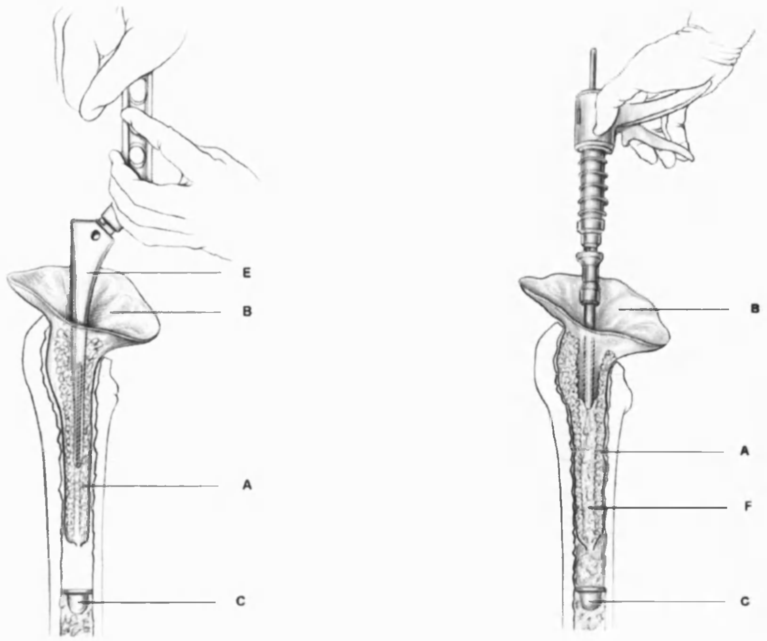

(a) Impacted with progressively larger tamps (b) Filling of the cement

Figure 1.19.: a) Allograft (A) impaction with trial tamps (E) of increasing size until the trial component is blocked and stable. b) Retrograde filling of the cement (F) enables its delivery distal to the graft (A), which is stabilized by Mersilene mesh (B) (adapted from [55]).

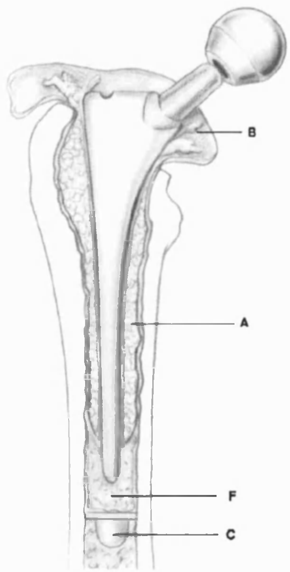

(a) Final insertion of implant

Figure 1.20.: Sealing of the definitive implant: four fifths at allograft level and one fifth directly in contact with host cortical bone (adapted from [55]).

By using this technique, no distal impaction is required. Instead, this technique allows cementing the distal stem directly to the host bone [55]. In other words, bone remodelling is not possible since no allograft is in place in the distal femur. Allograft is only impacted by proximal impaction with progressively increased impactor sizes. Therefore, the distal region around the stem tip has less graft stability compared with the Exeter technique. However, the major benefit of using this technique is to prevent dispersion of the graft by extrusion. However, placing the Mersilene mesh *in-vivo* is questionable as it may prevent host bone remodelling. Between 1996 and 2002, 45 revision hip operations were conducted by using this technique. Allograft transformation occurred in 36 hips and host bone remodelling occurred in 11 hips [55]. This technique, therefore, appears to be reliable.

1.7.3. Other non-standard techniques

In the last decade, there have been various attempts [14, 17, 47, 56–60] using other techniques for impaction bone grafting such as using collared, hydroxyapatite-coated stems or matt surface finished stems. Schreurs *et al.* [56] used a goat study using collared cemented prosthesis in impaction grafting with the use of bone cement. There were no stability differences after 6 and 12 weeks implantation in both rotational and axial subsidence. A histological study also showed revascularisation and bone remodelling of the graft. Kärrholm *et al.* [57] used a collared cemented non-polished cobalt-chrome alloy Spectron EF stem in 24 consecutive hip revision operations for patients who had loosening of the femoral stem, with the use of bone cement. There was evidence of trabecular remodelling, or graft resorption in both the proximal and distal femur after one year of implantation. Boldt *et al.* [47] used cemented non-polished Charnley stems for impaction bone grafting with the use of bone cement. The clinical results were promising with graft incorporation occurring in 48 of 73 (61%) femora. Van Kleunen *et al.* [17] used a collared textured stem for massive femoral impaction allograft with the use of bone cement and the clinical results were promising. Krupp *et al.* [14] used a non-polished bead-blasted stem for impaction bone grafting with the use of bone cement, and good clinical results were shown with respect to aseptic loosening. Einsiedel *et al.* [58] undertook impaction grafting with a partially cemented femoral stem. Bone cement was only injected in the proximal area. Clinical results demonstrated an average Harris Hip Score of 85.5, with a mean subsidence of less than 1.5 mm after 2 years implantation.

Only two studies were found of impaction grafting without the utilisation of bone cement. Schreurs *et al.* [59, 60] studied the possibility of impaction grafting without the use of bone cement. An *in-vitro* goat model was used [59]. A collared cemented prosthesis and an uncemented hydroxylapatite-coated titanium prosthesis were compared. It was found that the uncemented stem did not provide sufficient stability. The stems used, however, had different geometries and surface finishes. As a result, the results could not be directly compared and interpreted. An additional goat study [60], in which hydroxyapatite-coated femoral stems were used with impaction bone grafting without the use of bone cement, demonstrated that the rotational and axial subsidence stability of uncemented stems were improved at 12 weeks post implantation compared to 6 weeks. Histological studies also demonstrated revascularisation and bone remodelling of the graft in all the selected goats.

1.8. Complications in revision surgery

Stem subsidence and femoral fractures are two major complications with impaction grafting. Subsidence of femoral components can cause implant instability and subsequently cause pain and loosing [39]. Femoral fractures can occur per-operatively and post-operatively [61]. Per-operative femoral fracture occurs when the stress exceeds the strength of the bone during the operation, usually during graft impaction. Post-operative femoral fracture can also occur, possibly due to overloading, and this can cause severe pain [49].

1.8.1. Component subsidence

Component migration or gross movement with revision impaction grafting may represent a loss of fixation with the potential for failure of the procedure. The amount of subsidence of femoral components including the stem and the cement mantle is normally characterised by distal migration whilst the amount of subsidence of the acetabular components is normally described by the amount of proximal migration after operation [32, 39, 40, 62–64]. Subsidence of the femoral component can occur in two forms. One is the subsidence of the stem within the cement mantle, and the other is the subsidence of the cement mantle within the bone graft. The majority of the studies have only concentrated on the total subsidence of the stem without considering the two forms separately. Only a few reports [12, 65] have specified what type of subsidence was actually occurring. Radiostereometric analysis (RSA) is an effective method to examine the amount of distal, medial and posterior migration movements. This can be done by implanting 0.8 mm tantalum markers during hip revision in the greater and lesser trochanters, the acetabular roof and the socket [32]. Using this technique, the true subsidence can be found by measuring the subsidence of the stem tip since this is least influenced by stem rotations [40].

Ornstein *et al.* [62] found that most of the short-term stem migration occurs in the first seven days after surgery. Collarless, polished and tapered stems have the capacity to subside within the cement mantle without damaging the cement-bone interface [12] because of a centraliser with a hollow chamber attached at the end of the stem tip [45]. Figure 1.21 depicts the subsidence of stem within a cement mantle after 10 years. Cold flow or creep of the cement could also cause the subsidence of stem component [32]. Ornstein *et al.* [64] performed a long-term RSA study of Exeter revision femoral stems (Stryker-Howmedia International Ltd, London, UK). It was found that the majority of the stems migrated in the first 12 months and gradually became stable by two years due to bone graft consolidation and bone remodelling. The amount of distal, medial, lateral and posterior migration ranged from $1.4 - 4.3$ mm, $0.6 - 2.1$ mm, $0.5 - 1.0$ mm and $0.8 - 8.8$ mm respectively. This indicated that the femoral stem is not only exerting compressive forces but also torsional shear forces on the cement mantle and the bone graft during loading. It is, therefore, important to address the mechanical strength of the impacted graft particularly in these two directions.

Early massive subsidence is one of the problems with impaction grafting. It has been reported in one series that 11% (9 of 79) of revision femoral prostheses showed massive subsidence (> 10 mm) [41]. It was found that the amount of subsidence of the Exeter stem was correlated with deficiency of bone stock graded on the Gustilo and Pasternak classification [40] (see §1.5.2 on Page 11). This could be because of poor supportive structures and inadequate structural support of the radial compressive forces in the cortical host bone. This could also have been a result of inadequate graft impaction at the time of surgery which failed to provide a stable graft scaffold. Furthermore, *in-vitro* cadaveric experiments showed that impaction grafted stems demonstrates a greater subsidence compared with a primary total hip replacement (THR) stems because the MCB within the specimens was left uncompressed for a period before being placed in the testing machine [66].

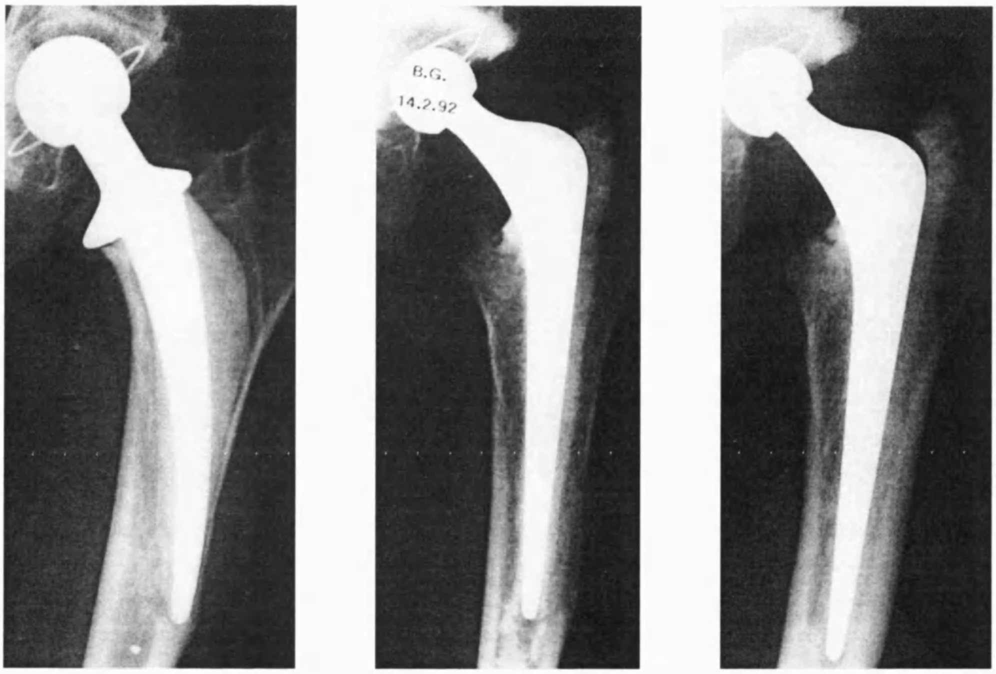

(a) Pre-operative (b) Post-operative (c) 10-year post-operative

Figure 1.21.: a) Pre-operative. b) Post-operative. c) 10-year radiographs of an impaction grafted femur. The subsidence between stem and cement appears to have stopped by 10 years in this very active patient (adapted from [67]).

1.8.2. Femoral fractures

Impaction grafting requires firm compaction of the bone graft using distal and proximal impactors in order to achieve initial stability. Initial secure fixation is provided mechanically by compacting of the allograft before impregnation of bone cement to overcome the inherent poor structural characteristics of cancellous bone [42, 43]. During the impaction, bone graft is compressed in both distal and radial directions. This creates transient peak stresses around the cortical bone [68]. Per-operative femoral fracture occurs when the stress exceeds the strength of the bone especially in an area of bone deficiency. Fracture usually occurs during impaction when reconstructing the neo-medullary canal. The proximal impactor has a tapered shape and generates high compressive forces. During impaction, a large amount of energy is delivered to the bone graft and is transmitted to the surrounding structures. However, it is essential to deliver sufficient impaction energy to consolidate the bone graft in spite of the threat of per-operative femoral fracture. Heal *et al.* [61] summarised various reports reviewing 35 per-operative and 14 post-operative femoral fractures occurring in a total of 399 revision hip arthroplasties. Ornstein *et al.* [48] reported an incidence of 15% (21 of 144) and 6% (9 of 144) of per- and post-operative fractures. Thus per-operative fractures occur more commonly than post-operative fractures. Establishing the adequacy of initial compaction per-operatively in order to achieve initial implant stability but at the same preventing per-operative fractures is an important criterion in revision impaction grafting. It is, however, extremely difficult to predict post-operative femoral fracture due to the unclear nature of consolidation and incorporation of bone grafts. Figure 1.22(a) depicts examples of a post-operative femoral fracture caused by the fatigue of the stem. Van Doorn *et al.* [49] reported a combination of stem and femoral fractures. Pekkarinen *et al.* [69] also reported that fracture of femur can also occur around the distal tip of the stem as shown in Figure 1.22(b). This could probably be caused by stress concentration around the tip of the prosthesis. Furthermore, morsellised bone graft has both time-dependent and viscoelastic behaviour [70] which both contribute to the difficulty in this prediction. Cerclage monofilament wire, cables, cortical strut grafts meshes or reconstructive plates are effective methods for repairing femoral cortical defects in proximal and distal areas for prophylactic reconstruction [18, 53]. These methods can, therefore, be used effectively to prevent per-operative femoral fractures in the presence of regions of inadequate or defective bone stock.

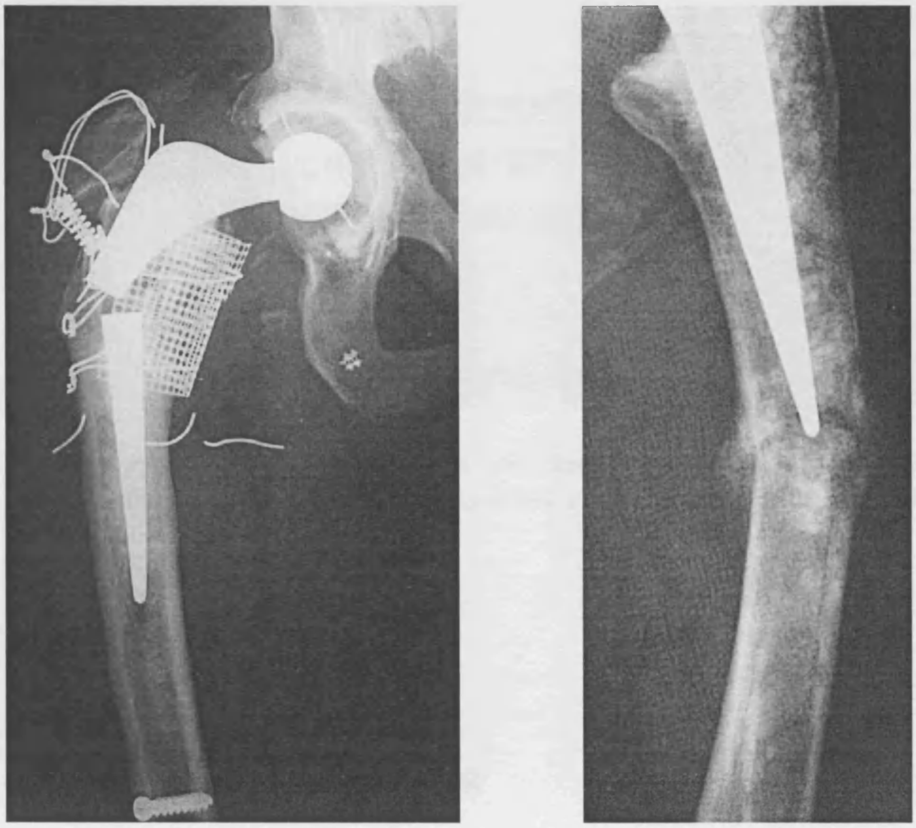

(a) Fractured stem (b) Fractured femur

Figure 1.22.: a) Fractured revision Exeter stem and graft shows incorporation distal to the lesser trochanter and resorption proximal to it (adapted from [49]). b) A fracture of the femur near the tip of the prosthesis four months after revision (adapted from [69]).

1.9. Post-operative events

Ornstein [32] summarised seven pre-requisites for stem migration that prevail in revision with impaction grafting with the use of bone graft and cement as shown in Figure 1.23. As can be seen, in this figure, the stem settles into the bone cement, the allograft is compressed and the cement may creep for several months. The femoral canal can also expand due to bone remodelling [32]. In the long term, allograft is re-modelled by host bone.

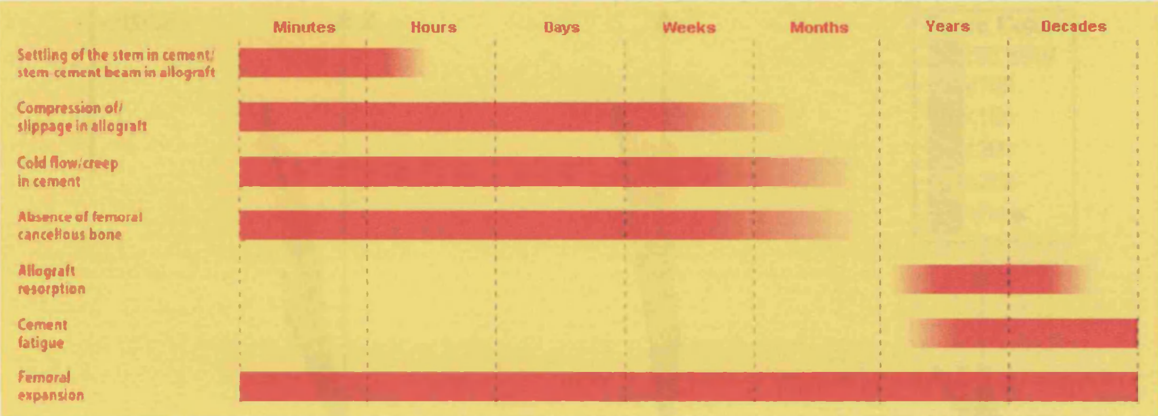

Figure 1.23.: Pre-requisites for migration of a collarless, double tapered and polished stem in femoral hip revision with impacted morselized allograft bone and cement (adapted from [32]).

1.10. In-vivo mechanical loading

1.10.1. Loading forces

In order to determine the *in-vitro* graft properties during impaction grafting, it is essential to understand how forces transfer to the host bone. The characteristics of load transfer to the hip joint depend on various factors: human activity, implant design (geometry and dimensions), implant technique (cemented or uncemented), the elasticity of materials (stem, graft and cement), and the quality of the bone (osteoporosis). *In-vivo* studies provide some valuable information on the loading direction and the amount of force acting on the femur during the gait cycle. Figure 1.24 depicts the most common method used to define the various forces in three dimensions. The forces acting on the hip joint during the gait cycle can also be represented in three mutually perpendicular directions F_x, F_y and F_z as shown in Figure 1.25.

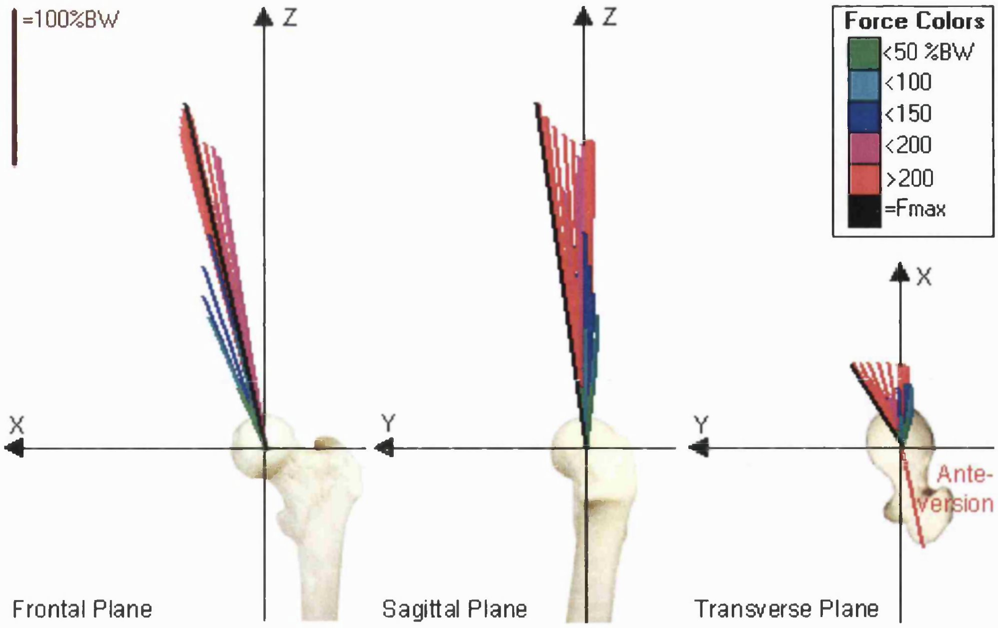

Figure 1.24.: Frontal, sagittal and transverse planes use for defining the direction of loading forces – normal walking cycle (adapted from [71]).

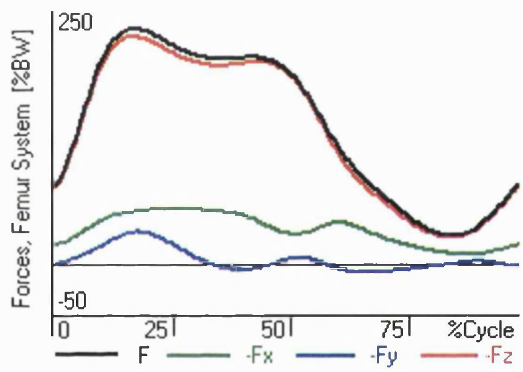

Figure 1.25.: A single cycle is represented by 0% to 100%. The level of forces is represented by the amount of body weight (BW%). The forces are dominant in the z-axis (adapted from [71]).

Bergmann *et al.* [72–77] have performed extensive studies using gait analysis and measuring the amount of hip contact forces using instrumentated hip implants with telemetry. Table 1.6 summaries the amount of force (in terms of % of body weight) occurring in the hip joint during various activities. As can be seen, the proximal-distal direction (z-axis) dominates most of the forces. The reason is obvious – the presence of body weight and the contribution of muscles to counteract the body weight component. Other factors include body posture, muscles forces, sex, and human activities such as walking and jogging. It can be observed that in most cases, there is about 250% body weight acting on the hip joint. For a typical body mass of 75 kg, there is, therefore, a force of (75 × 9.81 × 250% =) 1839 N exerted on the hip joint during the normal walking cycle.

	Force (% of body weight)			
	Medial-laterial	Ventral-dorsal	Proximal-distal	Resultant
Activity	$(-F_x)$	$(-F_y)$	$(-F_z)$	(F)
Upstairs	60	61	237	252
Downstairs	60	39	253	261
Downstairs [74]	180	10	500	530
Standing up	53	23	182	190
Sitting down	43	8	150	156
Standing [78]	40	10	90	100
Standing (One leg)	32	17	230	232
Walking (Slow)	51	36	235	243
Walking (Normal)	54	32	225	233
Walking (Normal)	40	-20	250	254
Walking (Fast)	52	33	243	251
Jogging upstairs [74]	250	85	550	610

Table 1.6.: *In-vivo* hip contact forces for various activities (adapted from [71, 72], unless otherwise stated).

Micromotion is an important factor for impaction grafting. Micromotion is defined as the recoverable movement of the implant relative to the bone under cyclic loading [79]. A small amount of micromotion can lead to a better fixation of implant, higher stability of implant and possibility of osteointergation. Various studies [80–82] have shown that bone remodelling occurs when the amount of micromotion between the implant and the bone is less than 40 μm. Bragdon *et al.* [80] and Engh *et al.* [81] showed that a micromotion of 150 μm could induce formation of fibrous tissue. Szmukler-Moncler [83] suggested that the tolerated micromotion threshold was found to lie somewhere between 50 μm and 150 μm. In impaction grafting, the morsellised bone graft material should be strong enough to withstand the aforementioned micromotion up to about 50 μm.

1.10.2. Gait analysis

Gait analysis is defined as the process of quantification and interpretation of animal (including human) locomotion [84]. Figure 1.26 illustrates how the body moves from 0% to 100% in one walking cycle. From the sagittal plane, it can be seen that the lower limb is moving with different velocities and accelerations. It can also be observed that in the frontal and transverse plane, the leg is moving across the neutral axis. Therefore, the motion is complex. For revision hip replacement with impaction bone grafting, the compacted morsellised bone graft experiences forces during the gait cycle. The loading is predominantly in one direction but varies in magnitude as shown in Figure 1.24. In addition to the different velocities and accelerations, an understanding of the viscoelastic properties of the bone graft could play an important role post-operatively.

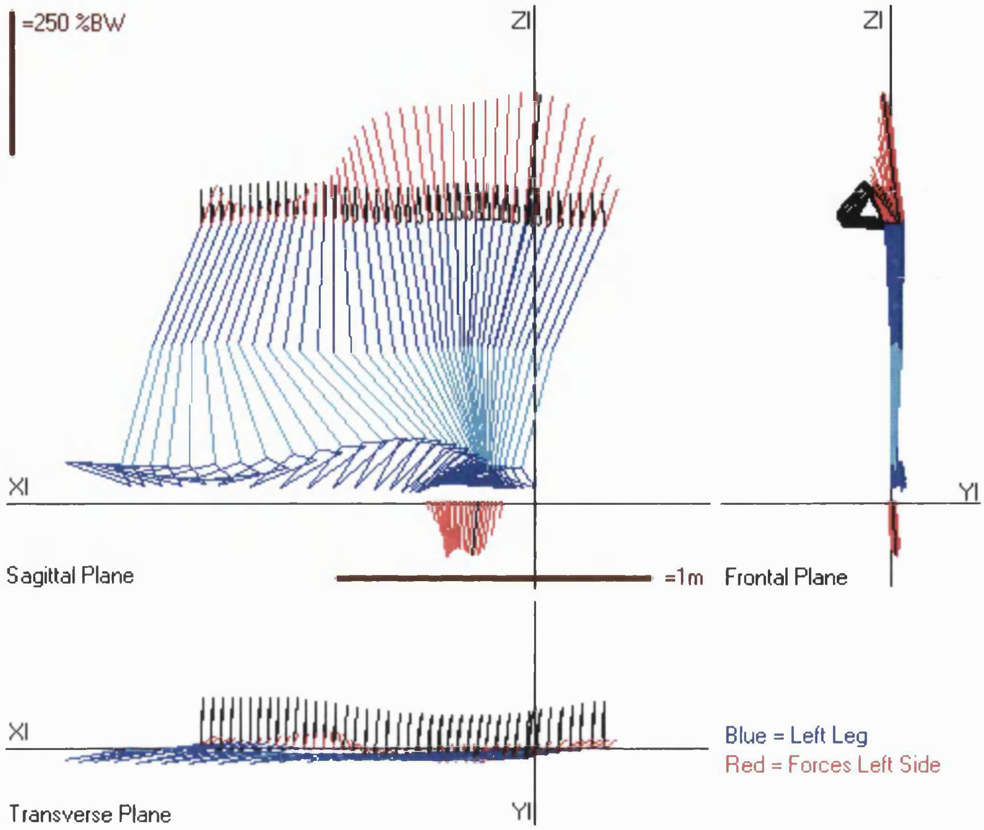

Figure 1.26.: The motion track of a gait analysis of the lower limb in a normal walking cycle was captured in three different planes including the sagittal plane, frontal plane and transverse plane. The corresponding applied force is represented by percentage body weight (%BW) (adapted from [71]).

1.11. Material considerations

Morsellised cancellous bone is essential in impaction grafting. It can be either autograft (taken from the patient) or allograft (taken from another person). Xenograft (taken from other species such as porcine and ovine bone) is usually used for pre-clinical testing and experiments. Autograft is usually preferable to allograft because transplanting allograft tissue can elicit immunogenicity [85] and run the risk of disease transmission such as hepatitis-A/B/C and HIV-1/2. Using autograft in acetabulum reconstruction has given promising results [33, 86]. However, there is not usually sufficient amounts of autograft available for impaction bone grafting in hip revision, due to the large amount of bone graft that is often needed [87]. Therefore, allograft is used in revision hip surgeries. A, B, O compatibility between graft donor and recipient is not necessary, Rhesus compatibility is important when the patient is a Rhesus negative woman of child bearing age [18]. The demand for allograft is, however, exceeding the availability. Therefore, much research [60, 88–90] has been done on investigating the use of artificial bone substitutes as an extender or an alternative to allograft bone. Hydroxyapatite and tricalcium-phosphate (HA-TCP) and glass ionomer [91] are widely used as bone graft extenders. Commercial products such as BoneSave (Stryker) are already available on the market. The major benefit of using bone graft extender materials is that they provide known and controllable properties compared to the variable bone qualities of autograft and allograft. The variability arises from donors' sex, size, age, sterilisation method, storage environment and the milling procedures used [88]. The mechanical properties of the bone graft in general depend on the type, size, grading, moisture and fat content, preparation methods, the amount of porosity as well as graft storage such as sterilisation. These factors can directly influence the mechanical stability after surgery. It takes a long period of time after operation for bone fusion and remodelling to occur, and during this time the supportive bone scaffold changes and the mechanical properties become difficult to predict. Heiner *et al.* [68, 92] tried to simulate the apparent modulus of femoral impaction grafts by mixing amine-based epoxy (Durabond 7120HP; Loctite Corp., Rocky Hill, CT) into bone graft. The apparent modulus of fused bone graft was found to be ten times greater than that of unfused bone graft. It is, therefore, important to pay attention to the effect of bone remodelling. Furthermore, the shear strength (τ) of bone graft is a function of cohesion (c), internal friction (ϕ) and normal compressive stress (σ). The relationship can be expressed by the Mohr Coulomb failure law $\tau = c + \sigma\, tan\phi$ [93, 94] as shown in Figure 1.27.

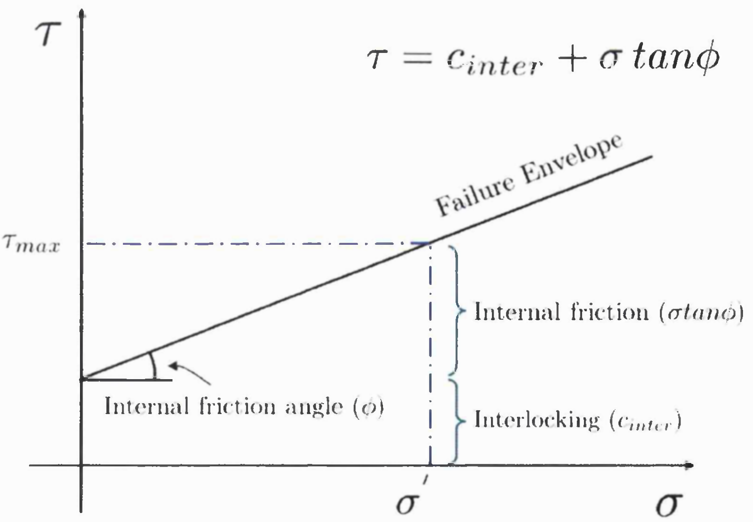

Figure 1.27.: Mohr Coulomb failure law.

1.11.1. Preparation techniques

Allograft bone graft can be prepared as fresh-frozen [12, 34], by lyophilisation (freeze-drying) [95–98], autoclaved [99–101], irradiated [102, 103], alkaline treated and acid treated [104, 105]. Gie *et al.* [12, 34] recommended that fresh-frozen femoral heads should be used in impaction grafting instead of freeze-dried femoral heads. Cornu *et al.* [96] found that the rate of compaction of freeze-dried bone was faster than that of fresh-frozen controls, and they both had about the same maximal apparent stiffness (~55 MPa). There have also been cadaveric experiments showing that using freeze-dried bone graft can minimise both micromotion and proximal subsidence [95]. Pelker *et al.* [106] found that freeze-drying significantly reduced the torsional and bending strength, but did not deleteriously affect the compressive or tensile strength. By contrast, fresh-frozen would be better than freeze-dried bone when the graft is subject to large torsional loads [103]. The findings by Cornu *et al.* and Pelker *et al.* were somewhat similar.

Irradiation of allograft is commonly used for minimising the risk of disease transmission. It is considered to be a very efficient and safe method, and can also be accomplished with freeze-dried allograft storage techniques. X-rays, gamma rays, or high-energy electrons are used to eradicate virus contamination by ionisation [107]. The effectiveness of radiation has a direct impact on the viability of viruses, and the amount of exposure to radiation is governed by a simple exponential function of dose. As a result, the probability of getting virus contamination by HIV cannot be completely eliminated [107]. The biomechanical strength of fresh-frozen allograft, which has been exposed to just 20 kGy, can be reduced up to 15% when compared with untreated pure fresh-frozen allograft [108]. Zhang *et al.* [109], however, found that there were no significant differences in mechanical or material properties for both fresh-frozen and freeze-dried tissues exposed to dosages of $20 - 25$ kGy. However, irradiation of bone with more than 30 kGy or irradiation combined with freeze-drying is likely to cause a significant reduction in breaking strength [106]. Furthermore, Anderson *et al.* [110] found that there was a significant differences in normalised failure stress ($P < 0.001$) and normalised elastic modulus ($P = 0.003$) when compared with the control specimens and specimens that had been irradiated with 60 kGy.

In terms of the effect of radiation on the biological properties, Hernigou *et al.* [107] summarised that a high-dose radiation can be harmful for the tissue and osteogenic potential. Fideler *et al.* [111] suggested that doses of 30 kGy of gamma radiation are necessary for the sterilisation of fresh-frozen allograft. Graft that had been irradiated with 30 kGy and 40 kGy did not have any deoxyribonucleic acid (DNA) of the human immunodeficiency virus that was detectable by a polymerase-chain-reaction test.

Autoclave sterilisation is a heat treatment method and is generally done by exposing allograft, under high pressure to heat or pressurised steam. It is performed at a temperature of 132°C for 60 mins [112]. Autoclaving can also be combined with other treatments such as acidic or alkaline sterilisation. Speirs *et al.* [105] noted that autoclaving significantly reduced both the ultimate and yield strengths in destructive compression tests of allograft. Autoclaving combined with alkaline sterilisation has also been reported to reduce both the ultimate strength and the elastic modulus [113].

Although fresh-frozen allograft generally provides better mechanical strength such as in torsion and compression, there have been numerous concerns about the transmission of disease from donor to patient. Risk of HIV can be effectively reduced by irradiation, but it still cannot be totally eliminated. A screening process is, therefore, crucial to minimise the risk [114]. Unfortunately, there is still no gold standard for bone graft sterilisation and mechanical testing.

1.11.2. Size and grading

Brewster *et al.* [93] proposed that MCB is a friable particulate aggregate, the mechanical behaviour of which should conform to established engineering theory. Well-graded aggregates composed of a mixture of materials are known to have superior mechanical characteristics compared with poorly graded aggregates of one material. The absolute particle size is less important than the grading. A well-graded specimen should have a coefficient of uniformity $C_u > 5$ (which is the ratio of the sieve diameter that 60% of particles will pass to that through which 10% will pass); some other authors recommended $C_u > 6$ [115]. A well-graded aggregate has a higher shear strength than an aggregate with uniform particle size because a well-graded aggregate has many interparticle contacts, and load per contact is therefore, less than that of a uniform aggregate [94]. Furthermore, the shear strength can be improved by adding measured quantities of small and very small fragments [93]. As a result, bone graft may be morsellised whilst still frozen without detriment to the size profile obtained.

Bolder *et al.* [116] recommended firm impaction by hammering large bone grafts for optimal stability of the cup. In a similar study, Ullmark [117] reported that large sizes of morsellised bone graft chips can provide better cup stability than a small fragment sized graft. In addition, the mechanical stability of the femoral stem could be improved by using large-size bone chips [118]. Larger-sized bone chips (> 1.5 mm) present a higher modulus under tri-axial compression testing [119]. However, mixing small and large-size bone grafts together was found to give a better shear strength (i.e. cohesion c, internal friction ϕ) than pure large-size bone grafts [94]. Furthermore, there have been experimental results showing that well-graded large-size bone chips have a slightly better shear strength than well-graded small-size bone chips [94]. In 2004, Tsiridis *et al.* [53] reported that they have used large nibbler-made chips in the proximal femur for five years since 1998. Fractures with impaction grafting associated with this technique were five times more likely to unite if a long rather than a short cemented stem was used. Overall, well-graded small-size and well-graded large-size bone grafts for the distal and proximal femur respectively would seem to provide best implant stability.

1.11.3. Defatting

MCB consists of small particles of cancellous bone and marrow and it can be considered as a combination of water, fat and complex biological substances. Impact compaction studies have shown that varying the moisture content influences the compacted sample density, and that maximising sample density decreases subsequent compressive strain [120]. Graft can be washed by pulsed lavage with a warmed 0.9% saline solution [94], soaked in chloroform [92], soaked in heated detergent solution at approximately 80°C [115] or soaked in acetone for 48 hrs [70]. High-pressure saline washing of allograft has also suggested as being able to improve allograft safety by reducing the superficial bacterial bioburden [121]. Dunlop *et al.* [94] investigated the effect of particle size and washing of bone graft. Fresh-frozen human femoral heads were milled by an air-powered mill with a pair of intermeshing 8 mm teeth. They discovered that washed graft has exactly the same particle-size distribution as it does in the pre-washed state, but it has an increased resistance to shear (i.e. cohesion c, internal friction ϕ). Dunlop *et al.* [94] also suggested that the fat and marrow acted as an interparticle lubricant. The present of interparticle lubricant can absorb the impaction energy. Therefore, for washed graft (i.e. without interparticle lubricant), more energy can be transmitted to the graft particles and a higher compaction can be achieved.

Brodt *et al.* [119] also found that both non-defatted and defatted bone graft have exactly the same particle size. Thus, the moduli and the stress-strain transition points of non-defatted and that of defatted MCB were statistically indistinguishable under an identical level of applied pressure. However, regardless of statistical tests, defatted bone graft has demonstrated higher average moduli for both the pre-crush (before yield) and crush phase (beyond yield). Voor *et al.* [120] stated reducing the water content alone had some influence on properties, whilst reducing the fat content improved both the static and dynamic behaviour. In another study by Voor *et al.* [115], it was confirmed that MCB with minimal fat but with optimal water content would have superior mechanical performance. It was shown that defatted graft had a higher constrained modulus, lower strain and creep rate compared with fresh-frozen graft. In addition, partly defatted bone chips were found to increase the stability of the acetabular cup and prevent rotation of a cup cemented on a graft bed [117].

Gie *et al.* [12, 34] has on the other hand recommended unwashed, cancellous allograft chips prepared from frozen femoral heads retrieved at primary hip arthroplasties. The effect of washing on bone remodelling is still unclear even it seems to promote better mechanical stability. There is still no standard washing technique for bone graft material. Nevertheless, from an engineering point of view, washing bone graft could provide a favourable mechanical environment for implant insertion.

1.11.4. Graft extenders

The original impaction technique proposed by Slooff *et al.* [33] and Gie *et al.* [12] for acetabular and femur reconstruction only involved the use of morsellised cancellous bone. Recently, much research [88, 93, 122–125] has been done on investigating mixing graft with different composite materials such as cortical bone, bioglass, xenograft, polymer, hydroxyapatite (HA), tricalcium-phosphate (TCP) and bone morphogenic proteins (BMP). During preparation, cartilage and soft tissue must be removed as the presence of cartilage prevents efficient impaction of the grafts, probably due to its elastic nature [126]. Recently, Tsiridis *et al.* [53] suggested using pure cancellous or cortico-cancellous chips and to remove thick cortical fragments from the donor bone.

The mechanical properties of pure allograft are different to those mixed with certain proportions of bone graft extenders. Some surgeons [42, 43, 53, 125] prefer including cortical bone for improved stability. Kligman *et al.* [122] reported significantly better results using morsellised cortical allograft when assessed by early clinical outcome, thigh pain, and stem subsidence greater than 5 mm. There have been *in-vitro* experiments showing that pure cortical allograft has less axial subsidence, high torsional resistance and stiffness compared with pure cancellous bone [124]. However, Bavadekar *et al.* [126] reported that cortico-cancellous bone has as good a stiffness value ($\sim$42 MPa) as pure cancellous bone. Mixing cortical and cancellous bone can also reduce the number of femoral heads needed, and minimise the preparation time.

Grimm *et al.* [88] showed that mixing an HA-TCP ceramic with the bone graft can significantly improve stability. Mixing of HA-TCP was also found to significantly increase the stiffness of the graft under cyclic loading [127]. The advantage of HA-TCP as a graft extender is that it has similar material composition to host bone hence bone remodelling and graft replacement with live bone is possible. The major advantage of using a ceramic material is that it has less variable and better controlled properties. It has also been reported that mixing bioglass with morsellised bone graft can provide improved mechanical stability [93]. A photomicrograph study has also shown new bone formation within the graft and around degrading ceramic synthetic graft particles [90].

1.11.5. Graft delivery

Savory *et al.* [54] suggested that a 10 cm^3 syringe should be used to deliver bone into the medullary canal. A spatula was not recommended as large amounts of graft can be dropped into the surrounding tissue. In order to expose the major diameter of the syringe, the distal tip was cut off. The rubber grommet should also be removed as shown in Figure 1.28. Graft was filled into the syringe barrel and slightly compressed by index finger pressure. Only $2-3$ cm^3 by volume of graft was loaded. It was not suitable to insert a large amount of graft at the same time (e.g. $3-4$ cm^3). This was because inserting a pack of graft can potentially block the medullary canal, and this leave voids between graft particles. As a result, the surgeon could be misled into thinking that a tight impaction had been achieved. Therefore, progressive loading of the graft can lead to the best compression results.

(a) 10 cm^3 empty syringe (b) $2-3$ cm graft is filled (c) Injection of graft

Figure 1.28.: a) The distal tip has been cut off showing the major diameter. b) Filled the 10 cm^3 barrel with about $2-3$ cm^3 amount of graft. c) Graft was injected directly into the medullary canal (adapted from [54]).

1.12. Mechanical properties

Bone is a specialised connective tissue and it has the capacity to alter its shape and structure in response to changes in its mechanical environment [128]. Bone cells are embedded in a matrix consisting of both organic and inorganic components and are surrounded by a ground substance. The organic component is $90-95\%$ type I collagen; the inorganic components are calcium and phosphorus in the form of hydroxyapatite [129]. Bone has both elastic and viscous properties. It can be considered to be a biphasic material with a mineral phase and an organic phase containing collagen and ground substance as shown in Figure 1.29. The strength of the composite allows a strong but brittle material to be embedded into a weaker but more flexible one [130]. In addition, bone has the ability to remodel, by altering its size, shape and structure, to meet the mechanical demands placed on it (Wolff's law). Bone presents non-isotropic behaviour and its mechanical properties differ depending on the loading direction as shown in Figure 1.30 [130]. The basic mechanical properties are well-defined and can be easily found from the literature. Morsellised bone graft microscopically has the same biological and mechanical properties to a piece of bone (e.g. femur and tibia). However, macroscopically, morsellised bone graft has completely different mechanical properties. An analogy can be comparing the properties of a small stone and a piece of rock.

Numerous studies [66, 68, 70, 93, 94, 115, 119, 120, 126, 131–135] have been carried out to quantity the mechanical properties of morsellised bone graft materials. Since the graft material is morsellised, it has to be constrained when carrying out experiments on it. Moreover, all the mechanical properties have to be characterised as apparent values in order to replicate the actual mechanical behaviour during impaction grafting. For instance, apparent bone density ($\rho_{app\,bone}$), apparent Poisson's ratio (ν_{app}) and apparent compressive stiffness (E_{app}) are the terms that should be used. Properties can be obtained from either *in-vivo* or *in-vitro* experiments depending on the project aims and targeted variables. There is currently no standard method to test morsellised bone graft materials. In addition, it has been suggested that morsellised bone graft should conform to established engineering theory and able to be tested experimentally [93]. Some studies [93, 94, 115, 119, 120] have used geotechnical engineering approaches to estimate the mechanical properties of bone graft.

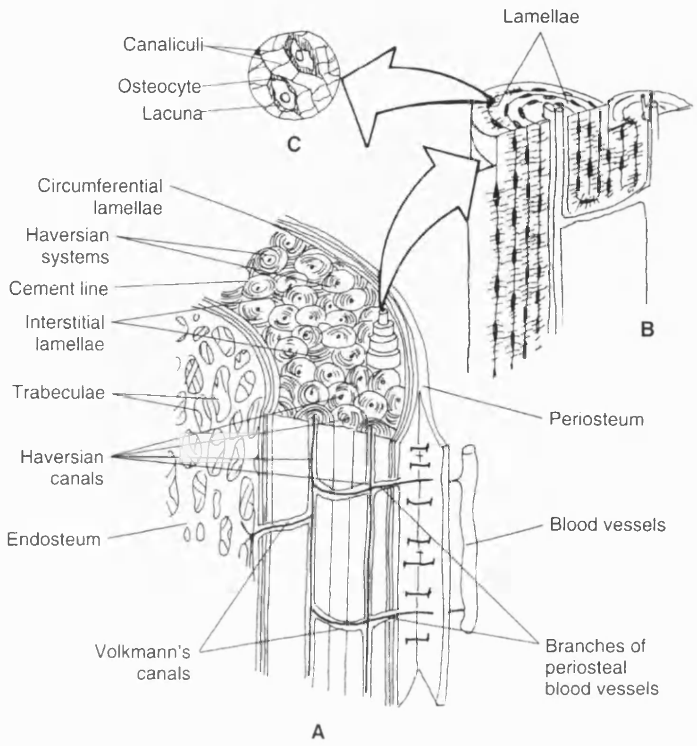

Figure 1.29.: a) Schematic illustration of a section of the shaft of a long bone depicted without inner marrow. The osteons, or Haversian systems, are apparent as the structural of bone. b) Each osteon consists of lamellae, concentric rings composed of a mineral matrix surrounding the haversian canal. c) Along the boundaries of the lamellae are small cavities known as lacunae, each of which contains a single bone cell, or osteocyte. Radiating from the lacunae are tiny canals, or canaliculi, into which the cytoplasmic processes of the osteocytes extend (adapted from [130]).

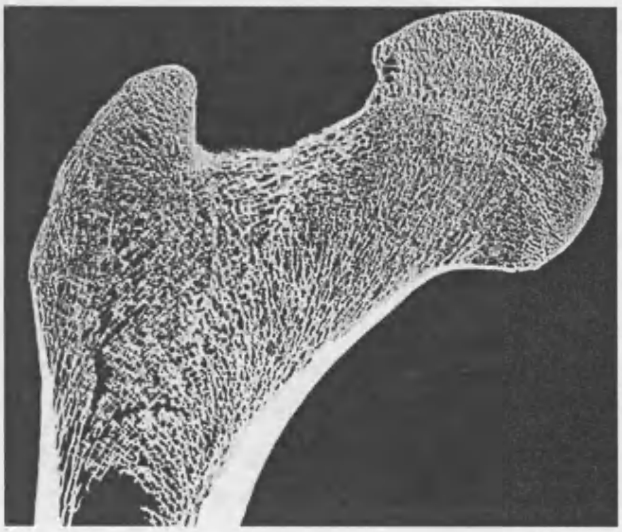

Figure 1.30.: Frontal longitudinal section through the head, neck, greater trochanter and proximal shaft of an adult femur. Bone grows to the direction in which it is subject to loading (adapted from [130]).

1.12.1. Mechanical strength

Mechanical strength of morsellised bone graft can be measured by compressive and shear testing. Compressive stiffness (modulus of elasticity or Young's modulus) provides information about the response of bone graft under the impaction process and post-operative cyclic loading during activities such as walking. Because of the tapered implant design, compression forces will cause radial displacement of the graft which can result in subsidence of the implant [66]. Therefore, higher mechanical strength can minimise the amount of subsidence. As bone and bone graft are viscoelastic materials, compressive stiffness differs depending on either the dynamic or static loading rates. Fosse *et al.* [132] categorised the stiffness of the bone graft according to the impact constrained modulus of elasticity (ICME) (i.e. transient modulus of elasticity), the consolidated constrained modulus of elasticity (CCME) (i.e. instantaneous modulus of elasticity) and the total constrained modulus of elasticity (TCME) (i.e. overall modulus of elasticity). ICME is important because it provides valuable information on the transient apparent stiffness and correlates directly with the transient peak stresses employing engineering stress equations. CCME provides the consolidated bone graft stiffness and indicates the static mechanical behaviour. TCME provides an overall view of the apparent stiffness. The stiffness of the bone graft varies and changes depending on the condition of the bone graft. In general, the higher the pre-compaction energy (i.e. high apparent bone density), the higher the apparent stiffness that can be observed. The apparent stiffness will tend to a steady value after a cumulative series of impactions [126]; in the steady state, the orientiation of the graft and bone density were optimised and had a maximum capacity to carry load. Compressive properties can be determined by uni-axial constrained compressive testing [68, 70, 88, 126], tri-axial compressive testing [119] or one-dimensional consolidation testing [120]. Tests can be carried out by using a drop-weight [68, 115, 126, 132] or cyclic compressive loading [88]. In addition, the geometry of the container (e.g. cylindrical or tapered), can have a direct influence on the apparent stiffness even when testing with the same graft material [68]. A wide range of apparent stiffnesses (8.0 – 100 MPa) have been reported in many studies [68, 116, 120, 126, 132]. For instance, Giesen *et al.* [70] calculated the confined apparent compressive modulus of 38.7 MPa after pre-loading their specimens by 2.75 MPa for 24 cycles, whereas Voor *et al.* [120] calculated the confined apparent compressive modulus of 8.0 MPa when the test sample was being loaded for the first time (i.e. without any pre-loading). It was observed that bone graft which has been pre-loaded yields a higher apparent stiffness. Pre-loading is recommended since it is very difficult to define the stiffness of the graft due to its viscoelastic behaviour (see §1.12.2 on Page 42) without any pre-loading. Pre-loading, therefore, provides a more predicable and representative result.

In addition, torsional shear forces are exerted on the cement mantle and the bone graft post-operatively, hence subsidence occurs in distal, medial, lateral and posterior directions [64]. Shear stiffness provides information about the resistiveness of bone graft under shear. Shear testing can be performed by a shear box [93, 94] similar to that described by British Standard 1377-7:1990 [136] as shown in Figure 1.31 and Figure 1.32. The test is performed by varying normal compressive loads on the specimen and the force required to produce the shear strain is measured. The relationship of bone graft can be expressed by the Mohr Coulomb failure law $\tau = c_{inter} + \sigma tan\phi$ (see §1.11 on Page 32). Dunlop *et al.* [94] found that the cohesion (c) ranged from -1.8 to 13.5 kPa, the internal friction (ϕ) ranged between 29.9° – 37.5° and the total shear strength (τ) ranged between 208 – 271 kPa.

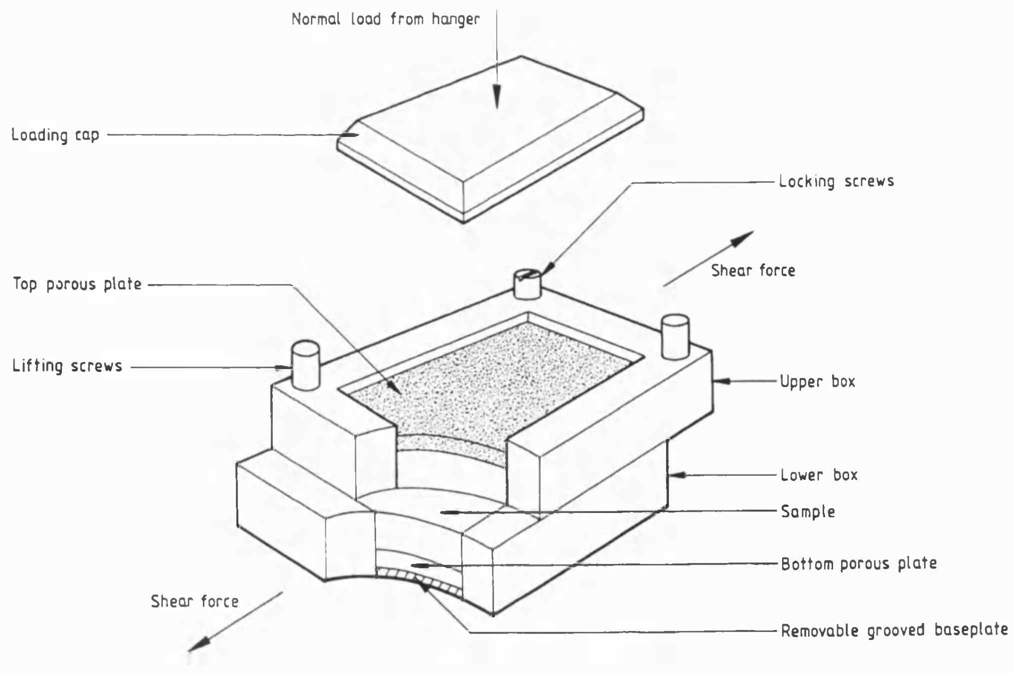

Figure 1.31.: Details of the shearbox (adapted from [136]).

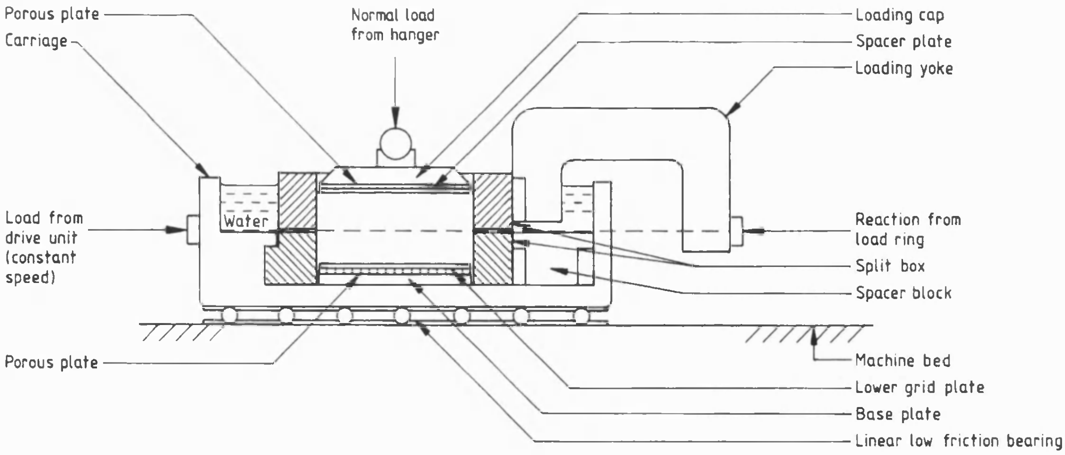

Figure 1.32.: Typical arrangement of shearbox apparatus (adapted from [136]).

Brewster *et al.* [93] discovered that the mechanical properties improved with increasing normal load and shear strain (strain hardening). The mechanical strength also increased with increasing compaction energy. Voor *et al.* [115] found that the greater the initial sample density, the lower the subsequent strain and the greater the initial modulus and ultimate strength. Malkani *et al.* [66] stated that compression will cause radial displacement of the graft which results in the subsidence of the implant. Shear forces along the interfaces may allow slippage of the cement along the graft or of the graft along the smooth cortical wall. However, it is less likely that slippage occurs at the cement-graft interface due to the wedge effect and interdigitation between the cement and the graft. Furthermore, the distal portion of the impaction graft is subjected to only axial compaction, whilst the proximal portion of the impaction graft is subjected to both axial and radial compaction. As a result, the radial component would tend to further compact the impacted morsellised bone graft; thus, increasing the effective modulus proximal impaction graft [68]. However, the actual elastic modulus will differ during impaction grafting since structurally damaged cancellous bone is known to have a much lower elastic modulus than undamaged cancellous bone [126].

1.12.2. Stress-strain behaviour

The relationship between the applied force and the deformation can be represented by a stress-strain ($\sigma - \varepsilon$) graph as shown in Figure 1.33. Stress (σ) is defined by the ratio of load (F) applied perpendicular to the specimen cross section by the cross section area (A). Strain (ε) is defined by the ratio of deformation elongation or compression (Δl) by initial length (l) [137]. The compressive modulus of elasticity (Young's modulus, E) is deduced by the slope of the stress-strain curve before the yield point. It can be calculated by overall changes (σ/ε), change of slope in a given time ($\Delta\sigma/\Delta\varepsilon$) or instantaneous slope ($d\sigma/d\varepsilon$).

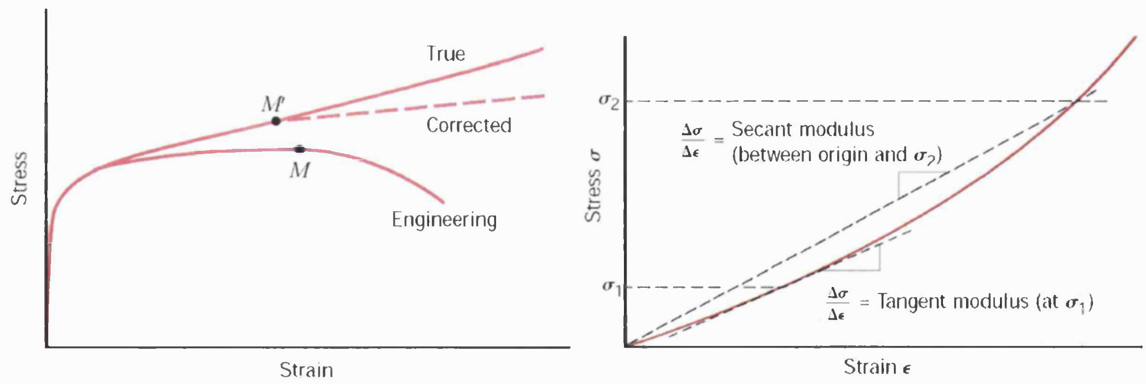

(a) True/Engineering stress-strain curve (b) Behaviour of bone graft material (not to scale)

Figure 1.33.: a) A comparison of typical tensile engineering stress-strain and true stress-strain behaviours. Necking begins at point M on the engineering curve, which corresponds to M' on the true curve. The 'corrected' true stress-strain curve takes into account the complex stress state within the neck region. b) Schematic stress-strain diagram showing nonlinear elastic behaviour, and how secant and tangent moduli are determined (adapted and modified from [137]).

Grimm [78] analysed the effect of mixing a ceramic graft extender with bone graft. The graft was compressed at a speed of 2 mm/min in a die plunger for pure ceramic, and 3 mm/min for bone graft and bone/ceramic mixes. The engineering force-strain curve (i.e. $\sigma - \varepsilon$) was plotted. A force of 500 N (= 1.59 MPa) was observed for a strain of 0.4. Graft or similar materials showed an exponential curve before yielding (i.e. the rate of change of stress increases as strain increases) [78, 127] as shown in Figure 1.33(b) and Figure 1.34. The exponential increase of stiffness demonstrates the toe-region of typical viscoelastic material properties. In compression testing, after the toe-region, a liner relationship of stress-strain is given [78].

If the loading rate is low, the viscoelastic effect can be eliminated. Practically, in the clinical situation, the viscoelastic behaviour should be considered during the impaction grafting. In an operation, timing is a crucial element. It is essential to finish the operation in least amount of time to minimise blood losses and minimise the risk of infection. As a result, it is unlikely to impact graft at a very slow rate. Fosse *et al.* [132] used an engineering strain-force curve instead of stress-strain curve. Therefore, the shape of the curve is displayed as an inverse shape (i.e. logarithmic curve) as shown in Figure 1.34. The shape of the curve is similar to that of Grimm [78]. A force of 800 N (= 0.8 MPa) was observed at a strain of about 0.23 [132]. Results presented by Grimm [78] also showed that the rate of change of stress increases as strain increases, the strain reaching a steady value in which the graft was fully compacted and no more deformation could be achieved.

Brodt *et al.* [119] investigated the true stress-strain behaviour of MCB by loading the graft under tri-axial compression. It was found that with stresses less than a few tenths of a megapascal, the curve was relatively steep. With additional stress (~0.1 – 0.2 MPa), a smooth transition was observed, followed by a nearly constant transition stiffness. It was concluded that the bone graft differs from classic soil behaviour in that it exhibits bi-linear true stress-strain curves, with no flattening of the curves to reflect an ultimate shear strength, at least within the strain regimes considered. Grimm [78] also found that bone graft exhibits a linear stress-strain relationship during re-compression, after pre-loading with static load of 1.59 MPa.

The difference between the studies of Brodt *et al.* [119] and Grimm [78] is that Brodt *et al.* obtained a nearly linear stress-strain relationship without any pre-loading, whereas Grimm only obtained a linear stress-strain relationship after pre-loading. Therefore, the test method used could probably affect the linearity. Furthermore, pre-loading of bone graft by static compressive loading [78] or cyclic loading [70] can positively influence the stress-strain relationship, hence, better linearity can be achieved. Pre-loading can also affect the initial position of stress-strain graph and the measured compressive modulus of elasticity. The engineering stress-strain curve should be sufficient for prediction of apparent stiffness in most situations. Pre-loading, therefore, would appear to be a useful technique to increase repeatability and predictability.

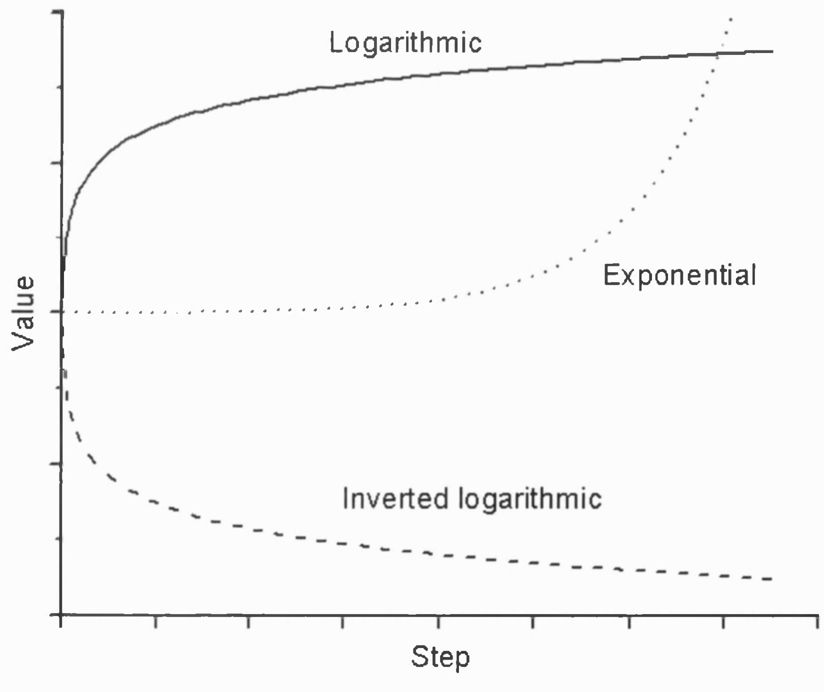

Figure 1.34.: Definition of logarithmic, inverted logarithmic and exponential curves.

1.12.3. Poisson's ratio

Poisson's ratio (ν) is defined as the ratio of the lateral (ε_x, ε_y) and axial strain (ε_z) when the force is applied from axial direction as shown in Figure 1.35. Theoretically, Poisson's ratio for isotropic materials should be 0.25 [137]. The nearer the Poisson's ratio is to 0.25, the more isotropic the material is and hence the engineering equation $E = 2G(1 + \nu)$, (where (E) is the elastic modulus, (G) is shear modulus and (ν) is Poisson's ratio), can be applied. Understanding the Poisson's ratio allows prediction of how graft behaves under different impaction conditions. Apparent Poisson's ratio should be used to describe the deformation of graft during impaction.

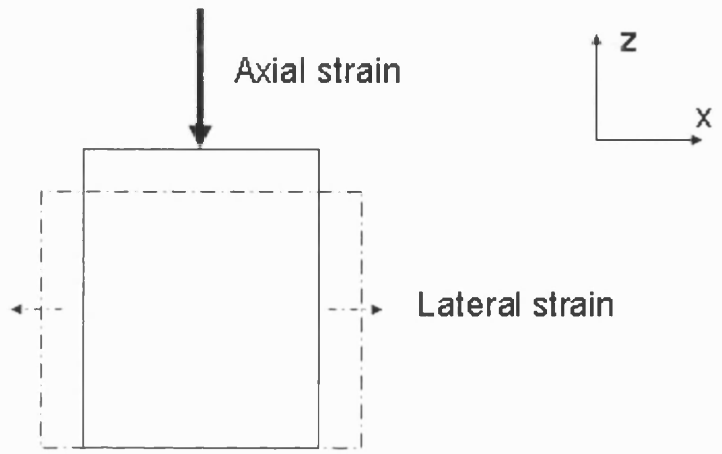

Figure 1.35.: Definition of Poisson's ratio.

It has been found that cancellous bone has a spring-back effect due to its viscoelastic behaviour [131]. Impact constrained apparent Poisson's ratio (ICPR) (i.e. transient Poisson's ratio) would be a crucial factor to assess the transient deformation changes due to impaction. Different loading rates should be considered to estimate the ICPR since the Poisson's ratio is not a constant value for bone. Thus, the volume expansion of MCB represents the stress exerted on the femur, which helps to forecast the risk of per-operative fracture. In addition, consolidated constrained apparent Poisson's ratio (CCPR) (i.e. instantaneous Poisson's ratio) can provide a static Poisson's ratio due to the cyclic loading post-operatively. Bavadekar *et al.* [126] showed that the apparent bone density increases with the number of impactions in a logarithmic manner. In other words, the denser the MCB, the more difficult it is to compact the graft and reduce the volume. Hence, the graft appears to be a high density aggregate and behaves in a similar manner to a solid substance, in which the CCPR can be easier to predict.

Brodt *et al.* [119] performed tri-axial compressive testing on MCB and calculated the effective Possion's ratio by assuming superposition of the deformations due to axial and hydrostatic loading over the entirety of the axial loading regime. The Poisson's ratio of MCB was found to be between $0.12 - 0.25$; therefore, MCB demonstrates anisotropic behaviour. The effective Possion's ratio represents total constrained apparent Poisson's ratio (TCPR) (i.e. overall Poisson's ratio) and it provides an indication of the overall deformation change due to impaction. Moreover, if both impact constrained apparent Poisson's ratio and impact constrained modulus of elasticity (see §1.12.1 on Page 40) are found, it is possible to combine both terms together to estimate the impact constrained shear modulus. To date, not much research has been carried out in investigating the effect of viscoelasticity on the Poisson's ratio of MCB.

1.12.4. Time dependent factors

Bone graft is a viscoelastic material and exhibits behaviour between an elastic solid and a viscous fluid. In addition, the mechanical properties of bone graft change depending on the loading situation. The creep test and the relaxation test are two common methods to characterise the viscoelastic properties of MCB. The creep test is done by applying a constant stress; the strain is then measured as a function of time as shown in Figure 1.36(a) and Figure 1.36(b); the relaxation test is done by applying constant strain, stress is then measured as a function of time as shown in Figure 1.36(c) and Figure 1.36(d). The creep test can be expressed as a logarithmic function; the relaxation test can be expressed as an inverted logarithmic function [138]. The creep modulus ($E_{creep,t} = \sigma/\varepsilon_t$) and relaxation modulus ($E_{relax,t} = \sigma_t/\varepsilon$) can be deduced from the instantaneous stress divided by the instantaneous strain. The recoil effect (also called spring-back, or recovery) is used to describe the volume expansion of graft. It is quantified by the strain change after removal of load.

Creep-recoil is determined by removal of load after the creep test as shown in Figure 1.36(a); the relaxation-recoil is determined by removing applied strain (i.e. removal of residual stress) after a relaxation test as presented in Figure 1.36(d). The recoil represents the volume change after impaction and it is particularly useful in determining the graft volume expansion after impaction by distal and proximal impactors. Nevertheless, most studies have not specified whether it is the creep-recoil or relaxation-recoil test which has been used.

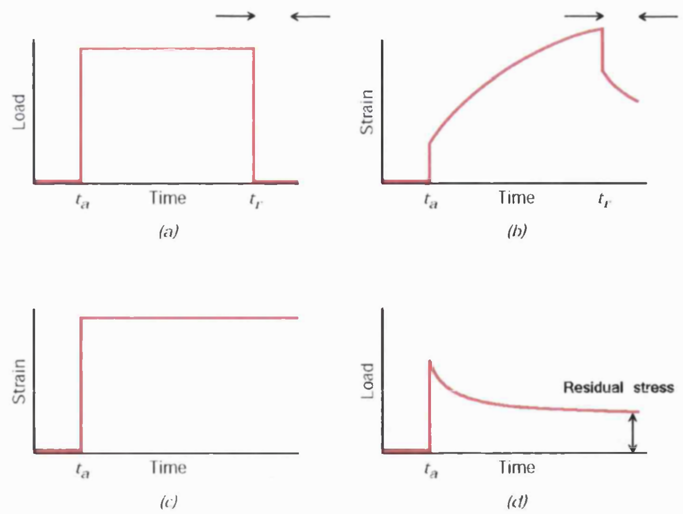

Figure 1.36.: Creep test – a) Load versus time, where load is applied instantaneously at time t_a and released at t_r; b) The strain-time responses for a viscoelastic material; the recoil effect is indicated by two arrows. Relaxation test – c) Stain versus time, where strain is applied instantaneously at time t_a and kept; d) The load-time response for viscoelastic material; residual stress is indicated by a double arrow (adapted and modified from [137]).

Giesen *et al.* [70] investigated the confined compression creep properties of MCB by pre-loading the graft with 2.75 MPa for 24 cycles. It was found that the creep behaviour can be described by a linear biphasic model (creep law), which has been originally been developed by Mow *et al.* [139] for modelling articular cartilage. Both the parameters and unknowns in this model can be quantified by experiment. However, these parameters change depending on the preparation of the graft. For instance, graft size and grading, defatting and the components of mixtures can affect the parameters. Furthermore, during the process of graft compaction, plastic deformation and intergranular motion occur, leading to denser packing and a permanent decrease in volume [140].

The die-plunger compressive test is an efficient and quick method to examine the relaxation of bone graft. The die-plunger used in various projects has a hollow cylinder of height of 80 mm with a polished bore of 20 mm [78, 141] as shown in Figure 1.37. The specimen is put into the die and compressed at a constant strain rate. The hollow cylinder is capped by a porous disc to allow fluid exudation. Stress is then measured for up to 120 s, and relaxation is calculated from the difference between the maximum stress and the stress at 120 s. Table 1.7 shows a summary of graft relaxation and strain recoil results taken from the literature. Generally the relaxation for synthetic graft extenders and natural graft materials ranges between 20 – 30% and 30 – 40% respectively; the recoil for synthetic graft extenders and natural graft materials ranges between 0.1 – 1.0% and 7 – 14% respectively [78, 142]. Giesen *et al.* [70] defined ‘relaxation’ after removal of the pre-loading load of 2.75 MPa (i.e. no load). Actually, the term 'relaxation' refers to the recoil effect since the relaxation test by definition does require constant strain.

Figure 1.37.: Die-plunger used in various projects at the University of Bath, United Kingdom.

Graft	Treatment(s)	Relaxation (%)	Strain-recoil (%)
Human	Fresh-frozen, unwashed	33.5	10.6
Human	Fresh-frozen, washed	36.7	12.5
Human	Freeze-dried, rehydrated	34.3 [142], 36.9	–
Human	Irradiated with 5 kGy	38.5	–
Human:HA-TCP	Mixed with ratio 20:80	19.5	–
Ceramics	25% porosity	18.7	0.77
Ceramics	50% porosity	18.9	0.10
Ovine	Fresh-frozen, unwashed	39.6	7.7
Ovine	Fresh-frozen, washed	31.9	–
Bovine	Fresh-frozen, unwashed	33.4	8.2
Porcine	Fresh-frozen, unwashed	29.7 [142]	–
Porcine	Fresh-frozen, washed	27.9 [142]	–

Table 1.7.: Relaxation of graft materials recorded at 120 s under compressive loading of 1.59 MPa (adapted from [78, 141], unless otherwise stated).

Kold *et al.* [131] stated that the increase in implant fixation found with compaction has been ascribed partly to the spring-back effect due to viscoelastic behaviour of cancellous bone. In reality, the recoil effect happens instantaneously after removal of the impactor. Therefore, the size of the neo-medullary canal will not be exactly the same size as the proximal impactor. In addition, the spring-back effect is neither complete nor symmetrical [131]. These factors might, therefore, contribute to variability of implant fixation. Nevertheless, under clinical conditions, the recoil effect is reduced per-operatively if the implant is loaded immediately and continually by muscle contractions [66]. As a result, cortical bone is subjected to an internal pressure because recoil cannot take place when the implant is in place. The recoil effect could be a useful value to assess the risk of post-operative femoral fracture since a large amount of recoil effect changes the size of neo-medullary canal. Thus, this affects the final stem position.

It has been discovered that the stiffness of the bone graft increases with time under static load, or cyclic loading [127]; this means the graft becomes stiffer with time under compression. Thus, the strain on the graft increases with time under loading, and can be represented as an exponential variation with time [127, 143]. This, therefore, suggests that stiffness versus time will give an inverse relationship (because $E \propto \varepsilon^{-1}$); this phenomenon being known as strain-hardening [93]. Eventually, the stiffness of the bone graft achieves a constant value with time when the graft reaches equilibrium.

1.12.5. Implant interfaces

1. Stem – Cement interface

   Cement is used to fix the implant into position. The shape of the interface depends on the design of the stem. In general, the thickness of the cement mantle varies from 1.7 – 2.0 mm and is occasionally greater than 2 mm [134]. Cement can consistently be found around the middle of the stem and is almost always absent around the distal stem [144]. Therefore, Masterson *et al.* [144] recommended the trial stem should be impacted a further 5 mm to allow room for cement. After impaction grafting, Malkani *et al.* [66] reported that the stem shows a rapid subsidence in the first few cycles during cyclic loading and this probably represents settling and wedging of the implant into the cement mantle. Subsidence can occur in either the cement mantle, or in the bone graft. If the subsidence occurs only within the cement mantle, a larger amount of compression will be exerted on the cement mantle and on the surrounding graft; however, if the subsidence of the stem and cement mantles occurs, the bone graft may be compressed. A centraliser is attached at the end of the stem and this allows stem-subsidence within the cement mantle. The centraliser is designed to prevent the stem from being end-bearing on the cement [45]. Various studies [145–148] have been carried out to estimate the debonding process using the finite element analysis (FEA) method. It has been suggested that debonding is governed by shear stress particularly starting at the tip, and the proximal and medial anterior regions of the stem [145].

2. Cement – Bone graft interface

   Mann *et al.* [135] measured the mechanical strength of the cement-graft interface under tensile and shear loading. It was shown that the cement-graft interface has a higher apparent shear stiffness than tensile stiffness under the same applied loading. Both stiffnesses are correlated with the amount of interdigitated bone. Therefore, high cement penetration can improve the mechanical strength of a graft. The depth of penetration depends on cement pressurisation pressure, duration of cement pressurisation, time of stem insertion, femoral stem profile and graft porosity [149, 150]. The graft porosity appears to be the most effective way to alter the cement flow in the impacted allograft bone [150]. Gruen *et al.* [151] grouped seven different zones which are widely used to specify different regions of the femur. Figure 1.38 illustrates seven zones starting from lateral to medial. Frei *et al.* [134] found that Gruen zones 7 and 1 give the highest cement penetration and Gruen zone 4 gives the lowest cement penetration as shown in Figure 1.39. Moreover, Gruen zone 1 gives the highest graft porosity (76%) and Gruen zone 4 gives the lowest graft porosity (52%). It was suggested that the distal graft has a higher apparent bone density than the proximal graft. Interestingly, a weak correlation was found between the penetration of cement and porosity of the graft. Masterson *et al.* [144] showed evidence of voids within the cement mantle of 2 mm or wider in 152 out of the 208 Gruen zones, and suggested this could induce cement-composite fractures and subsidence of the stem. The internal surface of the neo-medullary canal is determined by the size and shape of the proximal impactor, and relaxation of the bone graft can slightly change the shape of the canal, and affect the final stem position. The optimal cement thickness and the amount of interdigitation are, however, currently unknown.

3. Bone graft – host bone interface

The internal surface of the diaphyseal area varies from patient to patient and it is rather an uncontrollable variable. The uneven cortical surface is normally created by osteolysis, femoral fractures, removal of loose cement and removal of the implant. Impaction grafting is an efficient way to reshape the surface. Frei *et al.* [133] classified the graft-bone interface into three different failure types as shown in Figure 1.40. Stulberg [42, 43] recommended the use of tapered polished reamers to radially impact the graft onto the host bone, whereas Gie *et al.* [12, 34] recommended the use of a flat end distal impactor. From an engineering point of view, a radial impactor delivers a force perpendicular to the cortical surface; hence, it gives better surface contact between the bone graft and the host bone. However, not much research has been carried out on investigating the effect of graft contact on re-vascularisation although Ling *et al.* [35–37] proposed that allograft chips are replaced by viable cortical bone after impaction grafting. In reality, biopsies and post-mortem studies have shown that only a few millimetres of the allograft is replaced by viable bone. Therefore, a thin layer of graft with a viable cement-bone interface may be sufficient [134]. In some cases, cement can have direct contact with the host bone (e.g. Gruen zones 6 and 2) [133, 134]. Dai *et al.* [152] showed that inorganic particles (e.g. from a bone extender) embedded in cement can be replaced by new bone and create a viable cement-bone interface.

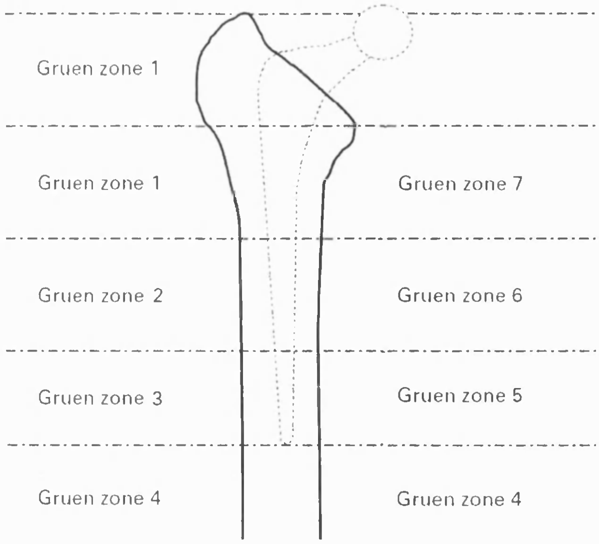

Figure 1.38.: Definition of Gruen zones 1 to 7 (adapted and modified from [134]).

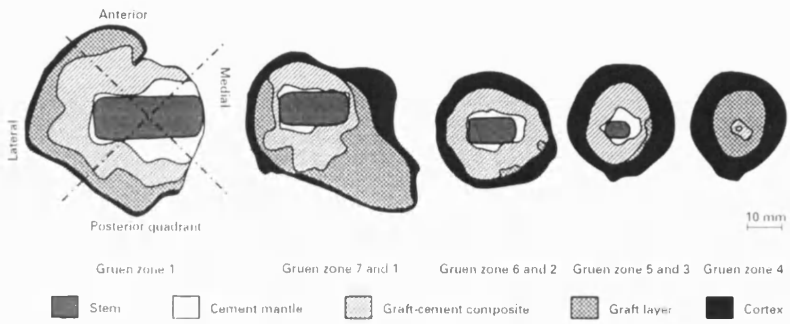

Figure 1.39.: Five sections of all the Gruen zones. The different patterns in the diagram indicate the materials present in each section. Each section is divided into anterior, posterior, medial and lateral quadrants (adapted from [134]).

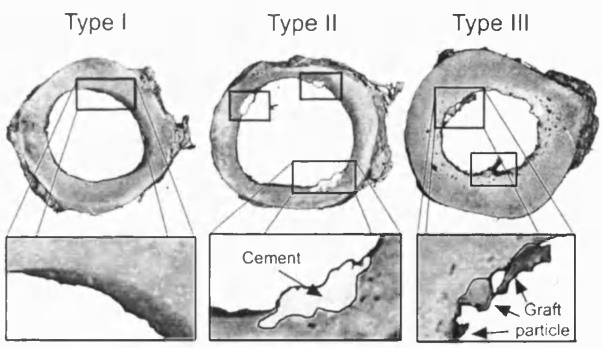

Figure 1.40.: Type I – pure interface failure (69%). Type II – remnants of cement remained on the endosteal surface indicating a local allograft-cement composite failure (19%). Type III – allograft particles remained on the endosteal surface indicating a local allograft layer failure (12%). Brackets indicate the % number of cases (adapted from [133]).

All three interfaces (stem-cement, cement-graft and graft-bone) are stronger in torsion than the bone itself [66]. Revision THR with impaction grafting gives a higher torsional mean stiffness (G) than primary THR, but with a lower maximum mean torque (T_{max}), but no statistically significant difference in strength or stiffness between the revision and primary groups was found. Malkani *et al.* [66] believed this is due to the variability in the quality of the bone in individual specimens. Re-revision cemented stems were also found to have less apparent shear strength (τ_{app}) than first revision cemented stems and primary THRs. In use, the implant is loaded with a combination of tensile, compressive and shear stresses. Testing these parameters separately may not successfully replicate the actual loading situation. A combined loading test might, therefore, be ideal to simulate the actual loading cycle during walking.

1.13. Impaction techniques

In the aforementioned discussion, the mechanical properties of bone graft and bone cement have been shown to depend on a number of variables such as graft preparation, impaction technique and design of instrumentation. Four types of variables (see below) have been categorised. Table A.1 (see §A.1 on Page 172 for full detail) lists 63 of the most common variables used in impaction grafting. Type I, II or III have been classified. Type IV is not included in the table since it is a combination of Type I, II or III.

- Type I – Preparation variables: This particular type is used for describing all variables in graft preparation. This value will be constant (or only change slightly) during the impaction grafting. For instance, the size of the graft (S) is determined by the blade size and shape of bone mill [78], the coefficient of the uniformity of the bone graft (C_u) is determined by the size and the grading of the graft [93]. Those variables will remain constant and are not affected by the impaction technique.

- Type II – Application variables: All variables can be controlled and have a known value. These types of variables usually depend on the design of instruments, surgical techniques and experience of the surgeon. For instance, a known force (F) or stress (σ) is applied on the system [120], and a known cement pressurisation pressure ($P_{pressure}$) is given by the cement gun [149].

- Type III – Impaction technique dependent variables: These variables do not have specific values and they change depending on the impaction technique used. In other words, they can be classed as passive variables. This kind of variable is generally difficult to control. For instance, the cement viscosity (η) increases with the mixing time [149], the cement penetration (t_{cement}) increases with the pressurisation pressure [150].

- Type IV – Hybrid variables: These are variables which can be classified into more than two of the above types. For instance, the stiffness (E) of the graft decreases with the amount of sterilisation (D) (Type I) [108], but also depends on the level or intensity of impaction (H) (Type II) [132]; the porosity ($P_{porosity}$) of the graft depends on the type of bone graft used (Type I) [127], but also depends on the impaction force (F) (Type II) [134].

In the past decade, numerous studies [78, 93, 94, 96, 105, 115, 118–120, 126, 141] have been performed to determine the optimal preparation techniques for bone graft to be used in impaction grafting. Although the optimal method has not yet been developed, the general understanding of Type I parameters is well known. For instance, less radiation, large particle size, better grading, defatting, removal of cartilage and soft tissue are known to improve the mechanical properties of the graft. In contrast, not much research [68, 115, 132] has been carried out to find the best impaction method. A good understanding of Type II parameters would be crucial to give a better control of Type III parameters leading to better mechanical properties of bone graft and a higher implant stability. Superior preparation techniques with a good impaction technique will lead to more successful impaction grafting.

1.13.1. Impaction energy

Table 1.8 shows the density and stiffness of the bone graft under different impaction conditions. It can be seen that higher impaction heights (i.e. higher impaction energy) gives better consolidated stiffness and apparent mass density, hence leading to high stability. Toms *et al.* [140] concluded that the migration distance of hip stems and tibial trays in knee surgery associated with impaction grafting can be largely predicted from the density of the compacted graft (i.e. the degree of compaction achieved). In addition, higher impaction energy and impact momentum were also found to provide higher implant stability under a cyclic compression test [78, 88]. A higher impaction force results in denser packing of graft chips (i.e. higher density) and a lower amount of graft porosity. During impaction grafting, the proximal impactor gives a higher impaction force than does the distal impactor for the same graft porosity [134]. However, the higher impaction force achieved with the use of the proximal impactor is probably required for the appropriate position of the canal.

Drop height (mm) x number of strokes	Number of pellets	AMD (g/cm^3)	BMD (g/cm^3)	ICME (MPa)	CCME (MPa)	TCME (MPa)
100×5	7	1.03	0.36	6.8	28.5	1.9
100×10	7	1.11	0.36	9.0	28.5	2.5
200×5	7	1.17	0.39	34.5	44.8	2.6
200×10	7	1.24	0.38	42.9	44.8	3.1
400×5	7	1.28	0.44	87.5	63.3	3.4
400×10	7	1.31	0.44	97.4	69.4	3.0

Table 1.8.: Comparison of apparent mass density (AMD), bone mineral density (BMD), impact constrained modulus of elasticity (ICME), consolidated constrained modulus of elasticity (CCME) and total constrained modulus of elasticity (TCME) under different impaction conditions (adapted from [132]).

1.13.2. Number of impactions

The degree of compaction is influenced by the total number of loading (impaction) cycles [153, 154]. Bavadekar *et al.* [126] investigated the effect of the number of impaction loads to the bone graft. It was found that the apparent stiffness increased with the number of impactions in a logarithmic manner, whereas the total deformation decreased with the number of impactions in logarithmic scale. The stiffness of the graft gradually reaches a steady state value ($\sim$42 MPa) starting from about 40 impactions [126]. Therefore, over-impaction will not improve the stiffness (i.e. CCME) of the graft, but does not jeopardise the implant stability. Nevertheless, over-impaction leads to an increase in the transient stiffness of graft (i.e. ICME), as shown in Table 1.8. If higher implant stability is desired, it is essential to increase the impaction energy rather than increase the total number of impactions, also over-impaction could predispose to femoral fracture. In addition, the effect of over-impaction on the graft can block the re-vascularisation needed for graft incorporation and prevent the new ingrowth of blood vessels.

1.13.3. Number of layers

Fosse *et al.* [132] demonstrated that surgeons can generate transient peak forces of around 250 – 750 N during impaction and this is an important value to determine the likelihood of a per-operative femoral fracture occurring. The peak force increases with the total number of impaction strokes as shown in Figure 1.41 because the material becomes stiffer with impaction [126]. However, the peak resistance force decreases with the number of graft layers because the fat and marrow within the bone graft damps out the applied compaction energy [94]. The first layer of bone graft has less damping ability to absorb impaction energy and hence it is subjected to the highest peak force.

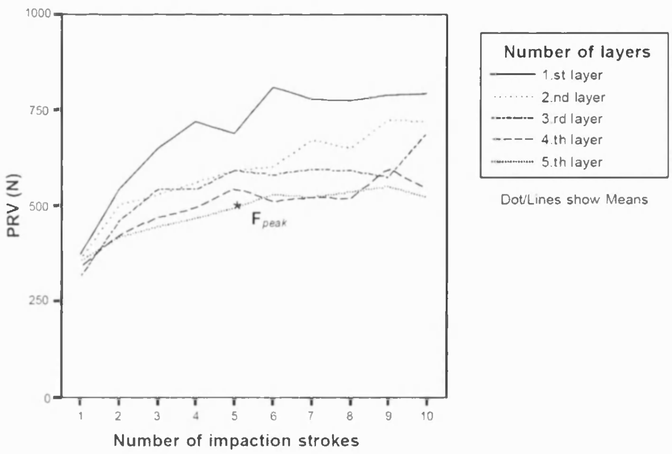

Figure 1.41.: Plot of peak resistance value (PRV) for each impaction showing the development for each of the five layers with slap hammer dropping from a height of 200 mm (adapted from [132]).

1.14. Lateral earth pressures

Brewster *et al.* [93] suggested that compacted morsellised bone is a friable particulate aggregate, and soil mechanics theory can be applied. The size and grading of graft were investigated. Voor *et al.* [115, 120] used geotechnical engineering testing techniques to study the mechanical properties of morsellised cancellous bone and the effects of defatting with hydroxyapatite. One-dimensional consolidation tests were used to determine the uni-axial strain, Young's modulus and creep rate. Brodt *et al.* [119] investigated the Young's modulus of the fresh-frozen human morsellised cancellous bone using a tri-axial compression test apparatus used in engineering soil mechanics tests.

As can be seen, there is an increasing interest in using engineering techniques from civil engineering because of the similarity of graft particles and soil particles. Various topics from a standard textbook of solid mechanics including lateral earth pressure, consolidation theory and compressibility were studied. When an implant is subjected to loading, it introduces a bending moment on the implant causing pressure differentiation of the bone graft (see Figure 5.9 on Page 151). This causes a different of pressure on the graft material around the stem. It was attempted to understand this phenomenon by lateral earth pressure. In the latter part of this section, a discussion was given on the correlation of lateral earth pressure to impaction grafting.

1.14.1. Introduction

In geotechnical engineering, it is often necessary to prevent lateral soil movements. As a result, it is necessary to estimate the lateral soil pressures acting on these structures, in order to be able to design them. In a homogeneous natural soil deposit, the forces acting on the granular material is determined by horizontal stress (α_h') and vertical stress (α_v'). The ratio of the horizontal stress and vertical stress (i.e. α_h'/α_v') is called the coefficient of earth pressure at rest (K_o) [155]. In the following sections (§1.14.2–§1.14.4), a cohesiveless material such as granular soil is discussed. Examples of the use of earth pressures are given in Figure 1.42.

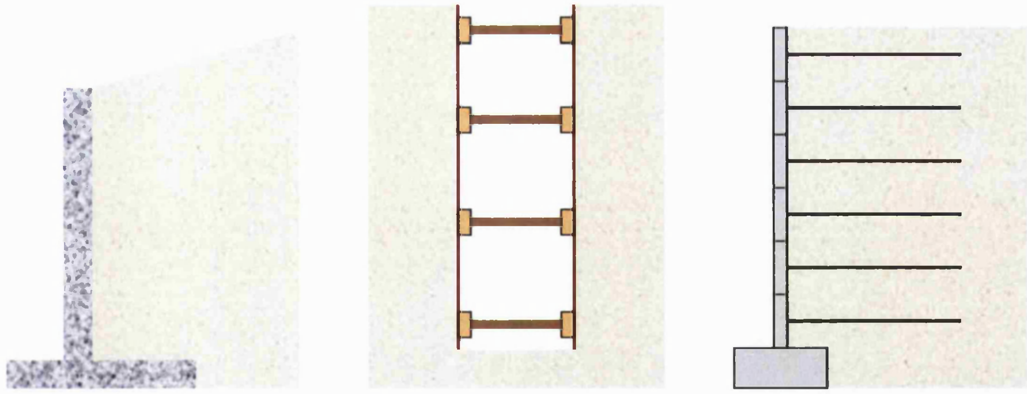

(a) Cantilever retaining wall (b) Braced excavation (c) Reinforced earth wall

Figure 1.42.: Examples of the use of lateral earth pressures (adapted from [155]).

Active and passive earth pressures are the two stages of stress in soils which are of particular interest in the design or analysis of shoring systems. Active pressure is the condition by which the earth exerts a force on a retaining system and the members tend to move toward the excavation. Passive pressure is a condition by which the retaining system exerts a force on the soil. Since soils have a greater passive resistance, the earth pressures are not the same for active and passive conditions [156]. Rankine's and Coulomb's theories are commonly used nowadays [157]. Positions of active and passive earth pressure are shown as A and B respectively in Figure 1.43.

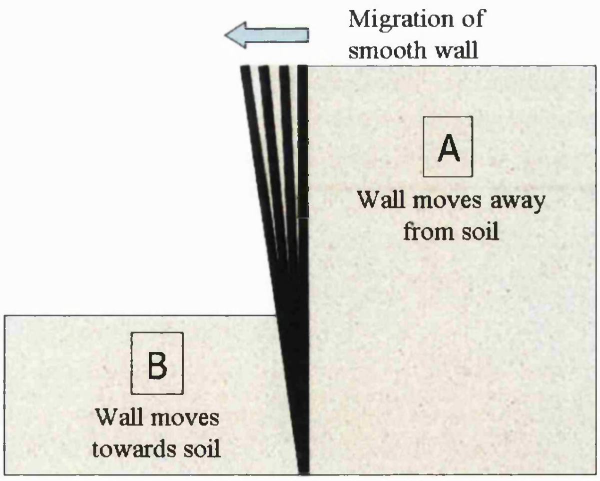

Figure 1.43.: Active earth pressure at point [A] and passive earth pressure at point [B] (adapted and modified from [155]).

1.14.2. Horizontal stress

In active condition, the wall moves away from the soil, $\alpha_v^{'}$ remains the same and the $\alpha_h^{'}$ decreases until failure occurs as shown in Figure 1.44(a); whereas in passive condition, the wall moves toward the soil, $\alpha_v^{'}$ remains the same and $\alpha_h^{'}$ increases until failure occurs as shown in Figure 1.44(b).

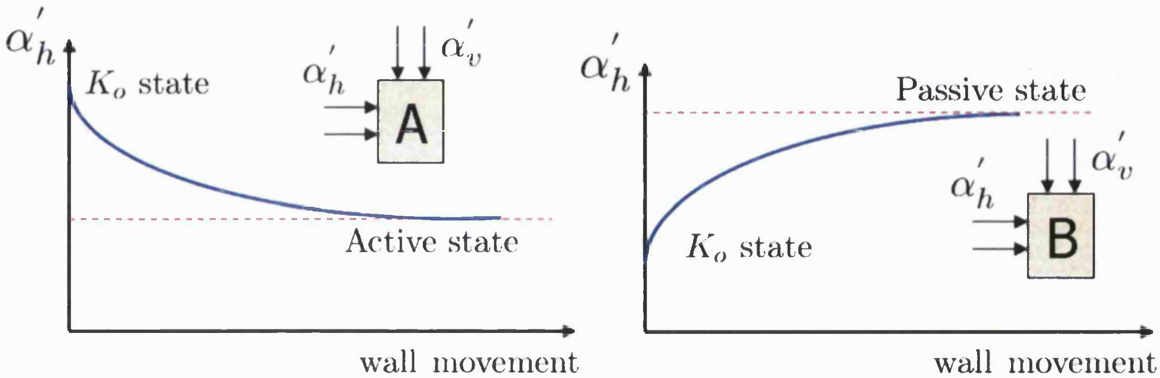

(a) Change of $\sigma_h^{'}$ at active mode (b) Change of $\sigma_h^{'}$ at passive mode

Figure 1.44.: Active and passive states (adapted and modified from [155]).

1.14.3. Modes of failure

At point A in Figure 1.43, the horizontal stress decreases as the wall moves away, so the soil appears less compressive. In terms of graphical representation, the size of the Mohr's circle increases as $\alpha_h^{'}$ decreases. The point at which failure occurs is called the active failure stress ($[\alpha_h^{'}]_{active}$). In contrast, at point B in Figure 1.43, the horizontal stress increases as the wall moves towards the soil due to the increasing level of compression force. Therefore, the size of the Mohr's circle decreases and then increases as $\alpha_h^{'}$ increases. The point at which failure occurs is called the passive failure stress ($[\alpha_h^{'}]_{passive}$). In both cases, failure occurs when the Mohr circle touches the failure envelope. Figure 1.45 shows the two different modes of failure. It should be noted that soil in the passive mode has a higher tensile failure stress than soil in the active mode.

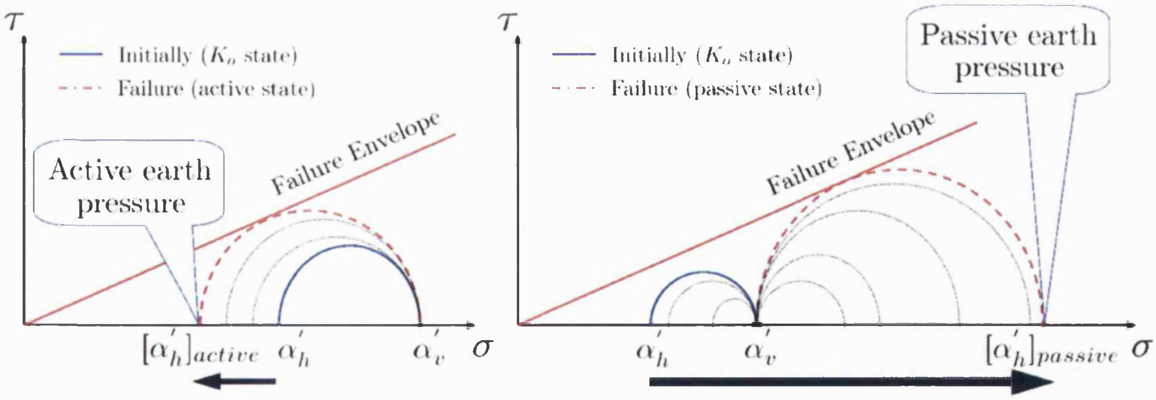

(a) Active failure mode (b) Passive failure mode

Figure 1.45.: Active and passive modes of failure (adapted and modified from [155]).

1.14.4. Angles of failure

The difference of active and passive pressures not only affect the failure stress, but also the angle of failure. In the active mode, the angle of failure with respect to the horizontal axis is $45° + \phi/2$ whilst in the passive mode, the angle of failure with respect to the horizontal axis is $45° - \phi/2$. Figure 1.46 presents the angles of failure at the two different modes. The relationship can be represented by Equation 1.1 and Equation 1.2.

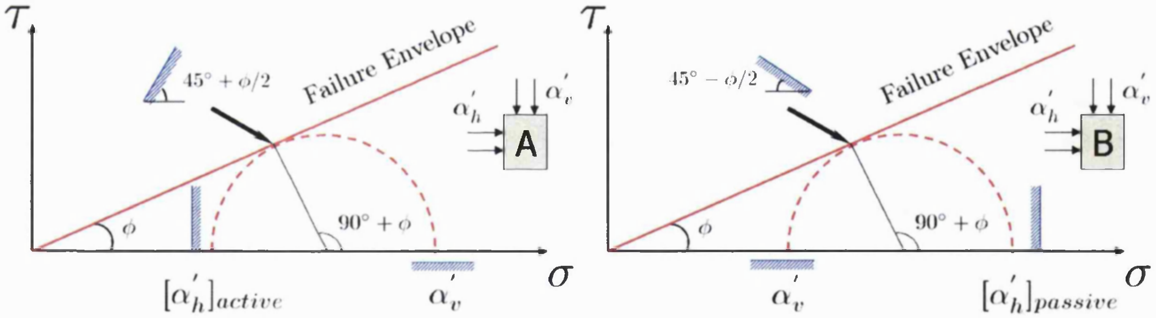

(a) Angle of failure at active mode (b) Angle of failure at passive mode

Figure 1.46.: Angle of failure at active and passive mode of failures (adapted and modified from [155]). Notes that figures are not in scale.

For granular soils (i.e. a cohesiveless material), the relationship can be represented by,

$$[\alpha_h^{'}]_{active} = K_a \alpha_v^{'} \tag{1.1}$$

where $K_a = tan^2(45° - \phi/2)$ = Rankine's coefficient of active earth pressure.

$$[\alpha_h^{'}]_{passive} = K_p \alpha_v^{'} \tag{1.2}$$

where $K_p = tan^2(45° + \phi/2)$ = Rankine's coefficient of passive earth pressure.

In the aforementioned discussion, the previous equations (Equation 1.1 and Equation 1.2) are only applicable to a cohesiveless material such as granular soils. However, for cohesive soils such as clays and clayey silts, constant cohesion (c) is required. This value of c is a material dependent constant. The equations can then be modified into Equation 1.3 and Equation 1.4.

$$[\alpha_h^{'}]_{active} = K_a \alpha_v^{'} - 2c\sqrt{K_a} \tag{1.3}$$

$$[\alpha_h^{'}]_{passive} = K_p \alpha_v^{'} + 2c\sqrt{K_p} \tag{1.4}$$

1.14.5. Correlation to impaction grafting

The theories of Rankine and Coulomb provide expressions for active and passive pressures for a soil mass at a state of failure [156]. It is assumed that the retaining wall is a smooth wall and the retaining structure is in a vertical position as happens most in civil engineering infrastructure applications. The inner surface of the medullary canal, however, is not a smooth surface due to bone loss after primary hip replacement. The angle of the position of the inner surface is also not vertical. Nevertheless, the Rankie and Coulomb expressions can provide a rough estimation of where the position of failure may occur.

In Rankine's mode, the vertical stress (α_v') stays constant during the wall movement. In total hip replacement, the joint is loaded under dynamic loading rather than statically. Therefore, the size of the Mohr's circle changes dynamically with respect to the loading force. Furthermore, the implant is loaded with an offset distance and because of the tapered design of the stem, the α_v' does need to be broken into vertical and horizontal components.

The horizontal stress (α_h') represents the stress acting horizontally on the bone graft material due to loading via the stem and cement mantle. As a result, the graft is compressed due to the movement of the stem and the cement mantle (i.e. wall movement). Graft is compressed as if under passive earth pressure. The horizontal stress could also partially contribute to the residual stress because of the relaxation of the graft after impaction. During full-load bearing, α_h' changes depending on the loading conditions, and the value varies from position to position. It is, therefore, very difficult to estimate the true value of α_h'.

Table 1.9 shows the value of cohesion, friction angle, and shear strength in two different studies. The value of cohesion has to be greater than zero. However, in the study of Dunlop *et al.* [94], a negative value of cohesion was found because of the extrapolation of results using a least squares fit as shown in Figure 1.47. Experimental results from these two studies showed that cohesion (c) was about $0 - 13.5$ kPa. The variability of cohesion comes from the donors' sex and age, size, grading, milling method, preparation technique and preservative method. The friction angle (ϕ) was found to be about $25.0° - 53.5°$. Mixing of ceramic into the graft gives the greatest impact on the value of cohesion and friction angle. Grimm [78] also reported that ceramic materials have a higher value of friction angle, but very low cohesion.

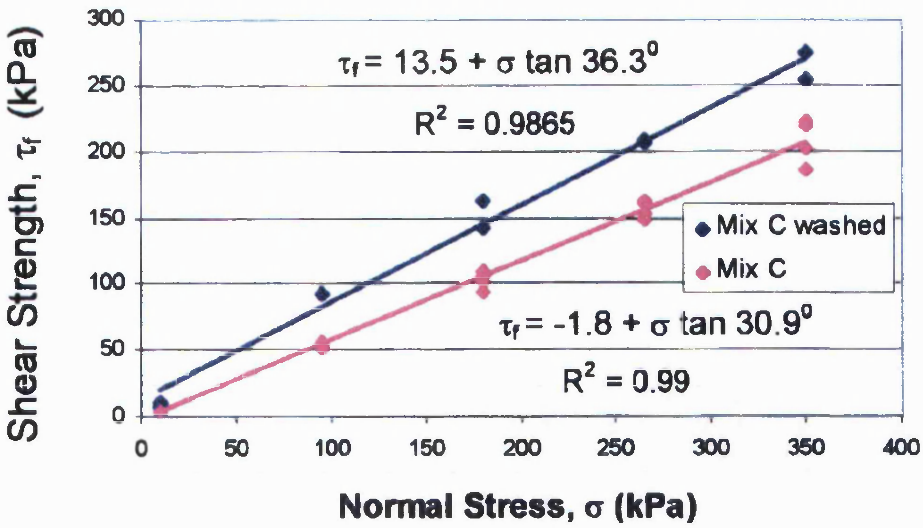

Figure 1.47.: Regression analysis trend lines of shear strength for non-defatted and defatted graft (adapted from [94]).

Graft	Defatting	Cohesion (c, kPa)	Friction angle (ϕ, deg)	Shear strength* (τ, kPa)	
Ovine	No	9.0	25.0	–	[78]
1 : 1 ovine/ceramic	No	5.5	43.6	–	..
1 : 9 ovine/ceramic	No	0.0	53.5	–	..
Mix A	No	10.2	29.9	212	[94]
Mix B	No	-0.9	35.0	244	..
Mix C	No	-1.8	30.9	208	..
Mix A	Yes	7.3	33.4	238	..
Mix B	Yes	13.5	37.5	282	..
Mix C	Yes	13.5	36.3	271	..

Table 1.9.: Cohesion, friction angle and shear strength of human graft. Mix A = Human graft, large particle size and with poor grading; Mix B = Human graft, intermediate particle size and with average grading; Mix C = Human graft, small particle size and with good grading. * Value was taken when graft was compressed at σ = 350 kPa.

The value of Rankine's coefficient K_a and K_p can be calculated by using the friction angle (ϕ) in Equation 1.1 and Equation 1.2. The calculated results are presented in Table 1.10. The higher the friction angle, the lower the Rankine's active coefficient and the higher the Rankine's passive coefficient. In other words, higher friction angle allowing the hip to carry higher loading capacity because of the bigger Mohr's circle.

Graft	Defatting	Friction angle (ϕ, deg)		Active coefficient (K_a)	Passive coefficient (K_p)
Ovine	No	25.0	[78]	0.41	2.46
1 : 1 ovine/ceramic	No	43.6	..	0.18	5.44
1 : 9 ovine/ceramic	No	53.5	..	0.11	9.19
Mix A	No	29.9	[94]	0.33	2.99
Mix B	No	35.0	..	0.27	3.69
Mix C	No	30.9	..	0.32	3.11
Mix A	Yes	33.4	..	0.29	3.45
Mix B	Yes	37.5	..	0.24	4.11
Mix C	Yes	36.3	..	0.26	3.90

Table 1.10.: Rankine's active and passive coefficients based on vary studies. Mix A = Human graft, large particle size and with poor grading; Mix B = Human graft, intermediate particle size and with average grading; Mix C = Human graft, small particle size and with good grading.

When a stem migrates toward one direction, for example the medial side, the graft on the medial side is under passive earth pressure and the lateral side is under active earth pressure. In other words, active and passive activities happen concurrently. Figure 1.48 demonstrates the active and passive regions when the implant is subjected to varus movement. The movement of the stem can be classified into a six degree of freedoms (DOFs) motion system. Table 1.11 gives the two pressures (either active or passive) which occurred in the 12 different types of movement at 16 possible positions. Ornstein *et al.* [64] found that the amount of distal (i.e. subsidence), medial, lateral and posterior migrations ranged from 1.4 – 4.3 mm, 0.6 – 2.1 mm, 0.5 – 1.0 mm and 0.8 – 8.8 mm respectively after two years post-operatively (see §1.8.1 on Page 25). Therefore, a low value of active failure pressure ($[\alpha'_h]_{active}$) and a high value of passive failure pressure ($[\alpha'_h]_{passive}$) can be expected in those directions listed by Ornstein *et al.* [64].

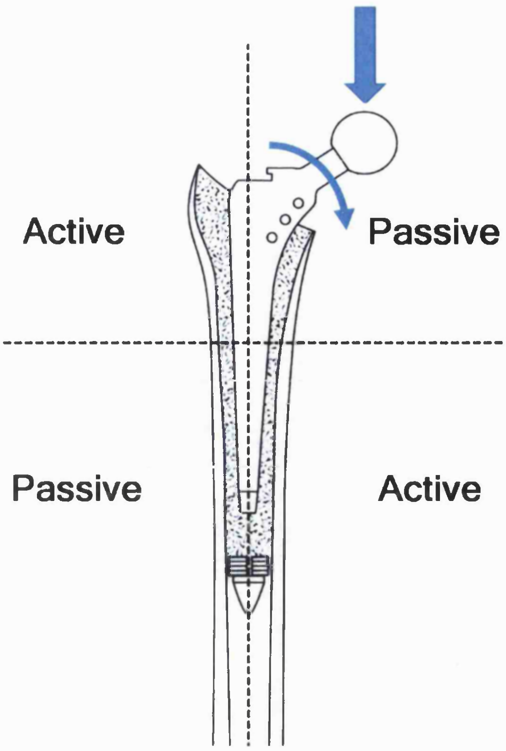

Figure 1.48.: Active and passive regions of bone graft under varus movement (adapted and modified from [18]).

Position	Direction(s)	Direction of movement											
		Anterior	Posterior	Medial	Lateral	Distal	Proximal	Varus	Valgus	Flexion	Extension	Anteversion	Retroversion
Medial	Distal	–	–	P	A	P	A	A	P	–	–	–	–
Lateral	Distal	–	–	A	P	P	A	P	A	–	–	–	–
Anterior	Distal	P	A	–	–	–	–	–	–	P	A	–	–
Posterior	Distal	A	P	–	–	–	–	–	–	A	P	–	–
Medial	Proximal	–	–	P	A	P	A	P	A	–	–	–	–
Lateral	Proximal	–	–	A	P	P	A	A	P	–	–	–	–
Anterior	Proximal	P	A	–	–	–	–	–	–	A	P	–	–
Posterior	Proximal	A	P	–	–	–	–	–	–	P	A	–	–
Anterior-medial	Distal/ Proximal	–	–	–	–	–	–	–	–	–	–	P	A
Anterior-laterial	Distal/ Proximal	–	–	–	–	–	–	–	–	–	–	A	P
Posterior-laterial	Distal/ Proximal	–	–	–	–	–	–	–	–	–	–	P	A
Posterior-medial	Distal/ Proximal	–	–	–	–	–	–	–	–	–	–	A	P

Table 1.11.: Classification of active and pressure in different positions at six degree of freedoms (A = Active pressure, P = Passive pressure, '–' = No change of pressure).

1.14.6. Discussion

The concept of geotechnical engineering has been recently used for determination of graft properties in impaction grafting. The concept of lateral earth pressures was proposed in this thesis. Active and passive earth pressures are two important concepts to understand the failure of granular materials including the modes of failure and angles of failure. The failure stress can be determined by the Rankine's coefficient and the amount of cohesivity of the material. However, the equations for lateral earth pressure were originally designed for small wall and retaining structure in its vertical position. The inner surface of the medullary canal, however, is not a smooth surface due to bone loss after primary hip replacement. The angle of position of the inner surface is also not vertical.

An extensive study would be required to modify those equations so that they can fit in with the real situation of impaction grafting. Furthermore, the modified equations would be very case specific, meaning that the equations will only be suitable for a specific geometry. It will be practically difficult to apply these equations. The dynamic movement of human activities would also be hard to simulate in *in-vitro* experiments. As a result, the theory of lateral earth pressures was not applied in this study. However it is recommended that further studies in this area could be performed to attempt to validate this particular theory for use in impaction grafting.

1.15. Conclusions

Impaction grafting used in the reconstruction of acetabular protrusio and the creation of a neo-medullary femoral canal has evolved for over a decade. It was originally proposed by Gie *et al.* [12, 34]. A number of promising results and numerous problems have been recorded. Primarily, the classification of Endo-Klinik [51] and Gustilo and Pasternak [52] are used to determine the amount of bone stock loss. Component subsidence and femoral fractures are the two main complications in impaction grafting.

Stulberg [42, 43] subsequently modified the technique by using a tapered polished impactor instead of a flat-end distal impactor, which resulted in radial impaction grafting (RIG). The initial seven year results associated with this technique were encouraging. De Thomasson [55] depicted a developed Exeter technique. A Mersilene mesh was used to prevent the dispersion and extrusion of the graft through potential cortical defects the during impaction grafting. The clinical results showed that this technique appears to be reliable.

Allograft is commonly used because of the lack of autologous bone stock. A wide range of preparation techniques have been suggested including fresh-frozen, freeze-dried, autoclaved, irradiated, alkaline treatment and acidic treatment. The fresh-frozen method is currently recommended because of its better mechanical properties. However, it has high risk of disease transmission such as hepatitis and HIV, so screening processes are essential to minimise this risk.

Morsellised bone graft materials have to be constrained in order to carry out experiments on them and be characterised by apparent values in order to replicate the actual loading environment behaviour during impaction grafting. The amounts of graft size, grading, defatting and mixing of extender into the graft have a significant effect on the mechanical properties of the graft such as compressive stiffness and resistance to shear. The mechanical properties can be quantified by the mechanical strengths such as Young's modulus, analysis of stress-strain behaviour and Poisson's ratio. In addition, time-dependent properties such as creep and relaxation are commonly used to determine the viscoelastic properties of the graft. To date, little research has been performed on investigating the viscoelasticity of the bone graft.

Superior graft preparation techniques, without a good impaction technique, will not lead to successful impaction grafting. Hence, four fundamental types of variables have been defined, Type I – Preparation variables, Type II – Application variables, Type III – Impaction technique dependent variables and Type IV – Hybrid variables. Relationships between different parameters have not been well explored to date. Currently, there is no standard test to quantify the mechanical properties of bone graft material [158]. As a result, much of the published data are not comparable because different test techniques have been used. For instance, a wide range of values of the modulus of elasticity have been measured (9.0 – 100 MPa). A good understanding of the variables would allow more accurate prediction of the results of the impaction grafting and impaction techniques used, and therefore contribute to achieving improved implant stability.

In an attempt to apply geotechnical engineering theories concepts to impaction grafting, the theory of lateral earth pressures was studied. Two factors were identified: active and passive earth pressures. These are important concepts to understand the failure of granular materials. However, it is practically very difficult to apply the theory of lateral earth pressure to impaction grafting as this theory is based on various assumptions such as a smooth surface and a vertical wall. Whilst it was not considered practical within the framework of this project to carry this work forward, it is recommended that further work could be carried out to modify this theory, to make it more applicable to impaction grafting.

1.16. Objectives

The primary objective of this study was to quantify the mechanical properties of the bone graft in terms of both static and dynamic behaviour. The secondary objective was to optimise the impaction grafting processes so that better implant stability can be obtained. Chapter 1 includes an extensive literature review on impaction grafting. Chapter 2 discusses the graft preparation techniques. Chapter 3 and Chapter 4 explore different aspects of bone graft mechanics; Chapter 5 focuses on the clinical aspects of impaction bone grafting.

In detail, this thesis is divided into the following chapters.

- Chapter 1 provides an extensive literature review on the principles of impaction grafting and the basic science behind impaction grafting.
- Chapter 2 discusses how bone graft is prepared during the experiments, and provides a comparison of defatting techniques. Various methods of defatting have been identified such as using acetone, chloroform, detergent and lavage as well as incubation.
- Chapter 3 identifies the viscoelastic properties of bone graft material. Dynamic properties including Poisson's ratio, stiffnesses, recoil and relaxation are measured. Parameters are analysed so as to identify the correlation between different combinations of settings. The stress-strain relationship, stiffness and strain energy of graft material are also discussed in detail. This is achieved by compressing morsellised bone chips in a thin-walled aluminum cylinder fitted with strain gauges. Three parameters are used including defatting of the graft, load rate and pre-loading.
- Chapter 4 investigates the effect of repetitive cyclic loading and the rate of impaction on morsellised bone graft. The effects of different impaction frequencies and rates are defined. Experimental results including strain-stress characteristics, recoil and relaxation are also presented. An uni-axial test with a thick-walled cylinder is employed for the investigation. Four loading frequencies are used 0 Hz, 0.17 Hz, 1 Hz and 2 Hz to simulate various *in-vitro* conditions. In addition, the effect of the rate of impaction is determined by compressing the graft using single ramp impactions at high stresses.
- Chapter 5 explores the effect of cementation on revision stem stability. An *in-vitro* study is carried out and the mechanical stability is examined. The experiment uses composite femurs with the 'cancellanous' bone removed and the diameter of the medullary canal increased to simulate the bone loss associated with the femur in revision surgery. The experiment compares a cemented stem with a larger uncemented stem using impaction grafting.
- Chapter 6 summarises the findings and discusses work that could be carried out in the future.
- Appendix A presents all the detailed experimental data.
- Appendix B lists publications produced during this study.

2. Bone graft preparation

2.1. Preparation of graft

Porcine bone from femoral heads was used in all of the experiments. Graft came from healthy pigs which were bred for food production. As a result, the variability between specimens should be reduced as the age, size and nutrition of the pigs would be the same. In addition to reduce to the variability, graft was obtained from the same batch for the same experiments. This variability would be less than human allograft used in impaction grafting. The primary source of human allograft comes from patients who receive primary hip replacement. These patients probably suffered from arthritis and osteoporosis. For the purposes of testing and a more consistent bone graft, porcine graft was used to allow better correlation of the different test regimes.

A standardised method of graft preparation was used. Porcine bone from femoral heads was used in all of the experiments. Raw material was obtained from a local abattoir and was frozen and stored at $-25°C$. Before preparation, the bone was defrosted at room temperature for 2 hrs. Cartilage and soft tissue were then removed with great care by a scalpel as illustrated in Figure 2.1. The femoral heads were cut off using a hacksaw, from the proximal femur just below the cartilage line to the distal end of the less trochanter as illustrated in Figure 2.2.

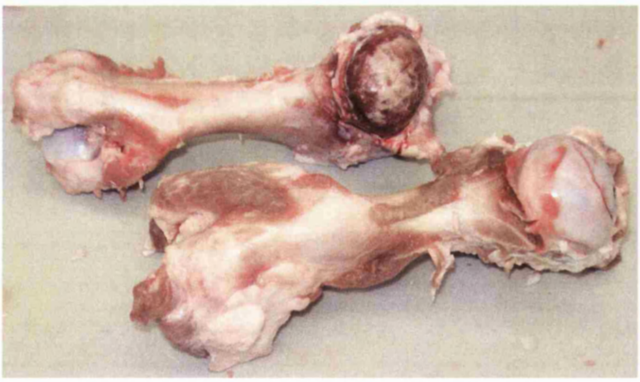

Figure 2.1.: A comparison between fresh (bottom) and prepared femur (top).

(a) Cartilage free porcine femoral head (b) Porcine femoral heads

Figure 2.2.: a) Cartilage and soft tissue were removed by a scalpel. b) Range of femoral heads cut off from the femur.

The preparation of graft can be summarised as follows:

- Defrosting raw material at room temperature for 2 hrs.
- Removal of cartilage and soft tissue arround the heads by a scalpel.
- Cutting the head off by a hacksaw.

2.2. Preparation of non-defatted MCB

A Norwich bone mill with a coarse blade was used in all of the experiments. A disassembly and general assembly diagram of the Norwich bone mill is shown in Figure 2.3. The Norwich bone mill consists of six different parts. The coarse blade and the graft delivery tube are the most important elements of the mill. Because of the design of the blade, various graft sizes were produced. During milling, the majority of the graft was stored inside the circular blade as shown in Figure 2.4. Graft was transferred and stored. Graft was then manually inspected. Any bigger, chunky cortical fragments and any visible soft tissue were removed. Large cancellous bone fragments (> 20 mm) were broken down to size by hand. Graft sizes smaller than 2 mm were also removed. As a result, graft sizes ranged from around 2 mm to 20 mm mean length. No particular attention was paid to the shape and the graft distribution. Finally, graft was stirred using a spatula to form a homogenous mixture. This helped to minimise the variation of bone quality from batch to batch. Graft was then stored at $-25°C$ and defrosted thoroughly at room temperature for 2 hrs prior to testing. In order to minimise the effect of multiple freeze-thaw cycles on the mechanical properties of the graft as discussed by Grimm [78], the graft was only defrosted when necessary. After each experiment, morsellised cancellous bone grafts (MCB) was not re-used due to internal fracture during impaction, new graft was used in each new test.

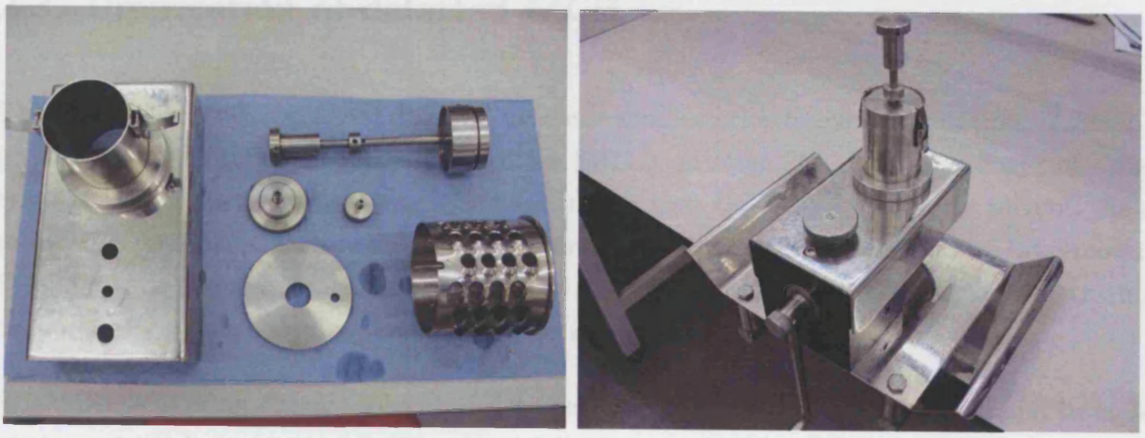

(a) Disassembly diagram (without base) (b) General assembly diagram

Figure 2.3.: a) Norwich bone mill consists of six different parts. b) Norwich bone mill general assembly diagram.

(a) Operation of bone mill (b) Extracted morsellised bone graft

Figure 2.4.: a) Majority of the graft was stored inside the circular blade. b) Graft was extracted from the circular blade and was ready to be stored or used.

The preparation of fresh MCB can be summarised as follows:

- Milling with Norwich bone mill.
- Removal of large cortical fragments and any visible soft tissue.
- Discarding small graft (< 2 mm) and breaking down large chips (> 20 mm) by hand.
- Storage of graft at −25°C.
- Defrosting graft material at room temperature for 2 hrs whenever necessary.

2.3. Preparation of defatted MCB

The morsellised graft used was defatted for some studies prior to experimentation. Table 2.1 gives different methods of defatting (also see §1.11.3 on Page 36). The advantages of using organic solvent such as acetone and cholorform are that they are a strong fat solvent. As a result, it is possible to achieve a very low fat content. Detergent is also an effective fat remover. Pulsed lavage is good for reducing superficial bacterial bioburden [121] and for penetrating deeper surfaces, but extra equipment may be required.

It is unlikely that an organic solvent or detergent can be used in clinical environment because of the potential chemical risk. For simplification and more clinical relevance, warm water was used in all cases. Defatted bone graft was prepared by soaking the graft in water at 35°C water for 20 mins so as to avoid thermal damage of the graft. The temperature was constantly monitored by a Fluke 52 thermometer (Fluke Inc.) at 1 min time intervals as shown in Figure 2.5(a). Graft was then extracted by a sieve as shown in Figure 2.5(b) and excessive water was absorbed using tissue paper. Bone graft was kept on a dry tissue at room temperature for 2 hrs prior to testing. Figure 2.6 shows the effect of washing of the graft. The actual amount of water content was not measured. Similarly, graft was then stored at −25°C and defrosted at room temperature for 2 hrs whenever necessary.

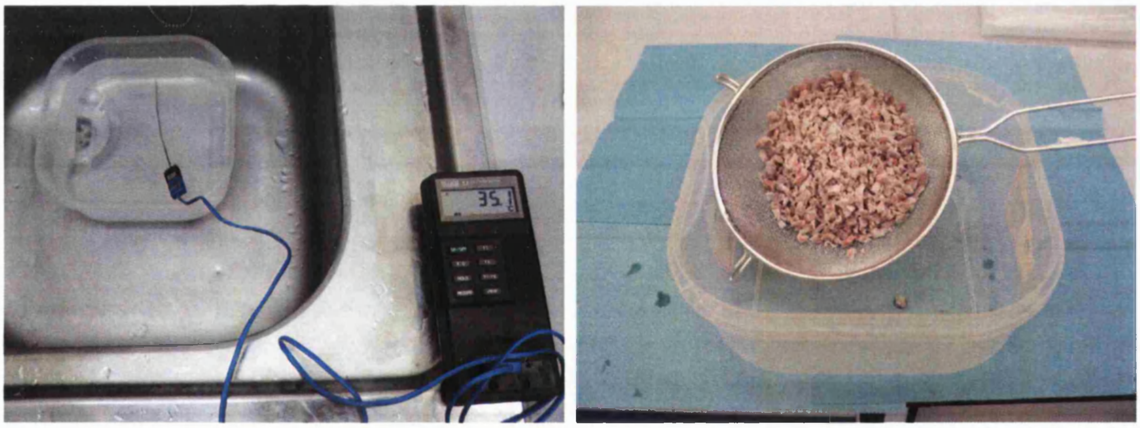

(a) Fluke 52 portable thermometer (b) Graft was washed and sieved

Figure 2.5.: a) The water temperture was controlled within 35 ± 1°C. b) MCB was soaked at 35°C water for 20 mins. Graft was then sieved and dried by tissue.

Method	Procedure	Advantages	Disadvantages
Acetone [70]	Soaked in acetone for 48 hrs	+ Cost effective + Strong fat remover + Strong organic solvent	– Can pass through skin [159] – Danger of breathing fumes – Flammable liquid – Irritant to eyes, nose and throat – Risk of damaging protein [160]
Chloroform [92]	Soaked in chloroform	+ Cost effective + Strong fat remover + Strong organic solvent	– Carcinogen [161] – Can pass through skin – Exposure can cause dizzy – Risk of damaging protein [160]
Detergent [115]	Soaked at 80°C detergent	+ Cost effective + Low temperature can be used + Strong fat remover	– Causes thermal-damage
Incubation [160]	Stored at 40°C for three weeks	+ No coagulation of protein + No mixing of harmful substances + No change of the graft distribution	– Fat retained within the graft – Time consuming – Graft dries out with time
Pulsed lavage [94]	Pulsed with warmed 0.9% saline	+ Capable of penetrating deeper + Completely safe + Reduce superficial bateria [121]	– Drying of graft required – Requires extra equipment
Water	Soaked at 35°C water for 20 mins	+ Completely safe + No thermal-damage + No coagulation of protein [160]	– Drying of graft required – Fat retained within the graft

Table 2.1.: Comparison of different defatting techniques.

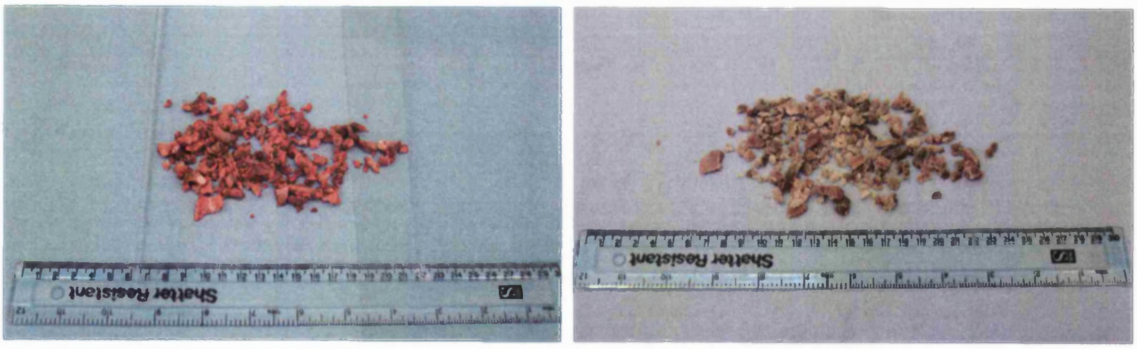

(a) Non-defatted bone graft (b) Defatted bone graft

Figure 2.6.: a) Fresh MCB with different particle sizes. b) Defatted MCB with different particle sizes. It can be observed that the colour faded out to white and grey as blood and fat were washed out.

The preparation of defatting MCB can be summarised as follows:

- Soaking graft at 35°C water for 20 mins.
- Extracting graft by a sieve.
- Drying graft on dry tissue for 2 hrs prior to testing.
- Storage of graft at −25°C.
- Defrosting graft material at room temperature for 2 hrs whenever necessary.

For illustration purposes, six large chips (i.e. ~ 20 mm) were selected as shown in Figure 2.7. They were milled by the Norwich bone mill. Three MCBs on the right hand side were defatted and dried in contrast the fresh MCBs on the left. It can be observed that the majority of the blood and fat was washed out as the colour faded significantly. In other words, the properties of the graft changed in terms of appearance and composition. Nevertheless, the shape of the graft (i.e. the volume) remained the same.

Figure 2.7.: A close look of large non-defatted MCB (left) and defatted MCB (right) chips. The porosity increased after washing as blood and fat were washed out.

3. Dynamic properties of morsellised bone graft

3.1. Introduction

The aim of this study was to examine the effect of loading rates, pre-loading and defatting on bone graft. Variables including hoop strain, compressive force, mass, total constrained apparent Poisson's ratio (TCPR) and recoil were determined. A simple thin aluminium tube with strain gauges attached was used in the experiment. The primary objective of this experiment was not to acquire precise material properties of the graft but to compare material properties of the graft under different impaction conditions.

3.2. Design of test rig

The test rig consisted of four parts, a plunger, a die, a base and a sample extractor as shown in Figure 3.1 and Figure 3.2. The plunger was made of mild steel (EN1A) and had a diameter of $18.5^{+0.00}_{-0.01}$ mm. The die was 60 mm long and made of aluminium (6082) and had a $19^{+0.00}_{-0.05}$ mm internal diameter and 20 mm external diameter. The small clearance between the plunger and the die allowed fluid to escape and also provided a constrained environment for bone graft during impaction. Both the plunger and the die were polished to minimise any friction generated during impaction. Two 350 Ω open-faced strain gauges (Model N2A-13-T004R-350, Vishay Measurements Group, UK) were mounted perpendicular to the cylinder axis (to measure hoop strains) opposite to each other on the outer surface of the die. The Sawbones surface was degreased and dry abraded. Then, the surface was cleaned and the position was marked. The strain gauges were attached by M-bond 200 adhesive (Vishay Measurements Group, UK). The strain gauges were aligned perpendicular to the long axis of the die such that the hoop strain could be measured. Three additional pins were installed near the bottom of the base (mild steel, EN1A) in order to fix the position of the die. These pins also provided an additional route for fluid escape.

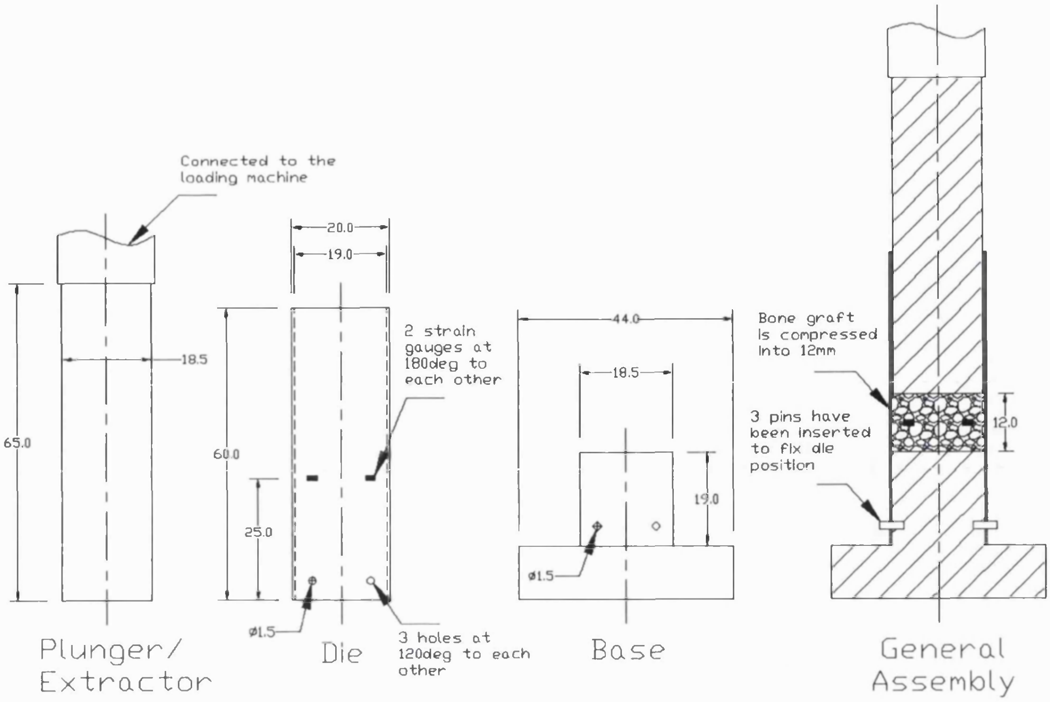

Figure 3.1.: Drawings of the plunger, extractor, die and base, and a general assembly diagram (unit in mm).

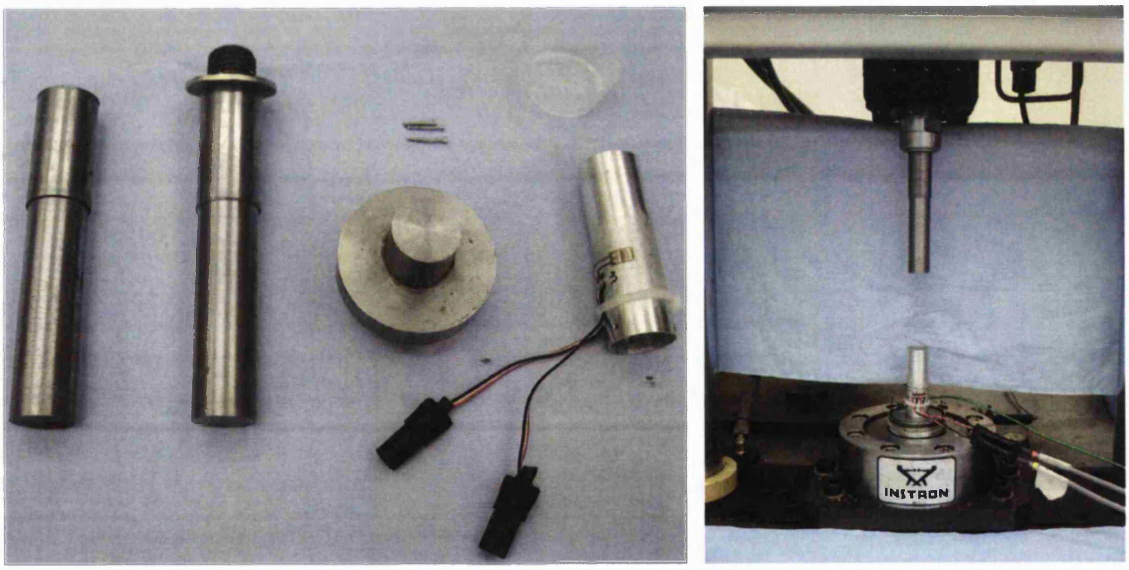

(a) Rig design

(b) Instron 8511 loading machine

Figure 3.2.: a) Illustration of the extractor, plunger, base, die, pins and measuring cup. b) General assembly rig mounted in the Instron loading machine.

3.2.1. Signal processing

The following calculations were used to estimate the strain of the strain gauges, viz.:

1. Quarter bridge configuration was used in this experiment.
   - The strain of the system was calculated by using $\varepsilon = 4 \times \frac{V_o}{V_s} \times \frac{1}{S}$, where ε= Output strain, V_o= Output voltage, V_s= Supply voltage = 4.021 V, S= Gauge factor = 2.11
2. In addition, the interfacing card had a built-in amplifier with amplification value of 2000.
   - Hence, the strain can be calculated by using $\varepsilon = \frac{4}{2000} \times \frac{V_o}{V_s} \times \frac{1}{S}$
3. In order to minimise the noise during data acquisition, the Instron load cell was grounded by wiring it to the computer.

3.3. Method

A fixed volume of prepared graft was loaded into the die. The amount of MCB was determined by volume rather than by mass because this is in practice similar to the clinical situation. 10 cm^3 of MCB was measured into a plastic measuring cup. The net weight was also measured by an electronic balance (AC-12K, Adam Equipment, UK). Graft was then inserted carefully into the aluminium die and lighly impacted using the index finger to make sure graft settled near the base. The desired load rate (either high or low speed) was inputted from the Instron control panel prior to testing. A single ramp input was used to provide a linear velocity during impaction as shown in Figure 3.3 on Page 81.

Material was uni-axial loaded in uni-axial compression using an Instron servo-hydraulic 8511 machine. Two different load rates, 7.5 mm/s (low speed) and 60 mm/s (high speed), were used. It is noted that 60 mm/s is the maximum speed of the material testing machine. Preliminary testing showed that 7.5 mm/s was sufficient to determine the viscoelastic effect. In order ensure the viscoelastic effect could be determined, the value of 7.5 mm/s was chosen. The specimen was pre-loaded either with 1 N (no load) or 250 N (high load, about one-third of the body weight). Non-defatted (no treatment) and defatted (with treatment) grafts were used.

When 'no load' was used, the graft was pre-loaded by 1 N in order to determine the contact position. The purpose of applying 1 N was not to compress the graft, but to determine the initial position. Therefore, this is defined as 'no load' condition. For the 'high load' test, in order to minimise the viscoelastic effect, the stroke moved at 0.5 mm/s and stopped provided load reached 250 N. It was observed that some relaxation occurred when the stroke was stopped. Due to the test set up constraints, it took time to setup the Instron and initiate the data acquisition system (HPVEE, Hewlett-Packard VEE). As a result, 1 min was allowed for setting up the equipment. Graft was then compressed into a thickness of 12 mm (equivalent to a volume of 3.77 cm^3 ($= \frac{\pi(2)^2}{4} \times 1.2$)). This thickness was chosen because it was found (by trial and error) that it gave reasonable strain readings without damaging the die. Primary parameters including stroke position, compressive force and strain gauge outputs were monitored by HPVEE at 8000 Hz per channel. After each test, the graft was extracted by the sample extractor. A vernier calliper was used to measure the sample thickness, and the amount of recoil was determined by the change of thickness of the graft.

3.4. Experimental design

3.4.1. Design of experiment

In the design of the experiment (DoE), a 2-level factorial design was employed. DoE is a method for determining the significant factor(s) and interaction between various parameters. Three parameters, defatting, pre-loading and load rate were classified as attribute data (i.e. low or high). A 3-factor full factorial experiment design (i.e. $2^3 = 8$ experiments) was chosen with a number of six replications of each setting for statistical purposes. Therefore, 48 ($= 2^3 \times 6$) experiments were performed. A 2^3 full factorial DoE is shown in Table 3.1. The run order represents the statistical order that the experiment was designed for. Following the run order to perform the experiment (as shown in Table A.2 on Page 174) introduces randomisation of the experiment and eliminates bias of experimental settings. When the run order is used, it practically means using non-defatted and defatted graft alternatively, and there was no enough time to finish the experiment within the same day. If the experiment cannot be finished within the same day, and the graft is re-frozen, the composite of the graft (i.e. water content) will change and the results will not be accurate on the next day. Therefore, the standard order was used. The standard order represents the actual order that the experiment was run. The statistics package Minitab 14.20 (Minitab Inc.) was used to analyse the experimental data.

Symbol	−	+
Fat content	Non-defatted	Defatted
Pre-loading	Pre-loaded with 1 N (i.e. no load)	Pre-loaded with 250 N
Load rate	Impact at 7.5 mm/s	Impact at 60 mm/s

Standard order	Run order	Defatting	Pre-loading	Load rate
1	1	−	−	−
2	5	+	−	−
3	6	−	+	−
4	2	+	+	−
5	3	−	−	+
6	7	+	−	+
7	4	−	+	+
8	8	+	+	+

Table 3.1.: Full factorial DoE with one replication.

The experimental procedures can be summarised as follow:

- Initialise the Instron and setup the rig.
- Measure 10 cm^3 of MCB and record the net sample weight by electronic balance.
- Insert the bone graft into the aluminium die.
- Adjust the load cell to zero.
- Pre-load with either 1 N (i.e. 'no load') or 250 N,
  - move the stroke at speed 0.5 mm/s and stop the actuator when 1 N compressive force was detected, in order to determine the contact position.
  - move the stroke at speed 0.5 mm/s and stop the actuator when 250 N compressive force was measured and wait for 1 min.
- Initialise the Instron and data acquisition system.
- Compress graft to a specimen thickness of 12 mm with the desired load rate (7.5 mm/s, 60 mm/s).
- Remove the sample using the extractor and measure the thickness of the sample with a vernier calliper.

3.4.2. Sources of error

Table 3.2 gives the sources of error that could effect the accuracy of this experiment.

Source of error	Likelihood
Assumption of $\varepsilon_{bone\,r} \simeq \varepsilon_{Al}$, accuracy depends on t_{Al}	Medium
Inaccuracy of the acquisition system at high speed	Low
Misalignment of strain gauges	Low
Strain gauges debonding	Low
Strain gauges not in optimised position	Medium
Variability of graft properties from batch to batch	Low

Table 3.2.: Sources of error.

3.5. Estimation of Poisson's ratio

Table 3.3 provides the variables which were used in the experiment. Total constrained apparent Poisson's ratio is defined by overall change of Poisson's ratio. In order to estimate the TCPR, it was essential to measure the deformation of aluminium during the impaction. The required equations are also listed below.

Variable	Value	Unit	Quantity	Remark
$\varepsilon_{Al\,\theta}$		$\mu\varepsilon$	Al hoop strain	Measured by strain gauges
$\varepsilon_{Al\,r}$		$\mu\varepsilon$	Al radial strain	Estimated by Equation 3.1 via HPVEE
r_{in}	9.5	mm	Al tube inner radius	Known
r_{out}	10	mm	Al tube outer radius	Known
r'_{out}		mm	Al tube outer radius (after impaction)	Used in Equation 3.1
l_{recoil}		mm	Graft thickness (after the graft was extracted)	Measured by vernier calliper
m		g	Graft mass	Measured by electrical balance
$\varepsilon_{bone\,r}$		$\mu\varepsilon$	Graft hoop strain (r)	Estimated by Equation 3.2
$\varepsilon_{bone\,z}$		$\mu\varepsilon$	Graft vertical strain (z)	Measured by Instron via HPVEE
ν_{app}		–	Graft apparent Poisson's ratio	Estimated by Equation 3.3
R_{recoil}		%	Recoil	Estimated by Equation 3.4

Table 3.3.: Notation, quantity and units used in the estimation of the Poisson's ratio.

The following calculation shows that the radial strain ($\varepsilon_{Al\,r}$) of the alumimium tube is the same as the hoop strain ($\varepsilon_{Al\,\theta}$).

$$\varepsilon_{Al\,\theta} = \frac{2\pi r'_{out} - 2\pi r_{out}}{2\pi r_{out}} = \frac{r'_{out}}{r_{out}} - 1$$
$$\varepsilon_{Al\,r} = \frac{2r'_{out} - 2r_{out}}{2r_{out}} = \frac{r'_{out}}{r_{out}} - 1$$

so,

$$\varepsilon_{Al\,r} = \varepsilon_{Al\,\theta} \tag{3.1}$$

By definition of a thin walled cylinder, $\frac{r_{in}}{r_{out}-r_{in}}$ has to be greater than 20. Currently the ratio is $\frac{9.5mm}{0.5mm} = 19 \simeq 20$, so that the thin walled cylinder equation can be applied. So $\varepsilon_{bone\,r} \simeq \varepsilon_{Al\,r}$, and the strain of the aluminium die was estimated by the expansion of bone graft.

$$\varepsilon_{bone\,r} \simeq \varepsilon_{Al\,r} \tag{3.2}$$

Using Equation 3.1 and Equation 3.2, the total constrained apparent Poisson's ratio (TCPR) was found by the following equation.

$$\nu_{app} = -\frac{\varepsilon_{bone\,r}}{\varepsilon_{bone\,z}} \simeq -\frac{\varepsilon_{Al\,\theta}}{\varepsilon_{bone\,z}} \tag{3.3}$$

The amount of recoil was calculated based on the expansion of the graft.

$$R_{recoil} = \frac{l_{recoil} - 12}{12} \times 100\% \tag{3.4}$$

3.6. Results and discussion

3.6.1. Summary of results

Table 3.4 shows a summary of all the experimental results. Full detailed experimental results are listed in Appendix A.2 on Page 174. The mean (i.e. the average) of each of the parameter was recorded. The standard deviation was calculated by the statistical package Minitab 14.2 (Minitab Inc.).

Run order	1 – 6	7 – 12	13 – 18	19 – 24
Defatting (D_{defat})	–	–	–	–
Pre-loading (P_{load})	–	+	–	+
Load rate (R_{load})	–	–	+	+
Mass (m, g)*	5.14 (0.31)			
Max. hoop strain ($\varepsilon_{bone\,\theta}$, $\mu\varepsilon$)	613 (254)	638 (162)	769 (96)	870 (264)
Max. axial force (F, N)	1492 (265)	1569 (253)	1898 (302)	1790 (551)
TCPR ($\times 10^{-3}$)	0.98 (0.42)	1.93 (0.50)	1.19 (0.13)	2.50 (0.39)
Recoil (R_{recoil}, %)	38.9 (2.37)	39.0 (1.96)	36.2 (4.12)	37.5 (5.52)

Run order	25 – 30	31 – 36	37 – 42	43 – 48
Defatting (D_{defat})	+	+	+	+
Pre-loading (P_{load})	–	+	–	+
Load rate (R_{load})	–	–	+	+
Mass (m, g)*	5.07 (0.27)			
Max. hoop strain ($\varepsilon_{bone\,\theta}$, $\mu\varepsilon$)	633 (152)	939 (261)	1246 (265)	1135 (327)
Max. axial force (F, N)	2021 (381)	2309 (432)	2560 (407)	2243 (367)
TCPR ($\times 10^{-3}$)	0.95 (0.25)	2.14 (0.59)	1.87 (0.44)	2.51 (0.57)
Recoil (R_{recoil}, %)	38.4 (2.55)	39.4 (3.43)	39.5 (3.58)	39.9 (4.34)

Table 3.4.: Summary of mean and one standard deviation (presented in parentheses). *Mass is a variable independent to pre-loading and load rate.

3.6.2. Typical experimental results

3.6.2.1. Displacement, axial force and hoop strain versus time

A typical impaction result is shown in Figure 3.3. The stroke movement, uni-axial force and the results of the two strain guages were plotted. All four lines share the same y-axis to allow better comparsion. The y-axes was labelled for the corresponding data so that direct comparison of results at same time step was possible. The values of the forces and displacements represent compressive forces when the stroke moves down; the values of the strain gauges represent the amount of extension of the aluminium. As can be seen, strain and the peak force reached the highest value just before the stroke stopped. As soon as the stroke was stopped, relaxation occurred instantaneously.

In Figure 3.3, at about 0.2 s, the reading from of the strain gauge (1) increased. This suggested that an individual bone graft particle was suddenly no longer able to provide mechanical support. Technically speaking, the stress exceeded the ultimate strength of individual bone graft particles, and this caused the fracture of the graft particle. After the testing, it was observed that the sizes of graft particles decreased. Furthermore, the difference in maximum value of the two strain gauges represented uneven distribution of load on the aluminium tube. Hence, bone graft presented non-homogenous behaviour. There was a possibility that the difference came from the misalignment between two strain gauges. In order to determine the strain, an average of the two strain gauges was used. The average result is shown in Table 3.4 on Page 80.

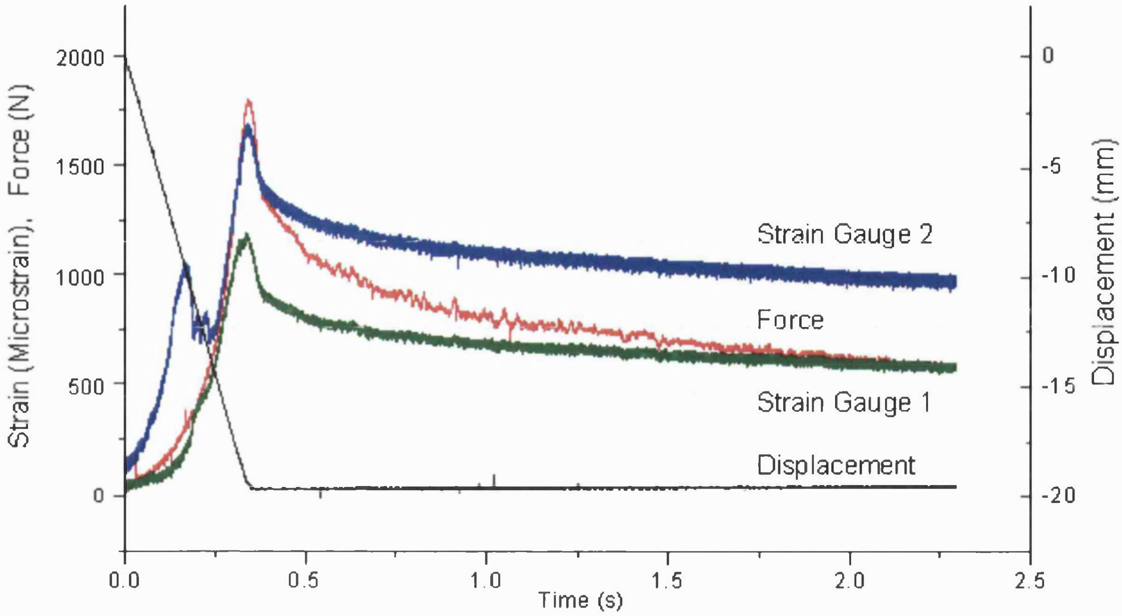

Figure 3.3.: Typical experimental result under uni-axial loading.

3.6.2.2. Loading, relaxation and unloading of graft

Figure 3.4 shows the stress-strain curve of bone graft in which the graft was not pre-loaded (i.e. no pre-load). A typical exponential curve was given during the loading phrase. At the end of the loading period (i.e. graft compressed to 12 mm), a transient drop of stress was observed because of stress relaxation. When the strain decreased (by moving up the plunger), the stroke was no longer in contact with the graft. Hence the stress dropped to zero.

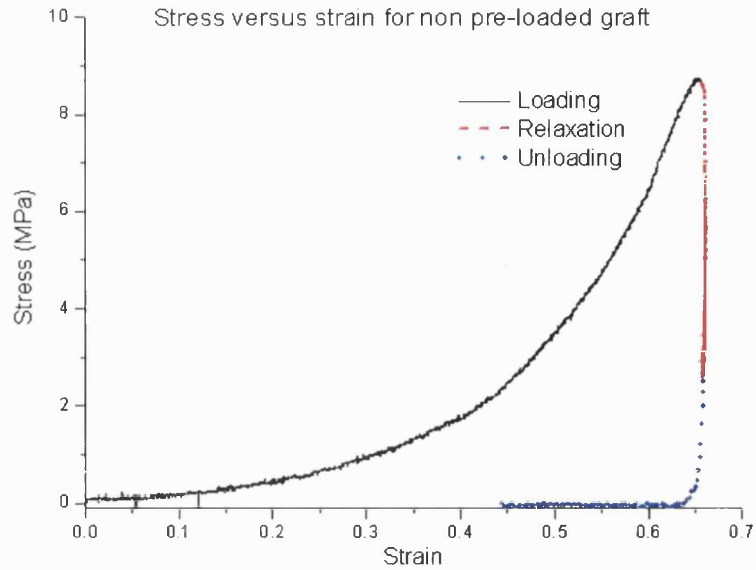

Figure 3.4.: Loading, relaxation and unloading phases in the stress-strain curve.

During loading, the area under the stress-strain curve represents the strain energy per unit volume (U, J/m^3) absorbed by the graft (detailed analysis is discussed in §3.6.6 on Page 111). Conversely, the area under the unloading curve is the energy released by the material. From Figure 3.4, it can be seen that the energy absorbed exceeds the energy released and the difference was probably dissipated as a form mechanical damage.

3.6.3. Statistical analysis

3.6.3.1. Effect of defatting on MCB

When the graft was defatting by soaking at 35°C in water for 20 mins as previously discussed, it was noticed that the colour of the MCB changed from red to pink because the fat and the bone marrow were washed out from the interstices of the graft as shown in Figure 2.6(b) on Page 72. Porosity of the bone within the particles can then be observed. It was also noticed that the mass of the graft dropped by about 1.5% ($\frac{5.142-5.067}{5.142} = 0.015$) for the same volume (10 cm^3) as shown in Figure 3.5. It was found that both non-defatted and defatted graft gave a similar standard deviation but the defatted graft gave a smaller mean value. The Student's t-test showed that there was no statistical significance ($P = 0.378$, $\alpha = 0.05$) between the mass of non-defatted and defatted graft (Minitab 14.20, Minitab Inc.). In other words, defatting of graft did not have a great impact on the mass of the graft. Nevertheless, in another study (see §4 on Page 116), a significant difference was found.

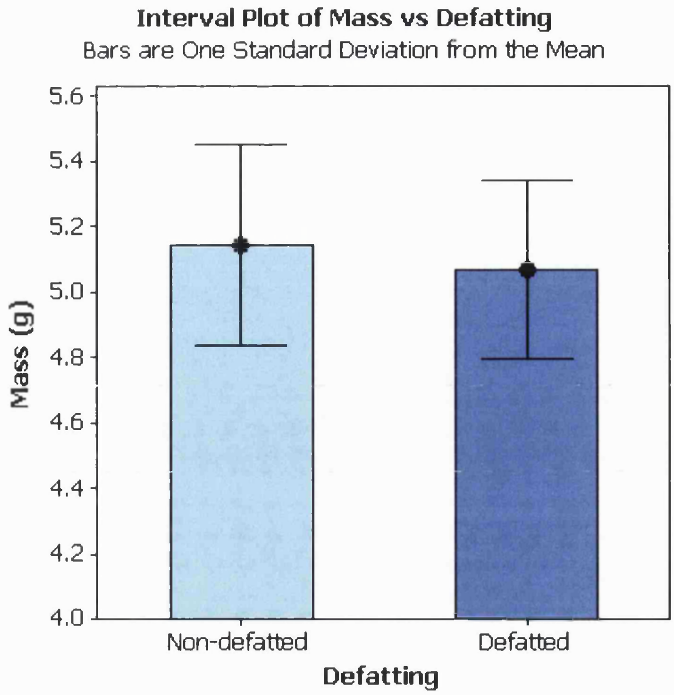

Figure 3.5.: Interval plot shows mean and one standard deviation of the mass (full results in Table 3.4).

3.6.3.2. Behaviour of hoop strain and axial force

During impaction grafting, the femur is subjected to a large amount of compressive stress. Part of the energy will be released in the radial direction due to the Poisson's Ratio effect. Hoop strain was, therefore, an important measure of how the graft responds in the radial direction. Figure 3.6 shows the value of the hoop strain measured on the aluminium die. It was found that defatted grafts showed higher hoop strains (statistical results in §3.6.3.4 on Page 87). This could be attributed to the absence of fat and marrow from the interstices of grafts, which dampens the compaction energy applied [94]. The result was similar to that of Dunlop *et al.* [94] and Voor *et al.* [115] in which the mechanical properties (shear strength and compressive stiffness) improved after washing.

When the graft was subjected to a high loading rate, the hoop strain found to be higher under the same condition. When the graft was compressed at high speed, it had no time to re-orientate itself into an optimised position so that all the stresses could be evenly distributed. In addition, viscoelastic effects became more significant and stress relaxation was not possible at this high loading rate. Hence, it was observed that higher load and hence strain rates gave higher hoop strains as shown in Figure 3.6 (statistical results in §3.6.3.4 on Page 87).

No statistical relationship was found between pre-loading and hoop strain.

Furthermore, the axial forces presented similar patterns to the hoop strain (Figure 3.7). Both defatting and loading rate were both found to have a significant effect on the axial forces (statistical results in §3.6.3.4 on Page 87). It is, therefore, suggested that the graft material is homogenous.

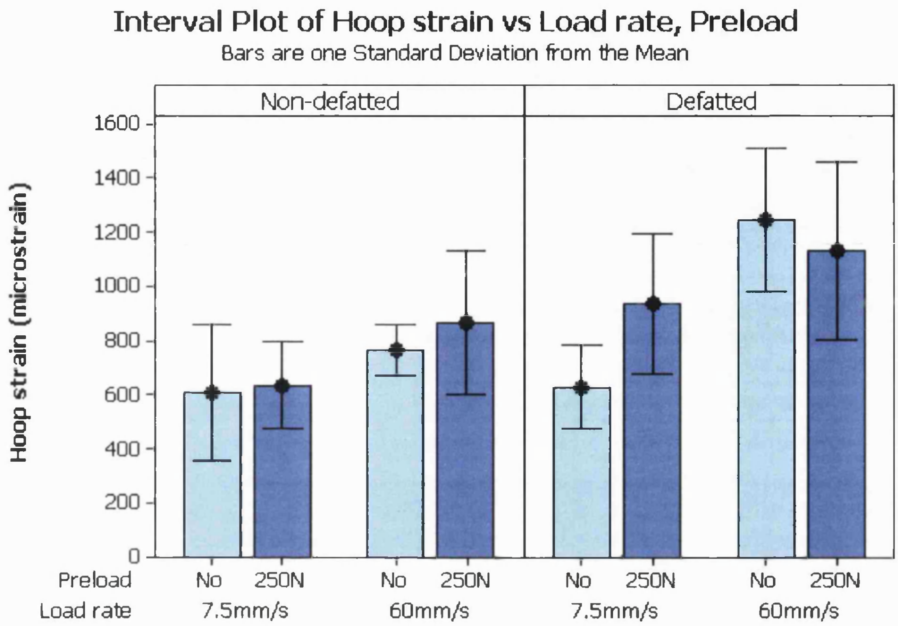

Figure 3.6.: Interval plot shows mean and one standard deviation of the measured hoop strain around the aluminium tube (full results in Table 3.4).

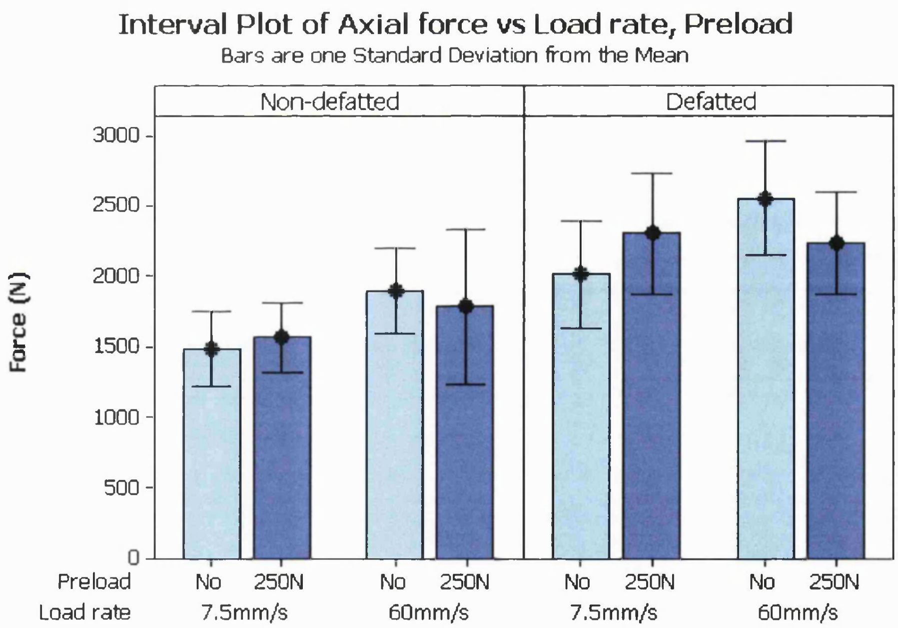

Figure 3.7.: Interval plot shows mean and one standard deviation of the measured axial force from the Instron load cell (full results in Table 3.4).

3.6.3.3. Behaviour of TCPR and recoil

Poisson's ratio is one of the most important parameters used to measure the mechanical properties of bone graft. It is an expression of the volume expansion of the graft during compression. In particular under dynamic conditions, with the effect of viscoelasticity, the volume changes vary with both time and loading rates. The total constrained apparent Poisson's ratio (TCPR) is one of the measures used to quantify this mechanical property. This is calculated by the ratio of the hoop strain in the aluminium die and the axial strain of the graft, as described in Equation 3.3 (see §3.5 on Page 78). Figure 3.8 shows the Poisson's ratio obtained under different settings. Firstly, considering pure non-defatted graft on the left hand side of the graph, pre-loading of graft gave a significantly higher value of the Poisson's ratio (statistical results in §3.6.3.4 on Page 87); similarly, a higher load rate gave a significantly higher value of the Poisson's ratio. In other words, higher radial volume expansion was observed. Nevertheless, defatting did not have significant impact on Poisson's ratio.

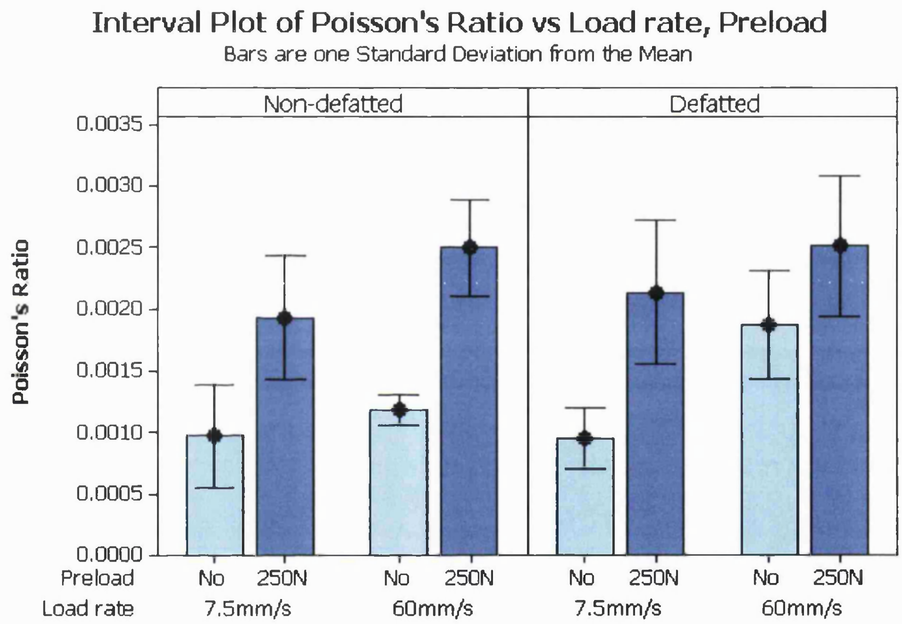

Figure 3.8.: Interval plot shows mean and one standard deviation of the calculated apparent Poisson's ratio (full results in Table 3.4).

The amount of recoil was measured as soon as the graft was extracted from the aluminium die. The result is shown in Figure 3.9. It was found that all three effects (i.e. defatting, preloading and loading rate) do not influence the recoil. No statistically significant effects were found in Pareto analysis (statistical results in §3.6.3.4 on Page 87). As a result, recoil should not be used as a measure of graft properties. Some of the graft samples are shown in Figure 3.10.

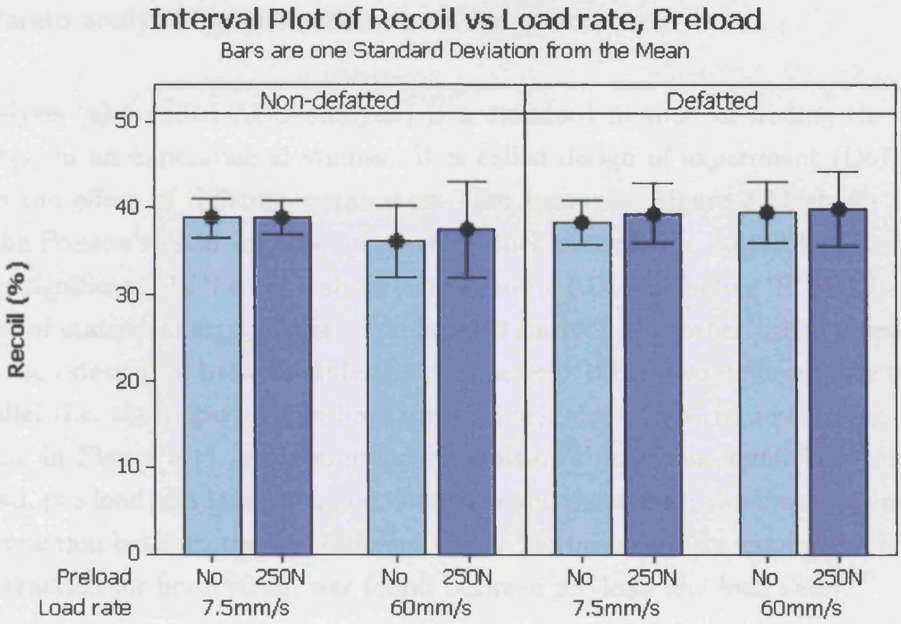

Figure 3.9.: Interval plot shows mean and one standard deviation of the measured recoil (full results in Table 3.4).

Figure 3.10.: Porcine graft was extracted after impaction and the recoil was measured with a vernier calliper. The first two rows in the figure was non-defatted MCB, whilst the other two rows were defatted MCB.

3.6.3.4. Pareto analysis and interaction between effects

Pareto analysis (also called ABC analysis) is a standard method of finding the significant parameters(s) in an experimental studies. It is called design of experiment (DoE) analysis. It analyses the effect of different parameters. For example, Figure 3.11 shows the Pareto chart for the Poisson's ratio: in this, any factor which exceeds the dotted line is classified as statistically significant. In this case, alpha (α) was set to 0.05 and factors 'B' and 'C' were both found to be of statistical significance. The interaction plot is another useful respresentation to present the interaction between different parameters. When two different effects are lined up in parallel (i.e. the slopes of two lines are similar), this means no interaction was found (for example in Figure 3.11, no interaction for Poisson's ratio was found between defatting and pre-load, pre-load and load rate, and, load rate and defatting); two crossing lines indicate that an interaction between the two different effects has occurred (for example in Figure 3.12, a small interaction for hoop strain was found between pre-load and load rate).

Figure 3.11 and Figure 3.12 show the Pareto chart of interaction plots for Poisson's ratio and hoop strain. It was interesting to note that the main effect for Poisson's ratio was pre-loading whilst the main effect for hoop strain was load rate. This suggested the viscoelastic effect became significant during high speed loading and the graft expanded rapidly. Hence, high strain was recorded. Also, during pre-loading, the total constrained apparent Poisson's ratio increased significantly because the toe region of the stress-strain was ignored. In other words, the material became much stiffer after pre-loading since the net strain was calculated after pre-loading. Also, no interaction was found for Poisson's ratio.

It is important to note that the most significant effect for hoop strain (i.e. hoop stress, hoop force) was load rate; defatting was the next most significant factor. For axial force (Figure 3.13), defatting was the most significant factor, load rate being the next most significant factor. Based on this statistical study, it is suggested that load rate has the biggest effect in the radial direction whilst defatting has the biggest effect in the axial direction.

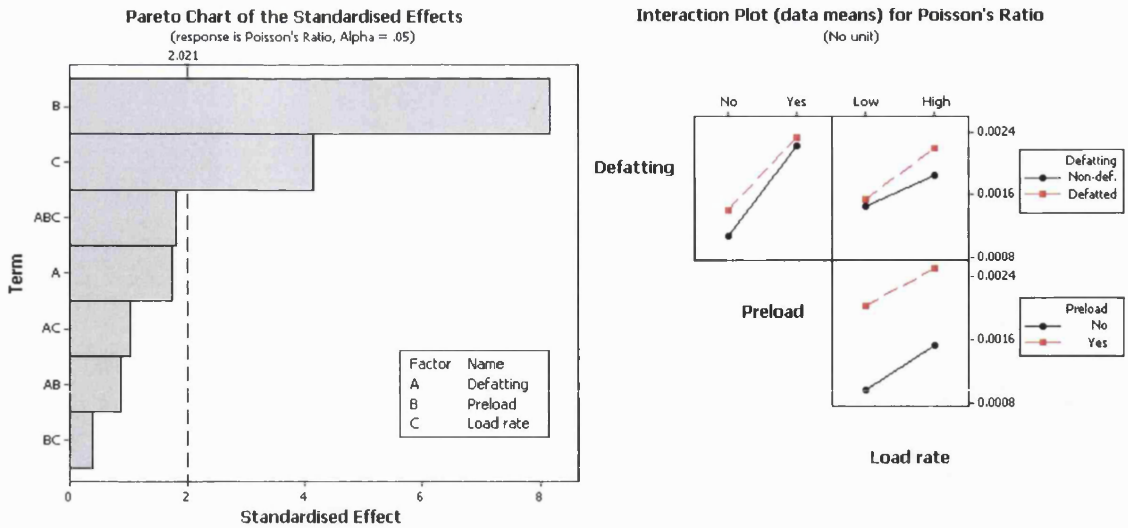

Figure 3.11.: Statistical analysis (Pareto analysis) of the calculated Poisson's ratio. The effect is statistically significant when the standardised value exceeds the vertical dotted line ($\alpha = 0.05$). Figure on the right hand side shows the interaction between different variables.

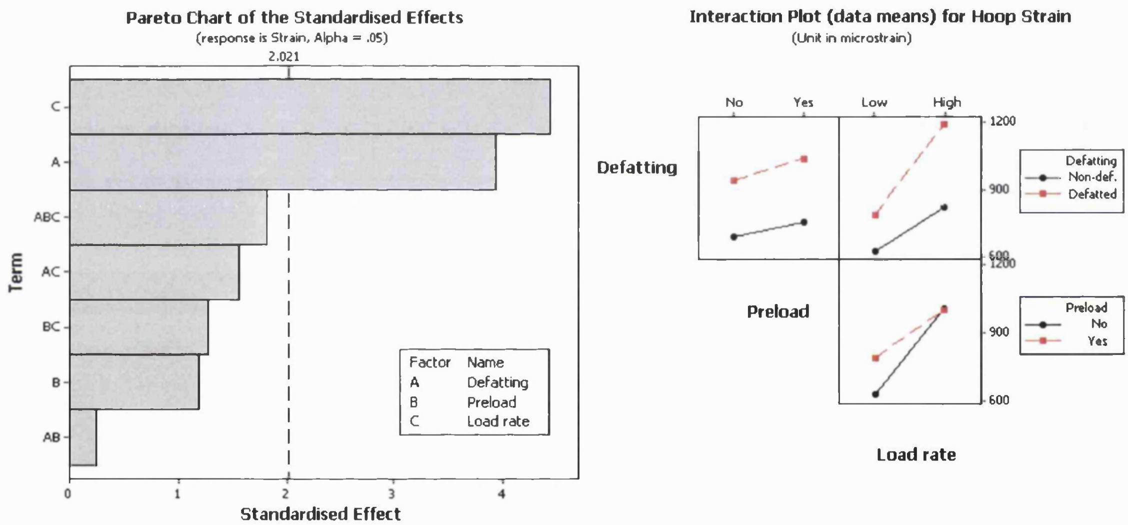

Figure 3.12.: Statistical analysis (Pareto analysis) of the measured hoop strain. The effect is statistically significant when the standardised value exceeds the vertical dotted line ($\alpha = 0.05$). Figure on the right hand side shows the interaction between different variables.

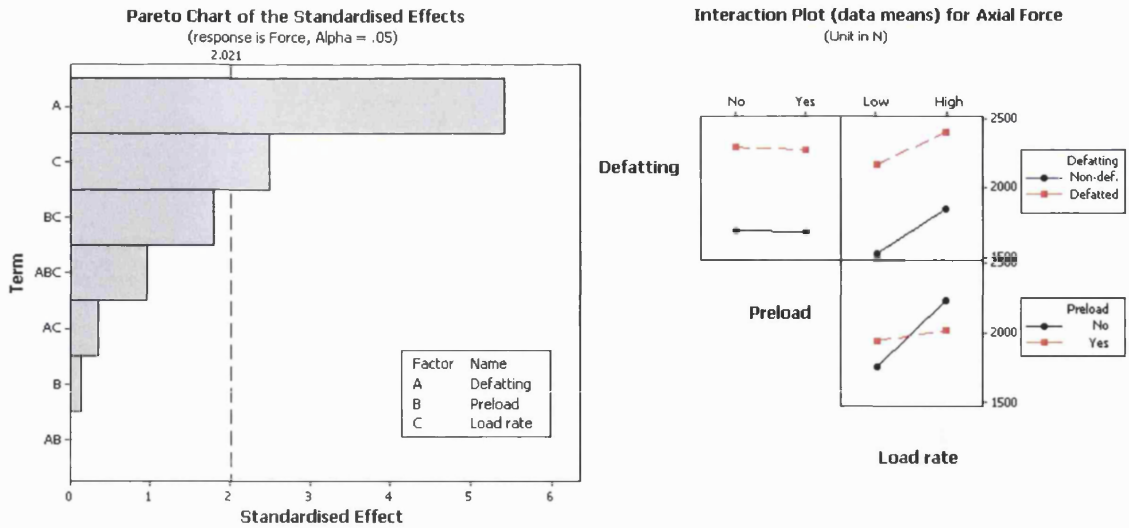

Figure 3.13.: Statistical analysis (Pareto analysis) of the measured axial force. The effect is statistically significant when the standardised value exceeds the vertical dotted line ($\alpha = 0.05$). Figure on the right hand side shows the interaction between different variables.

By repeating the previous analyses, a summary table for all the main effects and interactions was produced (Table 3.5). Recoil was the only parameter that was found to have no main effect. However, interactions between defatting and load rate were found. This could be probably because of the variability of graft material from batch to batch.

	Effect(s)							
Target	A	B	C	AB	BC	AC	ABC	Interaction
Poisson's Ratio (TCPR)	×	+	+	×	×	×	×	No relationship was found
Hoop strain	+	×	+	×	×	×	×	B − C
Axial force	+	×	+	×	×	×	×	B − C
Recoil	×	×	×	×	×	×	×	A − C

Table 3.5.: A = Defatting, B = Pre-loading and C = Load rate. Pareto analysis shows the relationship between targets and effects, '+' represents significance positive effect when setting changes from '−1' to '+1' ($\alpha = 0.05$). '×' indicates that no statistical significance was found. The last column shows the interactions between different effects.

3.6.4. Stress-strain behaviour

3.6.4.1. Baseline study

In order to enable data comparsion, a baseline study was defined: This used non-defatted (fresh) graft, pre-loaded with 1 N (i.e. no pre-load) and low load rate of 7.5 mm/s. Figure 3.14 gives the stress-strain results of this baseline study. Curves were plotted using similar techniques to the previous section (see Figure 3.4 on Page 82). It is also important to note that there was some noise encountered from the data acquisition system. As a result, small vertical and horizontal lines (i.e. noise) can be seen in the stress-strain curves in this section (§3.6.4.1–§3.6.4.6).

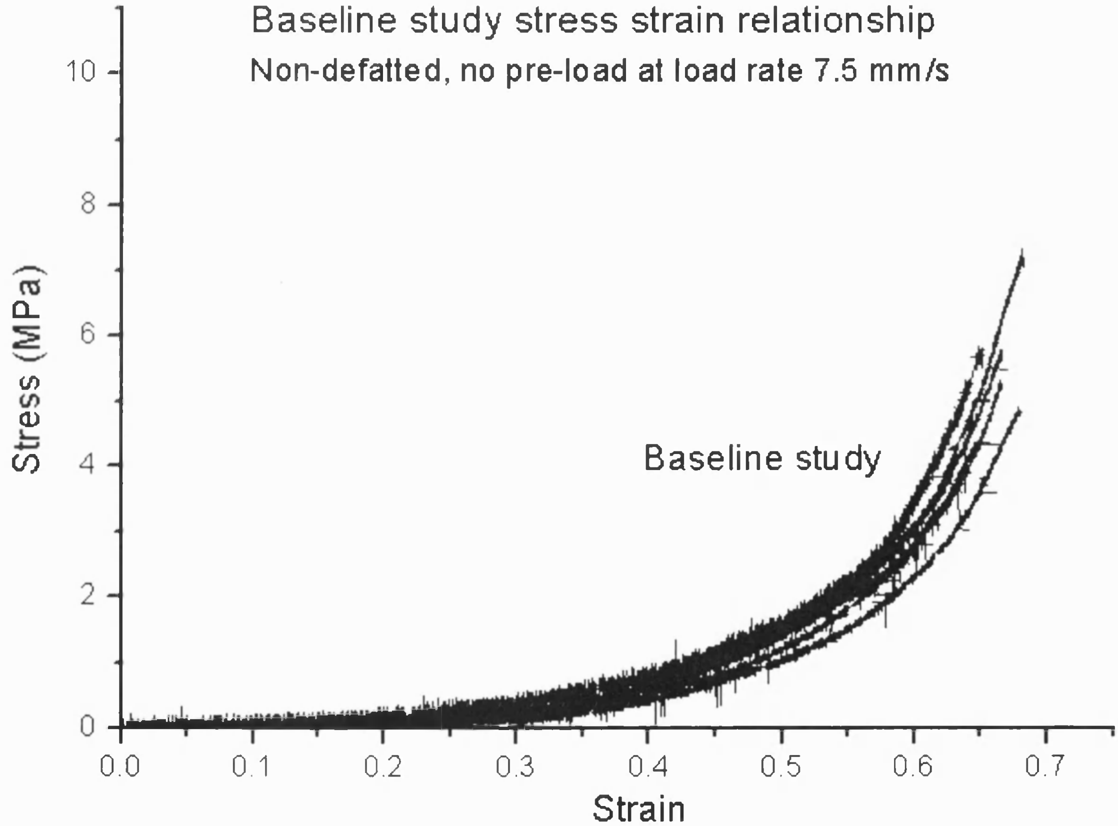

Figure 3.14.: Stress-strain curves for base line study. Results of experiments 1 – 6.

3.6.4.2. Effect of pre-loading

It is important to understand that the final thickness of the graft (i.e. 12 mm) in both non-preloaded and pre-loaded cases was the same. Figure 3.15 provides a schematic view of the effect of pre-loading. As can be seen, the starting point in the two cases is different. As a result, 0.1 strain (10% deformation) in the non-preloaded and pre-loaded cases represent different amounts of actual displacement.

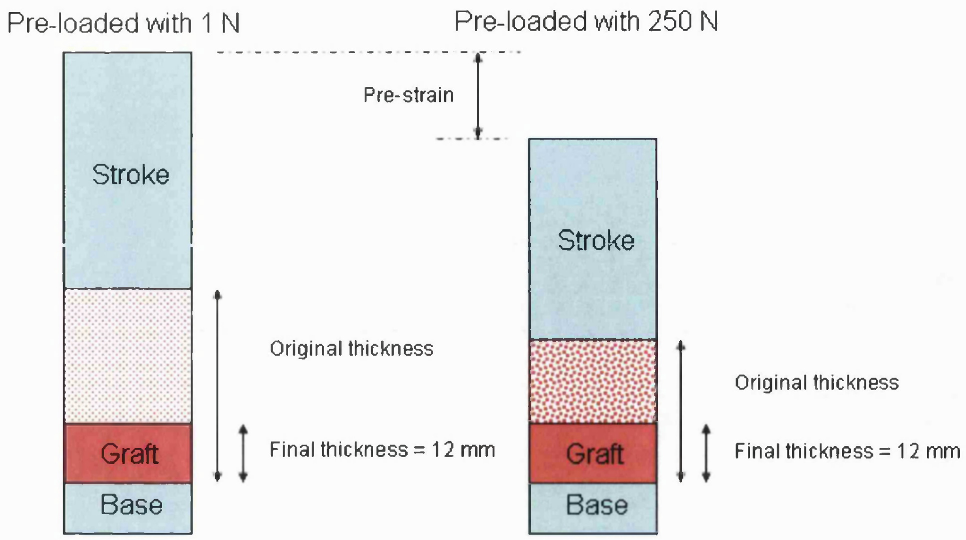

Figure 3.15.: Comparison of the non-preloaded and pre-loaded impaction.

From the baseline study shown in Figure 3.16, the graft was compressed to 12 mm in height. This created approximately 0.65 strain (65% deformation) at stress at about 6 MPa. When the graft was pre-loaded, only 0.35 strain (35% deformation) was required to get to the same final stroke position. Approximately the same amount of maximum stress was measured, which suggests that the maximum force acting on the femur would be independent of the amount of pre-loading force. It also suggests that pre-loading of the graft does not jeopardise the final stiffness. This can be explained by the similar forces generated with the same amount of total strains.

However, the initial gradient of the stress-strain curve of the pre-loaded graft gave an approximately logarithmic increase in stiffness. This means the initial stiffness (impact constrained modulus of elasticity) was very high. High transient force may therefore be expected. When the strain increased, the shape of the curve shifted towards that of an exponential nature. This could probably be attributed to the static friction of graft material.

The graft which was pre-loaded to 250 N represents a base study for pre-loaded cases and as shown in Figure 3.16.

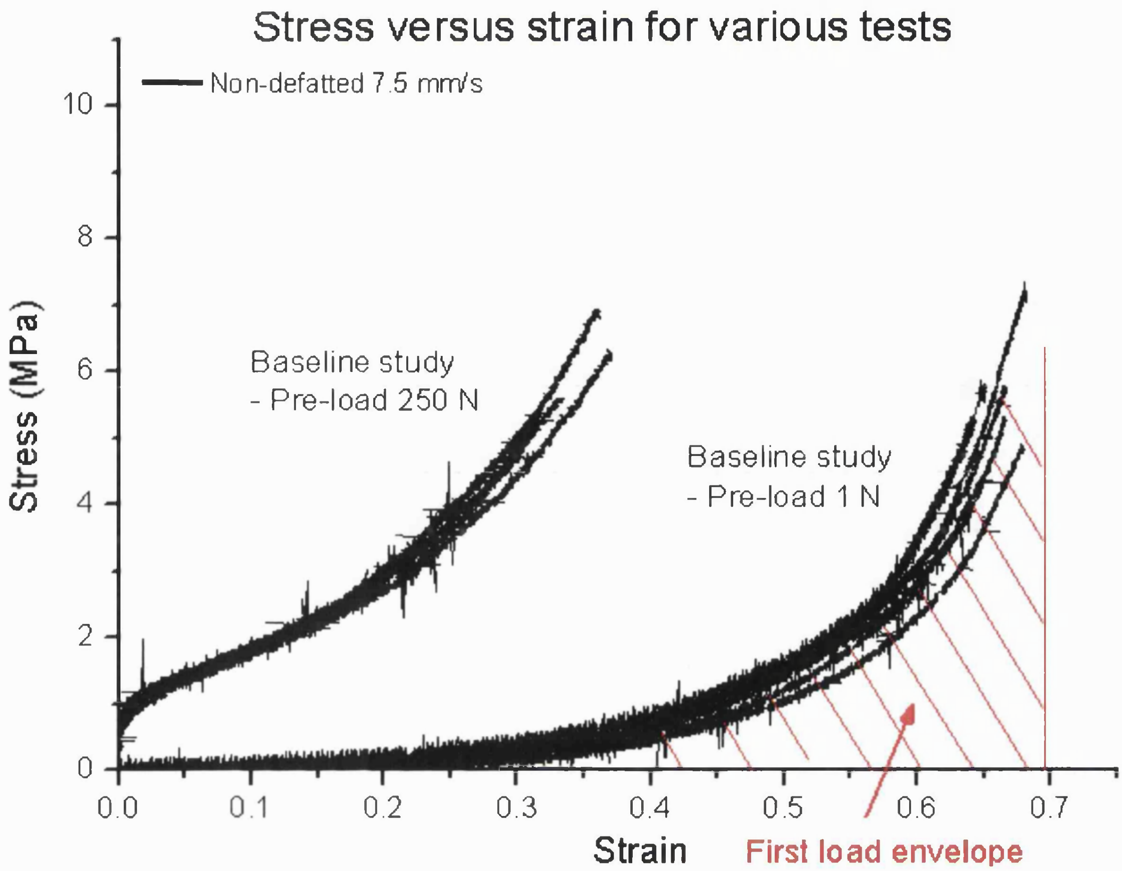

Figure 3.16.: Comparison of the effect of pre-loading under stress-strain curves. Results of experiments 1 – 6 and 7 – 12. (Remark: same strain in the non-preloaded and pre-loaded cases represent different amount of actual displacement).

In the baseline study, the first 'one-off' (i.e. no pre-load) compression is termed the first load envelope [162] and is shown in Figure 3.17. Phillips *et al.* [162] found that all re-compression (i.e. pre-load) stress-strain curves stay below the first load envelope. Therefore, the stress-strain curves of pre-loaded graft (i.e. pre-loaded with 250 N) would be located below the first load envelope if the initial strain during pre-loading is included. It is very important to note that Phillips *et al.* did not reset the strain to zero after the compression. However, in Figure 3.16, this was not the case as the strain was reset to zero after pre-loading with 250 N. So, it is important to keep this concept in mind as the same amount of strain value of two cases (pre-loaded with 1 N vs. pre-loaded with 250 N) represents different amounts of actual displacements.

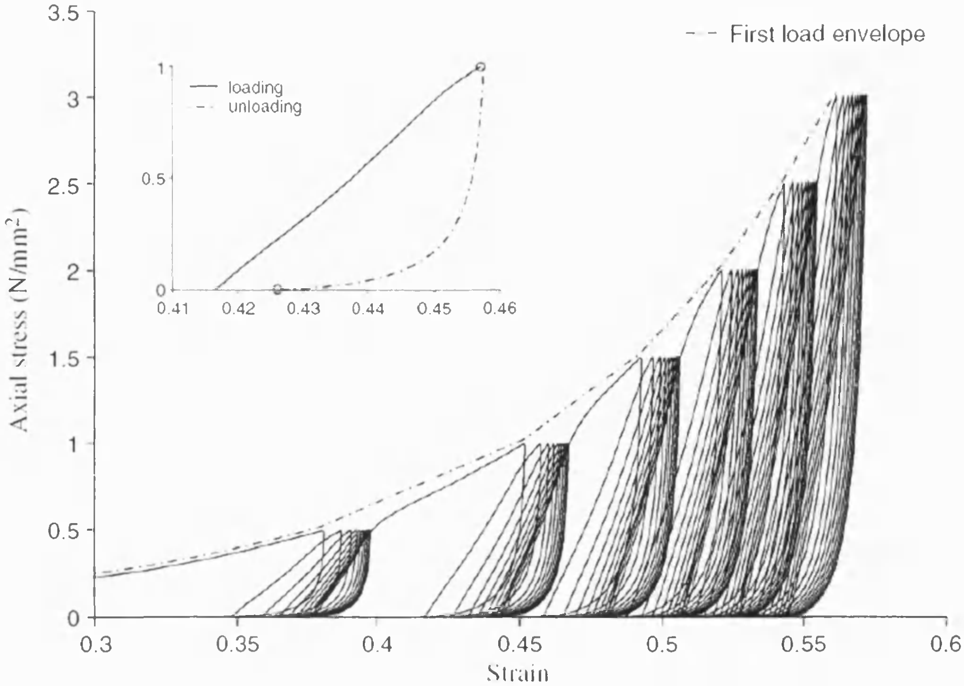

Figure 3.17.: Stress-strain characteristic of morsellised cortico-cancellous bone graft. It should be noted that all the re-compression characteristics fell below the first load envelope curve (adapted from [162]).

3.6.4.3. Effect of load rate

Figure 3.18 shows the effect of the higher load rate (60 mm/s). As can been seen, higher stress was observed for the same strain. Therefore, the higher the load rate, the higher is the stress (i.e. higher stiffness) exerted on the femur due to viscoelastic effects (see §4.7 on Page 136 (2nd experiment), the effect of the rate of impaction on stress is discussed in detail). It was also observed that the gradient of the stress-curves increased with the speed of impaction. The benefit of the higher load rate is that the static friction between graft particles can be overcome easily such that the stem can be quickly impacted into the desired position. Nevertheless, it could lead to a per-operative femoral fracture.

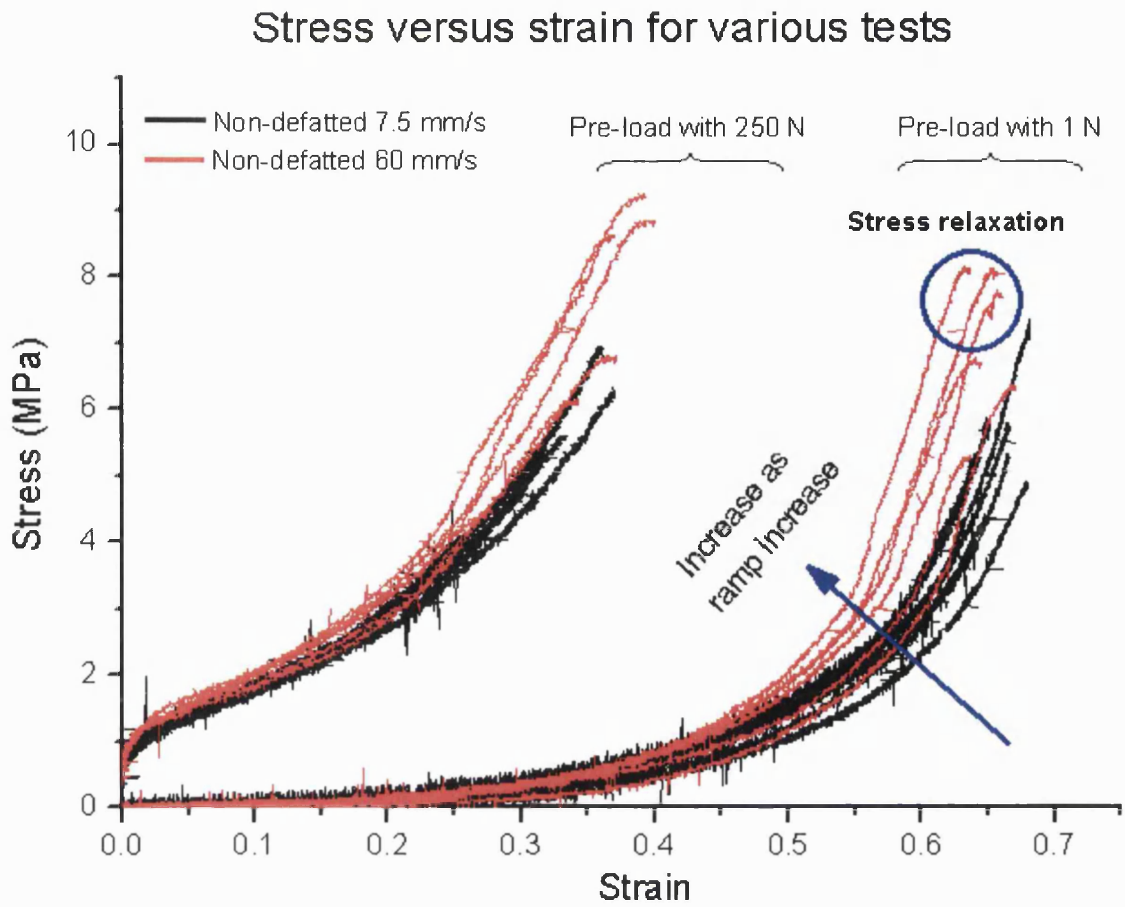

Figure 3.18.: Comparison of the effect of load rate under stress-strain graph. Results of experiments ($1-6$ and $7-12$, in black) and ($13-18$ and $19-24$, in red). (Remark: same strain in the non-preloaded and pre-loaded cases represent different amount of actual displacement).

In addition, in Figure 3.18 (also in Figure 3.21 on Page 97). It was found that the amount of stress dropped at the end of the loading (i.e. the end of the curve). It was probably due to the deceleration of the stroke from 60 mm/s to 0 mm/s. During the deceleration, stress relaxation occurred, causing a drop of stress in the stress-strain curve.

3.6.4.4. Effect of defatting on mechanical properties

It is known that the stiffness of the graft increases after defatting. At 250 N pre-load, the initial thickness of the defatted graft was higher compared with non-defatted graft as shown in Figure 3.19. So, a higher strain was required to compress the graft into 12 mm thickness as demonstrated in Figure 3.20.

In the clinical environment, if defatted graft was used, surgeons may be misled by the amount of feedback force produced, and as a result may assume the stem is fixed in position. Fortunately, there are depth markers for distal impactor, and indicators for proximal impactor which allow the surgeon to determine if the stem is in the correct position. Phipps *et al.* [163] attempted to use a modified Exeter slap hammer *in-vivo* to monitor the force level per-operatively. They recommended modifying the slap hammer to give immediate feedback to the surgeon on their level of force applied during impaction. This could be useful in attemption to avoid large forces which could lead to femoral fracture but should not be used as a reliable indication of final position of the stem.

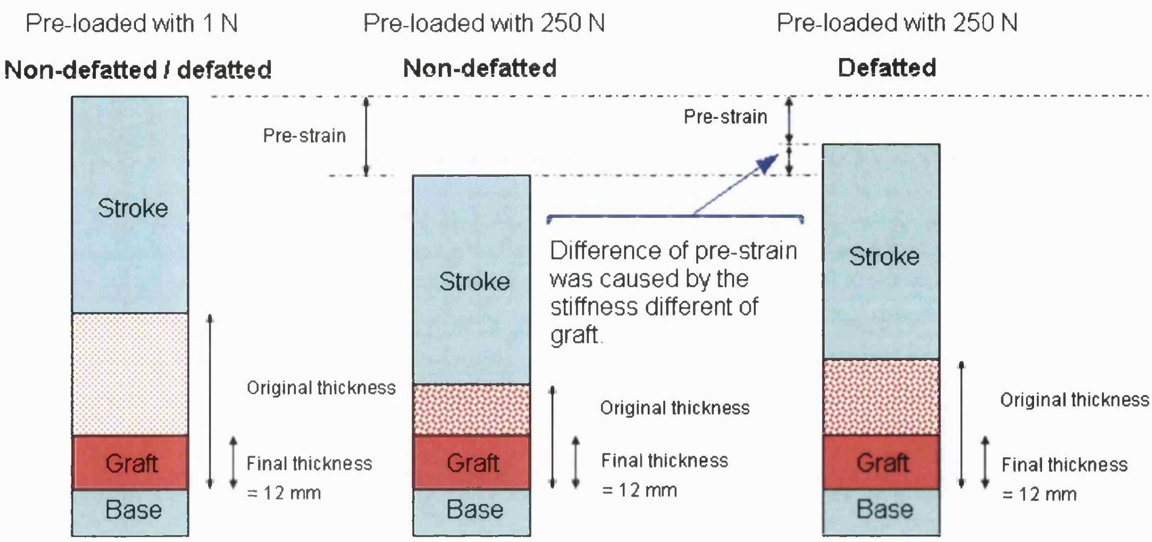

Figure 3.19.: Comparison of the effect of defatting on the initial thickness of graft.

Figure 3.20 demonstrates the effect of defatting of the graft and was carried out at a load rate 7.5 mm/s. Again, both the non-preloaded (i.e. 1 N) and pre-loaded (i.e. 250 N) results were plotted for comparsion. In both baseline studies, the maximum stress was about 6 MPa. After defatting, for both non-preloading and pre-loading cases, a maximum stress of approximately 9 MPa was obtained. So, a higher stress was observed (i.e. higher stiffness) with defatted graft.

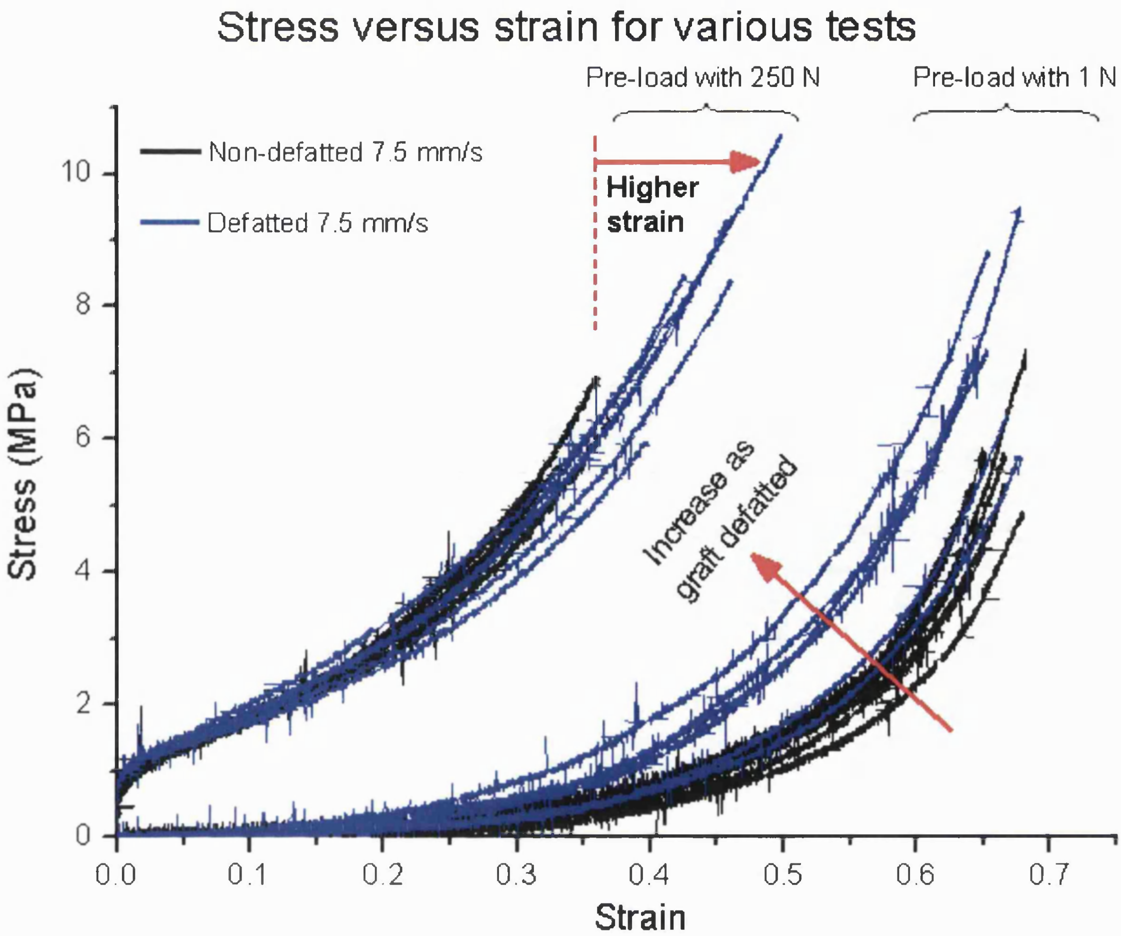

Figure 3.20.: Comparison of the effect of defatting under stress-strain curves. Results of experiments (1 – 6 and 7 – 12, in black) and (25 – 30 and 31 – 36, in blue). (Remark: same strain in the non-preloaded and pre-loaded cases represent different amount of actual displacement).

3.6.4.5. Effect on repeatability

Figure 3.20 and Figure 3.21 show the effect of defatting and pre-loading for load rate of 7.5 mm/s and 60 mm/s respectively. As can be easily, defatted graft which was pre-loaded with 250 N demonstrated high repeatability than non-defatted graft which was pre-loaded with 1 N.

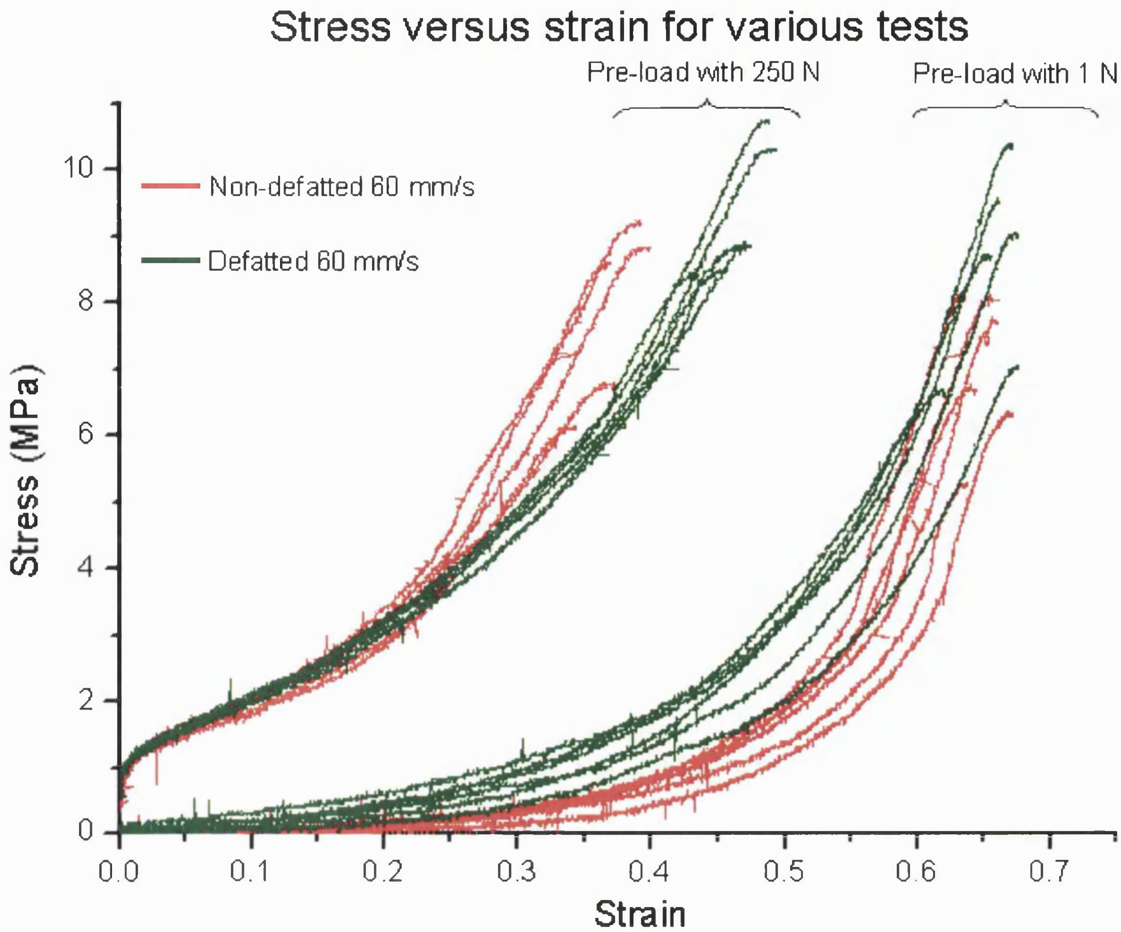

Figure 3.21.: Demonstration of stress-strain curves when all effects present. Results of experiments (13 – 18 and 19 – 24, in red) and (37 – 42 and 43 – 48, in green). (Remark: same strain in the non-preloaded and pre-loaded cases represent different amount of actual displacement).

3.6.4.6. Overall comparison

Figure 3.22 depicts all the experiments in a single figure. As can be seen, under all circumstances, pre-loading provides excellent repeatability as majority of the curves fall within a smaller envelope. However, a wide range of variation was observed if the graft was not pre-loaded.

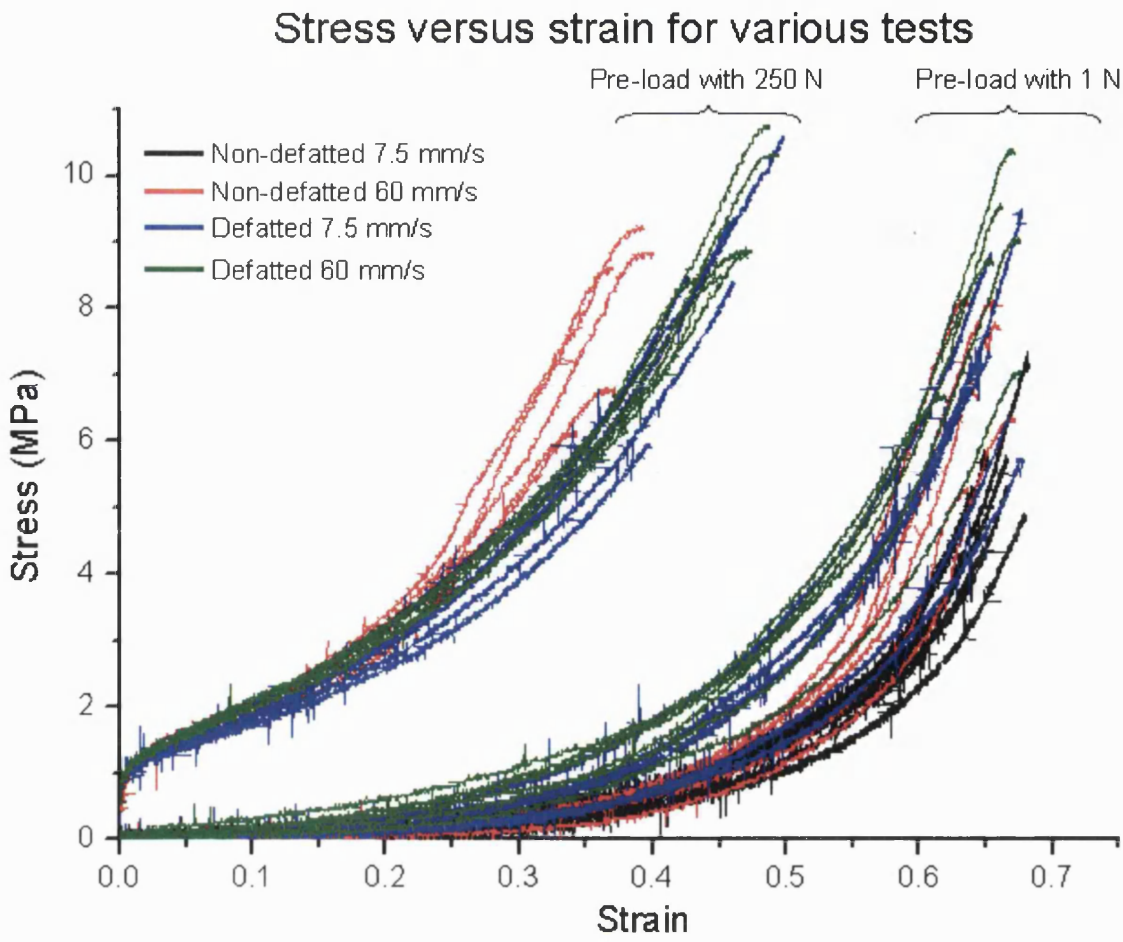

Figure 3.22.: Comparison of all experimental results under stress-strain curve. Results of experiments 1 – 48 in various colour. (Remark: same strain in the non-preloaded and pre-loaded cases represent different amount of actual displacement).

A summary of this section is also provided in Table 3.6.

Effect	Observations
When pre-loaded at 250 N	Higher initial stiffness, lower strain, transition of gradient from logarithmic to exponential, excellent repeatability
When impacted at 60 mm/s	Higher stress, higher stiffness, strain unchanged, gradient independent to the load rate
When defatting graft was used	Higher stress, higher stiffness, much better repeatability, higher strain in pre-loaded graft

Table 3.6.: Summary of stress-strain analysis.

3.6.5. Modulus of elasticity

3.6.5.1. Definition

This section is an extension of the previous section §3.6.4. The previous section discussed the stress-strain behaviour of the bone graft material. As morsellised bone graft is a highly viscoelastic material and presents completely non-linear characteristics, the objective of this section was, therefore, to quantify the slope of the stress-strain curves (i.e. modulus of elasticity) in a way that can be understood. In order to categorise this behaviour, three terms were used. These are: the impact constrained modulus of elasticity (ICME), the consolidated constrained modulus of elasticity (CCME) and the total constrained modulus of elasticity (TCME). Furthermore, the following definitions were used in this experiment, viz.:

- CCME – This is defined by the incremental change of stiffness of graft in steps of (5%, 10%, 20%...100%) of the 'actual' deformation (i.e. instantaneous modulus of elasticity). For instance, a total strain of 0.65 is measured with a compression of 12 mm. 20% of 'actual' deformation is equal to strain 0.13 (= 0.65 × 0.2). The full terminology of the CCME is given in Table 3.7.

Stiffness between	0 – 5%	0 – 10%	10 – 20%	20 – 30%	30 – 40%	40 – 50%
Terminology of CCME	5%	10%	20%	30%	40%	50%
	(cont.)	50 – 60%	60 – 70%	70 – 80%	80 – 90%	90 – 100%
		60%	70%	80%	90%	100%

Table 3.7.: Definition of consolidated constrained modulus of elasticity (CCME).

- TCME – This is defined by the overall apparent stiffness of the graft in steps of (5%, 10%, 20%...100%) of the 'actual' deformation (i.e. overall modulus of elasticity). The full terminology of the TCME is given in Table 3.8.

Stiffness between	0 – 5%	0 – 10%	0 – 20%	0 – 30%	0 – 40%	0 – 50%
Terminology of TCME	5%	10%	20%	30%	40%	50%
	(cont.)	0 – 60%	0 – 70%	0 – 80%	0 – 90%	0 – 100%
		60%	70%	80%	90%	100%

Table 3.8.: Definition of total constrained modulus of elasticity (TCME).

- ICME – This is defined by the change of stiffness of the graft in first 5% and 10% of the 'actual' deformation (i.e. transient modulus of elasticity) (whereas Fosse *et al.* [132] defined the ICME as the transient apparent stiffness during impaction). Based on the previous definition, (5% CCME) is the same as (5% TCME), and (10% CCMM) is the same as (10% TCME). For these two particular terms, they are defined as (5% ICME) and (10% ICME). The full terminology of the ICME is given in Table 3.9.

Definition	Represents	
5% ICME	5% TCME	or 5% CCME
10% ICME	10% TCME	or 10% CCME

Table 3.9.: Definition of impact constrained modulus of elasticity (ICME).

Figure 3.23 illustrates the three different stiffnesses in a graphical form so that they can be understood easily.

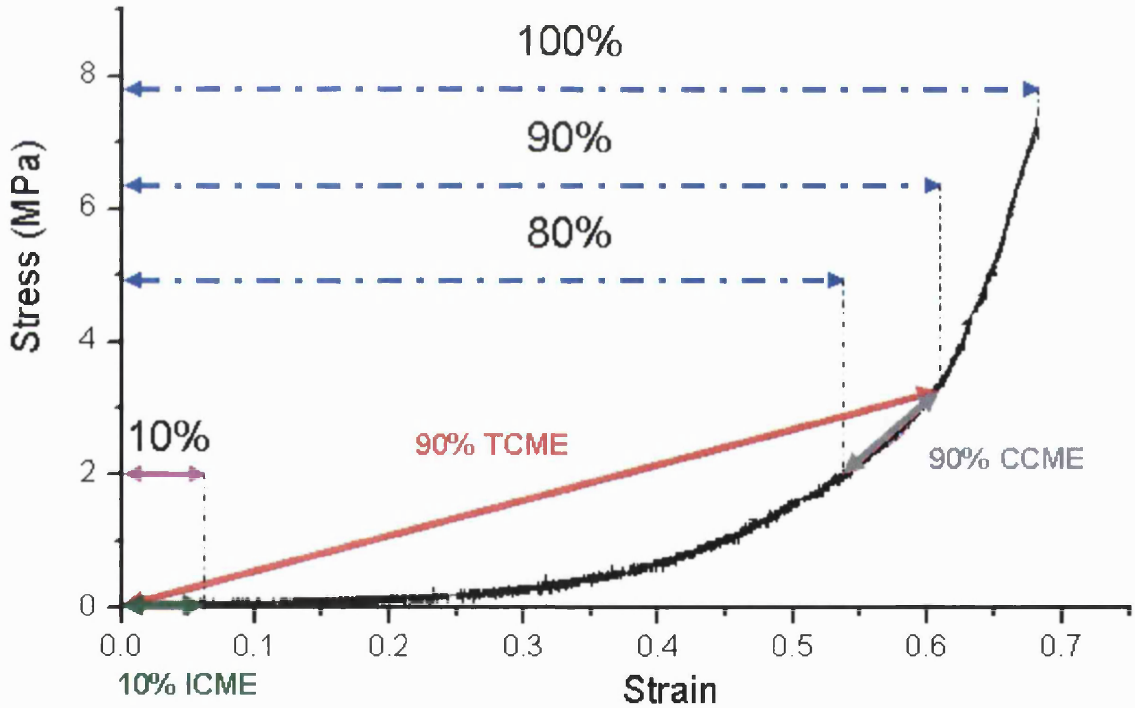

Figure 3.23.: Illustration of the 10% impact constrained modulus of elasticity (10% ICME), 90% total constrained modulus of elasticity (90% TCME), and 90% consolidated constrained modulus of elasticity (90% CCME).

3.6.5.2. Result of ICME, CCME and TCME

Table 3.10 (on Page 102) and Table 3.11 (on Page 103) summarise details of all the stiffnesses found for all of the experiments. The mean and the standard deviation (in parentheses) are also given. Full experimental results are shown in Table A.3 (on Page 176) and Table A.4 (on Page 178).

(This space intentionally left blank)

Run order	1 – 6	7 – 12	13 – 18	19 – 24	25 – 30	31 – 36	37 – 42	43 – 48
Defatting	−	−	−	−	+	+	+	+
Pre-loading	−	+	−	+	−	+	−	+
Load rate	−	−	+	+	−	−	+	+
5% ICME	0.00 (0.00)*	57.80 (5.97)	0.00 (0.00)*	50.70 (4.93)	0.00 (0.00)*	93.81 (16.56)	0.00 (0.00)*	78.28 (7.45)
10% ICME	0.00 (0.00)*	36.31 (1.60)	0.64 (0.23)	31.16 (0.70)	0.00 (0.00)*	51.23 (8.44)	1.56 (0.97)	40.12 (1.52)
20% CCME	0.56 (0.49)	8.12 (1.02)	0.97 (0.41)	7.79 (1.18)	0.89 (0.46)	9.19 (1.02)	1.70 (0.96)	9.12 (0.91)
30% CCME	0.95 (0.44)	8.52 (1.96)	1.62 (0.67)	8.61 (1.59)	0.90 (0.47)	7.53 (2.10)	2.48 (0.47)	9.09 (0.90)
40% CCME	1.00 (0.39)	9.13 (1.57)	2.47 (1.27)	10.71 (1.81)	1.44 (0.30)	10.30 (1.24)	3.40 (1.11)	11.74 (0.69)
50% CCME	2.33 (0.87)	10.71 (1.08)	4.32 (1.23)	12.66 (1.88)	2.53 (0.90)	12.26 (2.23)	5.53 (1.18)	13.10 (1.81)
60% CCME	3.82 (1.17)	12.71 (2.51)	7.17 (2.25)	14.78 (2.09)	4.58 (1.09)	15.49 (2.92)	8.80 (0.70)	16.77 (1.14)
70% CCME	6.35 (1.53)	15.97 (1.76)	11.13 (2.89)	19.78 (3.10)	7.21 (1.87)	26.69 (10.91)	12.76 (3.62)	19.86 (2.10)
80% CCME	9.28 (1.93)	19.65 (3.25)	16.74 (3.90)	22.43 (3.66)	14.54 (2.75)	26.55 (6.64)	21.15 (2.97)	24.49 (4.59)
90% CCME	14.79 (3.74)	22.19 (2.80)	25.70 (4.26)	28.31 (4.38)	32.22 (9.68)	32.02 (7.84)	34.61 (6.16)	36.30 (5.35)
100% CCME	33.10 (11.43)	26.01 (5.50)	41.89 (7.60)	32.59 (5.10)	47.50 (5.94)	20.03 (7.77)	44.09 (11.53)	23.25 (5.63)

Table 3.10.: Summary of mean and one standard deviation (presented in parentheses) of CCME (Units are MPa). *Values were too low to be determined because of low signal-to-noise ratio, and therefore, were assumed to be zero.

Run order	1 – 6	7 – 12	13 – 18	19 – 24	25 – 30	31 – 36	37 – 42	43 – 48
Defatting	−	−	−	−	+	+	+	+
Pre-loading	−	+	−	+	−	+	−	+
Load rate	−	−	+	+	−	−	+	+
5% ICME	0.00 (0.00)*	57.80 (5.97)	0.00 (0.00)*	50.70 (4.93)	0.00 (0.00)*	93.81 (16.56)	0.00 (0.00)*	78.28 (7.45)
10% ICME	0.00 (0.00)*	36.31 (1.60)	0.64 (0.23)	31.16 (0.70)	0.00 (0.00)*	51.23 (8.44)	1.56 (0.97)	40.13 (1.52)
20% TCME	0.27 (0.25)	22.38 (1.36)	0.72 (0.33)	19.62 (0.42)	0.58 (0.20)	27.26 (3.93)	1.63 (0.91)	22.28 (0.74)
30% TCME	0.46 (0.26)	18.05 (1.44)	1.01 (0.40)	16.03 (0.71)	0.63 (0.26)	19.68 (2.35)	1.92 (0.72)	17.32 (0.36)
40% TCME	0.60 (0.22)	15.72 (0.71)	1.39 (0.62)	14.71 (0.96)	0.84 (0.24)	17.01 (1.46)	2.29 (0.78)	15.84 (0.32)
50% TCME	0.94 (0.32)	14.72 (0.68)	1.96 (0.73)	14.25 (1.13)	1.19 (0.35)	15.96 (1.08)	2.94 (0.72)	15.25 (0.52)
60% TCME	1.42 (0.45)	14.38 (0.64)	2.84 (0.95)	14.34 (1.23)	1.76 (0.36)	15.89 (1.18)	3.92 (0.62)	15.51 (0.52)
70% TCME	2.12 (0.58)	14.61 (0.68)	4.00 (1.14)	15.08 (1.45)	2.56 (0.52)	17.30 (2.02)	5.18 (0.89)	16.15 (0.59)
80% TCME	3.02 (0.74)	15.19 (0.65)	5.60 (1.45)	15.98 (1.71)	4.07 (0.79)	18.54 (2.43)	7.15 (1.07)	17.21 (0.82)
90% TCME	4.32 (1.03)	15.98 (0.80)	7.82 (1.75)	17.34 (1.98)	7.18 (1.77)	20.04 (2.91)	10.12 (1.44)	19.32 (1.15)
100% TCME	7.20 (2.10)	16.95 (1.07)	11.23 (2.15)	18.99 (2.29)	10.70 (1.72)	20.07 (3.25)	12.87 (2.03)	19.63 (1.41)

Table 3.11.: Summary of mean and one standard deviation (presented in parentheses) of TCME (Units are MPa). *Values were too low to be determined because of low signal-to-noise ratio, and therefore, were assumed to be zero.

3.6.5.3. Baseline study

The baseline study was the same as described in §3.6.4.1 (i.e. non-defatted (fresh graft), pre-loaded with 1 N (i.e. non-preloaded) and a low loading rate (7.5 mm/s) as shown in Figure 3.24(a)). An average of the results was calculated and the slope of the 'average' stress-strain curve was determined. In the baseline study, the value of the stress exponentially increases as stain increases. As CCME, by definition, is the segmental stiffness change, the CCME is always larger than the TCME as shown in Figure 3.24(b). As the strain increases, the difference between CCME and TCME became larger. In particular, at 100% actual deformation, the value of the CCME is nearly five times higher than that of TCME (33.1 MPa versus 7.2 MPa).

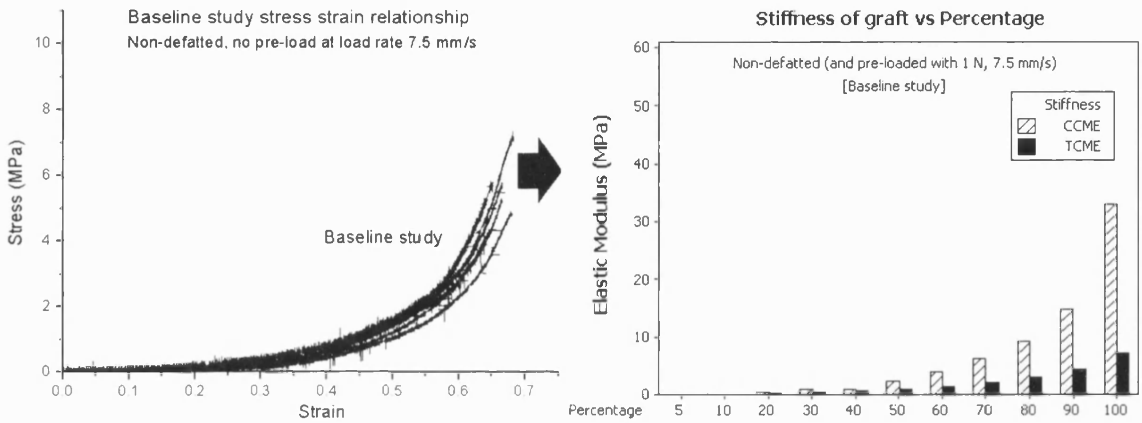

(a) Stress-strain curve (b) Slope of stress-strain curve

Figure 3.24.: a) Non-defatted, 1 N pre-loaded and 7.5 mm/s load rate is defined as baseline study. b) The associated slope (i.e. modulus of elasticity) was then averaged and plotted. Results of experiments 1 – 6.

3.6.5.4. Effect of pre-loading

The stress-strain curves showing the effect of pre-loading were plotted in Figure 3.25 (Remark: same as Figure 3.16 on Page 92). As was previously seen, the shape of the stress-strain curves for pre-loading were completely different. Therefore, a great difference in stiffness was expected. It is very important to note that the strain of non-preloaded and pre-loaded cases are different. In other words, 10% 'actual' deformation (i.e. strain) are different. So, direct comparsion of the stiffness value between two cases is inappropriate.

Figure 3.25 presents the impact of pre-loading on the modulus of elasticity. It can be seen that the 5% and 10% ICME in the baseline study showed zero stiffness whereas the 5% and 10% ICME in pre-loaded case showed nearly 60 MPa and 35 MPa respectively. As a result, a high instantaneous impaction force was expected; this can probably be attributed to the high static friction between the graft particles. In order to overcome the initial frictional force, high energy and high forces are required. Once the frictional force is overcome, the stiffnesses (both CCME and TCME) drop significantly before increasing steadily.

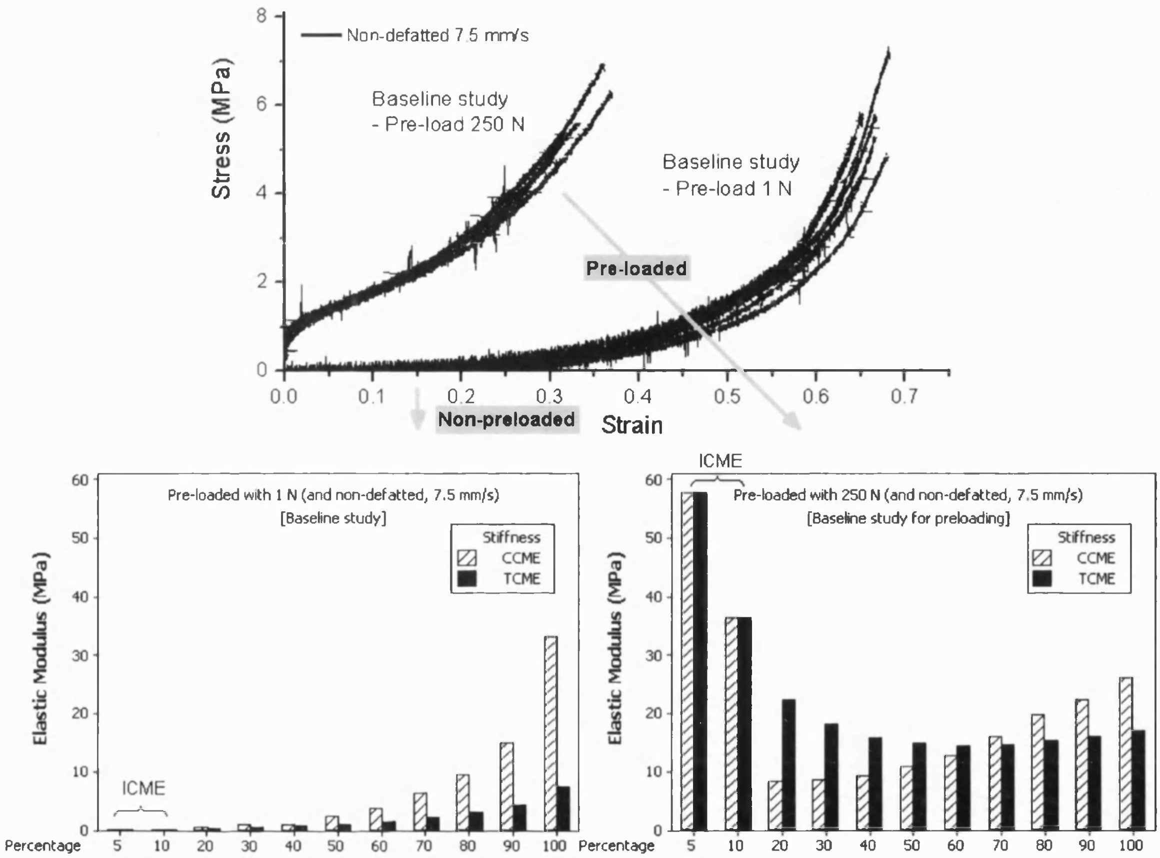

Figure 3.25.: Effect of the pre-loading on the modulus of elasticity (above), baseline study for non-preloaded graft (left), baseline study for pre-loaded graft (right). Average of results of experiments 1 – 6 (left) and 7 – 12 (right).

For the CCME of pre-loaded graft, the stiffness dropped from about 60 MPa to nearly 10 MPa when the stiffness percentage changed from 5% to 20%. From 20% to 50%, the stiffness was nearly ten times higher than the baseline study. The stiffness continues to increase from stiffness percentage 60% onward. Ultimately, at 100%, the magnitude of CCME of pre-loaded graft reached 26.1 MPa.

The TCME behaved in a similar manner to the CCME, although there was a significant drop of stiffness between 5% to 20%, showing a smooth transition and becoming steady at about 50%. As a result, if the graft is pre-loaded, compressing the graft to half of its height is sufficient to estimate the TCME.

It is also important to note that in the baseline study on the left hand side of Figure 3.25 (left), the CCME is always larger than the TCME at all times. As can be seen on Figure 3.25 (right), 20%, 30%, 40%, 50% and 60% TCME was larger than that of CCME. However, at 70%, 80%, 90% and 100%, the CCME was larger than that of TCME. Therefore, the way that the results can be interpreted yields a slight difference in the modulus of elasticity. This could be the reason why a wide range of apparent stiffnesses (8.0 – 100 MPa) have been reported in many studies [68, 116, 120, 126, 132].

3.6.5.5. Effect of load rate

The stress-strain curves showing the effect of pre-loading are plotted in Figure 3.26 (Remark: same as Figure 3.18 on Page 94). As can be seen, the shapes of the curves were similar. Therefore, the value of CCME, TCME and ICME would be similar for two different load rates. The effect of load rate on the Modulus of Elasticity is illustrated in Figure 3.26. Both the CCME and TCME show similar trends and magnitudes to the baseline study. It was found that material became stiffer at higher load rates due to viscoelastic properties of graft.

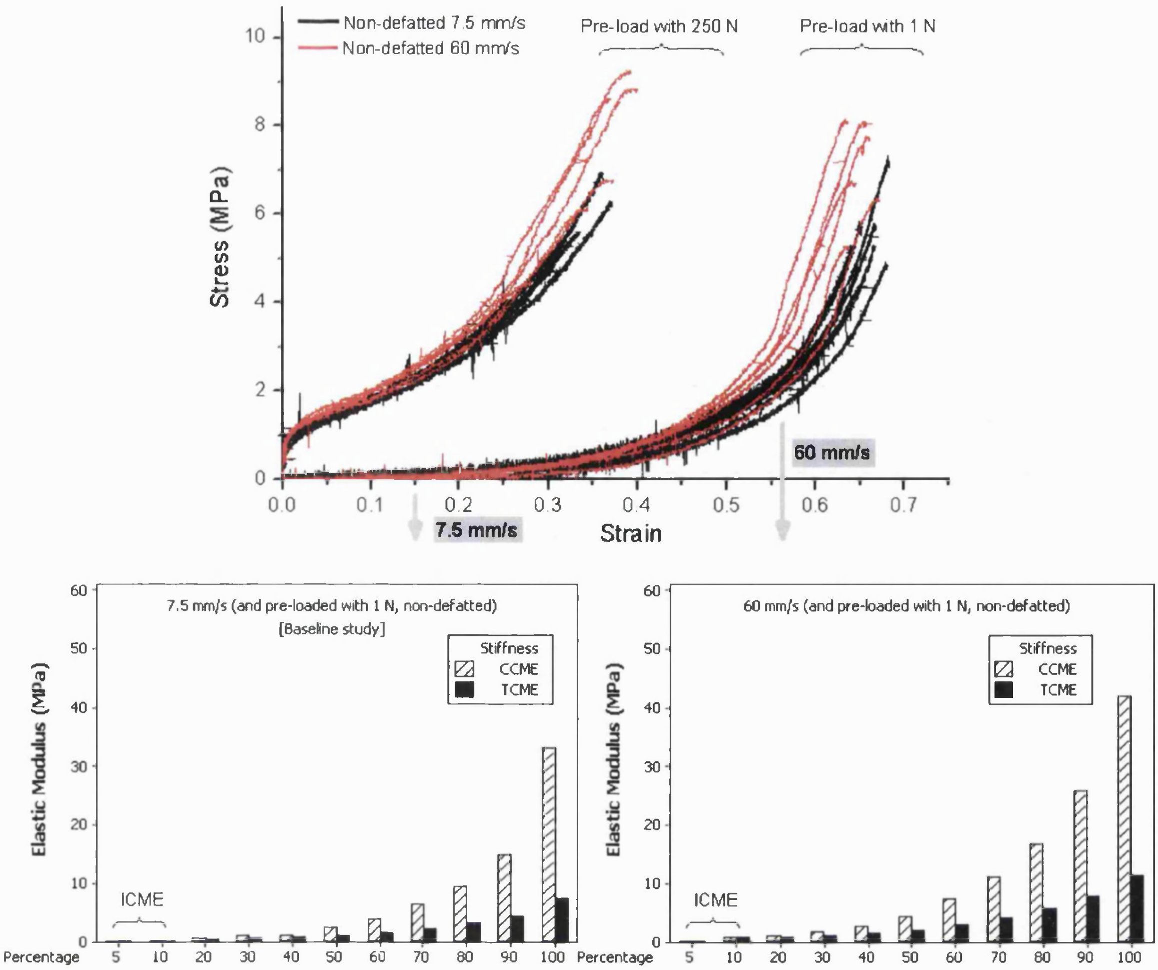

Figure 3.26.: Effect of the load rate without pre-loading on the modulus of elasticity (above). Low load rate (7.5 mm/s, left), high load rate (60 mm/s, right). Average of results of experiments 1 – 6 (left) and 13 – 18 (right).

Figure 3.27 (Remark: same as Figure 3.18 on Page 94) shows the effect of a higher load rate for which the graft was pre-loaded with 250 N. This gave similar results in which the stiffness increased with loading rate. In particular, at 60% actual deformation, CCME was slightly larger that TCME.

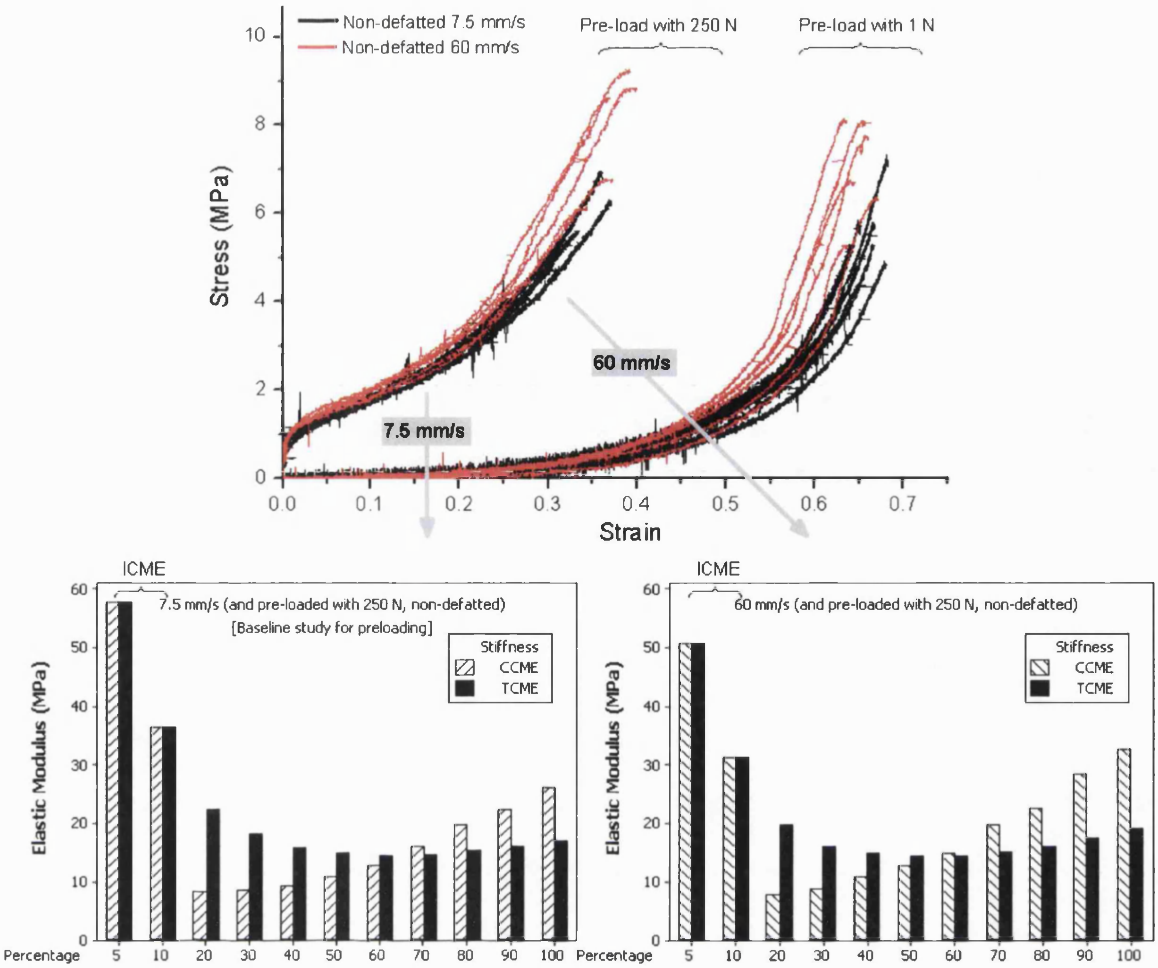

Figure 3.27.: Effect of the load rate with pre-loading on the modulus of elasticity (above). Low load rate (7.5 mm/s, left), high load rate (60 mm/s, right). Average of results of experiments 7 – 12 (left) and 19 – 24 (right).

3.6.5.6. Effect of defatting

The stress-strain curves showing the effect of defatting are given in Figure 3.28 (Remark: same as Figure 3.20 on Page 96). As can be seen, the shapes of the curves are similar. It was, therefore, expected that the values of CCME, TCME and ICME would be similar for the two different load rates. CCME, TCME and ICME gave similar trends and magnitudes to the baseline study. It was found that bone graft material became stiffer after defatting.

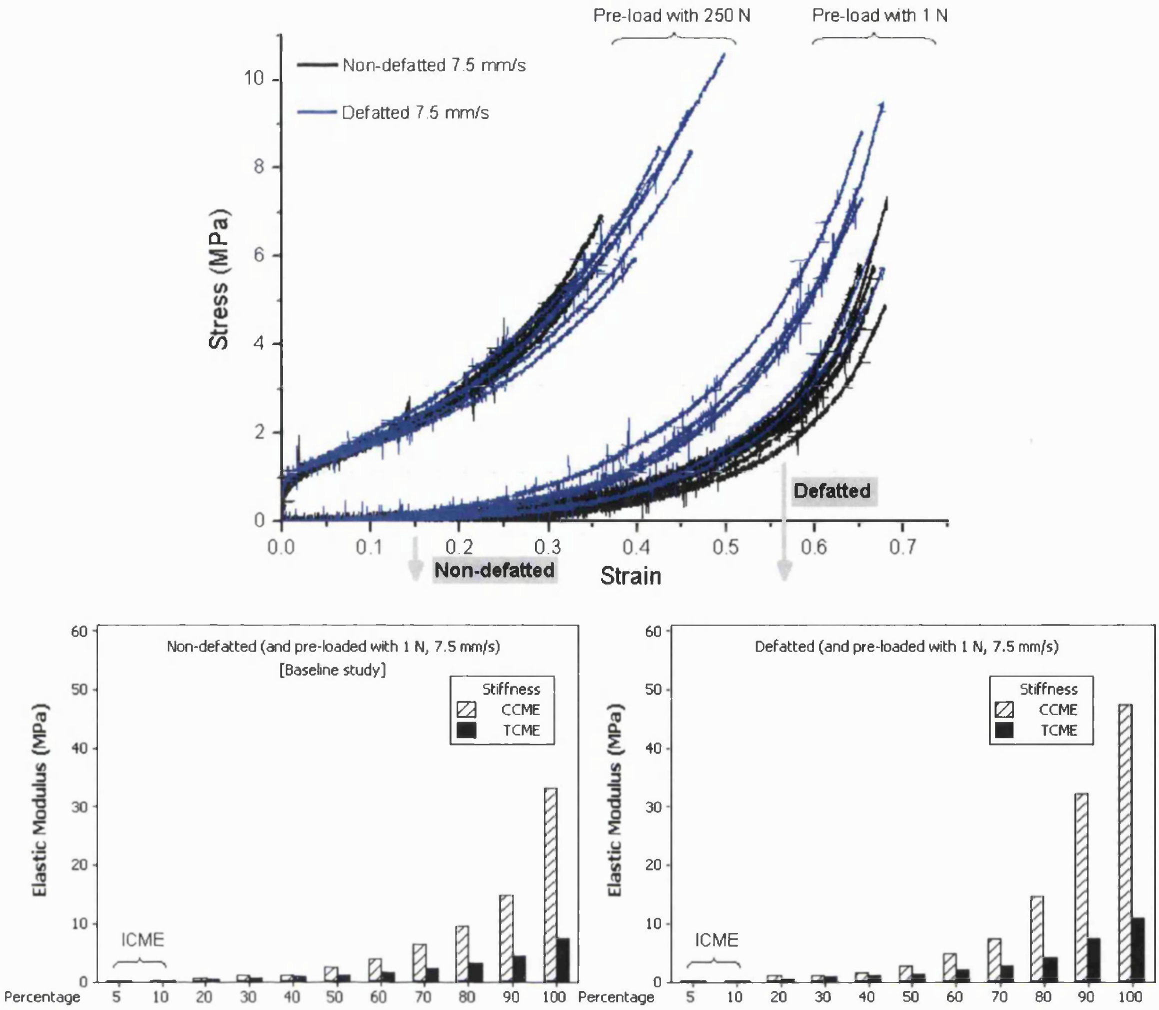

Figure 3.28.: Effect of the defatting without pre-loading on the modulus of elasticity (above). Non-defatted (left), defatted (right). Average of results of experiments 1–6 (left) and 25 – 30 (right).

As defatted graft has a higher compressive resistance, the inital position of displacement after pre-loading with 250 N was different to that of the non-defatted graft. In order to compress the graft to a height of 12 mm, more strain was needed because of a higher initial thickness (as shown in Figure 3.19 on Page 95). Since these curves had markedly different strains, to allow comparison between results, percentages of 'actual' deformation were used, thus 10% of the actual deformation in the two cases is different.

Figure 3.29 presents the effect of defatting for which the graft was pre-loaded with 250 N. After defatting, the 5% ICME increased from about 60 MPa to nearly 90 MPa. The TCME behaved in a similar manner to the baseline study for pre-loading. However, it was interesting to note that the CCME dropped from 90% to 100%. The reason for this was unclear.

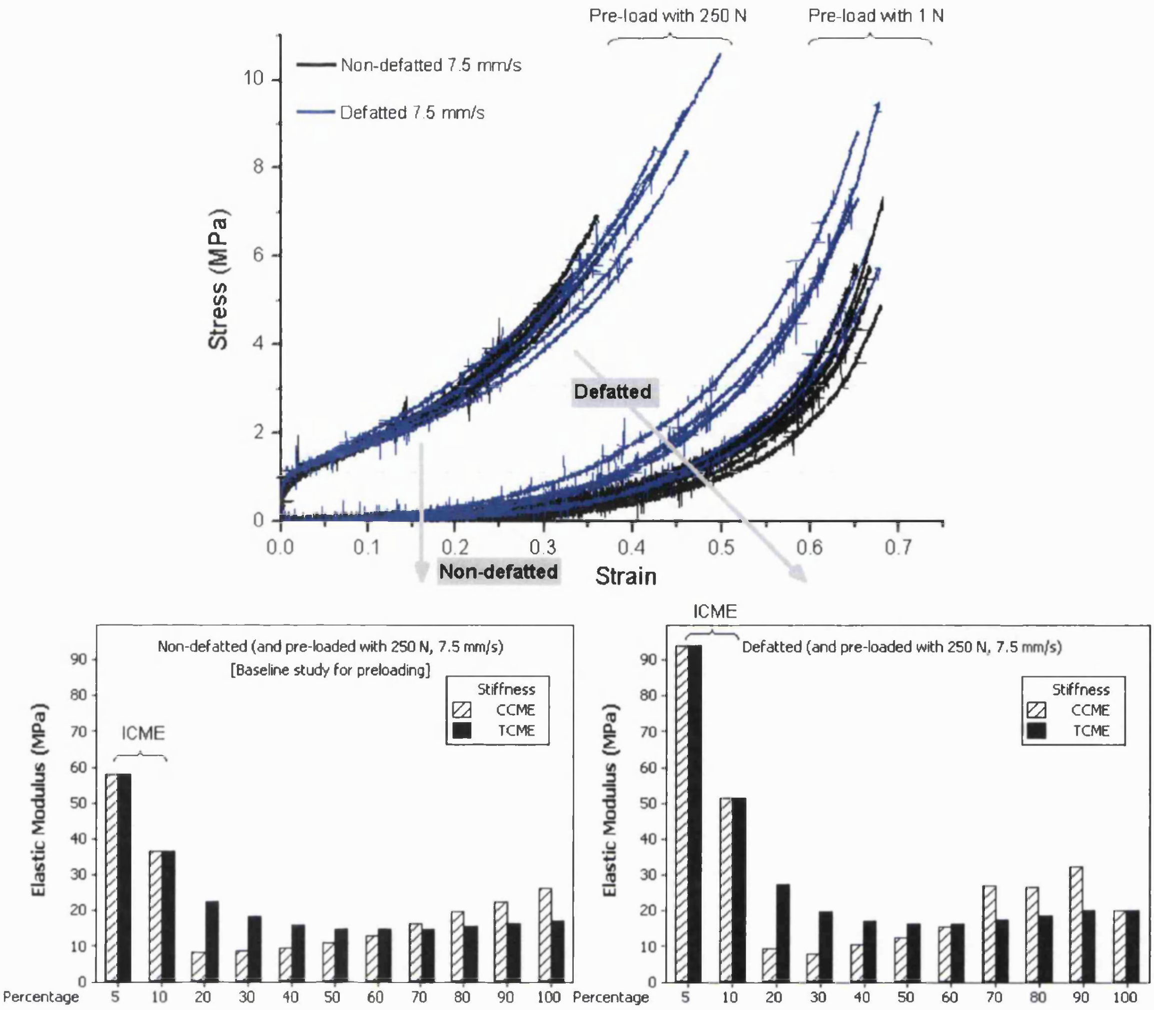

Figure 3.29.: Effect of the defatting with pre-loading on the modulus of elasticity (above). Non-defatted (left), defatted (right). Average of results of experiments 7 – 12 (left) and 31 – 36 (right). Notice that the y-axis scale (i.e. stiffness) is not the same as the previous figures (i.e. Figure 3.24(a)–Figure 3.29).

3.6.5.7. Overall comparison

Table 3.12 provides a summary of the whole section (§3.6.5).

Stiffness	Observations
CCME	Exponential increases when graft is not pre-loaded. Stiffness increases with load rate and defatting. However, if the graft is pre-loaded, CCME decreases dramatically and then increases. In particular, CCME dropped from 90% to 100% when defatted graft was pre-loaded with 250 N.
TCME	Exponential increases when graft is not pre-loaded. Stiffness increases with load rate and defatting. However, if the graft is pre-loaded, TCME decreases dramatically and then increases steadily. Furthermore, TCME is generally smaller than CCME, but CCME can be larger if the graft is pre-loaded.
ICME	Generally very low (nearly zero), but can be extremely high if graft is pre-loaded (can be up to $\sim$ 100 MPa).

Table 3.12.: Summary of modulus of elasticity.

3.6.6. Strain energy density

3.6.6.1. Methods

The strain energy was determined by the area under the stress-strain curve (i.e. trapezium rule). To do this, it is essential to remove any noise which can induce error (Figure 3.30) during the calculation of strain energy. From the curve, the noise did not show any periodic peaks. Therefore, the noise probably came from the mechanical vibration during testing. In order to minimise the amount of noise, data was manually adjusted so that obvious noise was removed.

The principle of finding strain energy is to sum up all the trapezoid areas under the stress-strain curve as shown in Figure 3.31. Matlab 7.0.4 (MathWorks, Inc.) was employed for this numerical analysis.

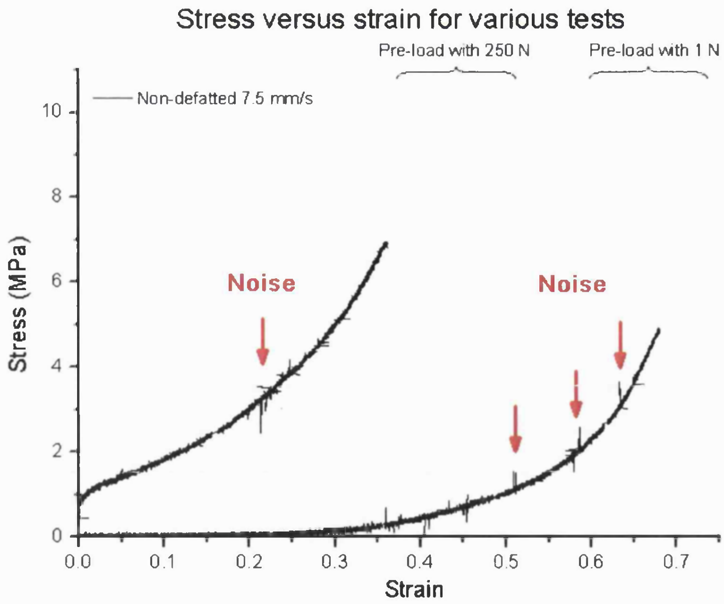

Figure 3.30.: Noises in raw data.

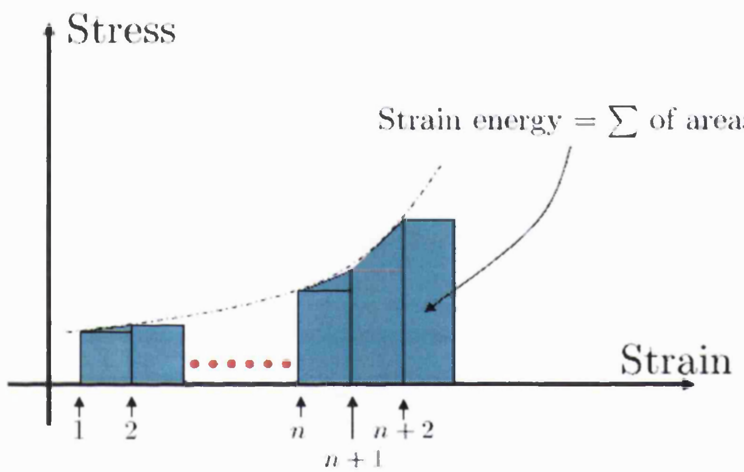


```
energy=0;
matrix_size=size(B);              % Obtain the size of the data matrix
rows=matrix_size(1,1);            % Obtain the number of rows

for n=1:(rows-1)                  % B(:,1)=stress, B(:,2)=strain
    step=B((n+1),2)-B(n,2);
    energy=energy+B(n,1)*step+(B((n+1),1)-B(n,1))*step/2;
end
```

Figure 3.31.: Method of calculating the area under the stress-stain curve and associated Matlab codes for estimating the strain energy.

3.6.6.2. Results of strain energy density

Table 3.13 shows a summary of all the strain energy found in the experiments. The mean and the standard deviation (in parentheses) are also given. Note that the run order represents the order in which the experiments were run.

Run order	1 − 6	7 − 12	13 − 18	19 − 24
Defatting	−	−	−	−
Pre-loading	−	+	−	+
Load rate	−	−	+	+
Energy ($\times 10^6$)	3.00 (0.59)	1.00 (0.25)	3.80 (0.62)	1.45 (0.58)
Normalised mean	1	0.33	1.27	0.48

Run order	25 − 30	31 − 36	37 − 42	43 − 48
Defatting	+	+	+	+
Pre-loading	−	+	−	+
Load rate	−	−	+	+
Energy ($\times 10^6$)	3.94 (0.72)	2.23 (0.59)	4.38 (0.90)	2.41 (0.44)
Normalised mean	1.31	0.74	1.46	0.80

Table 3.13.: Summary of mean and one standard deviation (presented in bracket) of strain energy density (U, J/m^3).

3.6.6.3. Statistical analysis

The strain energy (Table 3.13) was plotted in a bar chart as shown in Figure 3.32. As can be seen from this figure, the amount of strain energy density (U) ranges between 1×10^6 J/m^3 to 5×10^6 J/m^3. It is important to note that the strain energy was calculated per unit volume. Therefore, it was a specific value which was independent of the volume of the graft. The pre-loaded graft presented lower strain energy densities (40%−70% lower) for all cases since a certain proportion of energy was absorbed by the graft during pre-loading. The strain energy density increased (10%−50% higher) if a high loading rate was used because of the viscoelastic effect. Finally, defatted graft was also found to give a higher strain energy density (10%−120% higher) because the material became stiffer after washing.

Statistical analysis (Pareto analysis) showed that all three factors: defatting, pre-loading and load rate were statistically significant (i.e. all had a significant influence on the strain energy density). Pre-loading was found to have the biggest influence. This was because the stain energy was absorbed during pre-loading. Defatted graft and a high loading rate also showed significant influence on the strain energy density, as these caused a higher stiffness of the stress-strain curve. Hence a higher value of strain energy was measured.

In addition, no interaction was found between the different parameters. Results of the Pareto analysis and the interaction plot are illustrated in Figure 3.33, and a summary is given in Table 3.14.

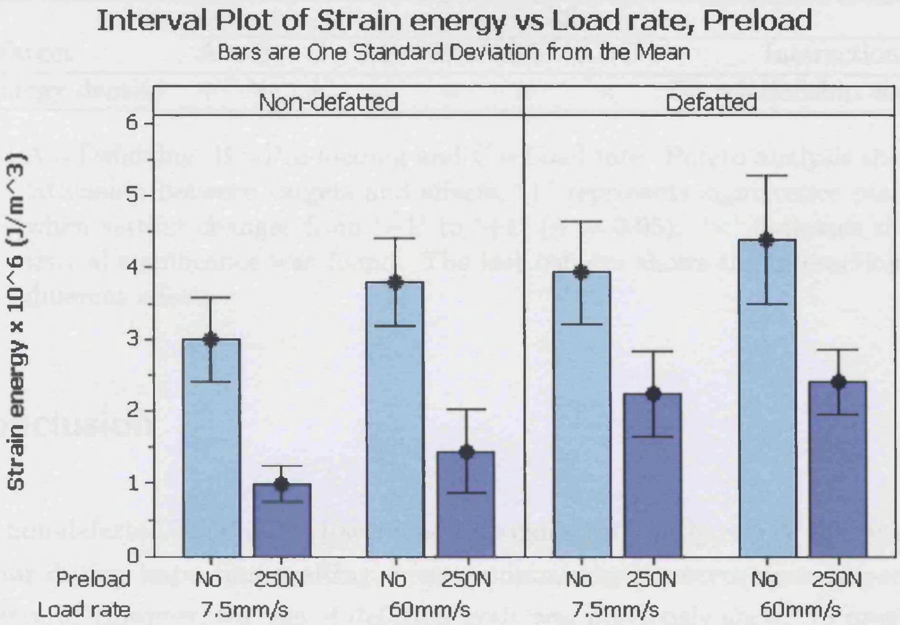

Figure 3.32.: Interval plot shows mean and one standard deviation of the strain energy (full results in Table 3.13).

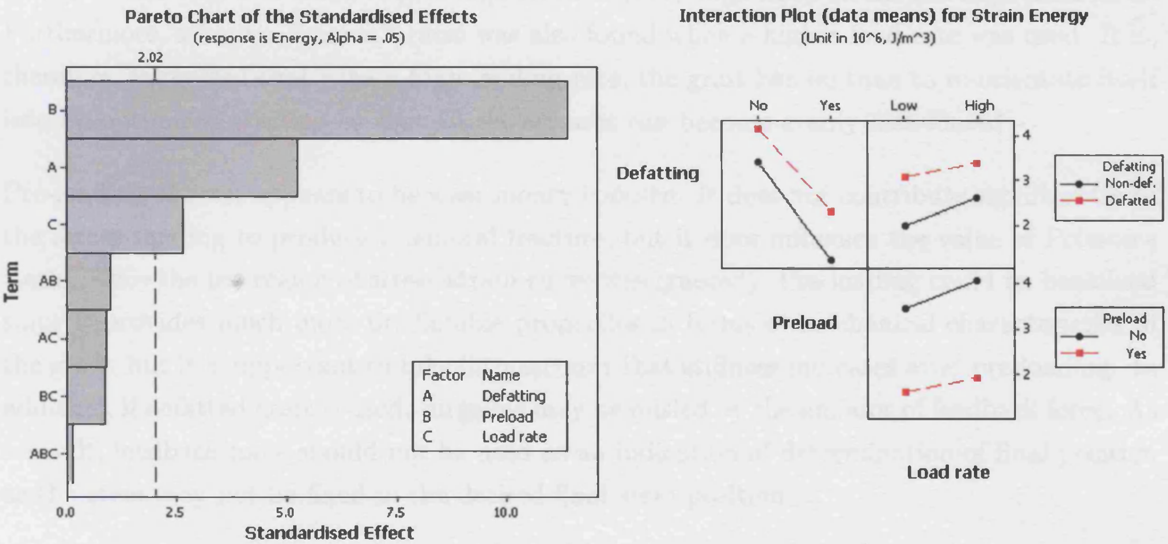

Figure 3.33.: Statistical analysis (Pareto analysis) of the calculated strain energy density. The effect is statistically significant when the standardised value exceeds the vertical dotted line ($\alpha = 0.05$). Figure on the right hand side shows the interaction between different variables.

Target	Effect(s)							Interaction
	A	B	C	AB	BC	AC	ABC	
Strain energy density	+	+	+	×	×	×	×	No relationship was found

Table 3.14.: A = Defatting, B = Pre-loading and C = Load rate. Pareto analysis shows the relationship between targets and effects, '+' represents significance positive effect when setting changes from '−1' to '+1' ($\alpha = 0.05$). '×' indicates that no statistical significance was found. The last column shows the interactions between different effects.

3.7. Conclusion

The use of non-defatted MCB and a lower load rate can significantly reduce the strain exerted on the femur during impaction grafting, hence, minimising the occurrence of per-operative femoral fracture. However, the use of defatted graft was previously shown to provide a high shear strength, cohesion and friction angle [94]. It was also found that defatting of graft does not greatly influence the Poisson's ratio.

A higher load rate was found to give high stiffness [115], high hoop strain and high axial force. Furthermore, a higher Poisson's ratio was also found when a higher load rate was used. It is, therefore, suggested that with a high loading rate, the graft has no time to re-orientate itself into an optimised position so that all the stresses can become evenly distributed.

Pre-loading of graft appears to be a secondary concern. It does not contribute significantly to the forces tending to produce a femoral fracture, but it does influence the value of Poisson's Ratio (since the toe region of stress-strain curve was ignored). Pre-loading could be beneficial since it provides much more predictable properties in terms of mechanical characteristics of the graft, but it is important to take into account that stiffness increases after pre-loading. In addition, if defatted graft is used, surgeons may be misled by the amount of feedback force. As a result, feedback force should not be used as an indication of determination of final position as the stem may not be fixed in the desired final stem position.

The mechanical properties of graft changed dramatically under different conditions. The dynamic behaviour of bone graft still remains unknown. To date, there is still no standard method to quantify the mechanical properties of MCB especially with respect to parameters such as Poisson's ratio and Young's modulus.

4. The effects of different loading regimes

4.1. Introduction

The aim of this study was to examine the effects of repetitive cyclic loading and the load rates on morsellised bone graft material. Variables including: compressive force, displacement and mass were recorded. Recoil and relaxation were also determined. The die plunger test was used in this study. Again, the primary objective was not to acquire precise material properties but to compare the material properties under different loading conditions.

4.2. Design of test rig

The test rig consisted of four parts, a plunger, a die, a base and a sample extractor. The die was of a similar design to the previous experiment described in §3 on Page 73. Figure 4.1 and Figure 4.2 illustrate the components and assembly of the rig. The plunger was made of mild steel (EN1A) and had a diameter of $20^{+0.00}_{-0.02}$ mm. The die was 77 mm long and made of mild steel (EN24T) which has a $20^{+0.05}_{-0.00}$ mm internal diameter and 40 mm external diameter (i.e. a thick cylinder). Therefore, the die was rigid enough to provide a constrainted environment. Both the plunger and the die were polished to minimise any friction generated during impaction. In addition, a brass porous disc was installed at the bottom of the die to allow escape of liquid materials when non-defatted graft was tested. The base was made of steel (EN1A) and mounted on the loading machine. The position of the die was aligned so that it remained parallel to the plunger at all times as shown in Figure 4.3.

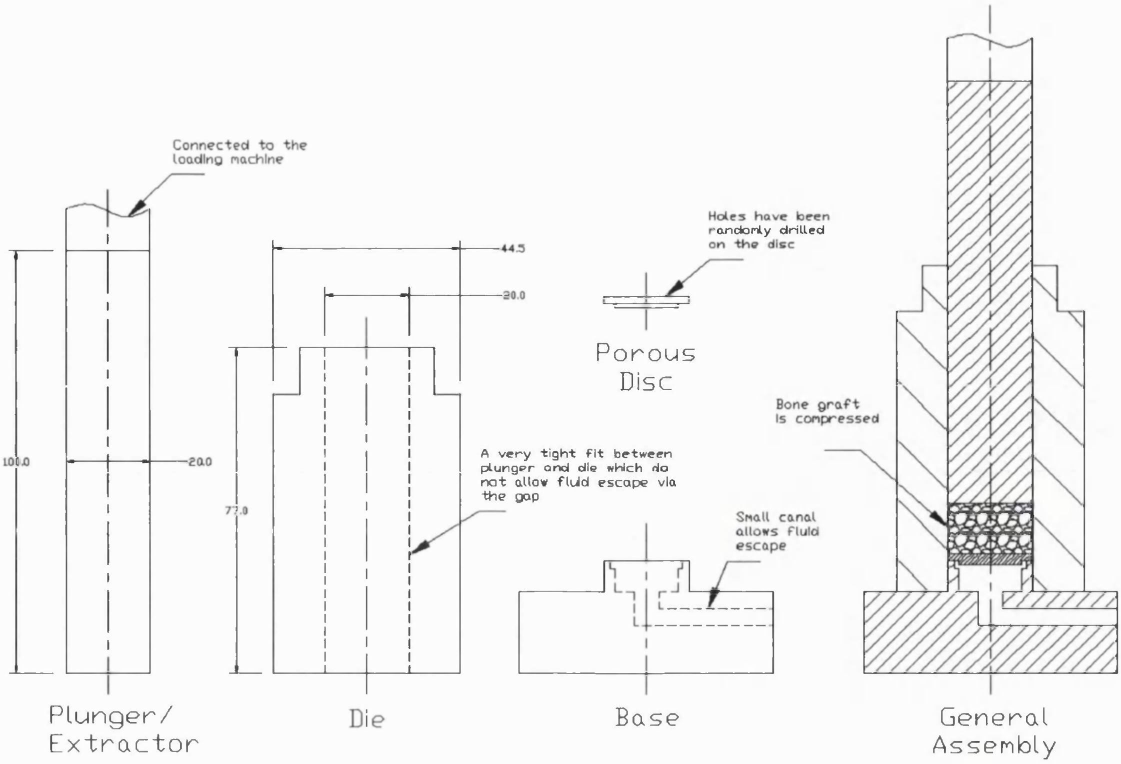

Figure 4.1.: Schematic diagrams of plunger, extractor, die, base, porous disc and a general assembly diagram (unit in mm).

(a) Disassembly diagram

(b) General assembly

Figure 4.2.: a) Diagrams of plunger, die, base and porous disc. b) Diagram shows a fully assembly rig.

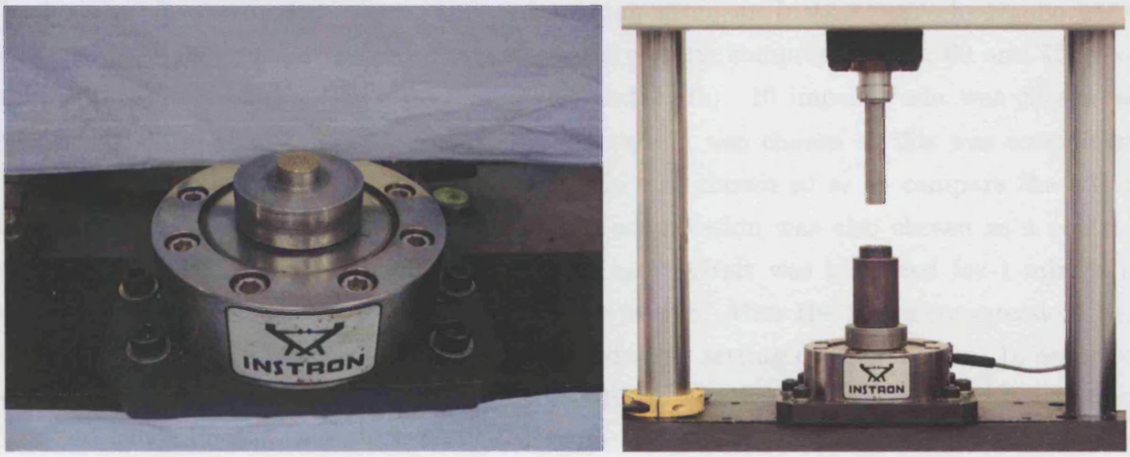

(a) Brass porous disc (b) Instron 8511 loading machine

Figure 4.3.: a) Brass porous disc is placed on top of the base and the load cell allows fluid penetration via the holes. b) Fully setup experimental rig allows variable loading conditions.

4.3. Methods

4.3.1. First experiment

The first experiment was to determine the effect of repetitive cyclic loading on morsellised bone graft.

The amount of MCB was determined by volume rather than by mass as is used in the clinical situation as previously described in §3 on Page 73. Porcine femoral heads were used and the graft preparation method was according to §2 on Page 67. 10 cm^3 of MCB was measured into a plastic measuring cup. The net weight was measured by an electronic balance (AC-12K, Adam Equipment, UK). It was noted that the diameter of the plastic measuring cup was about 20 mm whilst the length of the individual morsellised graft particles varied from around 2 mm to 20 mm. As a result, this could introduce large voids between particles. Therefore, great care was taken to ensure that a range of sizes of graft particles were used to fill all the voids within the 10 cm^3 cup. Graft was then inserted carefully into the die and impacted using an index finger to make sure graft settled near the base. The desired impaction frequency was inputted to the Instron control panel prior to testing.

Similar to the previous studies (see §3.3 on Page 75), the graft was pre-loaded with 100 N. A stroke rate of 0.5 mm/s was employed and stopped when the load reached 100 N. In addition, 1 min was allowed for setting up the equipments. Graft was then impacted with desired impaction rate. Primary parameters including stroke position and compressive force are monitored by HPVEE.

The bone graft was loaded in uni-axial compression using an Instron servo-hydraulic 8511 machine. Four different impaction frequencies: pure static compression, 10, 60 and 120 impacts/min, were used (i.e. 0 Hz, 0.17 Hz, 1 Hz and 2 Hz). 10 impacts/min was chosen as this approximates the clinical situation; 60 impacts/min was chosen as this was considered to represent high impaction rate; 120 impacts/min was chosen so as to compare the effect of doubling the impaction frequency; pure static compression was also chosen as a control experiment. A sinusoidal input was used in all cases. Graft was impacted for 1 min at a load of 1 kN, which was about 1.5 times the body weight. After the 1 min compression, the loading force was returned to 0 N as this was the default setting of the machine. In order to perform a relaxation testing, graft was additionally compressed to 1 kN. Both non-defatted (no treatment) and defatted (with treatment) graft were used.

After impaction, graft was left in compression for 2 mins, and the level of relaxation was measured. The graft was then extracted by the sample extractor. A vernier calliper was used to measure the sample thickness, and the amount of recoil was determined by the change of thickness of the graft.

4.3.2. Second experiment

The second experiment was to determine the effect of impaction rate on morsellised bone graft.

Graft material was loaded in uni-axial compression using an Instron servo-hydraulic 8511 machine. Seven different impaction rates (5, 10, 20, 30, 40, 50 and 60 mm/s) were chosen. 10 cm^3 of MCB was measured into a plastic measuring cup. The graft was then inserted carefully into the die as previously describe (see §4.3.1 on Page 118).

The 10 cm^3 of bone graft was compressed to a thickness of 8 mm (equivalent to a volume of 2.51 cm^3 ($= \frac{\pi(2)^2}{4} \times 0.8$)). After each experiment, graft was extracted by the sample extractor and the amount of recoil was determined by the change of thickness of the graft after extraction.

4.4. Experimental design

4.4.1. Design of experiment (First experiment)

A simple experimental design was used in this experiment. Two parameters, defatting and impaction frequency were used. The defatting variable was classified as attribute data (i.e. low or high). Four loading frequencies were used, static (i.e. 0 Hz), 0.17 Hz, 1 Hz and 2 Hz. Each test was repeated ten times. Therefore, 80 ($= 2 \times 4 \times 10$) experiments were performed. Table 4.1 summarises all the experimental settings. The run order represents the actual order that the experiment was run. The statistics package Minitab 14.20 (Minitab Inc.) was used to perform statistical analysis.

Symbol	−	+
Defatting	Non-defatted	Defatted

Run order	Defatting	Number of impacts in 1 min	⇒ Equivalent frequency (Hz)
1	−	Static	0
2	−	10	0.17
3	−	60	1
4	−	120	2
5	+	Static	0
6	+	10	0.17
7	+	60	1
8	+	120	2

Table 4.1.: Experimental design (first experiment) with one replication.

The experimental procedures can be summarised as follow:

- Initialise the Instron and set up the rig.
- Measure 10 cm^3 of MCB and record the net sample weight using an electronic balance.
- Insert the bone graft into the cast iron die.
- Adjust the load cell to zero.
- Move the stroke at speed 0.5 mm/s and stop the actuator at 100 N compressive force.
- Initialise the data acquisition system, which takes about 1 min.
- Impact with 1 kN compressive half-sine for 1 min (0 Hz, 0.17 Hz, 1 Hz or 2 Hz).
- Re-compress the graft to 1 kN.
- Stop the stroke in position and measure the stress relaxation for 2 mins.
- Remove the sample with the extractor and measure the thickness of the sample with a vernier calliper.

4.4.2. Design of experiment (Second experiment)

A simple experimental design was used in the second experiment. Seven different loading rates were used (5, 10, 20, 30, 40, 50 and 60 mm/s). Each test has ten replications. Therefore, 70 (= 7×10) experiments were performed. Table 4.2 summarises all the experimental settings. The run order represents the actual order in which the experiment was carried out. The statistics package Minitab 14.20 (Minitab Inc.) was used to perform statistical analysis.

Run order	Rates (mm/s)
1	5
2	10
3	20
4	30
5	40
6	50
8	60

Table 4.2.: Experimental design (second experiment) with one replication.

The experimental procedures can be summarised as follow:

- Initialise the Instron and set up the rig.
- Measure 10 cm^3 of MCB.
- Insert the bone graft into the cast iron die.
- Adjust the load cell to zero.
- Initialise the data acquisition system.
- Compress the graft into 8 mm thickness with desired impaction rate (5, 10, 20, 30, 40, 50 or 60 mm/s).
- Remove the sample with the extractor and measure the thickness of the sample with a vernier calliper.

4.4.3. Sources of error

Table 4.3 gives the sources of error that could effect the accuracy of the experiment.

Source of error	Likelihood
Frictional force generated due to stroke movement	Medium
Variability of graft properties from batch or batch	Low

Table 4.3.: Sources of error.

4.5. Estimation of stress and strain

Table 4.4 provides the variables which were used in the experiment. In order to estimate the stress and strain behaviour, the cross sectional area of the stroke and the deformation are required. Appropriate equations are also listed.

Variable	Value	Unit	Quantity	Remark
A		mm^2	Plunger cross section area	Calculated by Equation 4.1
d	0.02	m	Plunger diameter	Known
m		g	Mass of graft	Measured by electronic balance.
s		mm	Stroke displacement	Measured by Instron via HPVEE
$l_{initial}$		mm	Graft initial thickness (before impaction)	Converted by Equation 4.2
$l_{measured,\,t}$		mm	Graft measured thickness	Converted by Equation 4.2
l_{recoil}		mm	Graft thickness (after the graft was extracted)	Measured by vernier calliper
F_t		N	Applied force	Measured by Instron via HPVEE
$\sigma_{app,\,t}$		MPa	Applied stress	Calculated by Equation 4.3
$\varepsilon_{app,\,t}$		%	Apparent strain	Calculated by Equation 4.4
R_{relax}		%	Relaxation	Calculated by Equation 4.5
R_{recoil}		%	Recoil	Calculated by Equation 4.6 and Equation 4.7

Table 4.4.: Notation, quantity and unit used in estimation of stress and strain.

The cross sectional area was calculated through the standard equation.

$$A = \frac{\pi d^2}{4} \tag{4.1}$$

After calibration, the amount of thickness was converted using the following equation. (Remark: the value of 54 mm was the offset value to convert the recorded raw displacement data from the Instron linear variable displacement transducer (LVDT) displacement transducer to the thickness of the graft).

$$l = s + 54 \tag{4.2}$$

The stress was calculated by the following equation.

$$\sigma_{app,\,t} = \frac{F_t}{A} \tag{4.3}$$

The strain was calculated by the different of thicknesses.

$$\varepsilon_{app,\,t} = \frac{l_{initial} - l_{measured,\,t}}{l_{initial}} \tag{4.4}$$

The relaxation was calculated by the difference of residual forces.

$$R_{relax} = \frac{1000 - F_{t=180\,\mathrm{s}}}{1000} \times 100\% \tag{4.5}$$

The recoil (for first experiment, repetitive test) was calculated by the change of thickness after impaction.

$$R_{recoil\,(1st)} = \frac{l_{recoil\,(1st\,exp)} - l_{measured,\,t=180\,\mathrm{s}}}{l_{measured,\,t=180\,\mathrm{s}}} \times 100\% \tag{4.6}$$

The recoil (for second experiment, various impaction rates test) was calculated by the change of thickness after impaction.

$$R_{recoil\,(2nd)} = \frac{l_{recoil\,(2nd\,exp)} - 8}{8} \times 100\% \tag{4.7}$$

4.6. Results and discussion (1st exp)

4.6.1. Summary of results

Table 4.5 shows a summary of all the experimental results. Full detailed experimental results can be found in Appendix A.3 on Page 179. The mean (i.e. the average) of each experimental setting was determined. The standard deviation was calculated by the statistics package Minitab 14.2 (Minitab Inc.).

Run order	1 – 10	11 – 20	21 – 30	31 – 40
Defatting (D_{defat})	–	–	–	–
Frequency (f, Hz)	Static	0.17	1	2
Mass (m, g)		5.65 (0.10)		
Initial thickness*		23.58 (3.09)		
Impacted thickness**	11.49 (0.86)	11.16 (0.85)	11.11 (1.08)	11.19 (0.66)
Recoil ($R_{recoil\,(1st)}$, %)	42.92 (4.59)	41.64 (6.87)	33.78 (10.72)	38.45 (3.67)
Relaxation (R_{relax}, %)	14.73 (3.28)	20.69 (3.81)	25.65 (4.93)	18.70 (3.97)

Run order	41 – 50	51 – 60	61 – 70	71 – 80
Defatting (D_{defat})	+	+	+	+
Frequency (f, Hz)	Static	0.17	1	2
Mass (m, g)		4.67 (0.11)		
Initial thickness*		26.71 (2.08)		
Impacted thickness**	11.89 (0.40)	12.70 (0.59)	12.88 (0.55)	12.98 (0.54)
Recoil ($R_{recoil\,(1st)}$, %)	35.54 (1.10)	34.18 (2.06)	36.47 (4.07)	34.94 (4.38)
Relaxation (R_{relax}, %)	9.80 (3.94)	23.61 (2.67)	25.40 (1.43)	26.00 (1.25)

Table 4.5.: Summary of mean and one standard deviation (presented in bracket) of mass, Initial thickness, impacted thickness, relaxation and recoil. Mass is a variable independent to impaction frequency. *Unit in ($l_{initial}$, mm). **Unit in ($l_{measured,\,t=180\,s}$, mm).

4.6.2. Typical experimental results

4.6.2.1. Force and displacement against time

Figure 4.4 shows the typical experimental results obtained at four different impaction frequencies. Both force and displacement were measured against time. A zoom-in view is also plotted so that the effect of the change of frequency can been seen. For static compression, the stroke was set to compress at 1 kN. It was, however, found that the force oscillated over a range of 850 N to 1150 N due to the instabilites of the machine during static compression. (Remark: the machine problem was caused by the fault of the Proportional-Integral-Derivative (PID) controller, and was fixed subsequently after servicing). Despite repeated attempts, no improvement was able to solve this particular problem. When impacting at frequencies 0.17 Hz, 1 Hz and 2 Hz, the impaction force alternated from 0 N to 1 kN for 1 min. At the end of the cycle, the force returned to 0 N. A small additional compression of 1 kN was applied. A delay of approximately 5 seconds was required for the changeover of settings. The position (i.e. the displacement) of the stroke stopped at 1 min (i.e. no more impactions) and relaxation was measured for 2 mins.

It was observed that displacement dropped dramatically after a few cycles of compaction, and the displacement decreased in an inverted logarithmic manner (for a definition of 'inverted logarithmic' refer to Figure 1.34 on Page 44). After the compression of a force of 1 kN, the displacement was kept constant to allow measurement of relaxation. It can be seen that the magnitude of the force decreased with time.

Note that the displacement in Figure 4.4 was different to the thickness given in the experimental summary in Table 4.5 for the purpose of illustration. The displacement was converted to the thickness by Equation 4.2 on Page 122.

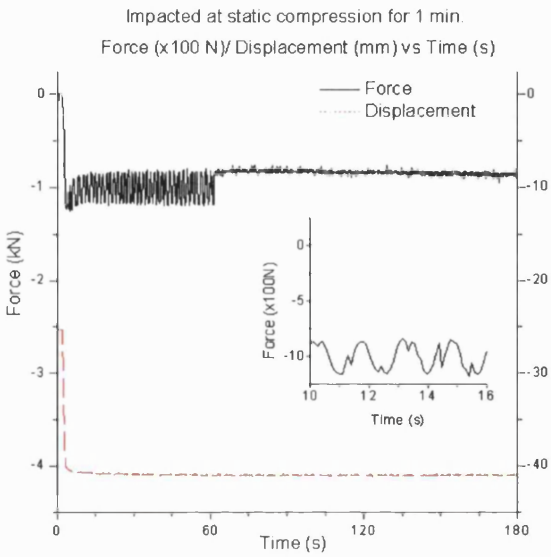

(a) Static compression

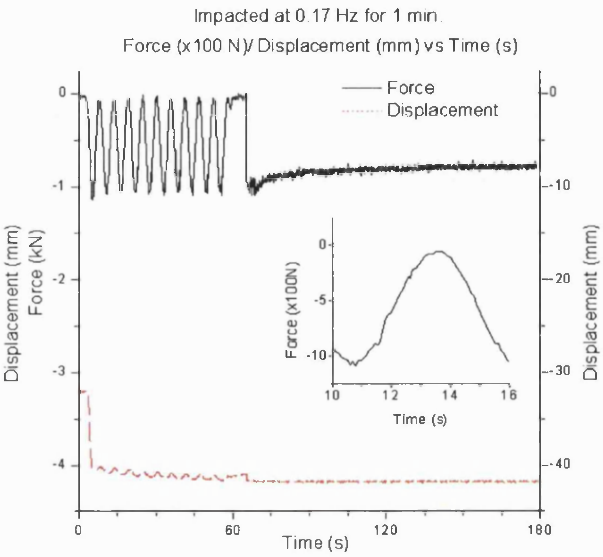

(b) Impaction frequency 0.17 Hz

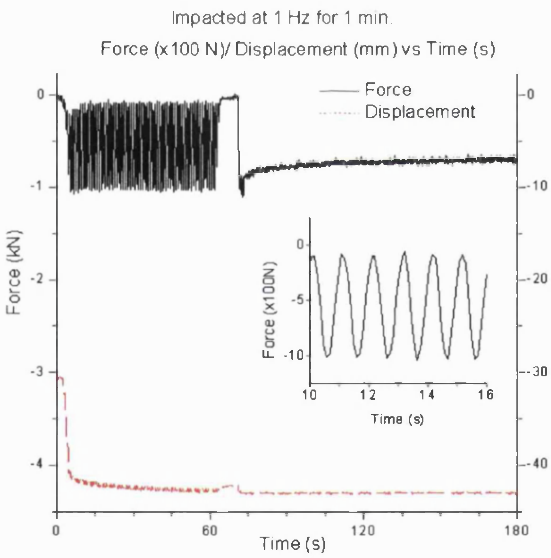

(c) Impaction frequency 1 Hz

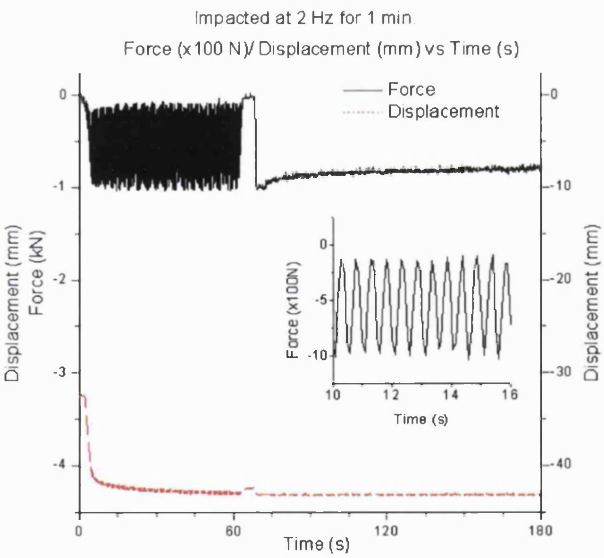

(d) Impaction frequency 2 Hz

Figure 4.4.: a) Typical force/time and displacement/time result at static compression for non-defatted and defatted graft. b) Typical result at 0.17 Hz. c) Typical result at 1 Hz. d) Typical result at 2 Hz.

4.6.2.2. Stress-strain behaviour

Figure 4.5 shows the typical stress-strain behaviour obtained. Note that the strain was measured after the 100 N pre-load was applied (i.e. the strain was reset to zero after pre-load), which effectively means the strain was measured just before impaction.

During loading, a sharp increase of stress was observed at a low strain value. This was due to the 100 N pre-load before impaction. During the loading period, an exponential increase in the gradient of the stress-strain curve was observed (for a definition of 'exponential' refer to Figure 1.34 on Page 44). Therefore, the material became stiffer with increased loading. At 0.17 Hz, the stress increased smoothly with strain and reached a peak value before the stroke oscillation. The stress value cycled from $0 - 3.5$ MPa due to the stroke oscillation. At 1 Hz and 2 Hz, a series of peaks were found on the stress-strain curve. This was due to the oscillation of the stroke (as detailed in §4.6.2.3 on Page 127) before reaching the maximum stress. For pure static compression, the stress-strain behaviour was similar to 0.17 Hz, but the stress did not return to zero. The stress oscillated around $2.4 - 3.8$ MPa because of instability of the loading machine.

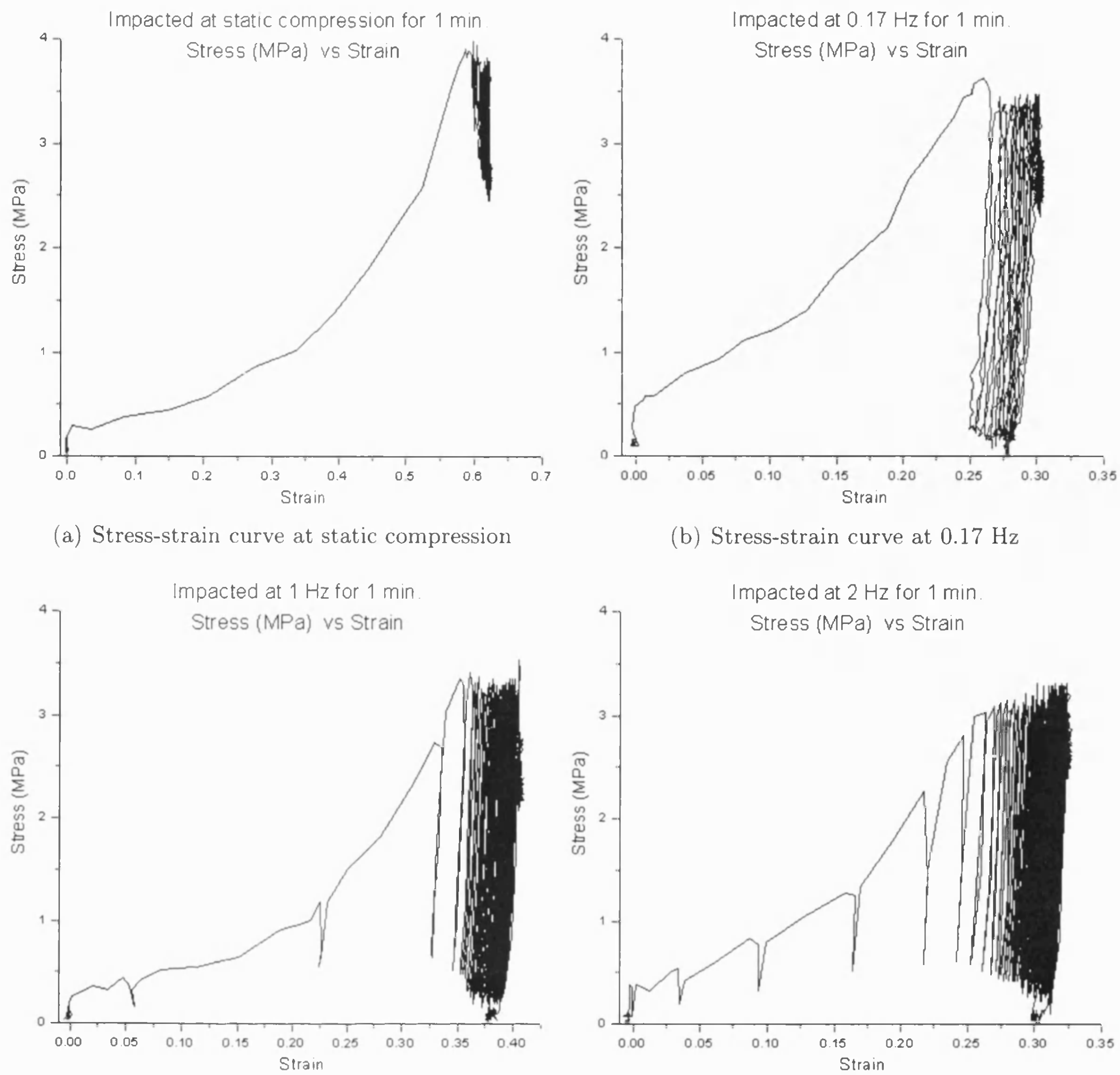

(a) Stress-strain curve at static compression

(b) Stress-strain curve at 0.17 Hz

(c) Stress-strain curve at 1 Hz

(d) Stress-strain curve at 2 Hz

Figure 4.5.: a) Typical stress-strain result at static compression for non-defatted graft. b) Typical result at 0.17 Hz. c) Typical result at 1 Hz. d) Typical result at 2 Hz. (Notes that all graphs have different x-axis scales).

4.6.2.3. Effect of re-compression

Figure 4.6 (extracted from Figure 4.4(c) and Figure 4.5(c)) presents the experimental results at 1 Hz compression for 3 mins. This allows direct comparision of force/displacement versus time and stress versus time. It is important to emphasise that these were plotted from the same experimental data (i.e. the force was converted into stress; the displacement was converted into strain). As can be seen, the gradient of the curve increases exponentially during compression. The graft, therefore, presents as a stiffer material with increased loading.

In the first few cycles of the loading period, a series of peaks were observed. These peaks were formed because the stroke required a few cycles to achieve the desired maximum force (i.e. 1 kN in this case). It was observed that the graft presented non-recoverable deformation because the structure of the graft collapsed (i.e. absorption of strain energy). As a result, graft may not be able to recoil back to the initial position. Fosse *et al.* [160] also reported the similar findings. Furthermore, it was observed that the change of strain became smaller at an increased number of cycles. As can be seen in Figure 4.6 (right), the change of strain between 3rd cycle and 2nd cycle was smaller than that of strain between 2nd and 1st cycle; the change of strain between 4th cycle and 3rd cycle was smaller than that of strain between 3rd and 2nd cycle. . . .As a result, the graft became denser with the increased number of cycles (i.e. higher density). At the same time, the stress increased with the numbers of cycles but reached to a a maximum of 3.5 MPa (in 4th, 5th, 6th cycle. . .).

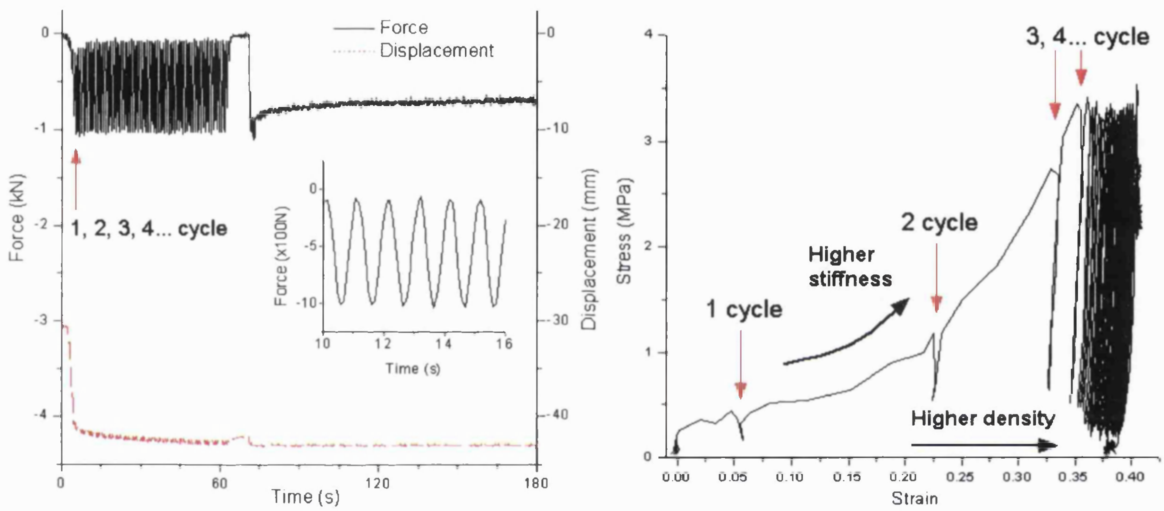

Figure 4.6.: Typical force/displacement against time (left), and associated stress-strain characteristic (right).

4.6.3. Statistical analysis

4.6.3.1. Effect of defatting on MCB

The defatting technique was discussed in §3 on Page 73. The porosity of the bone within the particles can then be observed after defatting. Figure 4.7 shows some examples of the grafts used in this experiment.

It was noted that the mass of the graft dropped by 17.3% ($\frac{5.65-4.67}{5.65} = 0.173$) for the same volume (10 cm^3) as is shown in Figure 4.8. Both non-defatted and defatted graft gave similar standard deviations. The amount of mass deviation was smaller compared with the experiment in §3 on Page 73 because a great care was taken to ensure various size of grafts were used. If a larger measuring cup was used (e.g. 50 cm^3), adjustment may not been necessary as the size of the voids would be less significant compared with the size of the measuring cup.

In both experiments, the deviation in the mass of the graft remained roughly constant after washing. It is, therefore, suggested that general distribution of graft in terms of size and grading remained the same. Dunlop *et al.* [94] discovered that washed graft has exactly the same particle-size distribution as in the pre-washed state. Nevertheless, the mass of the graft dropped significantly compared with the previous experiment as shown in Table 4.6 (a mass loss of 17.3% after washing). This could possibly have been caused by the over drying of the graft on tissue for a comparatively long period of time (about 3 – 4 hrs). This suggests that a precise control of the water removal process is required when defatting bone graft in this *in-vitro* model. However, this is practically very difficult in the *in-vivo* situation. A 2-sample t-test was also use to confirm that there was a statistical significance ($P < 0.001$, $\alpha = 0.05$) between non-defatted and defatted graft (Figure 4.8).

Figure 4.7.: Porcine graft was extracted after impaction and the recoil was measured with a vernier calliper. The first two rows in the figure are non-defatted MCB, whilst the other two rows are defatted MCB.

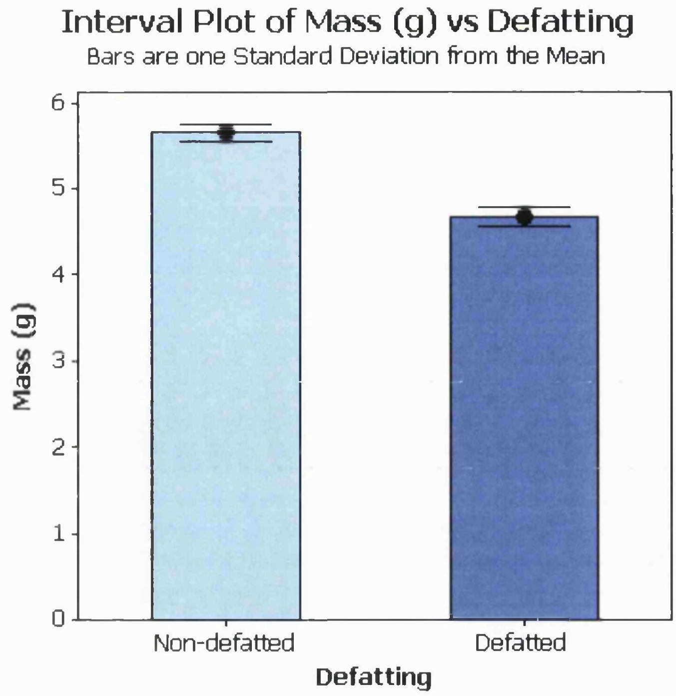

Figure 4.8.: Interval plot shows mean and one standard deviation of the mass (full results in Table 4.5 on Page 124).

Experiment	Graft	Non-defatted (g)	Defatted (g)	Difference	Significant*
Experiment in §3	Porcine	5.14 (0.31)	5.07 (0.27)	1.5%	No ($P = 0.378$)
This experiment	Porcine	5.65 (0.10)	4.67 (0.11)	17.3%	Yes ($P < 0.001$)

Table 4.6.: Effect of defatting on mass in different experiments. $^*\alpha = 0.05$.

4.6.3.2. Resistive strength of MCB at static condition

In the aforementioned discussion, all the specimens were pre-loaded. The stroke moved at 0.5 mm/s and was stopped when the load reached 100 N. The thickness of the graft was recorded so that the resistive strength of the material could be quantified after static compression. Figure 4.9 shows the thickness of the graft. It can be observed that the non-defatted graft had a smaller thickness compared with the defatted one. In other words, non-defatted fresh MCB was much more compressible than defatted graft for the same volume of graft and loading conditions. In this particular experiment, the defatted graft had 13.3% ($\frac{26.71-23.58}{23.58} = 0.133$) more resistive strength than non-defatted graft under uni-axial testing condition, this being statistically significance ($P < 0.001$, $\alpha = 0.05$, Student's t-test) (Minitab 14.20, Minitab Inc.). Therefore, washing of graft does help to improve mechanical properties of the graft during compression.

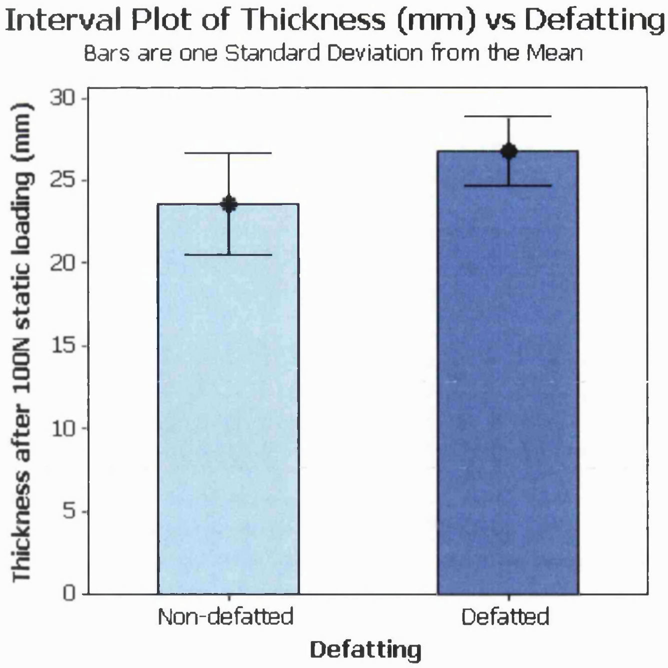

Figure 4.9.: Interval plot shows mean and one standard deviation of result of the measured displacement (full results in Table 4.5 on Page 124).

4.6.3.3. Resistive strength of MCB at dynamic condition

After a static compression of 100 N, the graft was impacted for 1 min at 1 kN. Four different frequencies were used (static for 1 min, 0.17 Hz, 1 Hz or 2 Hz) to investigate the dynamic properties of graft. Pure static compressive loading was used as a control experiment. The thickness of the graft was recorded after dynamic impaction. Figure 4.10 shows the thickness of the graft after impaction. Eight different results are plotted. Results on the left-hand side of this figure represent the thickness of the non-defatted graft whilst results on right-hand side represent the thickness of the defatted graft. The appropriate thickness and the frequency can be read directly from the x-axis and y-axis. The higher the thickness of the graft, the better the resistive strength of the graft. In general, it can be observed that defatted graft has a higher thickness compared to non-defatted graft. This agrees with the static condition in the previous discussion (see §4.6.3.2 on Page 130).

For the non-defatted group, all four results showed a similar range of standard deviation and mean values under different impaction frequencies. This suggests that the resistive strength of the graft was less dependent on the impaction frequency. All four results in defatted group showed a similar range of standard deviation, but the scale of standard deviation was lower compared to the non-defatted graft. Therefore, a defatted graft gives a slightly more consistent material in terms of resistive strength of the material under the same frequency of loading.

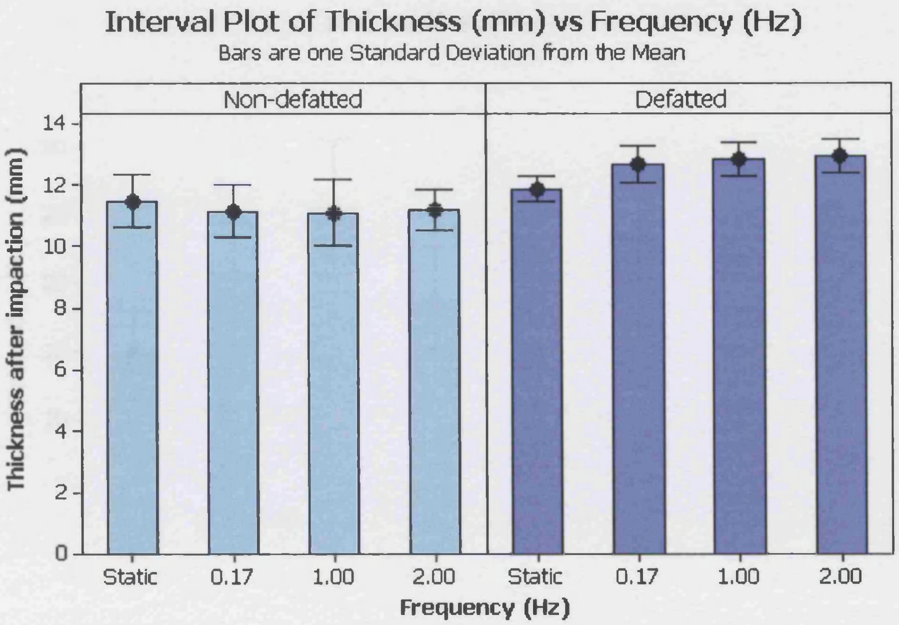

Figure 4.10.: Interval plot shows mean and one standard deviation of the measured displacement before relaxation test (full results in Table 4.5 on Page 124).

4.6.3.4. Behaviour of relaxation

After a series of 1 kN dynamic impactions, the stroke was stopped and relaxation occurred. Relaxation was measured for 2 mins. The amount of relaxation was calculated by the change of force divided by the impaction force (see Equation 4.5 on Page 123). Figure 4.11 shows the amount of relaxation under different impaction frequencies. Results of both non-defatted and defatted graft were plotted on the left and the right hand side of this figure respectively.

In a similar manner to the resistive strength of the graft under dynamic loading (see §4.6.3.3 on Page 131), non-defatted graft demonstrated a similar range of standard deviation under different impaction frequencies. Similarly, defatted graft had a similar range of standard deviation under different impaction frequencies, but the standard deviation of defatted graft was less than that of defatted graft.

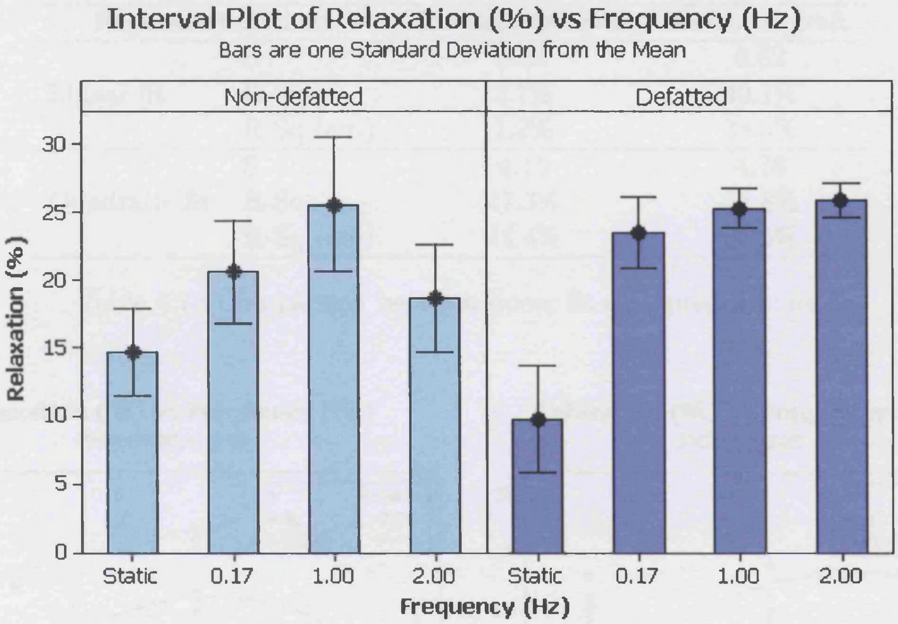

Figure 4.11.: Interval plot shows mean and one standard deviation of result of the measured relaxation (full results in Table 4.5 on Page 124).

In general, it was observed for the non-defatted graft that the amount of relaxation increased and then decreased when impaction frequency increased from static compression through 0.17 Hz, 1 Hz to 2 Hz. At static compression, the orientation of the individual graft particles did not change. For dynamic compression, when the impaction frequency increased, more kinetic energy was delivered to the graft and hence re-orientation of graft particles was possible. The re-orientation of graft into a new position improved the packing density. However, for pure static compression, it was not possible for the graft to re-orientate because the graft was only impacted once (at 1 kN). As a result, the orientation of the graft particles remained more or less the same and a lower relaxation was measured.

In order to determine the relationship between relaxation and frequency, linear and quadratic regressions were used. It was found that quadratic fit provided much better estimation than linear fit. Other regression methods were tried including cubic and polynomial regression, but the curves did not make any physical sense. A quadratic fit gave a better R-Squared (R-Sq) value than a linear fit as can be seen from Table 4.7. This confirmed that bone graft presents non-linear mechanical properties. Figure 4.12 shows the quadratic line fit for both non-defatted and defatted cases. As only four impaction frequencies were used, it would be difficult to conclude that there was a maximum value of relaxation at a certain frequency. Therefore, a wider range of frequencies would be necessary to fully estimate the relationship between relaxation and frequency. In addition, the optimised frequency may change depending on the graft size and grading. Therefore, the actual optimised frequency is very difficult to determine.

Regression method		Non-defatted graft	Defatted graft
	S	5.53	5.62
Linear fit	R-Sq	3.7%	40.1%
	R-Sq (adj)	1.2%	38.5%
	S	4.15	4.78
Quadratic fit	R-Sq	47.3%	57.8%
	R-Sq (adj)	44.4%	55.5%

Table 4.7.: Comparison between linear fit and quadratic fit.

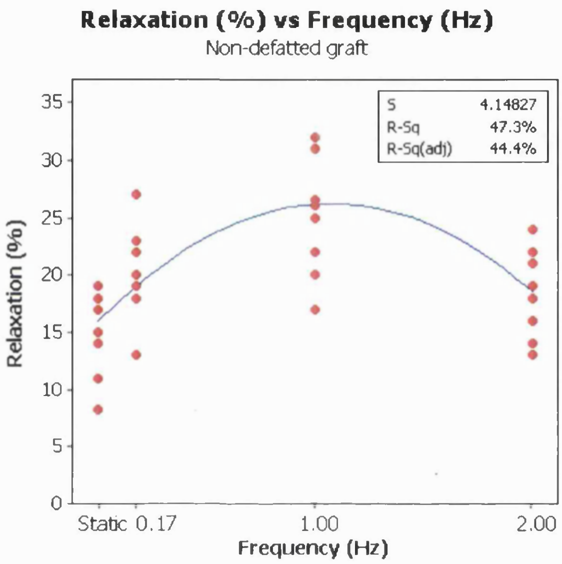

(a) Quadratic fit for non-defatted graft

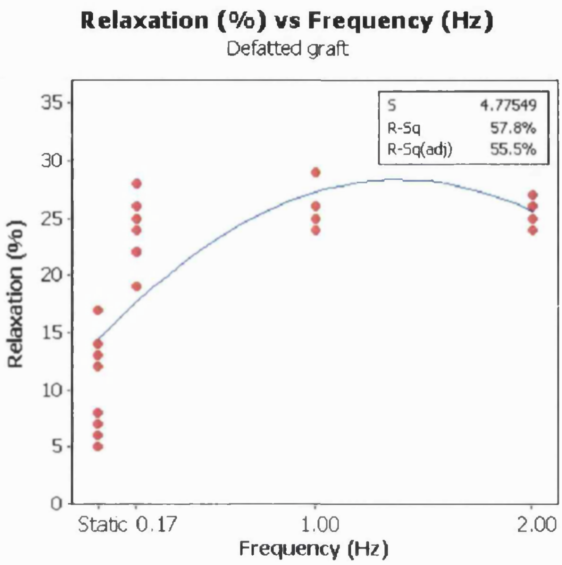

(b) Quadratic fit for defatted graft

Figure 4.12.: a) Quadratic line fit with data points for non-defatted graft. b) Quadratic line fit with data points for defatted graft.

Relaxation represents the change of force at a constant strain. In other words, it indicates the amount of residual force remaining within the graft after impaction when the implant is in place. In terms of the clinical situation, a high relaxation may be desirable as it could minimise the risk of per-operative femoral fractures. However, it could also lead to a loss of support for the implant even if the graft is fully impacted. Low relaxation may also be undesirable as it is associated with a high residual force. An optimised frequency of impaction could enable the best comprise to be obtained between the threat of per-operative femoral fracture and the amount of stability achieved.

4.6.3.5. Behaviour of recoil

The amount of recoil was measured after stress relaxation. The graft was extracted from the mild steel die. Figure 4.13 shows the amount of recoil against the four different testing frequencies. A large range of means and standard deviations were recorded for the non-defatted graft. No pattern in the results was observed in this particular case. Nonetheless, defatted graft appeared much more consistent (i.e. less standard deviation) and a smaller recoil was found. Lower recoil is desired because high recoil causes high changes in the shape of the medullary canal and may comprise the fit of the femoral stem.

The amount of recoil was relatively high compared with the results of Grimm [78]. Grimm found in fresh graft material the recoil ranged from 7 – 13%. Grimm measured the recoil after 500 N compression whilst in this experiment, the graft was compressed to 1000 N. In the previous experiment (see §3 on Page 73), the amount of recoil ranged between 36 – 40% at a compressive force of between 1500 – 2600 N. Table 4.8 shows a summary of results of recoil for the various experiments. It can be observed that the recoil was dependent on the amount of compressive force. At high compressive forces, the spring back effect became significant compared with low compressive forces. It could probably be that the material becames much stiffer at high compressive forces [78]. It was observed that the graft had a maximum recoil of around 35 – 40%, and the recoil remained around this value for a wide range of compressive forces (1000 N, 1500 N – 2600 N).

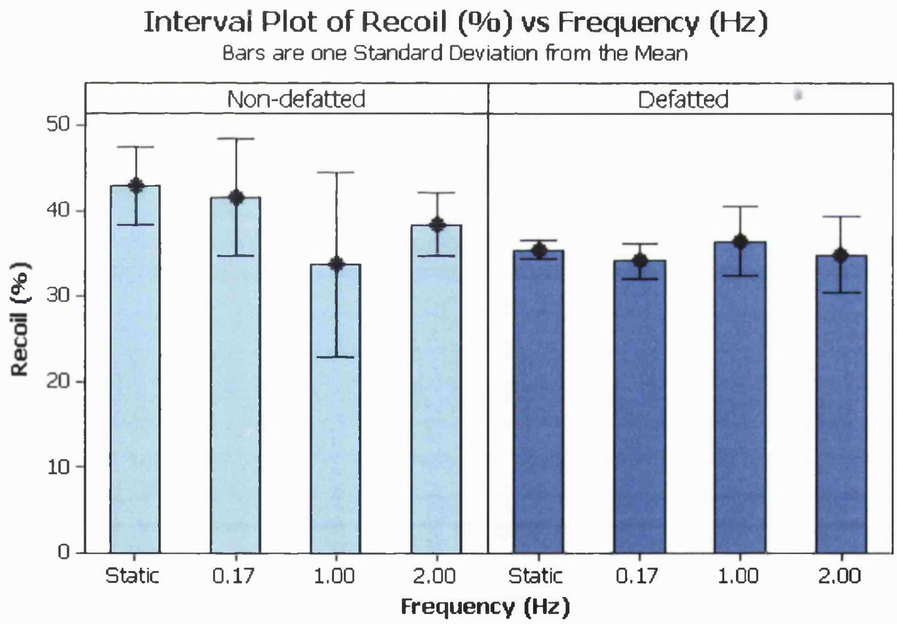

Figure 4.13.: Interval plot shows mean and one standard deviation of the measured recoil (full results in Table 4.5 on Page 124).

Experiment	Bone mill	Graft	Compressive method
Experiment in §3	Norwich	Porcine	High speed single stroke
This experiment	Norwich	Porcine	Multiple impactions
Grimm [78]	Howex, Norwich	Various (non-ceramic)	Low speed single stroke
Ullmark and Nilsson [164]	Howex, Tracer	Human	Flat bed

Experiment	Force (N)	Area (mm^2)	Stress (MPa)	Recoil (%)
Experiment in §3	1500 – 2600	$\frac{\pi \cdot 20^2}{4} = 314$	4.77 – 8.28	36.2 – 39.9
This experiment	1000	314	3.18	34.2 – 42.9
Grimm [78]	500	314	1.59	7.7 – 13.1
Ullmark and Nilsson [164]	Not mentioned	100 and 2000	0.55 – 1.95	11.0 – 34.0

Table 4.8.: Effect of force on recoil in different experiments. Stress was calculated by Equation 4.3 (see §4.5 on Page 122).

4.7. Results and discussion (2nd exp)

4.7.1. Summary of results

Table 4.9 shows a summary of all the experimental results. Full detailed experimental results can be found in Appendix A.3 on Page 179. The mean (i.e. the average) of each experimental setting was determined. The standard deviation was calculated using the statistics package Minitab 14.2 (Minitab Inc.).

	Rates (mm/s)			
	5	10	20	30
Stress (σ, MPa)	16.93 (2.96)	17.51 (2.18)	19.68 (2.37)	19.91 (2.25)
Recoil ($R_{recoil\,(2nd)}$, %)	46.88 (4.29)	46.14 (4.21)	45.56 (2.99)	45.56 (4.69)
	(cont.)	40	50	60
Stress (σ, MPa)		23.05 (3.31)	26.30 (4.44)	27.26 (4.35)
Recoil ($R_{recoil\,(2nd)}$, %)		44.98 (3.53)	43.28 (3.66)	44.70 (4.50)

Table 4.9.: Summary of mean and one standard deviation (presented in bracket) of stress and recoil.

4.7.2. Statistical analysis

4.7.2.1. Applied stress

Figure 4.14 shows the maximum stress exerted on the graft at different rates of impaction. As can be seen, the higher the rate of impaction, the higher the amount of stress. The Student's t-test showed that there was statistical significance ($P < 0.001$, $\alpha = 0.05$) in the level of maximum stress between 5 mm/s and 60 mm/s. Therefore, the viscoelastic effect became more significant at higher rates of impaction. When the graft was impacted at 60 mm/s, it was observed that blood sprayed out from the fluid escape canal of the die plunger (see Figure 4.1 on Page 117); in contrast, at 5 mm/s, the blood was squeezed out slowly from the fluid escape canal. Therefore, this showed a direct relationship between the rate of fluid escape and the value of maximum stress.

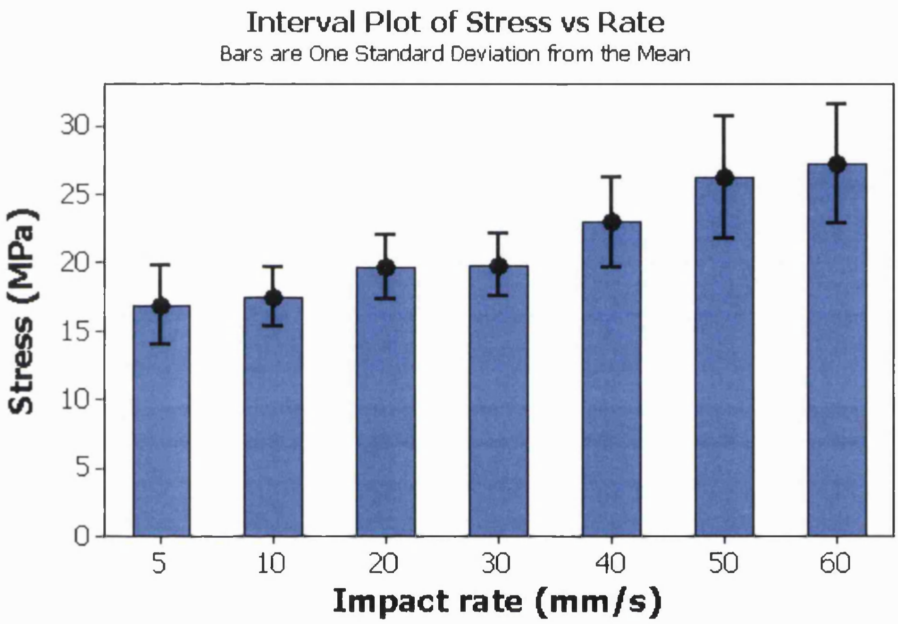

Figure 4.14.: Interval plot shows mean and one standard deviation of the applied stress at different rates of impaction (full results in Table 4.9 on Page 136).

4.7.2.2. Behaviour of recoil

Figure 4.15 shows the amount of recoil after impaction. As can be seen, at various rates of impaction, the amount of recoil was fairly similar. Statistical analysis using the Student's t-test showed that there was no statistical significance ($P = 0.284$, $\alpha = 0.05$) in the level of recoil between 5 mm/s and 60 mm/s. As the amount of recoil represents the deformation of the neo-medullary canal, this experiment demonstrated that the shape of the canal has no relationship to the rate of impaction.

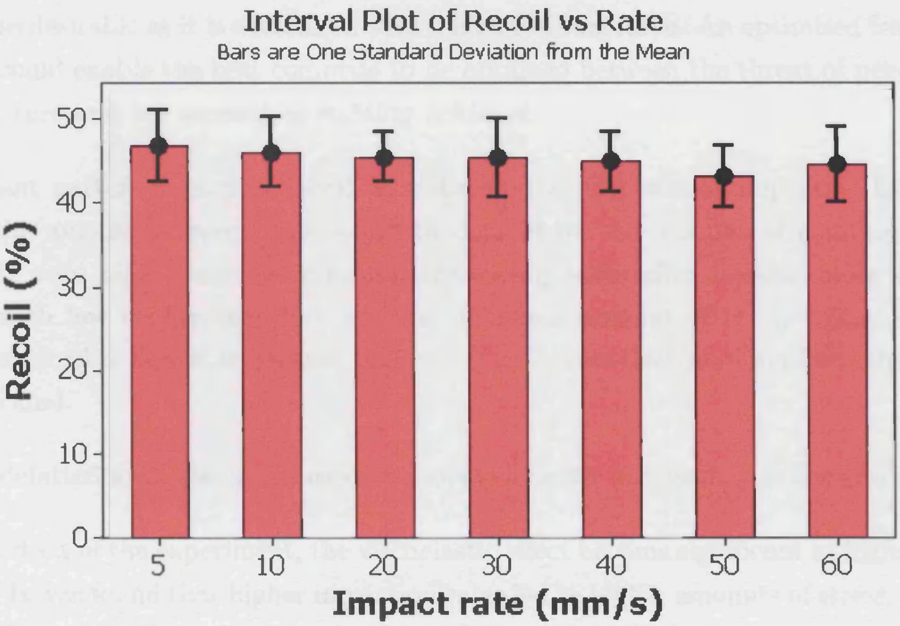

Figure 4.15.: Interval plot shows mean and one standard deviation of the measured recoil at different rates of impaction (full results in Table 4.9 on Page 136).

4.8. Conclusions

Defatted graft showed a huge mass drop (see Table 4.6 on Page 130) per unit volume. This could possibly have been caused by the over drying of the graft on tissue for a comparatively long period of time. Therefore, the length of drying time should be controlled precisely.

Defatted graft was found to have superior mechanical properties. The resistive strength of the material in both static and dynamic situations was improved after washing. Smaller standard deviations were found in resistive strength, relaxation and recoil in the defatted graft. Therefore, a defatted graft gives a slightly more consistent material in terms of resistive strength of the material under the same frequency of loading. In addition, changing the impaction frequency under the same level of force did not improve the resistive strength of the material.

It was observed that, for the non-defatted graft, the amount of relaxation increased and then decreased when the frequency increased from static compression, 0.17 Hz, 1 Hz to 2 Hz. At extremely low frequencies and under static compression, the orientation of the graft particles was kept the same so that re-orientation was not possible. At high frequencies, kinetic energy was delivered to the graft and hence re-orientation of graft particles was possible. The re-orientation of graft meant it took up a new position which could improve the packing density.

High relaxation could minimise the risk of per-operative femoral fractures, but it could also lead to a loss of support for the implant even if the graft is fully impacted. Low relaxation may also be underdesirable as it is associated with a high residual force. An optimised frequency of impaction could enable the best comprise to be obtained between the threat of per-operative femoral fracture and the amount of stability achieved.

No significant pattern regarding recoil was observed at the various impaction frequencies. However, the amount of recoil was found to depend on the amount of compressive force applied. At very high compressive forces, the spring back effect became more significant compared with low compressive forces. The maximum amount of recoil was around $35-40\%$. Lower recoil is desirable because high recoil can cause deformation of the shape of the medullary canal.

Generally, defatted graft should be used to provide a better consistency in the graft material.

In the second set of the experiment, the viscoelastic effect became significant at higher rates of impaction. It was found that higher impaction rates led to higher amounts of stress. However, the rate of impaction showed no relationship to the amount of recoil.

5. Comparison of the effect of cementation

5.1. Introduction

In the previous two chapters (see §3 on Page 73, and §4 on Page 116), a detailed discussion on the basic mechanical properties of graft has been given. This chapter focuses on the clinical application of impaction grafting. Studies in the previous chapters did not consider the use of bone cement. In this chapter, the influence of bone cement in impaction grafting was addressed. In §1.7.3 on Page 24, various non-standard impaction grafting techniques have been discussed. To date, no literature has been found on using collarless, polished and tapered stems for impaction graft without using bone cement in an *in-vitro* model. The hypothesis of this study was, therefore, to test whether the same or similar levels of mechanical stability could be achieved using a larger stem with the same surface finish and overall design without the use of bone cement, in comparison with a standard stem with the use of bone cement.

(This space intentionally left blank)

5.2. Design of test rig

An impactometer shown in Figure 5.1, developed at the Centre for Orthopaedic Biomechanics at the University of Bath, United Kingdom, which provides a known impaction energy and momentum, was used to standardise the impaction process. It consists of three core parts: a linear variable displacement transducer (LVDT), a variable height adjuster and a position market, a drop weight and a guide wire. An aluminium container is placed on the base allowing mounting of various models. In this case, a femur composite bone was used. The amount of impaction energy can be adjusted by altering the height of the drop weight. This rig has also been used in various research activities [78, 88, 165–169].

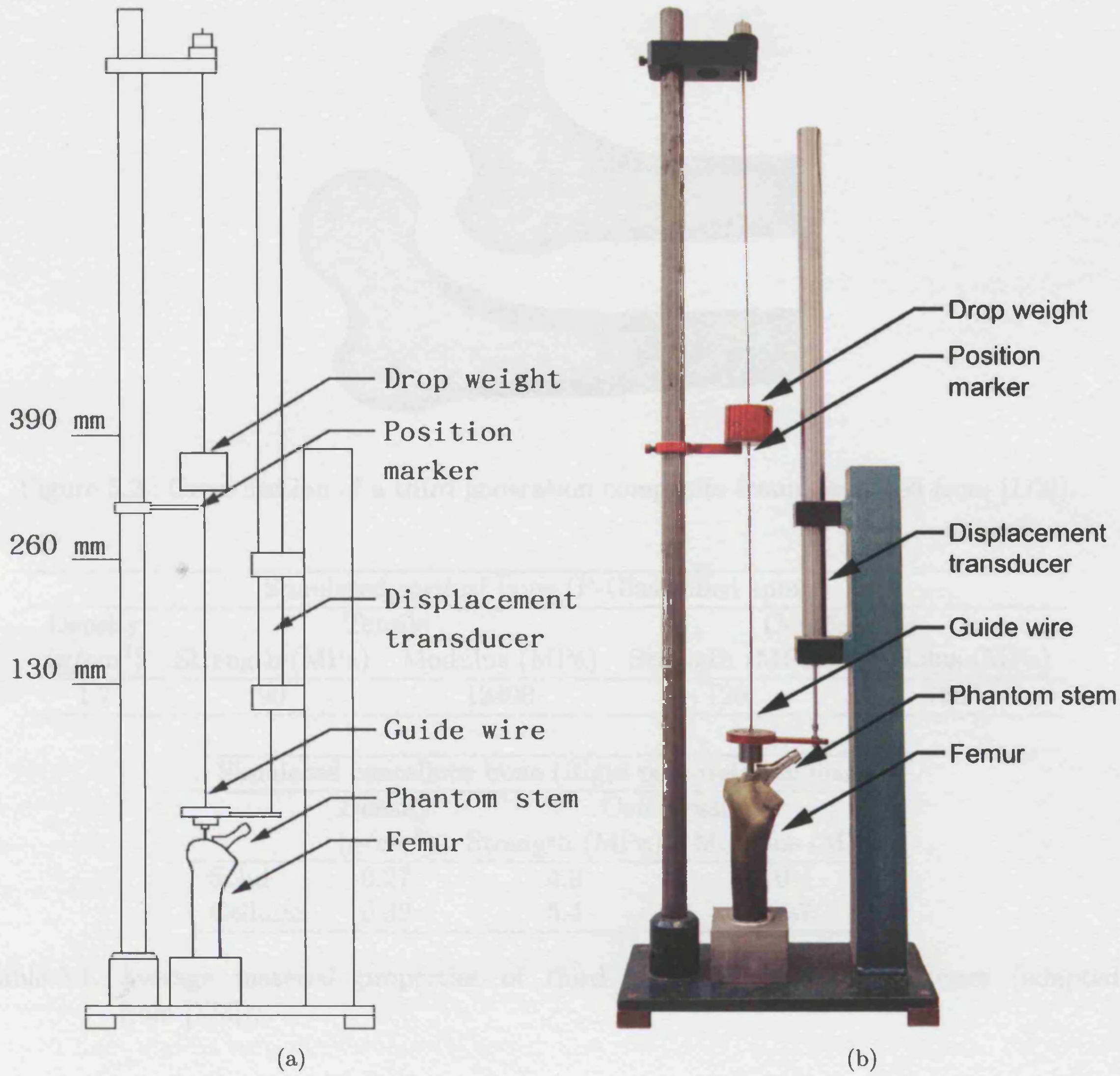

Figure 5.1.: a) Schematic diagrams of impactometer. b) Photograph of impactometer, designed to standardise the impaction grafting procedure.

5.3. Methods

5.3.1. Uncemented stem

Bone graft harvested from porcine femoral heads was used and the graft prepartion method was according to that given previously in §2 on Page 67. Six third generation Sawbones composite femora (Pacific Research Laboratories, Inc) were used. Previous studies showed that [170–172] the mechanical properties of these composite bones are similar to those of human bones. Figure 5.2 depicts the composite femora used in this experiment and the corresponding properties are shown in Table 5.1.

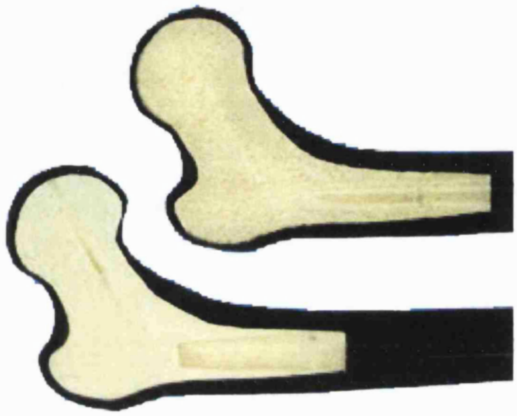

Figure 5.2.: Cross section of a third generation composite femur (adapted from [173]).

Simulated cortical bone (E-Glass filled epoxy)				
Density	Tensile		Compressive	
(g/cm^3)	Strength (MPa)	Modulus (MPa)	Strength (MPa)	Modulus (MPa)
1.7	90	12400	120	7600

Simulated cancellous bone (Rigid polyurethane foam)			
	Density	Compressive	
	(g/cm^3)	Strength (MPa)	Modulus (MPa)
Solid	0.27	4.8	104
Cellular	0.32	5.4	137

Table 5.1.: Average material properties of third generation composite bones (adapted from [173]).

The femoral head was cut, and the level of the cutting plane was controlled by a fixture in order to replicate the removal of femoral head during primary hip replacement. The distal end of the femur was cut at the location that the distal cement plug would be placed per-operatively. The ‘cancellous’ bone was removed by a rasp to replicate the bone loss. Care had to be taken to avoid breaking the fragile ‘cortical’ bone. To simulate a large femoral canal associated with bone loss, the internal diameter was reamed from ⌀15.7 mm to ⌀19.9 mm. The distal end of the composite femur was fixed in an aluminium container by potting with a low melting point alloy (Bend alloy, Lowden Metals Ltd, UK). This simulated the effect of the distal plug during a revision hip operation. After each experiment, the alloy was melted to facilitate the removal of the femur.

(a) Cutting (proximal section) (b) Reaming (femoral canal)

Figure 5.3.: a) The proximal part was cut with the aid of a fixture. b) Internal diameter increased from ⌀15.7 mm to ⌀19.9 mm.

After material and femur preparation, the Exeter femoral impaction technique was used as described by Gie *et al.* [12, 34]. The Stryker X-change revision femoral instrumentation was employed in this experiment. In addition, an impactometer (Figure 5.1) was used to standardise the impaction process including the amount of impaction energy and momentum as described in §5.2 on Page 141. A drop height of 260 mm was selected for this experiment as it provided an energy of 1.54 J and an impulse of 1.4 Ns. This has been shown to give an impaction energy and momentum as is typically achieved in the clinical scenario [78].

An 18 mm distal impactor was used for distal impaction, whilst Gie *et al.* [12, 34] recommended a progressive increase in size of distal impactor. The reason for using one size of distal impactor was because of the constant size of the internal diameter (i.e. ⌀19.9 mm). The distal impaction was divided into three stages. At each stage, a fixed volume of 30 cm^3 porcine bone graft was added and the volume of the graft was standardised using a 30 cm^3 measuring cup. As a result, a total of 90 cm^3 (= 30 × 3) of graft was used for each experiment. The porcine graft was impacted four times from a drop height of 260 mm. Then, a phantom impactor (size 2) was used for proximal impaction as shown in Figure 5.4. The proximal impactor migrated distally with the number of drops. When the secondary positional indicator (i.e. the second dot of the three dots located on the phantom impactor) of the phantom stem reached the proximal cut face of the femur, the impaction was stopped. At this stage, the femur was fully filled with graft and the phantom stem was firmly impacted. The stem was stiff and could not be extracted by hand as suggested by Savory *et al.* [54]. This stem represented a large stem and was employed for the uncemented stem study. It is important to note that the size of the phantom stem is larger than the final stem as depicted in Figure 5.4. This stem's dimensions effectively replaced the 2 mm cement mantle normally attained with the standard cemented stem used with this impactor.

Figure 5.4.: Exeter stem (size 2), Exeter phantom stem (size 2) and femoral head of 26 mm.

After proximal impaction, the femur was mounted on an Instron 8511 servohydraulic materials testing machine. The machine is capable of achieving a maximum load of 25 kN. Stability tests were carried out by a simplified uni-axial cyclic compressive loading test. The load was applied directly on the femoral head (26 mm diameter) by a flat adaptor which connected to the cross-head of the servohydraulic machine as shown in Figure 5.5. The cross-head moved up and down and hence the femoral head can slide on the flat adapter. There was no constraint or physical connection between the femoral head and the adaptor. Therefore, only the vertical force was transmitted to the femoral component which resulted in an axial and bending load on the femoral stem. The test was split into block loadings of 1500 cycles at 2 Hz (havesine cycle) in steps of 0.2 kN (i.e. 0 to 0.2 kN, 0 to 0.4 kN, 0 to 0.6 kN...) until the implant subsided by 4 mm. This was used as the failure criterion. Six tests were carried (one test for each femur, six femora were used in total). During the experiment, the force and the axial displacement were measured. After the stability testing, all the graft material was cleared from the femur so that the femur could be re-used for the next phase of the testing. The inner surface of the femur was then brushed using a toothbrush. The old graft material was discarded and fresh porcine graft was used for each test.

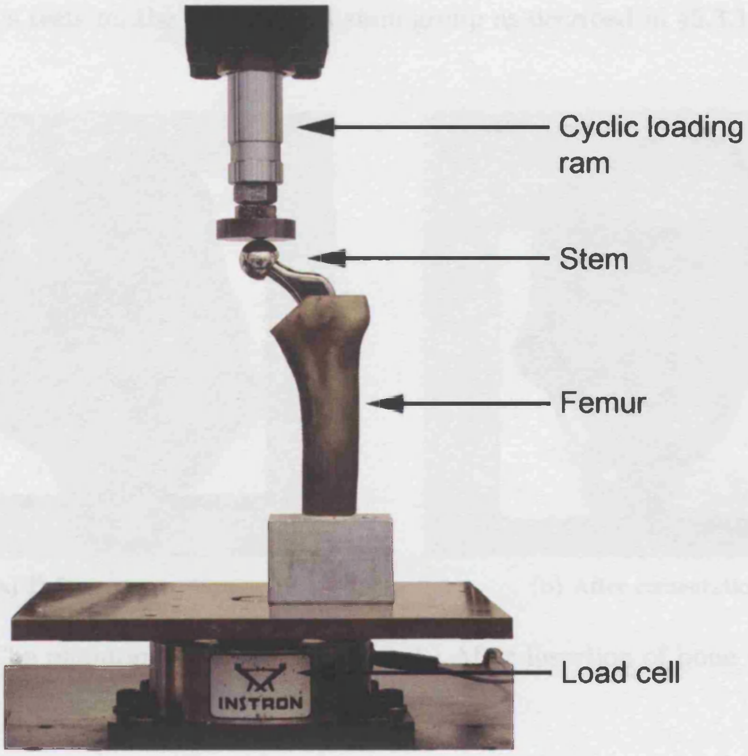

Figure 5.5.: Loading configuration showing a cemented Exeter stem implanted into composite femur.

5.3.2. Cemented stem

In the second series of experiments, similiar tests were carried out. Bone cement was used so that the effect of cementation on the stem stability could be simulated. The same impaction protocol was used during the distal and proximal impaction stages as aforementioned in §5.3.1 on Page 142. After the proximal impaction, the phantom stem was removed and Simplex (Stryker) bone cement was injected in a retrograde fashion. A third generation cement mixing technique was used. The cement was vacuum mixed for 30 s (HiVac Syringe, Summit Medical) according to the manufacturer's instructions. After 3 mins of mixing, the cement was injected into the neo-medullary femoral canal using a cement gun (DePuy Prism II 5401-34) in retrograde fashion. The cement was pressured for 1 min by a proximal pressuriser to maintain the pressure on the injected cement. After 4 mins, the Exeter stem (size 2) was manually inserted into the cement until the second positional marker of the stem (Figure 5.4) reached the edge of the proximal cut as shown in Figure 5.6. Before the stem insertion, the stem was smeared with a thin layer of silicon grease (RS 494-124) to facilitate removal of stem from the bone cement after the experiment. It should be noted that the size of the stem used in the cemented stem study was two sizes smaller than the size of the final stem used in the uncemented stem study. This allowed space for a 2 mm cement mantle between the bone graft and the stem [134]. Stability tests were then performed following the same procedure as in the previous tests on the uncemented stem group as decribed in §5.3.1 on Page 142.

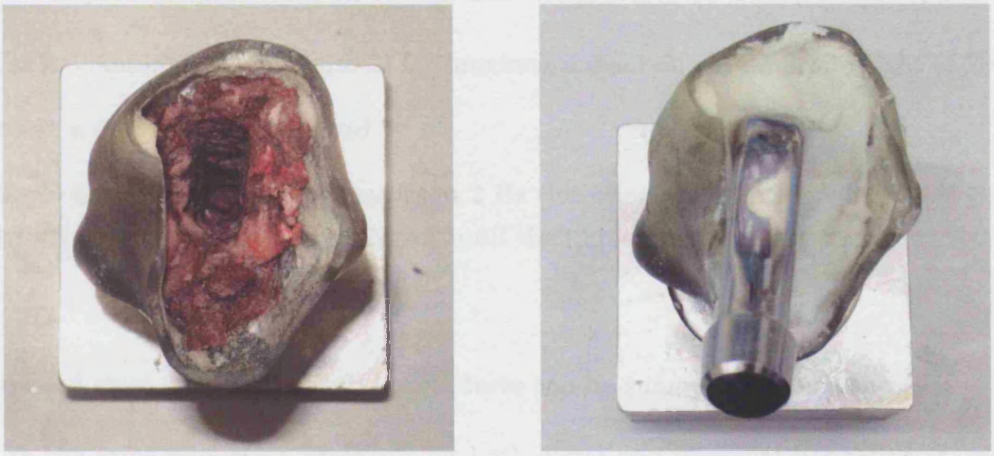

(a) Before cementation (b) After cementation

Figure 5.6.: a) The phantom stem was removed. b) After insertion of bone cement, the stem was inserted.

5.4. Experimental design

5.4.1. Design of experiment

A simple experimental design was used in this experiment. Two parameters, cemented and uncemented were used. Each setting has a number of six replications. Therefore, 12 ($= 2 \times 6$) experiments were performed. Table 5.6 summarises all the experimental settings.

Cementation	Stem used
Uncemented	Phantom stem (size 2)
Cemented	Exeter stem (size 2) + Simplex bone cement

Table 5.2.: Experimental design with one replication.

For the uncemented stem, the experimental procedure can be summarised as follow:

- Prepare six composite femora and ream the inner canal from ⌀15.7 mm to ⌀19.9 mm.
- Mount the femur on the impactometer and prepare for impaction.
- Repeat the following steps three times.
  - Insert 30 cm^3 of morsellised cancellous bone (MCB) into the femur.
  - Impact the graft with an 18 mm distal impactor with a drop height of 260 mm.
- Use a phantom impactor (size 2) for proximal impaction with a drop height of 260 mm.
- Insert a ⌀26 mm femoral head.
- Apply block loadings of 1500 cycles at 2 Hz (havesine cycle) in steps of 0.2 kN (i.e. 0 to 0.2 kN, 0 to 0.4 kN, 0 to 0.6 kN...) until the implant subsides by 4 mm.

For cemented stem, the experimental procedures can be summarised as follows:

- Use the same impaction protocols for both distal and proximal impaction stages as in the cemented stem.
- Use a phantom impactor (size 2) for proximal impaction with a drop height of 260 mm.
- Remove the phantom impactor and inserted bone cement in retrograde fashion.
- After 4 mins, insert an Exeter stem (size 2), which was previously smeared a thin layer of silicon grease on the surface, and pressurise the bone cement.
- Insert a ⌀26 mm femoral head.
- Apply block loadings of 1500 cycles at 2 Hz (havesine cycle) in steps of 0.2 kN (i.e. 0 to 0.2 kN, 0 to 0.4 kN, 0 to 0.6 kN...) until the implant subsides by 4 mm.

5.4.2. Sources of error

Table 5.3 gives the sources of error that could alert the accuracy of the experiment.

Source of error	Likelihood
Rotational misalignment of phantom/stem	High
Variability caused by cementation	Medium
Variability of graft properties from batch or batch	Low

Table 5.3.: Sources of error.

5.5. Measuring of subsidence

Table 5.4 shows the variables used in the experiment. The readings were measured by Instron and recorded via HPVEE.

Variable	Value	Unit	Quantity	Remark
s_{disp}		mm	Stroke displacement	Measured by Instron via HPVEE
F		N	Applied force	Measured by Instron via HPVEE

Table 5.4.: Notation, quantity and unit used in measuring of dispaclement and force.

5.6. Results and discussion

5.6.1. Summary of results

Table 5.5 shows a summary of all the experimental results. Full detailed experimental results can be found in Appendix A.4 on Page 182.

	Uncem. 1	Uncem. 2	Uncem. 3	Uncem. 4	Uncem. 5	Uncem. 6
Max. load (F_{max}, kN)	1.4	1.2	1.0	1.6	1.2	1.2

	Cement 1	Cement 2*	Cement 3	Cement 4	Cement 5	Cement 6
Max. load (F_{max}, kN)	4.4	–	5.6	4.4	4.0	4.6

Table 5.5.: The amount of force to achieve a subsidence of 4 mm, which was defined as the failure criterion, for both uncemented (Uncem.) and cemented stems. *The experiment setup was faulty and the date had to be discarded.

5.6.2. Movement pattern

5.6.2.1. Typical movement pattern

The stem subsidence consisted of two components: recoverable movement and non-recoverable subsidence as shown in Figure 5.7. The recoverable movement (micromotion) was the elastic range of movement within a given cyclic load (the peak-to-peak value); the non-recoverable subsidence (migration) was the amount of permanent subsidence of the stem within the graft (the different of the mean of peak-to-peak value at different time intervals). It is important to note that the magnitude of the applied loads increased with the number of cycles ($0-1500$ cycles at 0.2 kN, $1500-3000$ cycles at 0.4 kN, $3000-4500$ cycles at 0.6 kN...). In the absence of bone cement, uncemented stems demonstrated a catastrophic failure after a small number of cycles; there was also very little recoverable or elastic movement. When bone cement was used, the amount of non-recoverable subsidence gradually increased with respect to the number of cycles. The amount of recoverable movement also increased with the number of cycles.

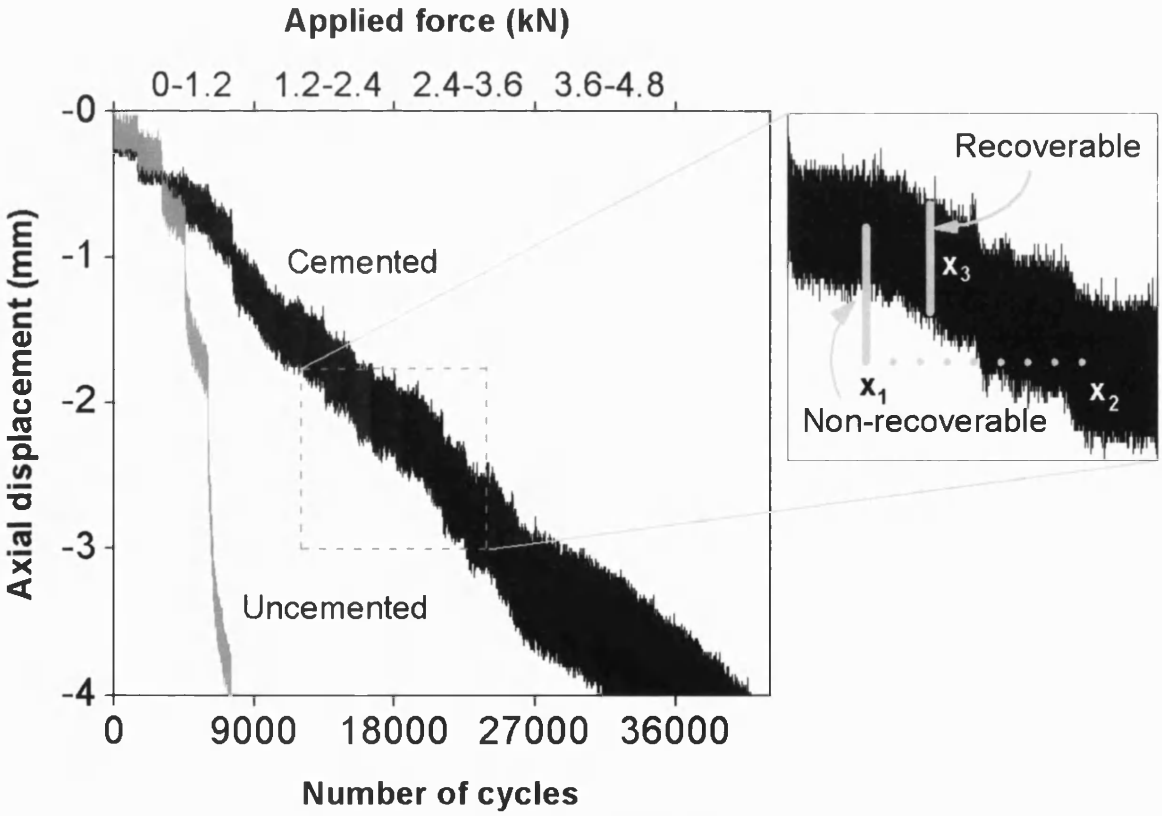

Figure 5.7.: Typical stem axial displacement curves at progressive increase of cycles and loading forces.

5.6.2.2. Uncemented stem

Figure 5.8 shows the subsidence of the uncemented stems. As can be seen, there was a massive subsidence when the applied load increased. In the absence of bone cement, all six stems failed in a similar fashion and a massive catastrophic non-recoverable subsidence was observed. The axial displacement was dominated by the non-recoverable subsidence of the uncemented stem within the bone graft. In other words, the bone graft was displaced distally and compressed as the stem subsided.

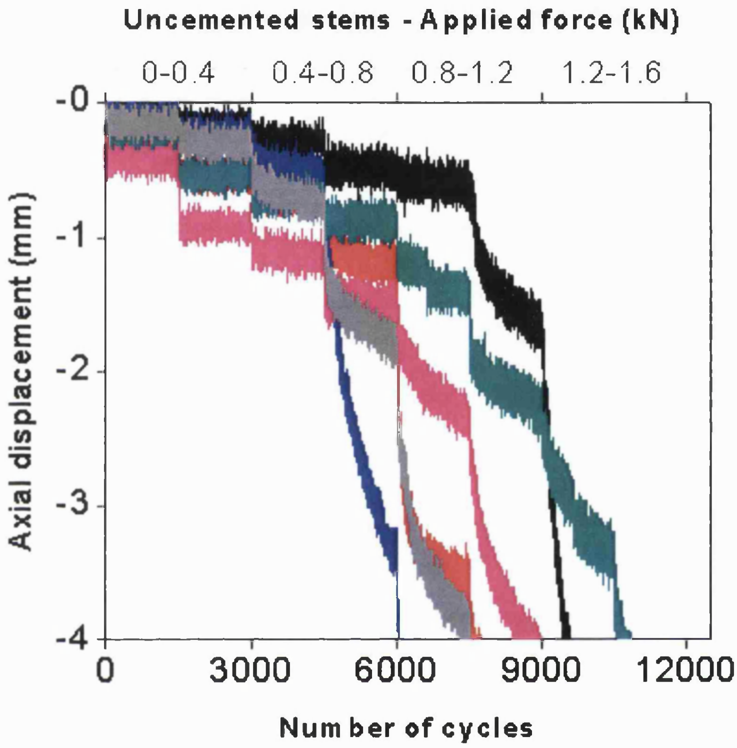

Figure 5.8.: Axial displacement of uncemented stem at progressive increase of cycles and loading forces.

During the stem subsidence, the cyclic forces were transmitted directly into the bone graft instead of the cortical bone of the femur. In the proximal-medial and distal-lateral areas of the femur (called the reaction zones) [174], the graft was compressed due to localised contact stresses as shown in Figure 5.9. In addition, only a very small amount of recoverable movement was demonstrated. Other studies have also found dramatic subsidence of the stem in similar *in-vitro* models [78, 88, 175].

For this experiment, a final stem of size 4 should have been used instead of the phantom stem (size 2). During the feasibility study for this experiment, the phantom stem was extracted and a size 4 final stem was inserted. However, it was found that graft recoil occurred immediately after phantom stem extraction. During the insertion of a size 4 final stem, it was difficult to locate the stem in the exactly same position as the phantom stem, and misalignment occurred. It was, therefore, decided for the actual experiment to leave the phantom stem in place after the proximal impaction.

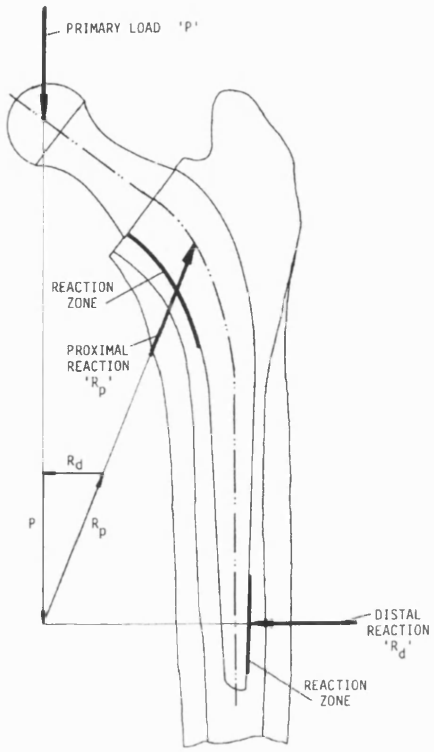

Figure 5.9.: Load transfer in femoral prosthesis (adapted from [174]).

5.6.2.3. Cemented stem

Figure 5.10 shows the subsidence of cemented stems. The amount of non-recoverable subsidence gradually increased with respect to the number of cycles. Unlike the mode of subsidence in uncemented stems, the measured displacement of the stem was mainly associated with the flexural loading of the femora, since the bone cement consolidated the stem, bone graft and the stem together. This was observed during the experiment. The consolidation of all three materials formed a composite structure, and enhanced the inter-locking of the graft. The load transfer distribution from the stem to the femur was, therefore, greatly improved.

In addition, the amount of elastic movement (i.e. the recoverable movement) increased with the number of cycles and the level of applied force due to the presence of bone cement. All six femora withstood forces of up to 6 $\times$ body weight ($\sim$4.2 kN).

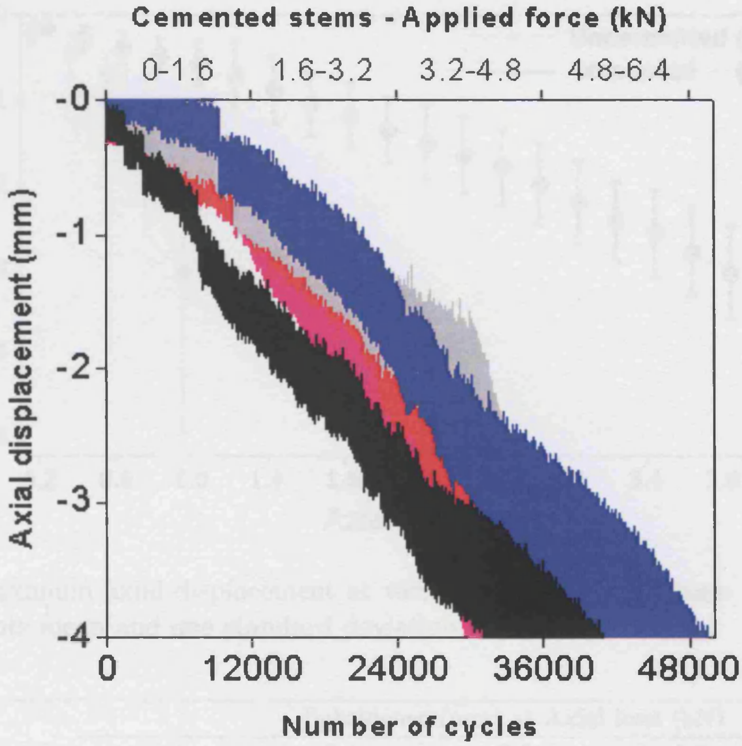

Figure 5.10.: Axial displacement of cemented stem at progressive increase of cycles and loading forces.

5.6.3. Statistical analysis

Figure 5.11 shows an interval plot of the results of uncemented and cemented stems. It is important to note that there were six samples for uncemented stems and five samples for cemented stems. This was because in one of the cemented stems, the setup was faulty and the data has to be discarded. At about $1 \times$ body weight ($\sim$0.80 kN), the uncemented stem showed non-recoverable subsidence (-1.61 ± 1.01 mm), three times that of the cemented stem (-0.48 ± 0.21 mm) as is shown in Table 5.6. The relationship between the non-recoverable subsidence and the loading force for the uncemented stem showed a sharp exponential increase; the relationship between the non-recoverable subsidence and the loading force for the cemented stem demonstrated a more gradual exponential increase.

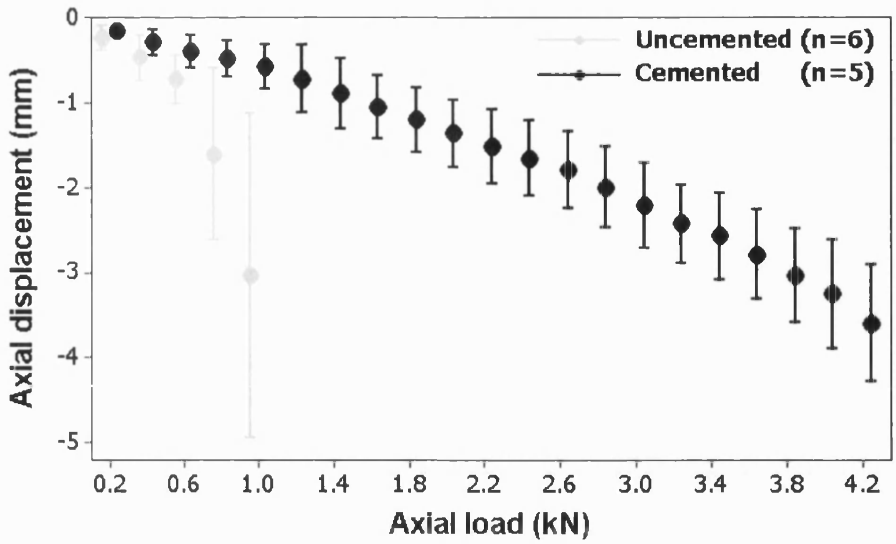

Figure 5.11.: Maximum axial displacement at various axial loading forces. Error bars represents mean and one standard deviation.

	Subsidence (mm) at Axial load (kN)				
	0.2	0.4	0.6	0.8	1.0
Uncemented ($n = 6$)	−0.24 (0.14)	−0.48 (0.27)	−0.74 (0.29)	−1.61 (1.01)	−3.05 (1.91)
Cemented ($n = 5$)	−1.64 (0.09)	−0.29 (0.14)	−0.40 (0.19)	−0.48 (0.21)	−0.59 (0.26)

Table 5.6.: The amount of non-recoverable subsidence at various loading forces. The sample size (n), mean and one standard deviation were shown (full results in Table A.7 and Table A.8 on Page 182).

5.7. Conclusion

In this study, the behaviour and the pattern of the axial displacement and subsidence depend strongly on the use of bone cement. In the case of uncemented stems, a large exponential increase relationship in non-recoverable subsidence was found. The high localised contact stresses on proximal-medial and distal-lateral areas of the femur caused only a small amount of elastic movement. In the case of cemented stems, a gradual exponential increase of non-recoverable subsidence was found, and the recoverable movement also increased with the number of cycles. Due to the presence of bone cement, the stem, bone graft and the femur form a composite structure, which allows an even transfer of forces to all regions of the stem and femur.

It would, therefore, appear that a large polished collarless stem is not a suitable design for substituting for the bone cement in impaction grafting. Other possible alternative solutions would be to incorporate a small collar to constrain the impacted graft proximally, although this design would be required to be evaluated thoroughly. From this experiment, it can therefore be concluded that it is not recommended to use an uncemented stem in impaction grafting.

6. Conclusion

6.1. Summary

This thesis focused on the investigation of the mechanical properties of morsellised bone graft. This involved extensive studies on basic material properties using a range of *in-vitro* mechanical tests.

Slooff *et al.* [33] and Gie *et al.* [12, 34] published work on acetabular and femoral reconstruction respectively using impaction bone grafting. In revision hip surgery, allograft bone graft is impacted into the femoral and acetabular cavities. The idea of impaction bone grafting is to provide a scaffold for mechanical support, and an appropriate biological scaffold for bone remodelling. Subsidence and femoral fracture are two main complications in impaction grafting of the femur.

The process of impaction grafting involves preparation of bone graft material, impaction of the graft and the insertion of a stem. The initial mechanical stability of the femoral stem is vital for bone remodelling. Good mechanical properties of graft, therefore, are crucial. This thesis focused on the understanding of the fundamental mechanical properties of morsellised bone graft.

Morsellised bone graft is a granular material. As a result, it has to be constrained in a representative way so that relevant experiments can be carried out. Morsellised bone graft is usually tested in compression as this is the primary way it is loaded *in-vivo*. In this thesis, the die-plunger compression test was employed for quantifying the mechanical properties of the bone graft. This produces information on the fundamental properties of the graft material. In addition, an impactometer, which simulates the impaction process in surgery and provides known impaction energy and momentum, was used to standardise the impaction process. This test rig has been used for various studies [78, 88, 166, 167, 169], such as measuring of hoop strain at various impaction energies.

In graft preparation, parameters such as defatting, graft size and grading, and the use of graft extenders have a significant influence on the mechanical properties of the graft. Defatted graft gives higher stiffness and provides a better mechanical support then non-defatted graft. Various key properties of the graft were identified including Poisson's ratio, the stress-strain characteristics of the graft, the modulus of elasticity, strain energy, stress relaxation and recoil. As the modulus of elasticity changed depending on the preparation of graft material, rate of loading, preloading and the method of measurement, it was important that the method of mechanical test used was standardised. It was found that morsellised bone graft was a highly viscoelastic, non-homogenous and anisotropic material. The viscoelastic behaviour was demonstrated using different rates and frequencies of loading. In general, the stiffness of the graft increased with the rate of loading.

Stability testing found that bone cement should be used in all cases when morsellised bone graft is used. Impaction grafting with an uncemented stem showed catastrophic failure at low loading values. The use of bone cement changed the load transfer characteristics and allowed better load transfer to all regions of the stem and femur. An *in-vitro* study of the strain in femoral canal during the impaction process (see Mak *et al.* [166]) suggested that a high impaction energy, 1.54 J, was required to impact the proximal impactor into the graft. The use of such a high impaction energy did not significantly affect the measured value of hoop strain (and hence increase the likelihood of producing femoral fracture).

A feasibility study of a proximal impaction cap (PIC) was also carried out. From this it was concluded that the PIC prevented graft extrusion into the joint space, but did not reduce the amount of hoop strain.

6.2. Further work

Suggested further work can be done on the characterisation of morsellised bone graft to improve the understanding of the properties of the graft, viz.:

- Standardised method of testing – The mechanical properties of the morsellised bone graft is highly dependent on the method of testing, the initial testing conditions, and the composition of the graft. The variability of the results from various published studies was primarily due to the inconsistencies in the methods of testing. Establishing a standardised testing methodology will allow better comparisons of different graft parameters to be established.

- Compactability of graft – The compactability test measures the capacity of a powder to be densified under an applied pressure and is defined by British Standard BS EN 23927 [176]. This specific standard was designed for metallic powder. By modifying the test rig and reducing the compressive pressure, it is possible to apply this standard to determine the compactibility of bone graft. A high level of compaction could mean that the graft is over impacted and there may therefore be reduced possibilities for re-vascularisation of the graft.

- Tackiness test – This is a test to determine how cohesive a material is. Compression tackiness testing is a simple version of the uni-axial compression test [177]. A high tackiness represents good cohesion of granular materials such as graft extender hydroxyapatite (HA) and tricalcium-phosphate (TCP).

- Various bone types – In this study, porcine graft was used in placed of human morsellised bone graft. Further work should be done on validating the experimental results using human allograft.

- Mixing of extenders – This thesis primarily focused on the characterisation of pure morsellised bone graft, and did not focus the use of graft extenders such as HA-TCP. Further work could be carried out on the characterisation of the mechanical properties of various mixtures of graft and graft extender.

- Numerical analysis – A numerical model of the bone graft could be developed. Provided the model has been validated against experimental data, this could be used to examine the consolidation of the graft at various impaction energies and impaction rates. It might also be possible to use this model to optimise the process of impaction by altering the appropriate parameters.

References

[1] National Audit Office. Hip replacement: Getting it right first time. [online] http://www.nao.org.uk; 2000 (Accesed 28 August 2006).

[2] Burns AWR, Bourne RB. (vi) Economics of revision total hip arthroplasty. Current Orthopaedics 2006;20(3):203–207.

[3] Huo MH, Cook SM. What's new in hip arthroplasty. J Bone Joint Surg [Am] 2001; 83-A(10):1598–1610.

[4] National Joint Registry 2005, 2nd Annual Report [online] http://www.njrcentre.org.uk/ ; 2005 (Accesed 28 August 2006).

[5] Annual report 2005. The Swedish national hip arthroplasty register. [online] http://www.jru.orthop.gu.se; 2005 (Accesed 29 August 2007).

[6] Murray DW, Carr AJ, Bulstrode CJ. Which primary total hip replacement? J Bone Joint Surg [Br] 1995;77(4):520–527.

[7] Robinson AH, Palmer CR, Villar RN. Is revision as good as primary hip replacement? A comparison of quality of life. J Bone Joint Surg [Br] 1999;81(1):42–45.

[8] Bozic KJ, Katz P, Cisternas M, Ono L, Ries MD, Showstack J. Hospital resource utilization for primary and revision total hip arthroplasty. J Bone Joint Surg [Am] 2005;87(3):570–576.

[9] Dupont JA, Charnley J. Low-friction arthroplasty of the hip for the failures of previous operations. J Bone Joint Surg [Br] 1972;54(1):77–87.

[10] eOrthopod. Artificial Joint Replacement of the Hip. [online] http://www.eorthopod.com/eorthopodv2/; 2003 (Accesed 28 August 2006).

[11] Coathup MJ, Blunn GW, Flynn N, Williams C, Thomas NP. A comparison of bone remodelling around hydroxyapatite-coated, porous-coated and grit-blasted hip replacements retrieved at post-mortem. J Bone Joint Surg [Br] 2001;83-B(1):118–123.

[12] Gie GA, Linder L, Ling RS, Simon JP, Slooff TJ, Timperley AJ. Impacted cancellous allografts and cement for revision total hip arthroplasty. J Bone Joint Surg [Br] 1993; 75-B(1):14–21.

[13] Burke DW, Rubash HE, Schutzer SF. Surgical technique for VerSys CRC cemented revision calcar hip prosthesis. Zimmer Inc.; 2006.

[14] Krupp RJ, Malkani AL, Crawford CH, Capello WN, Feinberg JR, Baker D. Impaction grafting for femoral component revision using a non-polished bead-blasted chrome cobalt stem-average 8 1/2-year follow-up. J Arthroplasty 2006;21(8):1180–1186.

[15] Berli BJ, Schafer D, Morscher EW. Ten-year survival of the MS-30 matt-surfaced cemented stem. J Bone Joint Surg [Br] 2005;87(7):928–933.

[16] Zwartele R, Peters A, Brouwers J, Olsthoorn P, Brand R, Doets C. Long-term results of cementless primary total hip arthroplasty with a threaded cup and a tapered, rectangular titanium stem in rheumatoid arthritis and osteoarthritis. Int Orthop 2007;[In Press].

[17] van Kleunen JP, Anbari KK, Vu D, Garino JP. Impaction allografting for massive femoral defects in revision hip arthroplasty using collared textured stems. J Arthroplasty 2006;21(3):362–371.

[18] Gie GA, Ling RS, Timperley AJ. X-change revision instruments system – Surgical protocol for revision of loose components of total hip arthroplasties utilising impaction cancellous grafting and cement. Stryker Corp.; 1993.

[19] Engh CA, Bobyn JD, Glassman AH. Porous-coated hip replacement. The factors governing bone ingrowth, stress shielding, and clinical results. J Bone Joint Surg [Br] 1987; 69-B(1):45–55.

[20] Hardy DC, Frayssinet P, Guilhem A, Lafontaine MA, Delince PE. Bonding of hydroxyapatite-coated femoral prostheses. Histopathology of specimens from four cases. J Bone Joint Surg [Br] 1991;73-B(5):732–740.

[21] Soballe K, Toksvig-Larsen S, Gelineck J, Fruensgaard S, Hansen ES, Ryd L, et al. Migration of hydroxyapatite coated femoral prostheses. A roentgen stereophotogrammetric study. J Bone Joint Surg [Br] 1993;75-B(5):681–687.

[22] ReCap femoral resurfacing system. Biomet Inc.; 2004.

[23] Biolox delta ceramic femoral heads. Biomet Inc.; 2005.

[24] Biomet offset femoral head. Biomet Inc.; 2000.

[25] Restoration modular revision hip system. Styker Inc.; 2007.

[26] Estok DM, Burroughs BR, Muratoglu OK, Harris WH. Comparison of hip simulator wear of 2 different highly cross-linked ultra high molecular weight polyethylene acetabular components using both 32- and 38-mm femoral heads. J Arthroplasty 2007; 22(4):581–589.

[27] Panagiotopoulos EC, Kallivokas AG, Koulioumpas I, Mouzakis DE. Early failure of a zirconia femoral head prosthesis: fracture or fatigue? Clin Biomech 2007;22(7):856–860.

[28] Lachiewicz PF. Metal-on-Metal hip resurfacing: A skeptic's view. Clin Orthop Relat Res 2007;465:86–91.

[29] Thanner J, Karrholm J, Herberts P, Malchau H. Hydroxyapatite and tricalcium phosphate-coated cups with and without screw fixation: a randomized study of 64 hips. J Arthroplasty 2000;15(4):405–412.

[30] Thanner J, Karrholm J, Herberts P, Malchau H. Porous cups with and without hydroxylapatite-tricalcium phosphate coating: 23 matched pairs evaluated with radiostereometry. J Arthroplasty 1999;14(3):266–271.

[31] Izquierdo RJ, Northmore-Ball MD. Long-term results of revision hip arthroplasty. Survival analysis with special reference to the femoral component. J Bone Joint Surg [Br] 1994;76(1):34–39.

[32] Ornstein E. Hip revisions with impacted morselized allograft bone and cement. Patient outcome, prosthetic fixation and risks. Acta Orthop Scand Suppl 2002;73(306):1–66.

[33] Slooff TJ, Huiskes R, van Horn J, Lemmens AJ. Bone grafting in total hip replacement for acetabular protrusion. Acta Orthop Scand 1984;55(6):593–596.

[34] Gie GA, Linder L, Ling RS, Simon JP, Slooff TJ, Timperley AJ. Contained morselized allograft in revision total hip arthroplasty. Surgical technique. Orthop Clin North Am 1993;24(4):717–725.

[35] Ling RS, Timperley AJ, Linder L. Histology of cancellous impaction grafting in the femur. A case report. J Bone Joint Surg [Br] 1993;75-B(5):693–696.

[36] Linder L. Cancellous impaction grafting in the human femur: histological and radiographic observations in 6 autopsy femurs and 8 biopsies. Acta Orthop Scand 2000; 71(6):543–552.

[37] Lind M, Krarup N, Mikkelsen S, Horlyck E. Exchange impaction allografting for femoral revision hip arthroplasty: results in 87 cases after 3.6 years' follow-up. J Arthroplasty 2002;17(2):158–164.

[38] Weidenhielm LR, Mikhail WE, Wretenberg P, Fow J, Simpson J, Bauer TW. Analysis of the retrieved hip after revision with impaction grafting. Acta Orthop Scand 2001; 72(6):609–614.

[39] Ornstein E, Franzén H, Johnsson R, Karlsson M, Linder L, Sundberg M. Hip revision using the Exeter stem, impacted morselized allograft bone and cement. Acta Orthop Scand 2004;75(5):533–543.

[40] van Doorn WJ, ten Have BL, van Biezen FC, Hop WC, Ginai AZ, Verhaar JA. Migration of the femoral stem after impaction bone grafting. First results of an ongoing, randomised study of the Exeter and Elite Plus femoral stems using radiostereometric analysis. J Bone Joint Surg [Br] 2002;84-B(6):825–831.

[41] Eldridge JD, Smith EJ, Hubble MJ, Whitehouse SL, Learmonth ID. Massive early subsidence following femoral impaction grafting. J Arthroplasty 1997;12(5):535–540.

[42] Stulberg SD. Impaction grafting: the science and clinical reality. Orthopedics 2000; 23(9):945–947.

[43] Stulberg SD. Impaction grafting: doing it right. J Arthroplasty 2002;17(4 Suppl 1):147–152.

[44] Miles AW, Clift SE, GC Bannister. The effect of the surface finish of the femoral component on load transmission in total hip replacement. J Bone Joint Surg [Br] 1990; 72-B(4):736.

[45] Williams HD, Browne G, Gie GA, Ling RS, Timperley AJ, Wendover NA. The Exeter universal cemented femoral component at 8 to 12 years. A study of the first 325 hips. J Bone Joint Surg [Br] 2002;84-B(3):324–334.

[46] Edwards SA, Pandit HG, Grover ML, Clarke HJ. Impaction bone grafting in revision hip surgery. J Arthroplasty 2003;18(7):852–859.

[47] Boldt JG, Dilawari P, Agarwal S, Drabu KJ. Revision total hip arthroplasty using impaction bone grafting with cemented nonpolished stems and charnley cups. J Arthroplasty 2001;16(8):943–952.

[48] Ornstein E, Atroshi I, Franzén H, Johnsson R, Sandquist P, Sundberg M. Early complications after one hundred and forty-four consecutive hip revisions with impacted morselized allograft bone and cement. J Bone Joint Surg [Am] 2002;84-A(8):1323–1328.

[49] van Doorn WJ, van Biezen FC, Prendergast PJ, Verhaar JA. Fracture of an Exeter stem 3 years after impaction allografting – a case report. Acta Orthop Scand 2002; 73(1):111–113.

[50] Kalteis T, Luring C, Gugler G, Zysk S, Caro W, Handel M, et al. Acute tissue toxicity of PMMA bone cements [Article in German]. Z Orthop Ihre Grenzgeb 2004;142(6):666–672.

[51] Engelbrecht E, Heinert K. Klassifikation and Behandlungsrichtlinien von Knochensubstanzverlusten bei Revisionsoperationen am Hüftgelenk - Mittelfristige Ergebnisse. In: Primär- und Revisions-alloarthroplastik, Hüft- und kniegelenk. Berlin: Springer-Verlag ; 1987. p. 189–20.

[52] Gustilo RB, Pasternak HS. Revision total hip arthroplasty with titanium ingrowth prosthesis and bone grafting for failed cemented femoral component loosening. Clin Orthop Relat Res 1988;(235):111–119.

[53] Tsiridis E, Narvani AA, Haddad FS, Timperley JA, Gie GA. Impaction femoral allografting and cemented revision for periprosthetic femoral fractures. J Bone Joint Surg [Br] 2004;86-B(8):1124–1132.

[54] Savory CG, Ling RS, Tilling JR, Gie GA, Timperley AJ. Femoral Impaction Grafting: The Exeter Technique [DVD]. Hughston Sports Medicine Foundation; 2003.

[55] de Thomasson E, Williams JB, Marmorat JL, Guigand O, Mazel C. Modified Exeter technique in revision hip surgery. Does distal fixation of the stem affect allograft transformation? J Arthroplasty 2005;20(4):473–480.

[56] Schreurs BW, Buma P, Huiskes R, Slagter JL, Slooff TJ. Morsellized allografts for fixation of the hip prosthesis femoral component. A mechanical and histological study in the goat. Acta Orthop Scand 1994;65(3):267–275.

[57] Kärrholm J, Hultmark P, Carlsson L, Malchau H. Subsidence of a non-polished stem in revisions of the hip using impaction allograft. Evaluation with radiostereometry and dual-energy X-ray absorptiometry. J Bone Joint Surg [Br] 1999;81(1):135–142.

[58] Einsiedel T, Arand M, Gebhard F, Kinzl L, Schultheiss M. Hip arthroplasty with proximal transmission of force: first clinical results with a new partially cemented femoral stem. Arch Orthop Trauma Surg 2007;127(3):147–151.

[59] Schreurs BW, Huiskes R, Slooff TJ. The initial stability of cemented and non-cemented femoral stems fixated with a bone grafting technique. Clin Materials 1994;16(2):105–110.

[60] Schreurs BW, Huiskes R, Buma P, Slooff TJ. Biomechanical and histological evaluation of a hydroxyapatite-coated titanium femoral stem fixed with an intramedullary morsellized bone grafting technique: an animal experiment on goats. Biomaterials 1996; 17(12):1177–1186.

[61] Heal JS, Blom AW, Miles AW, Learmonth ID. Morselized impaction bone grafting. A review article. Orthopaedic Update (India) 2001;11(3):28–35.

[62] Ornstein E, Franzén H, Johnsson R, Sundberg M. Radiostereometric analysis in hip revision surgery – optimal time for index examination: 6 patients revised with impacted allografts and cement followed weekly for 6 weeks. Acta Orthop Scand 2000;71(4):360–364.

[63] Ornstein E, Franzén H, Johnsson R, Stefánsdóttir A, Sundberg M, Tägil M. Hip revision with impacted morselized allografts: unrestricted weight-bearing and restricted weight-bearing have similar effect on migration. A radiostereometry analysis. Arch Orthop Trauma Surg 2003;123(6):261–267.

[64] Ornstein E, Atroshi I, Franzén H, Johnsson R, Sandquist P, Sundberg M. Results of hip revision using the Exeter stem, impacted allograft bone, and cement. Clin Orthop Relat Res 2001;(389):126–133.

[65] Stefánsdóttir A, Franzén H, Johnsson R, Ornstein E, Sundberg M. Movement pattern of the Exeter femoral stem; a radiostereometric analysis of 22 primary hip arthroplasties followed for 5 years. Acta Orthop Scand 2004;75(4):408–414.

[66] Malkani AL, Voor MJ, Fee KA, Bates CS. Femoral component revision using impacted morsellised cancellous graft. A biomechanical study of implant stability. J Bone Joint Surg [Br] 1996;78-B(6):973–978.

[67] Halliday BR, English HW, Timperley AJ, Gie GA, Ling RS. Femoral impaction grafting with cement in revision total hip replacement. Evolution of the technique and results. J Bone Joint Surg [Br] 2003;85-B(6):809–817.

[68] Heiner AD, Callaghan JJ, Brown TD. A laboratory simulation for morselized bone graft fusion: apparent modulus under operatively based femoral impaction kinetics. J Biomech 2005;38(4):811–818.

[69] Pekkarinen J, Alho A, Lepisto J, Ylikoski M, Ylinen P, Paavilainen T. Impaction bone grafting in revision hip surgery. A high incidence of complications. J Bone Joint Surg [Br] 2000;82(1):103–107.

[70] Giesen EB, Lamerigts NM, Verdonschot N, Buma P, Schreurs BW, Huiskes R. Mechanical characteristics of impacted morsellised bone grafts used in revision of total hip arthroplasty. J Bone Joint Surg [Br] 1999;81-B(6):1052–1057.

[71] HIP 98 [CD]. Biomechanics laboratory of Free University of Berlin; 2001.

[72] Bergmann G, Deuretzbacher G, Heller M, Graichen F, Rohlmann A, Strauss J, et al. Hip contact forces and gait patterns from routine activities. J Biomech 2001;34(7):859–871.

[73] Stansfield BW, Nicol AC, Paul JP, Kelly IG, Graichen F, Bergmann G. Direct comparison of calculated hip joint contact forces with those measured using instrumented implants. an evaluation of a three-dimensional mathematical model of the lower limb. J Biomech 2003;36(7):929–936.

[74] Bergmann G, Graichen F, Rohlmann A. Is staircase walking a risk for the fixation of hip implants? J Biomech 1995;28(5):535–553.

[75] Stansfield BW, Nicol AC. Hip joint contact forces in normal subjects and subjects with total hip prostheses: walking and stair and ramp negotiation. Clin Biomech 2002; 17(2):130–139.

[76] Bergmann G, Kniggendorf H, Graichen F, Rohlmann A. Influence of shoes and heel strike on the loading of the hip joint. J Biomech 1995;28(7):817–827.

[77] Bergmann G, Graichen F, Rohlmann A. Hip joint loading during walking and running, measured in two patients. J Biomech 1993;26(8):969–990.

[78] Grimm B. Mechanical properties of morsellised bone graft and synthetic graft extenders for impaction grafting. PhD dissertation. Department of Mechanical Engineering, University of Bath, United Kingdom; 2003.

[79] Clements JP, Gheduzzi S, Zweymuller K, Lintner F, Schmotzer H, Learmonth ID, et al. An in vitro cadaveric biomechanical evaluation of a cementless hip stem – Comparison of long and short term stability. Ortho Res Society 2005;51st Annual Meeting:266.

[80] Bragdon CR, Burke D, Lowenstein JD, O'Connor DO, Ramamurti B, Jasty M, et al. Differences in stiffness of the interface between a cementless porous implant and cancellous bone in vivo in dogs due to varying amounts of implant motion. J Arthroplasty 1996;11(8):945–951.

[81] Engh CA, O'Connor D, Jasty M, McGovern TF, Bobyn JD, Harris WH. Quantification of implant micromotion, strain shielding, and bone resorption with porous-coated anatomic medullary locking femoral prostheses. Clin Orthop Relat Res 1992;(285):13–29.

[82] Engh CA, Hooten JP Jr, Zettl-Schaffer KF, Ghaffarpour M, McGovern TF, Macalino GE, et al. Porous-coated total hip replacement. Clin Orthop Relat Res 1994;(298):89–96.

[83] Szmukler-Moncler S, Salama H, Reingewirtz Y, Dubruille JH. Timing of loading and effect of micromotion on bone-dental implant interface: review of experimental literature. J Biomed Mater Res 1998;43(2):192–203.

[84] Murphy VF. Medical engineering 2006 – Rehabilitation engineering. [online] http://rehabilitation.medicalengineer.co.uk/; 2004 (Accesed 28 August 2006).

[85] Langer F, Czitrom A, Pritzker KP, Gross AE. The immunogenicity of fresh and frozen allogeneic bone. J Bone Joint Surg [Am] 1975;57-A(2):216–220.

[86] Gates HS III, McCollum DE, Poletti SC, Nunley JA. Bone-grafting in total hip arthroplasty for protrusio acetabuli. A follow-up note. J Bone Joint Surg [Am] 1990;72(2):248–251.

[87] Boyce T, Edwards J, Scarborough N. Allograft bone. The influence of processing on safety and performance. Orthop Clin North Am 1999;30(4):571–581.

[88] Grimm B, Blom AW, Miles AW, Turner IG. In-vitro endurance testing of bone graft materials for impaction grafting. Bioceramics 14 2002;218-2:375–378.

[89] Greenwald AS, Boden SD, Goldberg VM, Khan Y, Laurencin CT, Rosier RN. Bone-graft substitutes: facts, fictions, and applications. J Bone Joint Surg [Am] 2001;83-A Suppl 2 Pt 2:98–103.

[90] Blom AW, Cunningham JL, Hughes G, Lawes TJ, Smith N, Blunn G, et al. The compatibility of ceramic bone graft substitutes as allograft extenders for use in impaction grafting of the femur. J Bone Joint Surg [Br] 2005;87-B(3):421–425.

[91] Eldridge JD, Cunningham JL, Samuels A, Blunn GW, Lawes TJ, Learmonth ID, et al. Glass ionomer as an expander of allograft in revision arthroplasty of the hip. Biomaterials 2003;24(3):499–508.

[92] Heiner AD, Brown TD. A physical model for simulating fusion of impaction-grafted morselized cancellous bone. J Biomech 2001;34(6):811–814.

[93] Brewster NT, Gillespie WJ, Howie CR, Madabhushi SP, Usmani AS, Fairbairn DR. Mechanical considerations in impaction bone grafting. J Bone Joint Surg [Br] 1999; 81-B(1):118–124.

[94] Dunlop DG, Brewster NT, Madabhushi SP, Usmani AS, Pankaj P, Howie CR. Techniques to improve the shear strength of impacted bone graft: the effect of particle size and washing of the graft. J Bone Joint Surg [Am] 2003;85-A(4):639–646.

[95] Cornu O, Bavadekar A, Godts B, van Tomme J, Delloye C, Banse X. Impaction bone grafting with freeze-dried irradiated bone. Part I. Femoral implant stability: cadaver experiments in a hip simulator. Acta Orthop Scand 2003;74(5):547–552.

[96] Cornu O, Bavadekar A, Godts B, van Tomme J, Delloye C, Banse X. Impaction bone grafting with freeze-dried irradiated bone. Part II. Changes in stiffness and compactness of morselized grafts: experiments in cadavers. Acta Orthop Scand 2003;74(5):553–558.

[97] Cornu O, Manil O, Godts B, Naets B, van Tomme J, Delloye C, et al. Neck fracture femoral heads for impaction bone grafting: evolution of stiffness and compactness during impaction of osteoarthrotic and neck-fracture femoral heads. Acta Orthop Scand 2004; 75(3):303–308.

[98] Cornu O, Libouton X, Naets B, Godts B, van Tomme J, Delloye C, et al. Freeze-dried irradiated bone brittleness improves compactness in an impaction bone grafting model. Acta Orthop Scand 2004;75(3):309–314.

[99] Allogo JJ, Fischer LP, Gonon GP, Minchella P, Fessy MH, Clermont N, et al. Analysis of restraint of the femur head. Experimental study of allograft of cold bone and autoclaved bone to kill the HIV virus [French]. Bull Assoc Anat (Nancy) 1995;79(244):11–13.

[100] Wangerin K, Ewers R, Kestel M. Interaction of bone resorption and bone synthesis using an autoclaved bone graft. Prog Clin Biol Res 1985;187:343–351.

[101] Wangerin K, Ewers R, Wottge HU, Randzio G. The autoclaved autogenous bone graft as a re-implant. Results of animal experiments. J Maxillofac Surg 1986;14(3):132–137.

[102] Robinson DE, Lee MB, Smith EJ, Learmonth ID. Femoral impaction grafting in revision hip arthroplasty with irradiated bone. J Arthroplasty 2002;17(7):834–840.

[103] Pelker RR, Friedlaender GE. Biomechanical aspects of bone autografts and allografts. Orthop Clin North Am 1987;18(2):235–239.

[104] Hotz MA, Speirs AD, Oxland T, Muller M, Hammerle C, Hausler R. Radiologic and mechanical properties of inactivated ossicle homografts. Laryngoscope 1999;109(1):65–69.

[105] Speirs AD, Hotz MA, Oxland TR, Hausler R, Nolte LP. Biomechanical properties of sterilized human auditory ossicles. J Biomech 1999;32(5):485–491.

[106] Pelker RR, Friedlaender GE, Markham TC. Biomechanical properties of bone allografts. Clin Orthop Relat Res 1983;(174):54–57.

[107] Hernigou Ph. Allograft sterility as exemplified by human immunodeficiency virus and sterilization by irradiation. J Arthroplasty 2000;15(8):1051–1058.

[108] Fideler BM, Vangsness CT Jr, Lu B, Orlando C, Moore T. Gamma irradiation: effects on biomechanical properties of human bone-patellar tendon-bone allografts. Am J Sports Med 1995;23(5):643–646.

[109] Zhang Y, Homsi D, Gates K, Oakes K, Sutherland V, Wolfinbarger L Jr. A comprehensive study of physical parameters, biomechanical properties, and statistical correlations of iliac crest bone wedges used in spinal fusion surgery. IV. Effect of gamma irradiation on mechanical and material properties. Spine 1994;19(3):304–308.

[110] Anderson MJ, Keyak JH, Skinner HB. Compressive mechanical properties of human cancellous bone after gamma irradiation. J Bone Joint Surg [Am] 1992;74(5):747–752.

[111] Fideler BM, Vangsness CT Jr, Moore T, Li Z, Rasheed S. Effects of gamma irradiation on the human immunodeficiency virus. A study in frozen human bone-patellar ligament-bone grafts obtained from infected cadavera. J Bone Joint Surg [Am] 1994;76-A(7):1032–1035.

[112] Ernst DR, Race RE. Comparative analysis of scrapie agent inactivation methods. J Virol Methods 1993;41(2):193–201.

[113] Hotz MA, Orr T, Speirs AD, Hausler R. A new inactivation/preservation procedure for ossicle homografts. Transplant Proc 2002;34(4):1325–1326.

[114] Caldwell PE III, Shelton WR. Indications for allografts. Orthop Clin North Am 2005; 36(4):459–467.

[115] Voor MJ, White JE, Grieshaber JE, Malkani AL, Ullrich CR. Impacted morselized cancellous bone: mechanical effects of defatting and augmentation with fine hydroxyapatite particles. J Biomech 2004;37(8):1233–1239.

[116] Bolder SB, Schreurs BW, Verdonschot N, van Unen JM, Gardeniers JW, Slooff TJ. Particle size of bone graft and method of impaction affect initial stability of cemented cups: human cadaveric and synthetic pelvic specimen studies. Acta Orthop Scand 2003; 74(6):652–657.

[117] Ullmark G. Bigger size and defatting of bone chips will increase cup stability. Arch Orthop Trauma Surg 2000;120(7-8):445–447.

[118] Eldridge JD, Hubble MJ, Nelson K, Smith EJ, Learmonth ID. The effect of bone chip size on initial stability following femoral impaction grafting. J Bone Joint Surg [Br] 1997;79-B(Supp. III):364.

[119] Brodt MD, Swan CC, Brown TD. Mechanical behavior of human morselized cancellous bone in triaxial compression testing. J Orthop Res 1998;16(1):43–49.

[120] Voor MJ, Nawab A, Malkani AL, Ullrich CR. Mechanical properties of compacted morselized cancellous bone graft using one-dimensional consolidation testing. J Biomech 2000;33(12):1683–1688.

[121] Hirn MY, Salmela PM, Vuento RE. High-pressure saline washing of allografts reduces bacterial contamination. Acta Orthop Scand 2001;72(1):83–85.

[122] Kligman M, Con V, Roffman M. Cortical and cancellous morselized allograft in revision total hip replacement. Clin Orthop Relat Res 2002;(401):139–148.

[123] Kligman M, Padgett DE, Vered R, Roffman M. Cortical and cancellous morselized allograft in acetabular revision total hip replacement: minimum 5-year follow-up. J Arthroplasty 2003;18(7):907–913.

[124] Kligman M, Rotem A, Roffman M. Cancellous and cortical morselized allograft in revision total hip replacement: A biomechanical study of implant stability. J Biomech 2003;36(6):797–802.

[125] Ullmark G, Hallin G, Nilsson O. Impacted corticocancellous allografts and cement for femoral revision of total hip arthroplasty using Lubinus and Charnley prostheses. J Arthroplasty 2002;17(3):325–334.

[126] Bavadekar A, Cornu O, Godts B, Delloye C, van Tomme J, Banse X. Stiffness and compactness of morselized grafts during impaction: An in vitro study with human femoral heads. Acta Orthop Scand 2001;72(5):470–476.

[127] Verdonschot N, van Hal CT, Schreurs BW, Buma P, Huiskes R, Slooff TJ. Time-dependent mechanical properties of HA/TCP particles in relation to morsellized bone grafts for use in impaction grafting. J Biomed Mater Res 2001;58(5):599–604.

[128] Freemont AJ. (i) Bone. Current Orthopaedics 1998;12(3):181–192.

[129] Glimcher MJ. The nature of the mineral component of bone and the mechanism of calcification. Instr Course Lect 1987;36:49–69.

[130] Nordin M, Frankel VH. Basic biomechanics of the musculoskeletal system. 3rd ed. Lippincott Williams and Wilkins; 2001.

[131] Kold S, Bechtold JE, Ding M, Chareancholvanich K, Rahbek O, Soballe K. Compacted cancellous bone has a spring-back effect. Acta Orthop Scand 2003;74(5):591–595.

[132] Fosse L, Ronningen H, Lund-Larsen J, Benum P, Grande L. Impacted bone stiffness measured during construction of morsellised bone samples. J Biomech 2004;37(11):1757–1766.

[133] Frei H, Mitchell P, Masri BA, Duncan CP, Oxland TR. Mechanical characteristics of the bone-graft-cement interface after impaction allografting. J Orthop Res 2005;23(1):9–17.

[134] Frei H, Mitchell P, Masri BA, Duncan CP, Oxland TR. Allograft impaction and cement penetration after revision hip replacement. A histomorphometric analysis in the cadaver femur. J Bone Joint Surg [Br] 2004;86-B(5):771–776.

[135] Mann KA, Werner FW, Ayers DC. Mechanical strength of the cement-bone interface is greater in shear than in tension. J Biomech 1999;32(11):1251–1254.

[136] Methods of test for soils for civil engineering purposes – Part 7: Shear strength tests (total stress). BS 1377-7:1990. British Standard; 1990.

[137] William DC. Fundamentals of materials science and engineering: An interactive E-Text. Paperback ed. John Wiley and Sons; 2001.

[138] Jäger IL. Viscoelastic behavior of organic materials: consequences of a logarithmic dependence of force on strain rate. J Biomech 2005;38(7):1451–1458.

[139] Mow VC, Kuei SC, Lai WM, Armstrong CG. Biphasic creep and stress relaxation of articular cartilage in compression? Theory and experiments. J Biomech Eng 1980; 102(1):73–84.

[140] Toms AD, Barker RL, Jones RS, Kuiper JH. Impaction bone-grafting in revision joint replacement surgery. J Bone Joint Surg [Am] 2004;86-A(9):2050–2060.

[141] Gozzard C, Grimm B, Miles AW, Learmonth ID. The effect of preparatory technique on the compressive properties of morsellised bone graft. Hip International 2002;12(2):116–118.

[142] Datta A, Gheduzzi S, Miles AW. A comparison of the viscoelastic properties of bone grafts. Clin Biomech 2006;21(7):761–766.

[143] Brown CU, Norman TL, Kish VL III, Gruen TA, Blaha JD. Time-dependent circumferential deformation of cortical bone upon internal radial loading. J Biomech Eng 2002; 124(4):456–461.

[144] Masterson EL, Masri BA, Duncan CP. The cement mantle in the Exeter impaction allografting technique. A cause for concern. J Arthroplasty 1997;12(7):759–764.

[145] Verdonschot N, Huiskes R. Cement debonding process of total hip arthroplasty stems. Clin Orthop Relat Res 1997;(336):297–307.

[146] Mann KA, Bartel DL, Wright TM, Burstein AH. Coulomb frictional interfaces in modeling cemented total hip replacements: a more realistic model. J Biomech 1995; 28(9):1067–1078.

[147] Verdonschot N, Tanck E, Huiskes R. Effects of prosthesis surface roughness on the failure process of cemented hip implants after stem-cement debonding. J Biomed Mater Res 1998;42(4):554–559.

[148] Verdonschot N, Huiskes R. Mechanical effects of stem cement interface characteristics in total hip replacement. Clin Orthop Relat Res 1996;(329):326–336.

[149] Churchill DL, Incavo SJ, Uroskie JA, Beynnon BD. Femoral stem insertion generates high bone cement pressurization. Clin Orthop Relat Res 2001;(393):335–344.

[150] Frei H, Gadala MS, Masri BA, Duncan CP, Oxland TR. Cement flow during impaction allografting: a finite element analysis. J Biomech 2006;39(3):493–502.

[151] Gruen TA, McNeice GM, Amstutz HC. "Modes of failure" of cemented stem-type femoral components: a radiographic analysis of loosening. Clin Orthop Relat Res 1979; (141):17–27.

[152] Dai KR, Liu YK, Park JB, Clark CR, Nishiyama K, Zheng ZK. Bone-particle-impregnated bone cement: an in vivo weight-bearing study. J Biomed Mater Res 1991; 25(2):141–156.

[153] Sawicki A, Swidzinski W. Cyclic compaction of soils, grains and powders. Powder Technology 1995;85(2):97–104.

[154] Sawicki A, Swidzinski W. Elastic moduli of non-cohesive particulate materials. Powder Technology 1998;96(1):24–32.

[155] Sivakugan N. Lateral earth pressure. [online] http://www.geoengineer.org; 2001 (Accesed 28 August 2006).

[156] California Department of Transportation. Earth pressure theory and application. [online] http://www.dot.ca.gov/hq/esc/; 2003 (Accesed 28 August 2006).

[157] Smith GN, Smith IGN. Elements of soil mechanics. Seventh ed. Blackwell Science; 1998.

[158] Liebschner MA. Biomechanical considerations of animal models used in tissue engineering of bone. Biomaterials 2004;25(9):1697–1714.

[159] State of New Jersey. Hazardous substance fact sheet – Acetone. [online] http://www.state.nj.us; 1999 (Accesed 28 August 2006).

[160] Fosse L, Ronningen H, Benum P, Sandven RB. Influence of water and fat content on compressive stiffness properties of impacted morsellized bone: an experimental ex vivo study on bone pellets. Acta Orthop 2006;77(1):15–22.

[161] State of New Jersey. Hazardous substance fact sheet – Chloroform. [online] http://www.state.nj.us; 1999 (Accesed 28 August 2006).

[162] Phillips AT, Pankaj, Brown DT, Oram TZ, Howie CR, Usmani AS. The elastic properties of morsellised cortico-cancellous bone graft are dependent on its prior loading. J Biomech 2006;39(8):1517–1526.

[163] Phipps K, Saksena J, Muirhead-Allwood S, Miles AW, Goodship AE, Blunn G. Intra-operative force measurement of impaction allografting. 12th Annual Meeting. Euro.Orthop.Res.Soc.; 2002. .

[164] Ullmark G, Nilsson O. Impacted corticocancellous allografts: Recoil and strength. J Arthroplasty 1999;14(8):1019–1023.

[165] Mak SY. Instrumentation design for use in impaction grafting. BEng dissertation. Department of Mechanical Engineering, University of Bath, United Kingdom; 2004.

[166] Mak SY, Holsgrove TP, Miles AW. In-vitro study of medial strain distribution in the femur during impaction grafting. Proc Inst Mech Eng [H] 2007;221(6):613–619.

[167] Farooq MA, Clements JP, Miles AW. In vitro monitoring of hoop strains during impaction grafting of the femur. Hip International 2006;16(3):223–231.

[168] Grimm B, Gozzard C, Miles AW, Turner IG. Compression testing of bone grafts for impaction grafting. In: Ortho. Res. Society. vol. 48th Annual Meeting; 2002. p. 568.

[169] Grimm B, Miles AW, Turner IG. Optimizing a hydroxyapatite/tricalcium-phosphate ceramic as a bone graft extender for impaction grafting. J Mater Sci Mater Med 2001; 12(10-12):929–934.

[170] Cristofolini L, Viceconti M, Cappello A, Toni A. Mechanical validation of whole bone composite femur models. J Biomech 1996;29(4):525–535.

[171] Cristofolini L, Viceconti M. Mechanical validation of whole bone composite tibia models. J Biomech 2000;33(3):279–288.

[172] Heiner AD, Brown TD. Structural properties of a new design of composite replicate femurs and tibias. J Biomech 2001;34(6):773–781.

[173] Sawbone worldwide catalog. Pacific Research Laboratories; 2006.

[174] Miles AW, Dall DM. Some design considerations on the stems of total hip replacement prostheses. S Afr J Surg 1978;16(2):157–165.

[175] Robinson MC, Fernlund G, Meek RMDominic, Masri BA, Duncan CP, Oxland TR. Structural characteristics of impaction allografting for revision total hip arthroplasty. Clin Biomech 2005;20(8):853–855.

[176] Metallic powders, excluding powders for hardmetals – Determination of compactibility (compressibility) in uniaxial compression. BS EN 23927:1993. British Standard; 1993.

[177] Monick JA. Measuring tackiness of detergent powders. Soap and Chemical Specialties 1966;(June):49–107.

[178] Mann KA, Bartel DL, Wright TM, Ingraffea AR. Mechanical characteristics of the stem-cement interface. J Orthop Res 1991;9(6):798–808.

A. Experimental data

A.1. Notation uses in classification of variables in §1.13

Symbol	Unit	Type	Quantity	Reference(s)
A	mm^2	II	Cross section area	[78, 92, 126, 132, 165]
δ	mm	III	Transient deformation	[132]
c	N/mm^2	I, III	Cohesion	[93, 94]
$c_{contact}$	%	III	Cement contact	[133]
C_u	–	I	Coefficient of uniformity	[93, 115]
C_{fat}	%	I, III	Fat content	[120]
C_{water}	%	I, III	Water content	[115, 120]
$C_{moisture}$	%	I, III	Moisture content	[120]
D	kGy	I	Irradiation	[106, 109, 111]
D_{defat}	Yes/No	I	Defatting	[78, 92, 94, 115, 119]
E_{mod}	N/mm^2	I, III	Young's modulus/ Axial stiffness	[68, 78, 92, 119, 120] [126, 127, 132, 178]
$E_{creep,t}$	N/mm^2	I, III	Creep modulus at time (t)	–
$E_{relax,t}$	N/mm^2	I, III	Relaxation modulus at time (t)	–
E_{energy}	kPa	III	Energy Density	[127]
G_{mod}	N/mm^2	I, III	Shear modulus/ Torsional stiffness	[66]
G_{energy}	N/mm	III	Failure energy	[133]
f_{fusion}	Yes/No	II	Fusion simulation	[68, 92]
f	Hz	II	Impaction frequency	[70, 88, 127, 166]
H	mm	II	Impaction height	[115, 120, 132]
K	J	II	Impaction energy	[88]
l	mm	I	Initial specimen length	[126]
m	mm	III	Stem migration	[40, 62]
M	Ns	II	Momentum/ Impulse	[68, 88]
ρ_{dry}	g/cm^3	I	Dry density	[115, 120]
ρ_{bone}	g/cm^3	I, III	Bone density	[70, 93, 126, 132]
$\rho_{mineral}$	g/cm^3	I, III	Bone mineral density	[132]
$P_{porosity}$	%	I, III	Porosity	[78, 127, 134, 150]
$P_{perm.}$	m^4/Ns	I, III	Permeability	[70]
$P_{pressure}$	kPa	II	Cement pressurisation pressure	[149, 150]
R_a	μm	II	Stem surface roughness	[147]
$R_{creep\,recoil,t}$	%	III	Creep-recoil at time (t)	[127]
$R_{relax\,recoil,t}$	%	III	Relaxation-recoil at time (t)	[70, 78, 131]
$R_{relax,t}$	%	III	Relaxation at time (t)	[78, 141, 142]
S	mm	I	Graft size	[78, 93, 94, 115, 116, 119]

(Continue on the next page)

Symbol	Unit	Type	Quantity	Reference(s)
t_{time}	s	II	Time	[70, 78, 92, 115] [120, 127, 132, 143]
t_{cement}	mm	III	Cement mantle thickness/ penetration	[134, 150]
t_{int}	mm·mg/cc	III	Amount of interdigitated bone	[135]
ϕ	deg	I, III	Internal friction angle	[93, 94]
μ	–	II, III	Coefficient of friction	[178]
U	J/m^3	II	Strain energy	–
ν	–	III	Poisson's ratio	[68, 119]
V	ml	II	Amount of MCB per layer	[68, 78, 165]
w_{ash}	g	I	Ash weight	[132]
η	cP	III	Cement viscosity	[149]
N_{layer}	–	II	Number of graft layers	[68, 115, 120, 132]
N_{impact}	–	II	Number of impactions per layer	[68, 115, 120]
$N_{impact\ total}$	–	II	Number of total impactions	[68, 94, 126, 132]
N_{cycle}	–	II	Number of cyclic loadings	[66, 88, 127, 165]
a	θ	II	Applied rotational angle	[66]
F	N	II	Applied force	[66, 78, 88, 132] [134, 135, 146, 178]
τ	N/mm^2	II	Applied shear	[94, 133]
σ	N/mm^2	II	Applied stress	[70, 92, 115, 120, 132]
ε	–	II	Applied strain	[66, 93, 132] [133, 178]
T	Nm	II	Applied torque	[66]
F_{max}	N	III	Maximum peak force	[132]
T_{max}	Nm	III	Maximum torque	[66]
σ_{max}	N/mm^2	III	Maximum stress strength	[119, 146]
τ_{max}	N/mm^2	III	Maximum shear strength	[78, 93, 94]
Δl	mm	III	Total deformation	[66, 70, 126, 135]
$\Delta\sigma$	N/mm^2	III	Change of stress in a given time	–
$\Delta\varepsilon$	–	III	Change of strain in a given time	–
$d\sigma$	N/mm^2	III	Instantaneous stress (for true $\sigma - \varepsilon$)	[119]
$d\varepsilon$	–	III	Instantaneous strain (for true $\sigma - \varepsilon$)	[119]

Table A.1.: Common variables and units use for describing impaction grafting. Type I – Preparation variables. Type II – Application variables. Type III – Impaction technique dependent variables. Remarks: '$_{app}$' can be attached if the material is tested as apparent value (e.g. $\tau \rightarrow \tau_{app}$), and non SI-unit is used (e.g. $N/m^2 \rightarrow N/mm^2$).

A.2. Detailed experimental results in §3

Standard order	1	2	3	4	5	6	7	8	9	10	11	12
Run order	1	9	17	25	33	41	3	11	19	27	35	43
Defatting	–	–	–	–	–	–	–	–	–	–	–	–
Pre-load	–	–	–	–	–	–	+	+	+	+	+	+
Load rate	–	–	–	–	–	–	–	–	–	–	–	–
Mass (g)	5.1	5.0	4.8	4.8	4.8	5.3	5.0	5.5	5.2	5.0	5.2	4.8
Max. strain ($\mu\varepsilon$)	870	453	457	275	725	895	818	524	810	400	650	630
Max. force (N)	1570	1552	1180	1410	1300	1940	1455	2010	1699	1455	1504	1290
TCPR ($\times10^{-3}$)	1.46	0.698	0.738	0.435	1.09	1.43	2.62	1.38	2.22	1.32	1.98	2.06
Recoil (%)	34.75	38.92	41.00	38.08	40.42	40.00	37.92	42.42	38.42	36.58	39.17	39.33

Standard order	13	14	15	16	17	18	19	20	21	22	23	24
Run order	5	13	21	29	37	45	7	15	23	31	39	47
Defatting	–	–	–	–	–	–	–	–	–	–	–	–
Pre-load	–	–	–	–	–	–	+	+	+	+	+	+
Load rate	+	+	+	+	+	+	+	+	+	+	+	+
Mass (g)	5.4	5.2	5.5	5.4	4.9	5.5	4.6	5.2	5.5	5.6	4.6	5.5
Max. strain ($\mu\varepsilon$)	840	838	758	700	617	862	440	870	950	1216	732	1010
Max. force (N)	2088	1709	1816	2185	1425	2165	1211	1650	2373	2480	1200	1826
TCPR ($\times10^{-3}$)	1.28	1.26	1.18	1.11	0.987	1.32	1.85	2.51	2.33	3.02	2.62	2.69
Recoil (%)	35.33	35.08	40.42	29.67	35.92	40.92	35.92	36.92	45.17	35.33	29.58	42.33

Standard order	25	26	27	28	29	30	31	32	33	34	35	36
Run order	2	10	18	26	34	42	4	12	20	28	36	44
Defatting	+	+	+	+	+	+	+	+	+	+	+	+
Pre-load	–	–	–	–	–	–	+	+	+	+	+	+
Load rate	–	–	–	–	–	–	–	–	–	–	–	–
Mass (g)	4.8	5.2	5.0	4.8	4.6	4.7	4.6	5.2	5.5	5.1	5.1	5.1
Max. strain ($\mu\varepsilon$)	555	642	628	890	660	425	675	802	1317	1208	755	879
Max. force (N)	1973	2548	2370	1972	1543	1718	1600	2675	2841	2256	2275	2207
TCPR ($\times10^{-3}$)	0.811	0.963	0.942	1.37	0.981	0.615	1.54	2.11	2.75	2.91	1.52	2.00
Recoil (%)	41.08	39.17	36.75	41.08	34.67	37.42	39.17	40.17	34.08	44.75	40.00	38.42

Standard order	37	38	39	40	41	42	43	44	45	46	47	48
Run order	6	14	22	30	38	46	8	16	24	32	40	48
Defatting	+	+	+	+	+	+	+	+	+	+	+	+
Pre-load	–	–	–	–	–	–	+	+	+	+	+	+
Load rate	+	+	+	+	+	+	+	+	+	+	+	+
Mass (g)	5.4	5.0	5.1	5.4	5.1	5.2	4.6	5.3	5.0	5.5	5.3	5.0
Max. strain ($\mu\varepsilon$)	1543	1431	1482	1016	1029	974	933	1619	999	1436	755	1066
Max. force (N)	2793	1807	2461	2939	2793	2568	1660	2392	2080	2773	2266	2285
TCPR ($\times10^{-3}$)	2.30	2.20	2.31	1.48	1.53	1.41	2.46	3.38	2.39	2.88	1.72	2.25
Recoil (%)	41.58	41.25	32.75	42.17	38.33	41.08	35.50	40.17	34.92	45.25	39.08	44.42

Table A.2.: Results of the 2^3 full factorial DoF with six replications, sorted by 'Run order'. Max. force should read as maximum axial force. The appropriate variables and units are Defatting (D_{defat}), Pre-load (P_{load}), Load rate (R_{load}), Mass (m, g), Max. hoop strain (ε_{boner}, $\mu\varepsilon$), Max. axial force (F, N), TCPR ($\times10^{-3}$) and Recoil (R_{recoil}, %).

Standard ord.	1	2	3	4	5	6	7	8**	9	10	11	12
Run order	1	9	17	25	33	41	3	11	19	27	35	43
Defatting	–	–	–	–	–	–	–	–	–	–	–	–
Pre-load	–	–	–	–	–	–	+	+	+	+	+	+
Load rate	–	–	–	–	–	–	–	–	–	–	–	–
5% ICME	0.00*	0.00*	0.00*	0.00*	0.00*	0.00*	56.33	65.01	54.15	50.56	55.62	65.13
10% ICME	0.00*	0.00*	0.00*	0.00*	0.00*	0.00*	37.05	35.55	34.94	36.48	34.81	39.05
20% CCME	0.56	1.12	0.00*	0.00*	0.61	1.09	7.13	6.64	8.67	8.39	8.54	9.33
30% CCME	1.15	1.06	1.69	0.56	0.66	0.57	11.21	7.37	8.60	8.34	5.59	9.98
40% CCME	1.60	0.56	0.58	1.06	1.20	1.03	8.12	9.81	10.35	8.34	11.19	7.00
50% CCME	2.91	2.66	2.12	2.81	0.66	2.84	11.21	10.04	12.70	9.99	10.07	10.26
60% CCME	4.85	4.47	2.95	4.86	1.94	3.85	13.65	13.69	16.56	9.99	12.31	10.04
70% CCME	6.98	7.89	5.58	6.61	3.67	7.38	17.44	17.07	15.97	12.66	17.01	15.68
80% CCME	9.46	11.18	8.38	10.05	5.90	10.70	20.21	18.96	22.57	23.60	17.90	14.66
90% CCME	16.69	17.18	15.51	15.91	7.26	16.21	21.40	22.94	26.95	22.02	21.48	18.33
100% CCME	40.54	41.25	28.88	35.78	11.79	40.35	21.60	26.41	33.32	31.21	24.52	19.01

Standard ord.	13	14	15	16	17	18	19**	20	21	22	23	24
Run order	5	13	21	29	37	45	7	15	23	31	39	47
Defatting	–	–	–	–	–	–	–	–	–	–	–	–
Pre-load	–	–	–	–	–	–	+	+	+	+	+	+
Load rate	+	+	+	+	+	+	+	+	+	+	+	+
5% ICME	0.00*	0.00*	0.00*	0.00*	0.00*	0.00*	55.95	41.56	52.11	49.77	53.38	51.44
10% ICME	0.54	1.11	0.56	0.57	0.54	0.55	32.42	30.43	30.73	30.86	31.36	31.17
20% CCME	0.57	1.04	1.62	1.05	1.04	0.49	6.30	9.85	7.28	8.09	7.42	7.79
30% CCME	1.70	1.66	2.87	1.14	1.10	1.24	6.71	10.61	7.46	7.47	9.89	9.53
40% CCME	2.27	3.11	4.26	3.09	1.03	1.06	8.36	13.16	8.90	11.85	10.71	11.26
50% CCME	4.49	4.39	6.32	4.63	2.77	3.33	9.64	15.44	12.35	12.98	12.27	13.25
60% CCME	6.10	8.73	10.22	8.13	5.69	4.14	11.71	17.41	14.21	16.59	15.28	13.48
70% CCME	12.05	11.53	12.38	15.04	6.64	9.15	13.93	22.26	19.20	20.42	20.61	22.27
80% CCME	16.45	20.93	20.79	17.73	11.60	12.92	16.72	27.10	19.74	23.70	23.08	24.25
90% CCME	24.96	31.85	29.61	24.92	21.59	21.28	19.50	29.90	29.76	31.56	29.67	29.44
100% CCME	43.35	53.87	45.44	36.27	32.08	40.32	23.01	34.11	31.04	36.06	36.77	34.54

Standard ord.	25	26	27	28	29	30	31	32**	33	34	35	36**
Run order	2	10	18	26	34	42	4	12	20	28	36	44
Defatting	+	+	+	+	+	+	+	+	+	+	+	+
Pre-load	–	–	–	–	–	–	+	+	+	+	+	+
Load rate	–	–	–	–	–	–	–	–	–	–	–	–
5% ICME	0.00*	0.00*	0.00*	0.00*	0.00 *	0.00*	103.42	97.18	76.31	120.51	83.92	81.53
10% ICME	0.00*	0.00*	0.00*	0.00*	0.00*	0.00*	50.80	46.72	42.31	67.13	49.46	50.97
20% CCME	0.52	0.52	0.52	1.08	1.64	1.05	9.55	9.20	8.73	10.27	7.44	9.98
30% CCME	1.60	1.06	1.12	0.55	0.55	0.53	5.30	7.81	9.75	8.31	4.65	9.33
40% CCME	1.60	1.04	1.08	1.64	1.70	1.59	8.56	10.67	10.61	9.07	11.17	11.75
50% CCME	3.14	1.06	3.35	3.29	2.19	2.17	11.41	13.88	14.60	9.07	10.58	14.00
60% CCME	4.85	4.18	5.41	4.39	2.77	5.90	10.83	14.29	19.45	14.96	16.23	17.18
70% CCME	7.47	5.85	7.18	9.32	4.43	9.03	19.41	30.37	32.88	11.08	24.20	42.19
80% CCME	16.01	12.53	14.76	17.38	10.08	16.47	24.62	31.24	36.07	16.62	24.20	26.52
90% CCME	33.96	23.02	33.51	43.18	18.70	40.96	30.53	37.51	41.34	19.00	28.85	34.91
100% CCME	54.16	50.55	38.76	51.37	41.96	48.20	14.45	24.29	22.81	11.51	15.00	32.14

(Continue on the next page)

Standard ord.	37**	38	39**	40	41	42**	43**	44	45**	46	47	48
Run order	6	14	22	30	38	46	8	16	24	32	40	48
Defatting	+	+	+	+	+	+	+	+	+	+	+	+
Pre-load	−	−	−	−	−	−	+	+	+	+	+	+
Load rate	+	+	+	+	+	+	+	+	+	+	+	+
5% ICME	0.00*	0.00*	0.00*	0.00*	0.00*	0.00*	68.48	74.72	75.65	81.13	90.64	79.08
10% ICME	3.39	1.18	1.59	0.59	1.58	1.04	38.27	39.93	38.49	41.55	40.65	41.87
20% CCME	2.86	0.51	2.12	0.51	2.13	2.07	10.70	8.47	8.38	8.41	9.42	9.37
30% CCME	2.79	2.57	2.67	1.54	2.69	2.61	9.99	8.99	9.40	8.37	10.03	7.77
40% CCME	4.00	2.59	4.28	1.54	4.31	3.68	12.38	12.00	11.87	10.39	11.99	11.79
50% CCME	5.71	6.22	5.88	4.71	7.01	3.65	14.27	14.93	12.32	13.25	13.92	9.89
60% CCME	7.90	9.33	9.72	8.30	9.16	8.42	16.07	19.05	16.43	16.37	16.11	16.57
70% CCME	10.04	17.43	13.36	8.22	16.34	11.16	20.10	22.32	21.64	20.27	16.85	17.98
80% CCME	18.97	24.30	20.73	16.59	23.67	22.63	19.97	26.82	32.11	23.76	19.93	24.31
90% CCME	28.91	44.18	35.09	28.02	32.62	38.87	26.96	42.64	39.23	35.15	35.32	38.51
100% CCME	26.44	53.75	58.27	38.60	40.01	47.49	24.17	32.43	25.29	22.68	18.54	16.40

Table A.3.: Results of the consolidated constrained modulus of elasticity (CCME) (Unit in MPa) of 2^3 full factorial DoF with six replications, sorted by 'Run order'. *Values were too low to be determined because of low signal-to-noise ratio. It was, therefore, assumed to be zero. **Experiment was re-taken since the original data set was insuffcent to estimate the CCME.

Standard ord.	1	2	3	4	5	6	7	8**	9	10	11	12
Run order	1	9	17	25	33	41	3	11	19	27	35	43
Defatting	−	−	−	−	−	−	−	−	−	−	−	−
Pre-load	−	−	−	−	−	−	+	+	+	+	+	+
Load rate	−	−	−	−	−	−	−	−	−	−	−	−
5% ICME	0.00*	0.00*	0.00*	0.00*	0.00*	0.00*	56.33	65.01	54.15	50.56	55.62	65.13
10% ICME	0.00*	0.00*	0.00*	0.00*	0.00*	0.00*	37.05	35.55	34.94	36.48	34.81	39.05
20% TCME	0.55	0.27	0.00*	0.27	0.00*	0.55	22.74	20.60	21.57	21.85	23.02	24.52
30% TCME	0.75	0.54	0.56	0.36	0.00*	0.56	19.13	16.40	17.51	17.60	17.29	20.36
40% TCME	0.97	0.54	0.56	0.54	0.31	0.68	15.80	14.72	15.75	15.39	15.78	16.90
50% TCME	1.34	0.97	0.89	0.98	0.38	1.10	14.98	13.64	15.05	14.39	14.65	15.64
60% TCME	1.94	1.54	1.22	1.63	0.63	1.56	14.76	13.65	15.29	13.70	14.26	14.63
70% TCME	2.64	2.47	1.84	2.34	1.08	2.37	15.11	14.15	15.39	13.51	14.73	14.76
80% TCME	3.49	3.53	2.66	3.33	1.66	3.44	15.72	14.71	16.22	14.61	15.11	14.75
90% TCME	4.92	5.06	4.15	4.67	2.31	4.80	16.33	15.68	17.41	15.50	15.82	15.15
100% TCME	8.65	8.55	6.55	7.85	3.22	8.40	16.86	16.71	18.90	16.94	16.63	15.63

Standard ord.	13	14	15	16	17	18	19**	20	21	22	23	24
Run order	5	13	21	29	37	45	7	15	23	31	39	47
Defatting	−	−	−	−	−	−	−	−	−	−	−	−
Pre-load	−	−	−	−	−	−	+	+	+	+	+	+
Load rate	+	+	+	+	+	+	+	+	+	+	+	+
5% ICME	0.00*	0.00*	0.00*	0.00*	0.00*	0.00*	55.95	41.56	52.11	49.77	53.38	51.44
10% ICME	0.54	1.11	0.56	0.57	0.54	0.55	32.42	30.43	30.73	30.86	31.36	31.17
20% TCME	0.55	1.07	1.09	0.82	0.27	0.52	19.36	20.25	19.01	19.75	19.54	19.80
30% TCME	0.93	1.26	1.67	0.92	0.54	0.73	15.32	17.06	15.22	15.79	16.35	16.44
40% TCME	1.26	1.74	2.34	1.49	0.67	0.82	13.59	16.11	13.63	14.79	14.95	15.16
50% TCME	1.91	2.26	3.11	2.09	1.07	1.31	12.71	15.94	13.33	14.40	14.38	14.75
60% TCME	2.61	3.38	4.27	3.11	1.87	1.80	12.55	16.17	13.47	14.76	14.53	14.54
70% TCME	3.93	4.52	5.46	4.74	2.53	2.80	12.74	17.03	14.21	15.51	15.39	15.59
80% TCME	5.48	6.61	7.35	6.31	3.68	4.13	13.22	18.22	14.90	16.54	16.33	16.65
90% TCME	7.63	9.35	9.89	8.43	5.61	5.98	13.90	19.70	16.45	18.18	17.79	18.04
100% TCME	11.29	13.86	13.37	11.07	8.35	9.45	14.77	21.08	18.07	20.13	20.16	19.71

Standard ord.	25	26	27	28	29	30	31	32**	33	34	35	36**
Run order	2	10	18	26	34	42	4	12	20	28	36	44
Defatting	+	+	+	+	+	+	+	+	+	+	+	+
Pre-load	−	−	−	−	−	−	+	+	+	+	+	+
Load rate	−	−	−	−	−	−	−	−	−	−	−	−
5% ICME	0.00*	0.00*	0.00*	0.00*	0.00*	0.00*	103.42	97.18	76.31	120.51	83.92	81.53
10% ICME	0.00*	0.00*	0.00*	0.00*	0.00*	0.00*	50.80	46.72	42.31	67.13	49.46	50.97
20% TCME	0.56	0.27	0.58	0.59	0.90	0.58	26.96	25.74	24.36	34.91	24.41	27.19
30% TCME	0.91	0.18	0.76	0.58	0.78	0.56	19.03	19.06	18.67	23.95	17.03	20.36
40% TCME	1.09	0.40	0.84	0.86	1.01	0.83	15.99	16.69	16.55	19.47	15.44	17.92
50% TCME	1.51	0.54	1.35	1.36	1.26	1.10	14.96	16.10	16.13	17.06	14.42	17.08
60% TCME	2.07	1.16	2.05	1.88	1.52	1.92	14.23	15.79	16.70	16.77	14.75	17.09
70% TCME	2.85	1.83	2.79	2.96	1.94	2.96	14.99	17.96	18.95	15.65	16.17	20.11
80% TCME	4.51	3.19	4.31	4.77	2.97	4.69	16.26	19.68	21.21	15.78	17.21	21.08
90% TCME	7.78	5.34	7.54	9.03	4.72	8.66	17.93	21.68	23.38	16.16	18.52	22.60
100% TCME	11.59	9.35	10.31	12.61	8.21	12.15	17.65	21.91	23.33	15.84	18.22	23.48

(Continue on the next page)

Standard ord.	37**	38	39**	40	41	42**	43**	44	45**	46	47	48
Run order	6	14	22	30	38	46	8	16	24	32	40	48
Defatting	+	+	+	+	+	+	+	+	+	+	+	+
Pre-load	–	–	–	–	–	–	+	+	+	+	+	+
Load rate	+	+	+	+	+	+	+	+	+	+	+	+
5% ICME	0.00*	0.00*	0.00*	0.00*	0.00*	0.00*	68.48	74.72	75.65	81.13	90.64	79.08
10% ICME	3.39	1.18	1.59	0.59	1.58	1.04	38.27	39.93	38.49	41.55	40.65	41.87
20% TCME	3.12	0.82	1.85	0.55	1.86	1.56	22.13	22.05	21.04	23.03	22.43	23.01
30% TCME	3.01	1.43	2.12	0.90	2.13	1.91	17.65	17.26	16.66	17.43	17.60	17.34
40% TCME	3.25	1.73	2.66	1.06	2.67	2.35	16.25	15.87	15.39	15.55	16.07	15.88
50% TCME	3.74	2.65	3.30	1.80	3.53	2.61	15.83	15.67	14.74	15.06	15.60	14.59
60% TCME	4.44	3.78	4.36	2.90	4.47	3.57	15.87	16.25	15.03	15.29	15.70	14.92
70% TCME	5.25	5.73	5.64	3.68	6.14	4.64	16.48	17.12	16.00	16.04	15.87	15.40
80% TCME	6.89	8.05	7.49	5.31	8.29	6.88	16.93	18.37	18.07	17.00	16.38	16.53
90% TCME	9.30	11.99	10.45	7.78	10.89	10.29	18.07	21.03	20.39	19.07	18.47	18.90
100% TCME	10.63	15.38	14.37	10.30	13.22	13.32	18.53	21.91	20.77	19.36	18.47	18.73

Table A.4.: Results of the total constrained modulus of elasticity (TCME) (Unit in MPa) of 2^3 full factorial DoF with six replications, sorted by 'Run order'. *Values were too low to be determined because of low signal-to-noise ratio. It was, therefore, assumed to be zero. **Experiment was re-taken since the original data set was insuffcent to estimate the TCME.

A.3. Detailed experimental results in §4

Standard order	1	2	3	4	5	6	7	8	9	10
Defatting (D_{defat})	–	–	–	–	–	–	–	–	–	–
Frequency (f, Hz)	Static	Static	Static	Static	Static	Static	Static	Static	Static	Static
Mass (m, g)	5.7	5.6	5.5	5.7	5.6	5.7	5.5	5.7	5.7	5.8
Initial thickness*	25.31	22.13	24.42	26.30	25.54	26.75	28.30	30.60	29.72	28.73
Impacted thickness**	12.09	10.63	10.53	11.98	11.80	10.18	11.50	11.22	12.01	12.98
Recoil (R_{recoil}, %)	36.31	39.04	41.88	41.99	45.76	50.69	46.00	47.96	41.47	38.06
Relaxation (R_{relax}, %)	18.00	17.00	14.00	8.26	11.00	19.00	15.00	17.00	14.00	14.00

Run order	11	12	13	14	15	16	17	18	19	20
Defatting (D_{defat})	–	–	–	–	–	–	–	–	–	–
Frequency (f, Hz)	0.17	0.17	0.17	0.17	0.17	0.17	0.17	0.17	0.17	0.17
Mass (m, g)	5.8	5.6	5.5	5.6	5.7	5.9	5.5	5.7	5.5	5.7
Initial thickness*	22.55	18.55	19.05	23.73	19.55	20.30	18.35	21.90	18.44	19.60
Impacted thickness**	11.75	10.43	9.80	12.00	10.74	12.31	11.14	12.18	10.67	10.59
Recoil (R_{recoil}, %)	36.94	41.61	49.18	35.42	42.09	28.43	43.99	39.90	50.52	48.35
Relaxation (R_{relax}, %)	22.00	27.00	17.90	19.00	23.00	13.00	20.00	23.00	19.00	23.00

Standard order	21	22	23	24	25	26	27	28	29	30
Defatting (D_{defat})	–	–	–	–	–	–	–	–	–	–
Frequency (f, Hz)	1	1	1	1	1	1	1	1	1	1
Mass (m, g)	5.5	5.8	5.7	5.7	5.6	5.6	5.6	5.5	5.6	5.5
Initial thickness*	23.42	25.75	21.70	24.73	22.46	20.53	24.37	22.43	23.03	25.62
Impacted thickness**	11.00	13.26	10.66	12.09	10.61	10.00	12.34	10.63	10.14	10.36
Recoil (R_{recoil}, %)	35.36	19.83	34.52	22.25	41.47	42.60	15.32	39.13	44.48	42.86
Relaxation (R_{relax}, %)	31.00	20.00	32.00	31.00	26.50	17.00	26.00	22.00	26.00	25.00

Standard order	31	32	33	34	35	36	37	38	39	40
Defatting (D_{defat})	–	–	–	–	–	–	–	–	–	–
Frequency (f, Hz)	2	2	2	2	2	2	2	2	2	2
Mass (m, g)	5.6	5.7	5.6	5.6	5.7	5.7	5.8	5.7	5.7	5.7
Initial thickness*	24.94	23.93	22.68	25.30	20.91	23.60	24.53	27.88	21.49	23.86
Impacted thickness**	11.50	10.69	10.09	11.24	11.80	11.06	11.14	12.55	10.83	11.04
Recoil (R_{recoil}, %)	38.70	41.91	46.68	39.50	36.19	35.35	38.42	33.86	36.84	37.05
Relaxation (R_{relax}, %)	13.00	21.00	22.00	18.00	16.00	14.00	24.00	16.00	19.00	24.00

Standard order	41	42	43	44	45	46	47	48	49	50
Defatting (D_{defat})	+	+	+	+	+	+	+	+	+	+
Frequency (f, Hz)	Static	Static	Static	Static	Static	Static	Static	Static	Static	Static
Mass (m, g)	4.3	4.8	4.9	4.6	4.7	4.8	4.6	4.9	4.7	4.8
Initial thickness*	23.54	23.00	26.49	25.73	25.90	26.39	26.67	29.35	32.14	27.95
Impacted thickness**	11.03	12.34	12.20	11.71	12.17	12.31	11.69	11.90	11.95	11.64
Recoil (R_{recoil}, %)	33.82	37.44	35.66	36.12	35.99	33.71	35.76	35.97	35.82	35.14
Relaxation (R_{relax}, %)	13.00	14.00	17.00	5.00	8.00	12.00	8.00	8.00	6.00	7.00

Standard order	51	52	53	54	55	56	57	58	59	60
Defatting (D_{defat})	+	+	+	+	+	+	+	+	+	+
Frequency (f, Hz)	0.17	0.17	0.17	0.17	0.17	0.17	0.17	0.17	0.17	0.17
Mass (m, g)	4.6	4.5	4.5	4.7	4.7	4.6	4.7	4.7	4.7	4.6
Initial thickness*	25.76	24.89	27.08	25.83	23.99	23.97	29.80	26.76	27.64	25.92
Impacted thickness**	12.10	11.69	13.35	12.84	12.02	12.61	12.92	12.90	13.50	13.06
Recoil (R_{recoil}, %)	35.79	33.53	36.03	33.10	36.52	29.58	34.67	32.87	35.56	34.15
Relaxation (R_{relax}, %)	22.00	24.00	25.00	26.00	22.00	26.00	19.00	22.00	22.10	28.00

Standard order	61	62	63	64	65	66	67	68	69	70
Defatting (D_{defat})	+	+	+	+	+	+	+	+	+	+
Frequency (f, Hz)	1	1	1	1	1	1	1	1	1	1
Mass (m, g)	4.6	4.6	4.7	4.6	4.8	4.8	4.6	4.7	4.6	4.6
Initial thickness*	30.56	26.72	27.20	24.21	26.16	27.99	24.26	24.03	28.45	27.97
Impacted thickness**	13.09	12.87	12.70	12.75	12.99	13.31	11.64	12.97	13.79	12.65
Recoil (R_{recoil}, %)	41.56	39.16	39.37	33.65	36.10	30.05	41.32	33.15	31.98	38.34
Relaxation (R_{relax}, %)	25.00	29.00	26.00	24.00	25.00	24.00	25.00	25.00	26.00	25.00

Standard order	71	72	73	74	75	76	77	78	79	80
Defatting (D_{defat})	+	+	+	+	+	+	+	+	+	+
Frequency (f, Hz)	2	2	2	2	2	2	2	2	2	2
Mass (m, g)	4.6	4.7	4.7	4.6	4.7	4.8	4.7	4.7	4.6	4.7
Initial thickness*	29.31	24.21	27.88	27.74	26.15	24.42	26.14	28.36	28.53	29.10
Impacted thickness**	12.25	13.19	13.43	12.61	12.65	13.01	12.50	13.65	12.64	13.90
Recoil (R_{recoil}, %)	35.59	28.20	33.36	45.68	36.21	34.20	34.56	32.53	34.81	34.24
Relaxation (R_{relax}, %)	27.00	26.00	25.00	24.00	27.00	27.00	27.00	24.00	26.00	27.00

Table A.5.: Results of the vary cyclic loading conditions with ten replications for each experimental setting, sorted by 'Run order'. *Unit in ($l_{initial}$, mm). **Unit in ($l_{measured,\, t=180\,\mathrm{s}}$, mm).

Standard order	1	2	3	4	5	6	7	8	9	10
Rates (mm/s)	5	5	5	5	5	5	5	5	5	5
Stress (σ, MPa)	20.56	15.53	16.20	20.69	20.69	15.25	13.21	13.94	14.48	18.78
Recoil (R_{recoil}, %)	40.38	49.75	42.00	52.50	49.00	50.88	50.50	44.00	42.63	47.13

Standard order	11	12	13	14	15	16	17	18	19	20
Rates (mm/s)	10	10	10	10	10	10	10	10	10	10
Stress (σ, MPa)	15.66	17.63	19.99	20.18	17.13	18.05	14.04	15.34	16.71	20.34
Recoil (R_{recoil}, %)	43.13	50.63	53.25	44.25	51.00	46.00	43.50	39.88	43.63	46.13

Standard order	21	22	23	24	25	26	27	28	29	30
Rates (mm/s)	20	20	20	20	20	20	20	20	20	20
Stress (σ, MPa)	15.85	20.44	18.97	21.55	16.90	20.79	23.30	18.72	22.06	18.18
Recoil (R_{recoil}, %)	46.63	47.50	45.50	49.75	43.63	41.50	44.13	41.00	46.75	49.25

Standard order	31	32	33	34	35	36	37	38	39	40
Rates (mm/s)	30	30	30	30	30	30	30	30	30	30
Stress (σ, MPa)	18.81	17.51	17.95	23.52	19.58	21.77	20.91	16.33	21.68	21.04
Recoil (R_{recoil}, %)	44.50	46.25	49.88	40.25	41.38	44.50	43.00	56.63	44.50	44.75

Standard order	41	42	43	44	45	46	47	48	49	50
Rates (mm/s)	40	40	40	40	40	40	40	40	40	40
Stress (σ, MPa)	23.14	22.70	27.50	24.64	25.40	22.73	19.83	26.61	21.68	16.30
Recoil (R_{recoil}, %)	40.38	41.00	50.25	45.75	47.38	41.25	42.75	49.25	44.75	47.00

Standard order	51	52	53	54	55	56	57	58	59	60
Rates (mm/s)	50	50	50	50	50	50	50	50	50	50
Stress (σ, MPa)	23.94	25.75	19.16	26.83	22.35	30.11	27.88	27.25	24.29	35.40
Recoil (R_{recoil}, %)	38.25	43.88	49.00	39.38	42.63	45.50	47.25	46.13	39.75	41.00

Standard order	61	62	63	64	65	66	67	68	69	70
Rates (mm/s)	60	60	60	60	60	60	60	60	60	60
Stress (σ, MPa)	28.07	21.42	28.81	28.52	31.42	20.34	28.81	25.59	24.89	34.73
Recoil (R_{recoil}, %)	38.50	42.75	46.13	52.63	45.38	38.25	44.88	47.75	42.00	48.75

Table A.6.: Summary of mean and one standard deviation (presented in bracket) of stress and recoil.

A.4. Detailed experimental results in §5

Load (kN)	Unce. 1	Unce. 2	Unce. 3	Unce. 4	Unce. 5	Unce. 6	Mean (SD)
0.2	−0.09	−0.37	−0.12	−0.25	−0.44	−0.19	−0.24 (0.14)
0.4	−0.21	−0.55	−0.26	−0.56	−0.94	−0.34	−0.48 (0.27)
0.6	−0.32	−0.75	−0.59	−0.75	−1.21	−0.80	−0.74 (0.29)
0.8	−0.56	−1.27	−3.44	−0.95	−1.59	−1.87	−1.61 (1.01)
1.0	−0.70	−3.66	−6.00	−1.51	−2.43	−3.99	−3.05 (1.91)
1.2	−1.75	−4.97		−2.42	−4.22	−5.58	−3.79 (1.64)
1.4	−5.33	−6.00		−3.52	−6.00	−6.00	−5.37 (1.07)
1.6	−6.00			−4.96			−5.48 (0.74)
1.8				−6.00			−6.00 (nil)

Table A.7.: Axial displacement of stem movement at various loads for both uncemented (Unce.) stems. Remarks: A subsidence of 4 mm was defined as the failure criterion.

Load (kN)	Cem. 1	Cem. 2*	Cem. 3	Cem. 4	Cem. 5	Cem. 6	Mean (SD)*
0.2	−0.13		−0.03	−0.23	−0.26	−0.17	−0.16 (0.09)
0.4	−0.29		−0.07	−0.41	−0.39	−0.27	−0.29 (0.14)
0.6	−0.43		−0.12	−0.64	−0.47	−0.35	−0.40 (0.19)
0.8	−0.53		−0.18	−0.76	−0.54	−0.40	−0.48 (0.21)
1.0	−0.61		−0.24	−0.96	−0.63	−0.49	−0.59 (0.26)
1.2	−0.69		−0.30	−1.37	−0.73	−0.54	−0.73 (0.40)
1.4	−0.76		−0.62	−1.61	−0.87	−0.63	−0.90 (0.41)
1.6	−0.90		−0.69	−1.67	−1.07	−0.94	−1.05 (0.37)
1.8	−1.02		−0.82	−1.80	−1.34	−1.05	−1.21 (0.38)
2.0	−1.19		−0.99	−2.00	−1.49	−1.15	−1.36 (0.40)
2.2	−1.33		−1.11	−2.22	−1.67	−1.27	−1.52 (0.44)
2.4	−1.44		−1.23	−2.31	−1.92	−1.41	−1.66 (0.44)
2.6	−1.55		−1.36	−2.42	−2.11	−1.53	−1.79 (0.45)
2.8	−1.76		−1.53	−2.67	−2.34	−1.71	−2.00 (0.48)
3.0	−2.04		−1.74	−2.90	−2.59	−1.85	−2.22 (0.50)
3.2	−2.39		−2.00	−3.10	−2.68	−2.01	−2.44 (0.47)
3.4	−2.48		−2.18	−3.37	−2.78	−2.10	−2.58 (0.52)
3.6	−2.77		−2.45	−3.61	−2.91	−2.25	−2.80 (0.52)
3.8	−2.91		−2.79	−3.68	−3.50	−2.34	−3.04 (0.55)
4.0	−3.08		−2.90	−3.78	−4.04	−2.49	−3.26 (0.64)
4.2	−3.46		−3.10	−3.93	−4.62	−2.92	−3.61 (0.69)
4.4	−6.00		−3.24	−4.08	−5.44	−3.51	−4.45 (1.21)
4.6			−3.36	−4.26	−6.00	−6.00	−4.91 (1.32)
4.8			−3.50	−4.42			−3.96 (0.65)
5.0			−3.66	−4.58			−4.12 (0.65)
5.2			−3.81	−4.78			−4.30 (0.69)
5.4			−3.98	−4.99			−4.49 (0.71)
5.6			−4.16	−5.21			−4.69 (0.74)
5.8			−4.33	−5.46			−4.90 (0.80)
6.0			−4.53	−5.73			−5.13 (0.85)
6.2			−4.76	−6.00			−5.38 (0.88)
6.4			−5.02				−5.02 (nil)
6.6			−5.27				−5.27 (nil)
6.8			−6.00				−6.00 (nil)

Table A.8.: Axial displacement of stem movement at various loads for cemented (Cem) stems. Remarks: A subsidence of 4 mm was defined as the failure criterion. *The experiment setup was faulty and the date had to be discarded.

B. Publication lists

Journal

- Mak SY, Holsgrove TP, Miles AW, *In-vitro* study of medial strain distribution in the femur during impaction grafting. Proc Inst Mech Eng [H] 2007;221(6):613–619.

Conference

- Mak SY, Katsimihas M, Miles AW. The effect of repetitive cyclic loading on the relaxation of morsellised bone graft. 6th Combined meeting, Orthopaedic Research Societies 2007. [Podium presentation]

- Mak SY, Cunningham JL, Miles AW. Elastic modulus and stress-strain characteristics of morsellised bone graft under different loading conditions. 6th Combined meeting, Orthopaedic Research Societies 2007. [Podium Presentation]

- Mak SY, Cunningham JL, Miles AW. The effect on rate of impaction on morsellised bone graft. 6th Combined meeting, Orthopaedic Research Societies 2007. [Podium presentation]

- Mak SY, Cunningham JL, Miles AW. Determination of Poisson's ratio and hoop strain of morsellised bone graft under uni-axial compressive loading. 53rd Annual meeting, Orthopaedic Research Societies 2007. [Poster presentation]

- Mak SY, Holsgrove TP, Miles AW. *In-vitro* study of influence of impaction energy on medial strain distribution in the femur during impaction bone grafting. 53rd Annual meeting, Orthopaedic Research Societies 2007. [Poster presentation]

- Mak SY, Smith SD, Miles AW. *In-vitro* predication of cemented and non-cemented revision stem stability in impaction bone grafting. 53rd Annual meeting, Orthopaedic Research Societies 2007. [Poster presentation]

- Mak SY, Holsgrove TP, Miles AW. *In-vitro* study of medial strain distribution in the femur during impaction grafting. Royal Academy of Engineering Futures Meeting 2006. [Podium presentation]

In-vitro study of medial strain distribution in the femur during impaction grafting

S Y Mak*, T P Holsgrove, and A W Miles
Centre for Orthopaedic Biomechanics, Department of Mechanical Engineering, University of Bath, Bath, Avon, UK

The manuscript was received on 31 July 2006 and was accepted after revision for publication on 4 April 2007.

DOI: 10.1243/09544119JEIM220

Abstract: Impaction bone grafting (IBG) is widely used for revision hip surgery to compensate for bone stock loss. It is performed by impacting morsellized allograft into the femoral canal and acetabulum prior to cementing new total hip components. Per- and post-operative femoral fractures and post-operative implant subsidence are major complications in IBG. The aim of this study was to investigate the strain distribution on the medial side of the femur during impaction grafting and the subsequent stability of the stem under uniaxial cyclic loading. The Exeter IBG technique was used in conjunction with Howmedica X-change instrumentation. Sawbones® composite femora were used. An impactometer, which provides a known impaction energy and momentum, was used to standardize the impaction process. Three drop heights, 130, 260, and 390 mm, were used for proximal impaction. *In-vitro* medial hoop strains and the number of impacts were recorded. A drop height of 260 mm was found to provide sufficient energy for impaction without introducing excessive strains to achieve implant stability. Furthermore, a feasibility study was performed on the use of a proximal impaction cap (PIC) to restrain extrusion of the graft during impaction. Although no significant difference in impaction strains or stem stability in uniaxial cylic loading was found by using a PIC, it is postulated that the design of a proximal impactor could be improved to assist with proximal stem alignment and graft containment.

Keywords: bone graft, impaction grafting, mechanical stability, revision hip replacement

1 INTRODUCTION

Impaction bone grafting with cement was first used for restoration of the acetabulum in protrusion secondary to arthrosis, rheumatoid arthritis, or trauma [**1**]. Gie *et al.* [**2**, **3**] subsequently modified this technique and applied it to femoral reconstruction by impacting morsellized cancellous bone graft (MCB) into the medullary canal. The principal objective of impaction grafting is to replace the bone stock loss and provide a mechanical and biological scaffold for bone formation. Thus, the ultimate goal is to provide a favourable biological environment for bone remodelling. This technique allows the insertion of a standard size femoral implant during revision total hip arthroplasty (THA). There has been scientific evidence of osteointegration showing that allograft chips have been replaced by viable bone after impaction grafting [**4–6**].

During the past decade, a number of authors have reported promising results [**2**, **4**, **6–12**], whereas numerous problems such as early subsidence and femoral fractures have also been reported [**13–15**]. Impaction grafting is a technically demanding surgical process and the outcome depends on both biological and mechanical issues. Heal *et al.* [**16**] summarized various papers which showed an incidence of 9 per cent (35 of 399) per-operative and 4 per cent (14 of 399) post-operative femoral fractures due to impaction grafting revision hip arthroplasties. Ornstein *et al.* [**14**] reported an incidence of 15 per cent (21 of 144) and 6 per cent (9 of 144) of per- and post-operative fractures respectively. Eldridge *et al.* [**17**] reported massive subsidence in nine cases of 71 (11 per cent) and Mikhail *et al.* [**18**] reported 18.6 per cent (8 of 43) of patients had subsidence

* *Corresponding author: Centre for Orthopaedic Biomechanics, Department of Mechanical Engineering, University of Bath, Bath, Avon, BA2 7AY, UK. email: S.Y.Mak@bath.ac.uk*

of 5–9 mm. Summarizing data given in a paper by Fetzer *et al.* [**19**], there was a 44 per cent incidence (140 of 316) of femoral component subsidence. However, it is important to note that the Exeter stem is designed to subside initially within the cement mantle, owing to the highly polished surface and the presence of a cavity within the distal centralizer. Studies have also shown that the amount of subsidence gradually decreases and the stem becomes more stable [**13, 20**]. Therefore, up to a few millimetres of subsidence of stem within the cement mantle is not an indication of failure or complications.

The stability of the implants can be influenced by the mechanical properties of the bone graft, the impaction technique, or the implant design. Various studies [**21–23**] have shown that the mechanical strength of the MCB can be improved by increasing the impaction energy. Higher stem stability was also found at higher impaction energies [**24, 25**]. However, a high impaction energy can lead to per-operative femoral fractures. An *in-vitro* experimental study [**26**] has shown that the medial side of the femur experiences higher strains than other locations on the femur during impaction grafting.

The aim of the present study was to investigate the strain distribution on the medial side of the femur during impaction grafting at different impaction energy levels. In addition, experiments were carried out to test whether the use of a proximal impaction cap to contain the graft during impaction could improve the implant stability during uniaxial cyclic testing.

2 METHODS

Bone graft harvested from porcine femoral heads was used. Studies have shown that porcine graft demonstrates similar mechanical properties to human allograft [**24, 27**]. During the preparation stage, soft tissue and articular cartilage were removed and a Norwich bone mill was employed to mill the femoral heads. The graft was inspected to ensure there were no cortical fragments. The graft was stored at $-25\,^{\circ}$C and defrosted thoroughly at room temperature for 2 h before use. Two third-generation Sawbones® composite femora (Pacific Research Laboratories, Inc.), which have identical dimensions and geometry, were used. Previous tests with these bone models have demonstrated good repeatability and reproducibility in biomechanical tests. The femoral head was cut and all the 'cancellous' bone was removed to replicate bone loss. A fixture was used to control the level of the cutting plane of the proximal femur. The distal end of the femur was cut at the level that the distal plug would be positioned per-operatively. This ensured that a similar amount of graft would be used and the behaviour of the graft would also be representative of the clinical situation. Four 1000 Ω open-faced strain gauges (Model N2A-06-S108N-10C, Vishay Measurements Group, UK) were mounted on the medial side of each of the femurs as shown in Fig. 1. The Sawbones® surface was degreased and dry abraded. Then, the surface was cleaned and the position was marked. The strain gauges were attached by M-bond 200 adhesive (Vishay Measurements Group, UK). The position was determined by having all four strain gauges equally spaced. All the strain gauges were aligned perpendicular to the long axis of the femur such that the hoop strain could be measured. The distal end of the femur was mounted in an aluminium container and fixed by potting with a low-melting-point alloy (Bend alloy, Lowden Metals Ltd, UK). The medial hoop strains were monitored and recorded continuously during testing with a personal computer using an analogue-to-digital interface card. In addition, the number of proximal impactions was recorded.

The Exeter IBG technique was used in conjunction with the Stryker X-change instrumentation [**2**]. The impactometer shown in Fig. 2, developed at the Centre for Orthopaedic Biomechanics at the University of Bath, which provides a known impaction energy and momentum, was used to standardize the impaction process [**24**]. The desired impaction energy can be achieved by altering the height of the drop weight (602 g). The distal impaction was broken down into three stages, using progressively larger distal impactors (14, 18, 20 mm respectively). A fixed

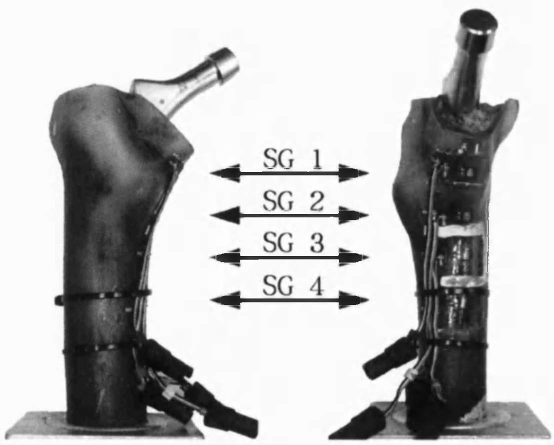

Fig. 1 Sawbones® femur with four strain gauges (SG 1–SG 4) positioned on the medial side to measure hoop strains

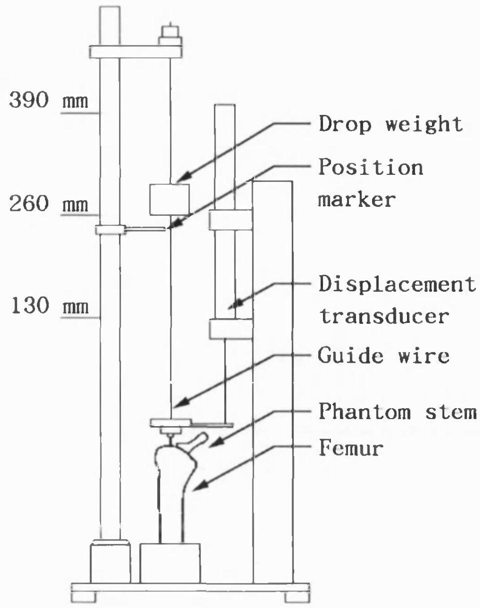

Fig. 2 Impactometer, designed to standardize the impaction grafting procedure

volume of 30 cm^3 porcine bone graft was added at each stage and impacted 4 times from a drop height of 260 mm. The graft volume was standardized by loosely packing it in a 30 cm^3 measuring cup. Proximal impaction was performed by impacting a phantom stem (size 3). Three drop heights were used to vary the proximal impaction energy: 130, 260, and 390 mm. A drop height of 260 mm, defined as the 'baseline level', produces an energy of 1.54 J and an impulse of 1.4 N s, which provides a similar amount of energy and momentum to that applied in the clinical scenario [**24**]. Drop heights of 130 and 390 mm represent 50 per cent lower and higher impaction energy than the baseline level, respectively. An experiment was stopped when the secondary positional indicator on the phantom stem reached the proximal cut face of the femur. The phantom stem at this stage was firmly impacted into the femur and could not be extracted by hand. Six tests (three using each femur) were performed for each of the drop heights. After each test all the graft material was cleared from the femur so that it could be re-used and the old graft material was discarded. Fresh porcine graft was used for each test.

In a second series of experiments, a proximal impaction cap (PIC) was used to contain the proximal area so as to prevent graft extruding during proximal impaction. The cap consisted of an aluminium rectangular-shaped plate with a central rectangular aperture to allow the phantom stem to pass through the cap during impaction; a dense foam gasket was bonded to the underside of the plate (Fig. 3). The same impaction technique was performed as in the previous experiments. The PIC was held in position with the index finger and the middle finger during the impaction process to ensure it was aligned properly. As one of the Sawbones® femurs was fractured during stem removal, only one femur was used for the PIC testing. (Previous results had shown that both composite femora gave similar results, therefore it was considered acceptable to use just one femur.) A drop height of 260 mm was used (i.e. baseline level). The femoral strains and the number of impacts were recorded. After impaction, the PIC was removed and the femur was mounted on an Instron 8511 servohydraulic materials testing machine. Stability tests were carried out by uniaxial cyclic compressive loading using an adaptor connected to the phantom stem (Fig. 4). Bone cement was not used as this test was simply to compare the effect of the PIC with regard to the impaction of the graft. Simplified uniaxial loading was likewise used to simplify this comparative test. The test

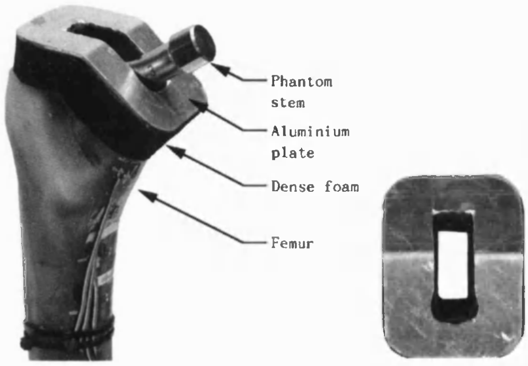

Fig. 3 Proximal impaction cap

Fig. 4 Uniaxial loading configuration

was split into block loadings of 3000 cycles at 2 Hz (sine cycle) in steps of 0.4 kN (i.e. 0–0.4 kN, 0–0.8 kN, 0–1.2 kN, ...) until the implant had subsided by 6 mm. Six tests were carried out without the use of the PIC, another six tests were carried with the use of the PIC.

3 RESULTS

3.1 Impaction energy

The total accumulated energy (= number of impacts × energy per impact) required fully to impact the phantom stem to the predetermined position decreased when the drop height increased from 130 mm to 260 mm and to 390 mm (Fig. 5). It was found that a drop height of 130 mm did not provide

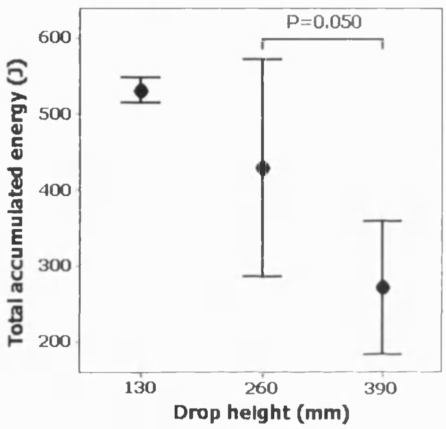

Fig. 5 Total accumulated energy required for proximal impaction at different drop heights. Mean and standard deviation ($n = 6$)

sufficient energy to impact the phantom stem into the final predetermined position. A test was therefore abandoned if subsidence was observed to have ceased after 700 impacts and the phantom stem had still not reached the final position. Drop heights of both 260 mm and 390 mm provided sufficient energy for graft consolidation to seat the stem in the final predetermined position. An unpaired two-sample t-test was performed to compare the effect of two different drop heights (i.e. 260 mm and 390 mm) on the total required energy. A drop height of 390 mm required 37 per cent less mean total accumulated energy than one of 260 mm. Increasing the drop height showed a significant reduction in the required total accumulated energy ($P = 0.050$) (Fig. 5).

During proximal impaction, as expected, the strain in the femur increased progressively as the stem migrated distally (see Fig. 6). It was found that stress relaxation occurred immediately after an impact. Therefore, the maximum strain was defined as the highest strain measured at the time the drop weight impacted. Strain gauge (SG) 1 demonstrated the lowest strain; SG 3 demonstrated the highest strain. An Anderson–Darling normality test was performed (Minitab 14.20, Minitab Inc.) for all four strain gauges at all three drop heights. Statistical results showed that the maximum value of all strain gauges demonstrated normal behaviour ($P > 0.050$). As a drop height of 130 mm was not sufficient to provide the required graft consolidation, an unpaired two-sample t-test was performed on strains associated with drop heights of 260 mm and 390 mm. No statistical difference was found between two different drop heights, as shown in Fig. 7 ($P > 0.050$ for all strain gauge locations).

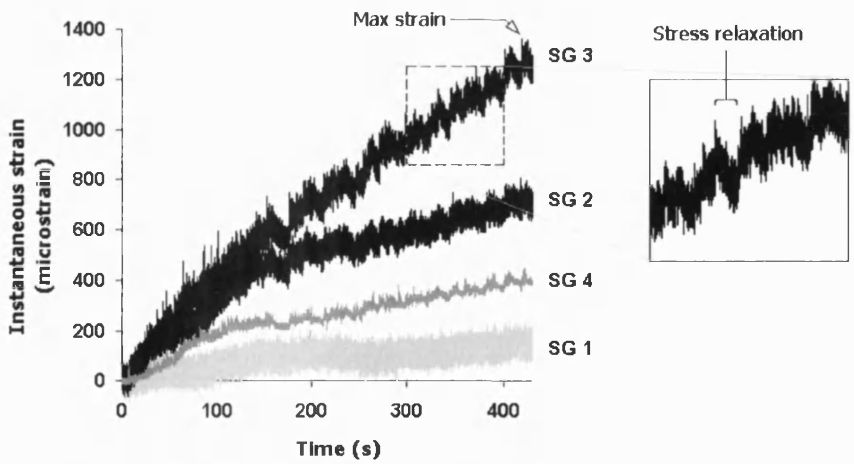

Fig. 6 Typical experimental result showing a progressive increase in strain during proximal impaction. Maximum strain was defined as the highest strain measured before stress relaxation occurred

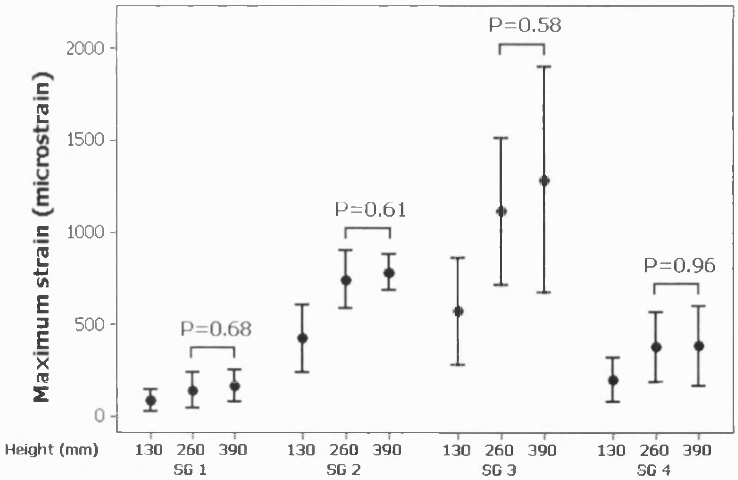

Fig. 7 Maximum strain against different drop heights and the position of the strain gauges. Mean and standard deviation ($n = 6$)

3.2 Use of the PIC

It was observed that, during proximal impaction, graft extruded from the proximal opening of the femoral canal. This led to the development of a PIC.

As with the previous testing, an Anderson–Darling normality test was performed for all four strain gauges with and without the PIC. Statistical results showed that the maximum value of all strain gauges demonstrated normal behaviour ($P > 0.050$). The effects of the PIC on the maximum strain, the number of cycles, and the maximum load were analysed using an unpaired two-sample t-test. Using the PIC resulted in no significant difference in the maximum strain at any gauge location ($P > 0.050$) (Fig. 8), or the stability, measured by means of the number of loading cycles ($P = 0.37$) (Fig. 9(a)) and the maximum carried load ($P = 0.49$) (Fig. 9(b)).

4 DISCUSSION

4.1 Effect of impaction energy

No statistical difference was found as regards the effect of a higher drop height on the maximum strains. Strain increased as the phantom stem moved distally, which was due to the double-tapered design of the Exeter stem. Less total accumulated energy was required to consolidate the graft with the phantom stem when using a higher drop height. A drop height of 390 mm required 37 per cent less total energy than a drop height of 260 mm. Using a drop height of 260 mm and 390 mm provided sufficient impaction energy to drive the phantom stem into the final position.

A drop height of 130 mm was not sufficient to impact the phantom stem distally. Towards the latter

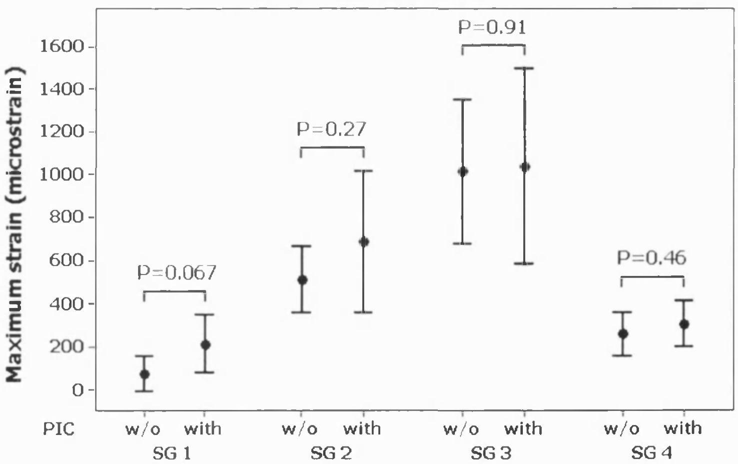

Fig. 8 Maximum strain against the effect of the use of a PIC. Mean and standard deviation ($n = 6$)

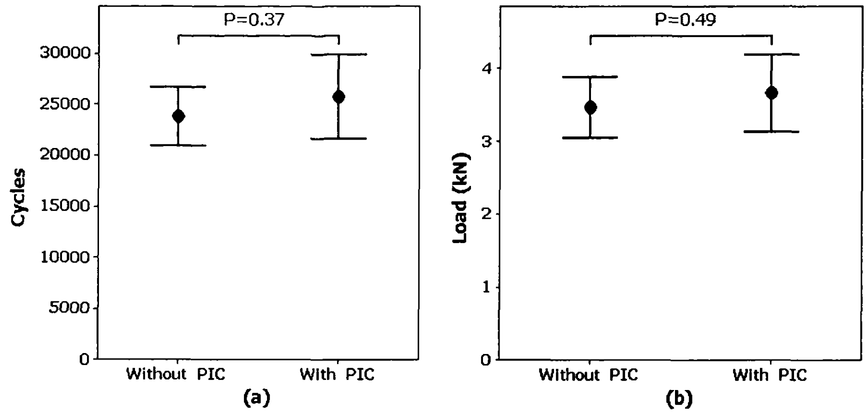

Fig. 9 Number of cycles to failure (a), and the maximum load capacity (b), with and without the use of a PIC. Mean and standard deviation ($n = 6$)

stages of proximal impaction, the reaction forces between the phantom stem and the bone graft increased because of the double-tapered design. A drop height of 130 mm was not able to provide sufficient energy to seat the stem fully.

4.2 Effect of the use of a PIC

The use of a PIC showed no statistical difference on the strain at any of the strain gauge locations. During proximal impaction, improved graft consolidation was observed at the top of the femur as the cap effectively closed the proximal femoral canal, preventing graft extrusion. The PIC formed a close constrained structure and may provide a better medium for energy transfer. When the PIC was not used, it was observed that the graft around the proximal area was more loosely packed in comparison with the experiments where the PIC was employed. Although statistical analysis shows no difference in graft stability with the use of the PIC, it is possible that, with design modifications, the PIC could improve both the stability and maximum load-carrying capability.

In addition, the PIC helped to prevent rotational misalignment during proximal impaction. The prototype used was made from dense foam, reinforced by a thin aluminium plate. The drawback of this was that it was difficult to observe the three positional dots on the side of the phantom stem. In a clinical environment, a disposable transparent PIC, available in different sizes, would be ideal to accommodate different stem sizes and patients, and to provide improved graft visibility. Further work on the design of the PIC in terms of geometry and materials may result in an improvement to the proximal impaction process.

5 CONCLUSION

The emphasis of this experiment was on the measurement of hoop strain along the medial side of the femur at different impaction energy levels. A drop height of 260 mm provides an energy of 1.54 J and a momentum of 1.4 N s. Although a drop height of 390 mm reduces the impaction time and requires 37 per cent less total accumulated energy compared with a drop height of 260 mm, no significant difference was found on the maximum values of the strain gauges. A drop height of 130 mm did not produce sufficient energy to drive the phantom stem into the final predetermined position. A PIC helps to prevent graft extrusion during the proximal impaction stage and also provided a close constrained structure so that the impaction energy could be more efficiently deployed to consolidate the graft in the proximal area. Further work on optimizing the impaction energy level and additional development of the proximal impaction cap may contribute to improving clinical outcomes in revision impaction grafting of the femur.

REFERENCES

1 **Slooff, T. J., Huiskes, R., Van Horn, J.,** and **Lemmens, A. J.** Bone grafting in total hip replacement for acetabular protrusion. *Acta Orthop. Scand.*, 1984, **55**(6), 593–596.

2 **Gie, G. A., Linder, L., Ling, R. S., Simon, J. P., Slooff, T. J.,** and **Timperley, A. J.** Impacted cancellous allografts and cement for revision total hip arthroplasty. *J. Bone Jt Surg. Br.*, 1993, **75**(1), 14–21.

3 **Gie, G. A., Linder, L., Ling, R. S., Simon, J. P., Slooff, T. J.,** and **Timperley, A. J.** Contained morselized

allograft in revision total hip arthroplasty. Surgical technique. *Orthop. Clin. N. Am.*, 1993, **24**(4), 717–725.
4 **Ling, R. S., Timperley, A. J.,** and **Linder, L.** Histology of cancellous impaction grafting in the femur. A case report. *J. Bone Jt Surg. Br.*, 1993, **75**(5), 693–696.
5 **Linder, L.** Cancellous impaction grafting in the human femur: histological and radiographic observations in 6 autopsy femurs and 8 biopsies. *Acta Orthop. Scand.*, 2000, **71**(6), 543–552.
6 **Lind, M., Krarup, N., Mikkelsen, S.,** and **Horlyck, E.** Exchange impaction allografting for femoral revision hip arthroplasty: results in 87 cases after 3.6 years' follow-up. *J. Arthroplasty*, 2002, **17**(2), 158–164.
7 **Ornstein, E., Franzén, H., Johnsson, R., Karlsson, M., Linder, L.,** and **Sundberg, M.** Hip revision using the Exeter stem, impacted morselized allograft bone and cement. *Acta Orthop. Scand.*, 2004, **75**(5), 533–543.
8 **Van Doorn, W. J., Ten Have, B. L., Van Biezen, F. C., Hop, W. C., Ginai, A. Z.,** and **Verhaar, J. A.** Migration of the femoral stem after impaction bone grafting. First results of an ongoing, randomised study of the Exeter and Elite Plus femoral stems using radiostereometric analysis. *J. Bone Jt Surg. Br.*, 2002, **84**(6), 825–831.
9 **Stulberg, S. D.** Impaction grafting: doing it right. *J. Arthroplasty*, 2002, **17**(4, Suppl. 1), 147–152.
10 **Williams, H. D., Browne, G., Gie, G. A., Ling, R. S., Timperley, A. J.,** and **Wendover, N. A.** The Exeter universal cemented femoral component at 8 to 12 years. A study of the first 325 hips. *J. Bone Jt Surg. Br.*, 2002, **84**(3), 324–334.
11 **Edwards, S. A., Pandit, H. G., Grover, M. L.,** and **Clarke, H. J.** Impaction bone grafting in revision hip surgery. *J. Arthroplasty*, 2003, **18**(7), 852–859.
12 **Boldt, J. G., Dilawari, P., Agarwal, S.,** and **Drabu, K. J.** Revision total hip arthroplasty using impaction bone grafting with cemented nonpolished stems and charnley cups. *J. Arthroplasty*, 2001, **16**(8), 943–952.
13 **Ornstein, E.** Hip revisions with impacted morselized allograft bone and cement. Patient outcome, prosthetic fixation and risks. *Acta Orthop. Scand. Suppl.*, 2002, **73**(306), 1–66.
14 **Ornstein, E., Atroshi, I., Franzén, H., Johnsson, R., Sandquist, P.,** and **Sundberg, M.** Early complications after one hundred and forty-four consecutive hip revisions with impacted morselized allograft bone and cement. *J. Bone Jt Surg. Am.*, 2002, **84**(8), 1323–1328.
15 **Van Doorn, W. J., Van Biezen, F. C., Prendergast, P. J.,** and **Verhaar, J. A.** Fracture of an Exeter stem 3 years after impaction allografting – a case report. *Acta Orthop. Scand.*, 2002, **73**(1), 111–113.
16 **Heal, J. S., Blom, A. W., Miles, A. W.,** and **Learmonth, I. D.** Morselized impaction bone grafting. A review article. *Orthop. Update (India)*, 2001, **11**(3), 28–35.
17 **Eldridge, J. D., Smith, E. J., Hubble, M. J., Whitehouse, S. L.,** and **Learmonth, I. D.** Massive early subsidence following femoral impaction grafting. *J. Arthroplasty*, 1997, **12**(5), 535–540.
18 **Mikhail, W. E., Wretenberg, P. F., Weidenhielm, L. R.,** and **Mikhail, M. N.** Complex cemented revision using polished stem and morselized allograft. *Arch. Orthop. Trauma Surg.*, 1999, **119**(5–6), 288–291.
19 **Fetzer, G. B., Callaghan, J. J., Templeton, J. E., Goetz, D. D., Sullivan, P. M.,** and **Johnston, R. C.** Impaction allografting with cement for extensive femoral bone loss in revision hip surgery. *J. Arthroplasty*, 2001, **16**(8, Suppl. 1), 195–202.
20 **Ornstein, E., Franzén, H., Johnsson, R., Stefánsdóttir, A., Sundberg, M.,** and **Tägil, M.** Hip revision with impacted morselized allografts: unrestricted weight-bearing and restricted weight-bearing have similar effect on migration. A radiostereometry analysis. *Arch. Orthop. Trauma Surg.*, 2003, **123**(6), 261–267.
21 **Brewster, N. T., Gillespie, W. J., Howie, C. R., Madabhushi, S. P., Usmani, A. S.,** and **Fairbairn, D. R.** Mechanical considerations in impaction bone grafting. *J. Bone Jt Surg. Br.*, 1999, **81**(1), 118–124.
22 **Bavadekar, A., Cornu, O., Godts, B., Delloye, C., Van Tomme, J.,** and **Banse, X.** Stiffness and compactness of morselized grafts during impaction: an *in vitro* study with human femoral heads. *Acta Orthop. Scand.*, 2001, **72**(5), 470–476.
23 **Fosse, L., Rønningen, H., Lund-Larsen, J., Benum, P.,** and **Grande, L.** Impacted bone stiffness measured during construction of morsellised bone samples. *J. Biomechanics*, 2004, **37**(11), 1757–1766.
24 **Grimm, B.** *Mechanical properties of morsellised bone graft and synthetic graft extenders for impaction grafting.* PhD Thesis, Department of Mechanical Engineering, University of Bath, UK, 2003.
25 **Grimm, B., Blom, A. W., Miles, A. W.,** and **Turner, I. G.** *In-vitro* endurance testing of bone graft materials for impaction grafting. *Bioceramics 14 Key Engng Mater.*, 2002, **218-2**, 375–378.
26 **Farooq, M. A., Clements, J. P.,** and **Miles, A. W.** *In-vitro* monitoring of hoop strains during impaction grafting of femur. *Hip Int.*, 2006, **16**(3), 223–231.
27 **Datta, A., Gheduzzi, S.,** and **Miles, A. W.** A comparison of the viscoelastic properties of bone grafts. *Clin. Biomech.*, 2006, **21**(7), 761–766.

THE EFFECT OF REPETITIVE CYCLIC LOADING ON THE RELAXATION OF MORSELLISED BONE GRAFT

Mak, Siu Yan[1]; Katsimihas, Mike[2]; Miles, Anthony W[1]
1. Centre for Orthopaedic Biomechanics, University of Bath, UK. 2. Royal United Hospital, Bath NHS Trust, United Kingdom
S.Y.Mak@bath.ac.uk

Introduction: Morsellised bone graft (MCB) is widely used in revision hip surgery to replace bone stock loss associated with aseptic loosening in primary hip replacement. The initial implant stability is essential for incorporation and osteointegration of the graft material. Graft relaxation is one of the important parameters which contributes to the structural properties of the MCB after impaction grafting. Creep and relaxation tests are the standard methods for testing viscoelastic materials (i.e. time-dependent properties). Various studies have [1-5] addressed quantifying, graft properties but the viscoelastic properties are still poorly understood. In terms of the clinical situation, graft relaxation properties could have an influence on the incidence of per and post-operative femoral fractures. A low graft relaxation value may result in a significant amount of residual strain in the graft. The aim of this study was to evaluate the relaxation properties of MCB under different impaction frequencies.

Materials and Methods: Porcine graft was used as it presents similar mechanical properties to human graft [3,5]. Porcine femoral heads were cleared of soft tissue and articular cartilage using a scalpel and a Norwich bone mill was employed to mill the femoral heads. The graft was inspected to ensure there were no cortical fragments. Graft was then stored at -25°C and defrosted thoroughly at room temperature for at least two hours before use. A fixed volume of 10 cm^3 of MCB was employed in this study. Two sets of graft material were used: normal and defatted. Defatted graft was prepared by soaking the graft in water at 35°C for 20 mins.

The MCB was then inserted carefully into a die for compression. The die has an internal and external diameter of 20.0 mm and 44.0 mm respectively (i.e. thick cylinder). The plunger diameter was selected to provide a tight sliding fit. A porous disc placed at the base of the die allowed fluid escape (Fig 1).

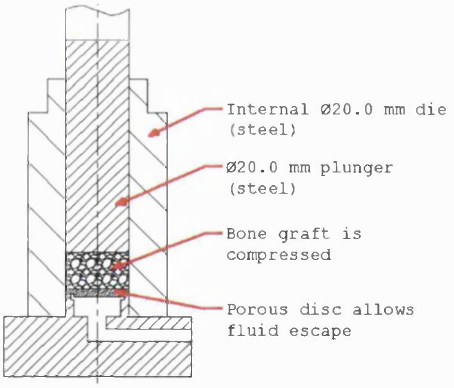

Fig 1: Die plunger test rig.

All the specimens (n=10) were first pre-loaded to 100 N at a stroke speed 0.5 mm/s. Four different loading frequency regimes were used: static, 0.17 Hz, 1 Hz and 2 Hz at a force of 1 kN using a haversine load cycle for 60 seconds. The graft was then left for 120 seconds and the amount of relaxation was measured. Relaxation is defined as the amount of residual force remaining after impaction with the plunger left in place; this was carried out by measuring the change in force at a constant strain. The loading history axial force vs. displacement was also recorded. Pure static compression was used to replicate the situation when the stem is impacted by a single stroke. Regression analysis was used for prediction of trends (Minitab 14.20).

Results: A typical load history of force and displacement is shown in Fig 2 (left). The force and displacement were then converted into a stress-strain curve as shown in Fig 2 (right). During loading the stress increased exponentially with strain, the material became stiffer. The stress-strain curve demonstrated a series of local minimum points after each loading cycle. This was associated with the relaxation in the graft during the unloading stroke.

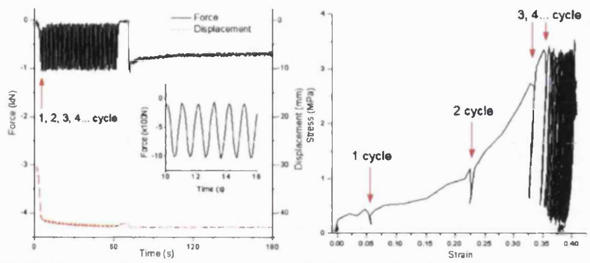

Fig 2: Typical force/displacement against time (Loading frequency 1 Hz) (left), and associated stress-strain characteristic (right).

Fig 3 depicts the relaxation behaviour of the non-defatted and defatted graft. It can be seen that static compression gave the lowest relaxation values (~15%). When the frequency increased, the amount of relaxation increased and it appeared that there was a peak value (~25%) at 1 Hz. A quadratic curve fit was used showing that there was a non-linear relationship between the relaxation and the frequency. Similar trends were observed with both forms of graft material. When the impaction frequency increased there was less time for the fluid within the graft to escape and this probably accounted for the higher relaxation that was observed. As the frequency increased further, the relaxation decreased and this was probably due to a higher packing density in the graft resulting in fluid being trapped within the compacted graft.

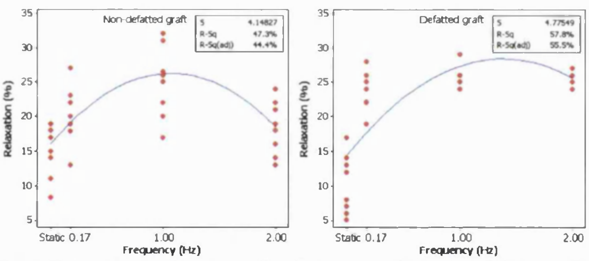

Fig 3: Relaxation against impaction frequency with quadratic fit (n=10).

Discussion: MCB shows non-linear characteristics in both the stress-strain behaviour and the relaxation-frequency relationship. Strain energy is absorbed by the MCB during impaction and there is a non-recoverable deformation. The material becomes stiffer and denser with increasing impaction frequency. An optimised frequency is required to find the best compromise between the risk of per and post-operative femoral fractures and the amount of graft consolidation to achieve stability.

References: [1] Jäger *et al.*, J Biomech 2005;38(7):1451-1458. [2] Giesen *et al.*, J Bone Joint Surg [Br] 1999;81-B(6):1052-1057. [3] Datta *et al.*, Clin Biomech 2006;21(7):761-766. [4] Verdonschot *et al.*, J Biomed Mater Res 2001;58(5):599-604. [5] Grimm, PhD dissertation, University of Bath, UK 2003.

ELASTIC MODULUS AND STRESS-STRAIN CHARACTERISTICS OF MORSELLISED BONE GRAFT UNDER DIFFERENT LOADING CONDITIONS

Mak, Siu Yan[1]; Cunningham, James L[1]; Miles, Anthony W[1]
1. Centre for Orthopaedic Biomechanics, University of Bath, UK
S.Y.Mak@bath.ac.uk

Introduction: Impaction bone grafting is widely employed in revision surgery to compensate for bone stock loss after failed primary hip replacement. It is performed by impacting allograft bone chips from morsellised cancellous bone (MCB) obtained from human femoral heads into the medullary canal. A femoral stem is then cemented into the impacted neo-medullary cavity. The stability of the stem is highly dependent on the stiffness of the impacted graft material. High graft stiffness provides good stability against stem subsidence. However, achieving a high stiffness can contribute to intra-operative femoral fractures. A wide range of apparent graft stiffnesses (8.0–100 MPa) have been found in investigations [1-5]. The aim of this study was to evaluate the stress-strain behaviour of MCB and to qualify the graft stiffness in a systematic way. A die-plunger was employed in the study and three different parameters were investigated: graft defatting, loading rate and graft pre-loading.

Materials and Methods: Porcine graft obtained from femoral heads was used as it presents similar mechanical properties to human graft [6]. Soft tissue and articular cartilage were removed with a scalpel and a Norwich bone mill was employed to mill the femoral heads. No particular attention was paid to the shape and the graft distribution. Graft was inspected to ensure that there were no cortical fragments. The graft was stored at -25°C and defrosted thoroughly at room temperature for two hours before use. A fixed volume of 10 cm^3 of MCB was used. The MCB was then inserted carefully into the aluminium die for compression. The die has internal diameter of 19.0 mm. The plunger has a diameter of 18.5 mm which provides clearance for fluid escape (e.g. blood and fat). The graft was then compressed to a thickness of 12 mm and the loading history axial force vs. displacement was recorded.

Three parameters were used to characterise the graft as shown in (Table 1). Defatted graft samples were prepared by soaking the graft in water at 35°C for 20 mins. Pre-loading was performed by loading the graft with 250 N. Two different loading rates (7.5 mm/s and 60 mm/s) were used to determine the time dependent properties.

Parameter	Low (–)	High (+)
Fat content	Non-defatted	Defatted
Pre-loading	Non pre-loaded	Pre-loaded with 250 N
Ramp speed	7.5 mm/s	60 mm/s

Table 1: Three major parameters used.

Result: Fig 1 illustrates the stress-stain behaviour of the two sets of graft materials. As can be seen, the graft without pre-loading gave a typical non-linear material characteristic including the presence of a toe region. On the other hand, graft pre-loaded to 250 N gave a low initial strain since the graft was partially compressed. Higher stresses and stiffnesses were observed at the higher loading rates for both sets of graft samples (Fig 1). Relaxation was inhibited at the higher loading rates since the fluid components including fat, blood and water stored in the interstices of the graft had no time to escape. The graft particles also had no time to re-orientate into the most optimised position at the higher loading rates. As a consequence the graft appeared to be stiffer.

Two types of stiffnesses are defined as described by Fosse *et al.* [5]: the consolidated constrained modulus of elasticity (CCME), and the total constrained modulus of elasticity (TCME). CCME is defined by the incremental change of stiffness of graft in steps of (5%, 10%, 20%...100%) of the 'actual' deformation, whereas TCME is defined by the overall apparent stiffness of graft. CCME provides a better representation of the instantaneous stiffness of the graft. This allows a better predication of the actual force that might be transferred to the femur during impaction grafting. By contrast, TCME provides a simplified model of the stiffness of the graft.

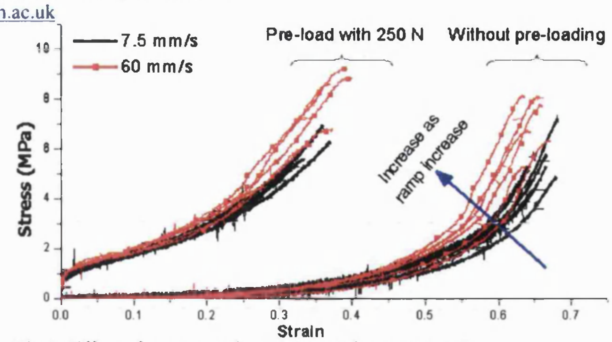

Fig 1: Effect of ramp speed on stress-strain curve (n=6).

It was found that graft without pre-loading demonstrated an exponential increase in stiffness and the CCME was always higher than TCME (Fig 2, left). When the graft was pre-loaded with 250 N, the graft appeared to be stiffer as the toe-region of the stress-strain graft was absent. It is important to note that graft pre-loaded with 250 N has a higher initial stiffness (Fig 2, right). These findings can be explained by assuming that there was a relatively high static force between graft particles.

In addition, numerical studies have shown that mechanical properties of MCB (e.g. modulus of elasticity) increased after washing (defatting) [3,7-9]. A similar finding was also observed in this study.

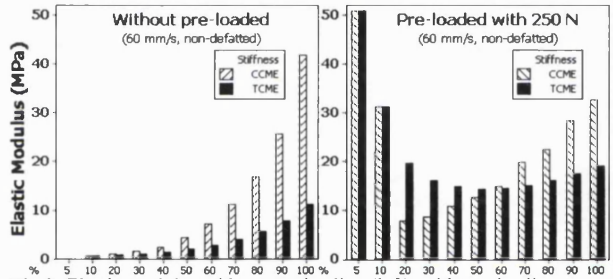

Fig 2: Elastic modulus without pre-loading (left), with pre-loading (right).

Discussion: This study provided a systematic method of establishing the equivalent elastic modulus of graft materials and demonstrated the dependence of graft preparation and loading conditions on graft stiffness. Of the two graft stiffness parameters examined, CCME is more suitable for the prediction of the instantaneous force acting on the femur during impaction whilst TCME provides a simple representation of the apparent graft stiffness for comparison purposes.

References: [1] Heiner *et al.*, J Biomech 2005;38(4):811-818. [2] Bolder *et al.*, Acta Orthop Scand 2003;74(6):652-657. [3] Voor *et al.*, J Biomech 2000;33(12):1683-1688. [4] Bavadekar *et al.*, Acta Orthop Scand 2001;72(5):470-476. [5] Fosse *et al.*, J Biomech 2004;37(11):1757-1766. [6] Grimm, PhD dissertation, University of Bath, UK 2003. [7] Dunlop *et al.*, J Bone Joint Surg [Am] 2003;85-A(4):639-646. [8] Voor *et al.*, J Biomech 2004;37(8):1233-1239. [9] Brodt *et al.*, J Orthop Res 1998;16(1):43-49.

THE EFFECT ON RATE OF IMPACTION ON MORSELLISED BONE GRAFT

Mak, Siu Yan[1]; Cunningham, James L[1]; Miles, Anthony W[1]

1. Centre for Orthopaedic Biomechanics, University of Bath, UK

S.Y.Mak@bath.ac.uk

Introduction:
Impaction bone grafting is widely used for revision hip replacement. It involves impaction of morsellised cancellous bone graft into the femur to form a neo-medullary canal. It is carried by impacting with a proximal phantom impactor. Per-operative femoral fracture is one of the concerns in impaction grafting [1]. One of the parameters that can be used to determine the possibility of fracturing the femur is the amount of stress exerted on the femur. Various authors have [1-6] studied the viscoelastic properties of bone graft. However, no study has attempted to understand the effects on the stress and the amount of recoil in the graft at different impaction rates. In terms of the clinical situation, high stresses should be avoided to minimise the risk of per-operative femoral fracture however good consolidation of the graft is also essential for stable fixation. High graft recoil should also be avoided as the shape of the neo-medullary canal depends on the amount of graft deformation when the proximal phantom impactor is removed. The aim of this study was to evaluate the stress and the recoil of MCB under different impaction rates.

Materials and Methods: Porcine graft was employed in this study as it has similar mechanical properties to human graft [2,3]. Porcine femoral heads were cleared of soft tissue and articular cartilage with a scalpel and a Norwich bone mill was used to mill the femoral heads. The graft was inspected to ensure there were no cortical fragments. The graft was then stored at -25°C and defrosted thoroughly at room temperature for two hours before use. A fixed volume of 10 cm^3 of graft was employed in this study.

The MCB was then inserted carefully into a die for compression. The die has an internal and external diameter of 20.0 mm and 44.0 mm respectively (i.e. a thick cylinder). The plunger has a diameter of 20.0 mm and was a close sliding fit in the die. A porous disc is placed at the base of the die to allow fluid escape (Fig 1).

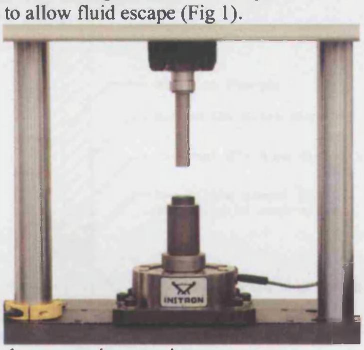

Fig 1: Uni-axial compressive test rig.

A uni-axial compressive test was then carried out. Seven different rates of impaction were used (5, 10, 20, 30, 40, 50 and 60 mm/s). Ten experiments were performed on each of the settings (i.e. n=10). The graft was then compressed to a thickness of 8 mm. After compression, the graft was left in the die for 120 seconds to allow for stress relaxation. The graft was then extracted and the thickness was measured immediately using a vernier calliper. During the experiment, the loading history of the axial force vs. displacement was also monitored and recorded. This allowed analysis of the stress applied to the graft at different stages during impaction. Recoil is defined as the percentage change of strain in comparison to the final thickness. The strain was calculated by [(Measured thickness - compressed thickness) / (compressed thickness) x 100%].

Results: The maximum mean forces generated ranged from 5.3 kN (equivalent to 16.9 MPa) to 8.6 kN (equivalent to 27.3 MPa) at 5 mm/s and 60 mm/s respectively. This was equivalent to about 7 to 11 times body weight (Body weight=750 N). The measured forces were then transformed into stresses as shown in Fig 2 (left). As can be seen, the amount of the maximum stress increased with the rate of impaction. Statistic software package (Minitab 14.20) was used to perform statistical analysis. It was shown that there was significant difference (Student's t-test, P=0.00) between loading rates of 5 mm/s and 60 mm/s on the amount of stress.

Fig 2 (right) depicts the amount of graft recoil after 120 seconds of stress relaxation. It was found that the amount of graft recoil was about 45% and was independent of the rate of the impaction. Statistical test (Student's t-test) also showed that there was no significant difference (P=0.28) between impaction rates of 5 mm/s and 60 mm/s.

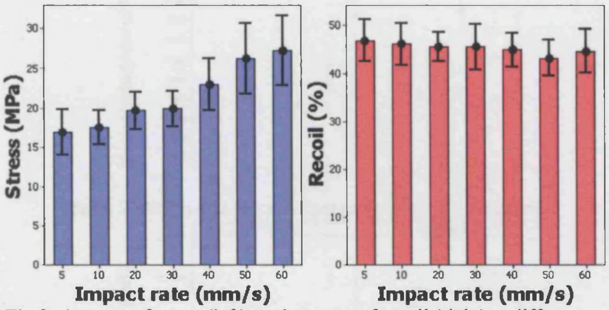

Fig 2: Amount of stress (left), and amount of recoil (right) at different impaction rates (Mean and one standard deviation).

Discussion: Since morsellised bone graft is a viscoelastic material [2], the blood, fat and marrow contribute the viscous components whilst the bone matrix demonstrates the elastic component of the graft. As a result, bone graft is a time dependent material. The viscoelastic properties are also affected by the rate of fluid escape. A lower impaction rate gives the graft more time for the blood and marrow to penetrate the porous graft matrix. Therefore, the higher the impaction rate, the higher the resulting measured stress. A high level of compression was employed so that the viscoelastic properties could be fully evaluated. In the clinical situation, high impaction energy is required for fully impacting the stem into desired position [7]. This could potentially be accomplished by lower impaction rate, high energy (e.g. using a larger drop mass and lower dropping height).

The amount of recoil is a measure of the deformation of the graft. It provides an indication of the deformation of the shape of the neo-medullary canal when the phantom stem is removed. As the thickness of the graft is not uniform in the neo-medullary canal, a high level of recoil could lead to misalignment of the implant during stem insertion. A lower amount of recoil is always desired. However, this was proven to be independent to the rate of impaction.

References:
[1] Heal *et al.*, Orthopaedic Update (India) 2001;11(3):28-35. [2] Datta *et al.*, Clin Biomech 2006;21(7):761-766. [3] Grimm, PhD dissertation, Uni. of Bath, UK 2003. [4] Giesen *et al.*, J Bone Joint Surg [Br] 1999;81-B(6):1052-1057. [5] Jäger *et al.*, J Biomech 2005;38(7):1451-1458. [6] Verdonschot *et al.*, J Biomed Mater Res 2001;58(5):599-604. [7] Mak *et al.*, Proc Inst Mech Eng [H] 2007:In-Press.

DETERMINIATION OF POISSON'S RATIO AND HOOP STRAIN OF MORSELLISED BONE GRAFT UNDER UNI-AXIAL COMPRESSIVE LOADING

+*Mak, S Y; *Cunningham, J L; *Miles, A W
+*Centre for Orthopaedic Biomechanics, University of Bath, UK
S.Y.Mak@bath.ac.uk

INTRODUCTION:

Although impaction bone grafting (IBG) with the use of bone graft and cement has been used for over ten years, per and post operative femoral fractures and stem subsidence are still major complications in IBG. Heal *et al.* [1] summarised various reports reviewing 35 per-operative and 14 post-operative femoral fractures occurring in a total of 399 revision hip arthroplasties. Ornstein *et al.* [2] reported an incidence of 15% (21 of 144) and 6% (9 of 144) of per- and post-operative fractures. Thus per-operative fractures occur more commonly than post-operative fractures. The initial stability is achieved by consolidation of graft material and initial graft compaction per-operatively. Preventing per-operative fractures is an important criterion during IBG. The aim of this study was to investigate the influence of axial force, hoop strain, Poisson's ratio and recoil existing in the femur using a simple experimental model.

MATERIALS AND METHODS:

Porcine graft was used as it presents similar mechanical properties to human graft [3]. Porcine femoral heads were used, soft tissue and articular cartilage were removed by a scalpel and a Norwich bone mill was employed to mill the femoral heads. The graft was inspected to ensure there were no cortical fragments. The graft was then stored at −25°C and defrosted thoroughly at room temperature for two hours before use. A fixed volume of 10 cc of graft was employed in this study.

A die-plunger test was employed for uni-axial compression testing (Figure 1). Two strain gauges were mounted on a thin walled aluminium die. The ratio of internal diameter and wall thickness of the die was 19 so that hoop strain could be estimated by thin wall cylinder theory. A clearance of 0.5 mm between the plunger and die was used for fluid escape (e.g. blood and fat).

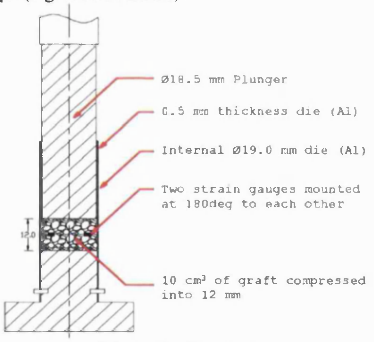

Figure 1 : Rig design.

Two sets of graft material were used: normal and defatted. Defatted graft was prepared by soaking the graft in water at 35°C for 20 mins. Pre-conditioning was preformed by pre-loading the graft to 250 N. Two different loading rates (7.5 mm/s and 60 mm/s) were used to demonstrate the time dependent properties. A fixed volume of 10 cc of MCB was then compressed to a thickness of 12 mm in the die. The experimental design employed a 2-level, 3-factor factorial design (n = 6). This Design of Experiment (DoE) was employed to evaluate the most significant factor(s) ($\alpha = 0.05$) and interaction between parameters (Minitab 14.20). A Pareto analysis was also performed.

RESULTS AND DISCUSSION:

The mean hoop strains measured are depicted in the interval plots in Figure 2. The loading rate, followed by defatting, contributed the most significant influence on hoop strains. The effect of pre-loading of graft showed no statistical significance (Table 1). Therefore, although a high impact energy and momentum could increase the risk of intra-operative femoral fractures; pre-loading of graft with a higher static force may not contribute to minimising the risk of femoral fracture.

The Poisson's ratio, shown in Figure 3, is defined as the ratio of the hoop and axial strain. In this study, the total constrained Poisson's ratio (TCPR) was used and measured by the change of strain between the initial position at pre-loading and after loading. It was found that both pre-loading and the loading rate showed statistically significant differences in the results. Establishing the Poisson's ratio can thus allow an estimation of the shear modulus, as the stiffness of the graft can be measured by compressive testing,

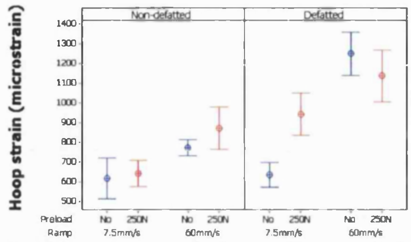

Figure 2 : Mean and one standard error of hoop strain (n=6).

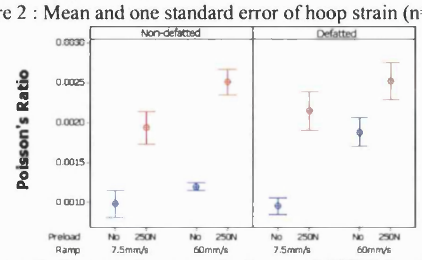

Figure 3 : Mean and one standard error of TCPR (n=6).

The amount of graft recoil was also measured by a vernier caliper and was defined by the change of volume after impaction when the plunger was removed. Graft recoil of approximately 40% was found. However, there were no significant factors related to graft recoil. The recoil was found to be only dependent on the final positions of the plunger, but independent to the impaction methods. Dunlop *et al.* [4] proposed that the defatted graft has exactly the same particle-size distribution as it does in the pre-washed state. Therefore, the shape of neo-medullary canal changes depended on the volume of the graft and the final stem position only. A lower amount of recoil is desirable as the shape of the neo-medullary canal changes immediately when the proximal impactor is removed. Overall, the general observation was that: the TCPR, hoop strain and axial force increased when the graft was defatted. However, the values of the standard error were similar and this suggested that the repeatability did not improve when defatted graft was used.

	Effect(s)							
Target	A	B	C	AB	BC	AC	ABC	Interaction
Poisson's	×	+	+	×	×	×	×	None
Hoop strain	+	×	+	×	×	×	×	B – C
Axial force	+	×	+	×	×	×	×	B – C
Recoil	×	×	×	×	×	×	×	A – C

Table 1: A = Defatting, B = Pre-loading, C = Ramp. Pareto analysis ($\alpha = 0.05$) shows the relationship and interactions between targets and effects, '+' statistical significance, '×' not statistical significance.

CONCLUSIONS:

High loading rates and graft defatting can significantly increase both hoop and axial force. The TCPR provides the concept of graft volume change during axial movement and allows an estimation of the shear modulus, in which the stiffness can be found by uni-axial testing. The amount of recoil is only dependent on the amount of graft and final plunger position, but independent on the impaction methods.

REFERENCES:

[1] Heal JS *et al.*, Orthopaedic Update [India] 2001;11(3):28–35.
[2] Ornstein E *et al.*, J Bone Joint Surg [Am] 2002;84-A(8):1323–1328.
[3] Grimm B, PhD dissertation, University of Bath, UK 2003.
[4] Dunlop DG *et al.*, J Bone Joint Surg [Am] 2003;85-A(4):639–646.

IN-VITRO STUDY OF INFLUENCE OF IMPACTION ENERGY ON MEDIAL STRAIN DISTRIBUTION IN THE FEMUR DURING IMPACTION BONE GRAFTING

+*Mak, S Y; *Holsgrove, T P; *Miles, A W

+*Centre for Orthopaedic Biomechanics, University of Bath, UK

S.Y.Mak@bath.ac.uk

INTRODUCTION:

Impaction bone grafting (IBG) using morsellised bone graft and cement has been used for over ten years, per and post operative femoral fractures are however still major complications. Per-operative femoral fracture is one of the common problems during reconstruction of the medullary canal and occurs in 12% of revision hip operations [1]. During impaction, a large amount of energy is delivered to the bone graft and is transmitted to the surrounding structures. This is essential to deliver sufficient impaction energy to consolidate the bone graft since the initial stability is vital for osteointegration.

The primary objective of this study was to establish the levels of strain occurring on the medial side of the femur during IBG under different impaction energy. The secondary objective was to investigate the feasibility of using low-force, high-frequency impaction to achieve the same level of bone graft consolidation.

MATERIALS AND METHODS:

Bone graft harvested from porcine femoral heads was used. Soft tissue and articular cartilage were removed and a Norwich bone mill was employed to mill the femoral heads. The graft was inspected to ensure there were no cortical fragments. Graft was stored at −25°C and defrosted thoroughly at room temperature for two hours before use. Third generation composite Sawbone® femora were used.

The Exeter IBG technique was used in conjunction with the Stryker X-change instrumentation [2]. An Impactometer [3] which provides a known impaction energy and momentum, was used to standardise the impaction process. A 602 g weight dropped from 260 mm, which produced an energy of 1.54 J and a momentum of 1.4 Ns. This represented the typical levels of achieved in the clinical scenario and was defined as the baseline level in this study. Drop heights of 130 mm (0.77 J) and 390 mm (2.31 J) were also used to represent impaction levels of 50% above and below the baseline study.

Four strain gauges were mounted on the medial side of the femur as shown in Figure 1. The distal impaction was broken down into three stages. A fixed volume of 30 cc porcine bone graft was added at each stage and then impacted four times at drop height of 260 mm. Proximal impaction was performed by impacting with a phantom stem. In aforementioned, three different drop heights were used. The numbers of drops were determined by the achievement of the same ultimate level of compaction; and this was determined by a predetermined final position of the proximal impactor. Strains were recorded in both distal and proximal impaction. The number of proximal impactions was also recorded.

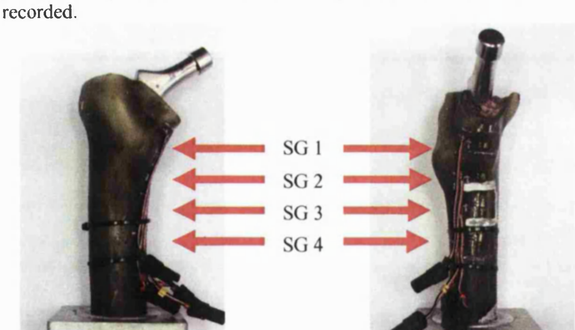

Figure 1 : Four strain gauges were mounted from proximally to distally along the medial side of a composite Sawbone® femur.

RESULTS:

Table 1 shows the amount of total accumulated energy required to perform proximal impaction. This was calculated by the number of blows multiplied by the given energy for a specific drop height. The baseline level required approximately 400 J at a drop height of 260 mm for full consolidation. A drop height of 130 mm required a higher total accumulated energy and was still not sufficient to consolidate the graft. A drop height of 390 mm required less total accumulated energy (a lower number of impacts) to achieve the same level of consolidation.

Drop height	130 mm*	260 mm	390 mm
Energy (J)	530.89 (6.53)	427.9 (58.2)	270.2 (35.9)
Normalised	124%	100%	63%

Table 1 : Total accumulated energy required for proximal impaction. Mean and one standard error are shown (n=6). * Experiments were stopped at 700 impacts if no further consolidation was achieved.

Figure 2 depicts the interval plots of the strain on the medial side of the femoral under three different impaction levels. The position of strain gauges 2 and 3 were situated in the region of Gruen zones 6 and 7. As can be seen, strain gauge 3 gave the highest value of strains. The general pattern was that the higher the drop height, the higher the strain experienced by the femur. Furthermore, very low strain values were measured in strain gauges 1 and 4 (i.e. proximal and distal end).

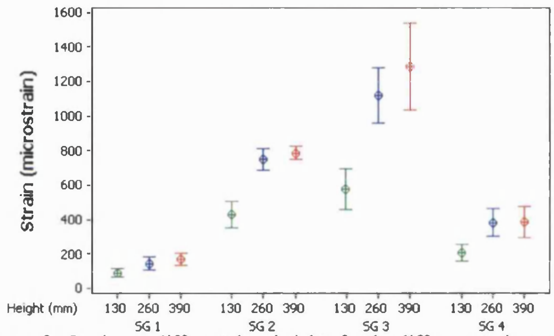

Figure 2 : Strains at different drop heights for the different strain gauge (SG) locations (n=6). The mean and one standard error are shown.

DISCUSSION:

When a drop height of 130 mm was used, there was insufficient energy to impact the stem into the compacted distal graft. Therefore, a larger number of impacts with a 'low-force' were shown not to be an appropriate method for proximal graft impaction. In contrast, a drop height of 360 mm gave 50% more energy per impact than the baseline study. This required 37% less accumulated energy in total, but could induce a higher risk of per-operative femoral fractures.

Higher strain levels were expected on the medial side of the femur because of the curvature and the design of the stem. Particular attention should be paid around Gruen zone 6 and 7. Femoral reinforcement with cerclage, meshes, cortical strut grafts or reconstructive plates are essential, especially in massive femoral reconstruction cases [4]. The location of the highest strain levels is dependent on the applied force, the stem geometry, bone quality of the femur and the load transmission ability of graft and cement.

CONCLUSIONS:

It was found that and energy level of 0.77 J was not sufficient to achieve graft compaction. Therefore, a low-force impaction is not an appropriate method for IBG to achieve the same amount of graft consolidation. A high impaction energy (2.31 J) causes higher strains and has a greater potential to cause per-operative fractures. In addition this level of impaction did not achieve improved consolidation over that achieved at the baseline impaction energy level.

REFERENCES:

[1] Heal JS *et al.*, Orthopaedic Update [India] 2001;11(3):28–35.
[2] Gie GA *et al.*, J Bone Joint Surg [Br] 1993;75-B(1):14–21.
[3] Grimm B, PhD dissertation, University of Bath, UK 2003.
[4] Van Kleunen JP *et al.*, J Arthoplasty 2006;21(3):362–371.

IN-VITRO PREDICTION OF CEMENTED AND NON-CEMENTED REVISION STEM STABILITY IN IMPACTION BONE GRAFTING

+*Mak, S Y; *Smith, S D; *Miles, A W
+*Centre for Orthopaedic Biomechanics, University of Bath, UK
S.Y.Mak@bath.ac.uk

INTRODUCTION:

Impaction bone grafting (IBG) has been used in revision hip replacement for more than 15 years. The objective is to impact allograft bone chips into the medullary canal to compensate for bone stock loss after failed primary hip replacement. Initial stability is crucial for osteointegration. A previous study attempted to assess the initial stability of cemented and non-cemented stems [1]. It was concluded that in the absence of cement, the graft could not provide sufficient stability. The aim of this study was to investigate the use of a large non-cemented stem with IBG, and to compare this with a smaller cemented stem to ascertain if sufficient stability could be achieved.

MATERIALS AND METHODS:

Bone graft harvested from porcine femoral heads was used. Soft tissue and articular cartilage were removed and a Norwich bone mill was employed to mill the femoral heads. The graft was inspected to ensure there were no cortical fragments. Graft was stored at –25°C and defrosted thoroughly at room temperature for two hours before use. Third generation composite Sawbone® femora were used and the internal diameter was reamed from Ø15.7 mm to Ø19.9 mm to simulate the femoral canal associated with bone loss.

The Exeter IBG technique was used in conjunction with the Stryker X-change instrumentation [2]. An Impactometer [3] which provides a known impaction energy and momentum, was used to standardise the impaction process. A 602 g weight dropped from 260 mm, which produced an energy of 1.54 J and a momentum of 1.4 Ns was used for both distal and proximal impaction. The distal impaction was broken down into three stages. A fixed volume of 30 cc porcine bone graft was added at each stage and then impacted four times. In the non-cemented experiments, the proximal phantom stem was left in place after impaction (Note: the size of the phantom stem was two sizes larger than the stem used for cement fixation). For the cemented experiments, the proximal phantom stem was removed and Simplex bone cement (Stryker Orthopaedics) was injected in a retrograde fashion, pressurised and the appropriate Exeter stem was inserted.

Stability testing was carried out by loading the stem on the femoral head (Figure 1). A progressively increasing cyclic load was employed, the test was split into block loadings of 1500 haversine cycles at frequency of 2 Hz in an Instron 8511 servo hydraulic test machine The load was initially set to 0.2 kN and increased in steps of 0.2 kN for each new block loading cycle (i.e. 0.4, 0.6, 0.8 kN...etc). This step was repeated until a 4 mm axial displacement was measured on the Instron test machine. Six tests were carried out for each test condition.

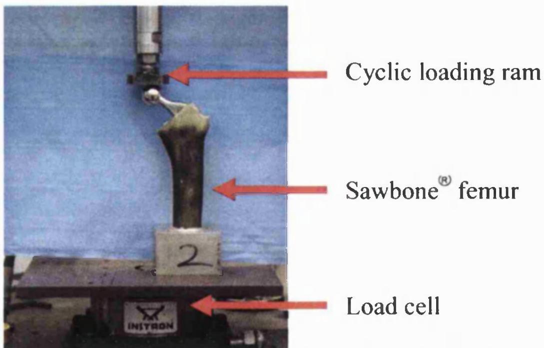

Figure 1 : Loading configuration showing Exeter stem implanted into Sawbone® femur.

RESULTS:

Figure 2 depicts the box plots of the axial displacement under cyclic loading tests. As can be seen, the relationship between the axial displacement and the loading for the non-cemented stem shows an exponential relationship. Grimm *et al.* [3, 4] also obtained similar relationship when evaluating different graft materials. In the case of the cemented stem the relationship between axial movement and of loading appears to demonstrate a gradual exponential increase.

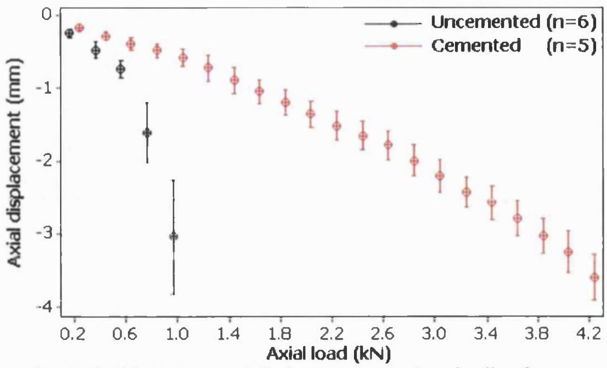

Figure 2 : Maximum axial displacement at various loading forces. Mean and one standard error are shown.

DISCUSSION:

In this experiment, the impaction grafting kit and Exeter stem were used. It is important to note that the collarless, polished and tapered stem was designed to allow subsidence within the bone cement [3]. When bone cement was not used, massive axial movement was observed. This movement was caused by the subsidence of the stem within the graft. All six stems failed in a similar way. In the absence of bone cement, all forces were transmitted into the bone graft. In addition, the graft was not fully in contact with the stem in all areas of the stem and, therefore, high localised contact stresses were generated. Most of the forces were exerted on the proximal-medial and distal-lateral areas (called reaction zone) [5]. Hence, graft material appeared to fail due to high localised contact stresses

When bone cement was used, the axial movement of the prosthesis was associated with subsidence of the stem within the cement and subsequent flexural loading of the femurs. The bone cement enhanced the load transfer distribution to the graft and provided an inter-locking between the graft and the femur. This consolidated all three materials to form a composite structure so as to provide resistance to the applied loading. As a result, the majority of the axial movement measured by the test machine was associated with the elastic bending of the femur. This study shows that it is essential to use bone cement during mechanical testing to evaluate impaction parameters for use in impaction grafting.

CONCLUSIONS:

The pattern of axial movement associated with impaction grafting is different for the two cases examined with and without the use of cement. Non-cemented stems demonstrated an exponential relationship between loading and subsidence since most of the force was exerted on the graft in the proximal femur, whilst in the case of the cemented stem a more gradual exponential relationship existed since the forces were more evenly transferred to the graft in all regions of the stem. The use of bone cement consolidates the graft, and the femur to form a more stable structural material. In conclusion, prediction of impaction graft stability without use of bone cement does not sufficiently characterise the graft behaviour and caution should be exercised in using such tests to screen graft materials.

REFERENCES:

[1] Schreurs BW *et al.*, Clinical materials 1994;16(2):105–110.
[2] Gie GA *et al.*, J Bone Joint Surg [Br] 1993;75-B(1):14–21.
[3] Grimm B, PhD dissertation, University of Bath, UK 2003.
[4] Grimm B *et al.*, Bioceramics 14 2002;218-2:375–378.
[5] Miles AW *et al.*, S Afr J Surg 1978;16(2):157–165.